(NASA-CR-159451) BASIC RESEARCH IN FAN SOURCE NOISE: INLET DISTORTION AND TURBULENCE NOISE Final Report, 16 Sep. 1976 - 16 Apr. 1978 (General Electric Co.) 161 p HC A08/MF A01 CSCL 20A G3/71

N79-14875

Unclas 42024

NASA CR 159451

BASIC RESEARCH IN FAN SOURCE NOISE - INLET DISTORTION AND TURBULENCE NOISE -

FINAL REPORT

By R.A. Kantola and R.E. Warren

GENERAL ELECTRIC COMPANY
Corporate Research and Development
Schenectady, New York 12345

NATIONAL AERONAUTICS AND SPACE ADMINISTRATION
Lewis Research Center
21000 Brookpark Road
Cleveland, Ohio 44135

Contract No. NAS3-17853

1 Report No NASA CR 159451	2 Government Accession No	3 Recipient's Catalog No
4 Title and Subtitle Basic Research in Fan Source Noise - Inlet Distortion and Turbulence Noise		5 Report Date December, 1978 6 Performing Organization Code
7 Author(s) R. A. Kantola and R. E. Warren		8 Performing Organization Report No SRD-78-186 10 Work Unit No
9 Performing Organization Name and Address General Electric Company Corporate Research and Development Schenectady, New York		11 Contract or Grant No Contract NAS3-17853
12 Sponsoring Agency Name and Address National Aeronautics and Space Administration Washington, D.C. 20456		13 Type of Report and Period Covered Contractor Report 76 September 16 - 78 April 16 14 Sponsoring Agency Code

15 Supplementary Notes

Project Manager, James H Dittmar, NASA Lewis Research Center, Cleveland, Ohio.

16 Abstract

A widely recognized problem in jet engine fan noise is the discrepancy between inflight and static tests This discrepancy consists of blade passing frequency tones, caused by ingested turbulence that appear in the static tests but not in flight. To reduce the ingested distortions and turbulence in an anechoic chamber, a reverse cone inlet is used to guide the air into the fan. This inlet also has provisions for boundary layer suction and is used in conjunction with a turbulence control structure, TCS, to condition the air impinging on the fan The program has been very successful in reducing the ingested turbulence, to the point where reductions in the acoustic power at blade passing frequency are as high as 18 dB for subsonic tip speeds Even with this large subsonic tone suppression, the supersonic tip speed tonal content remains largely unchanged, indicating that the TCS did not appreciably attenuate the noise but effects the generation via turbulence reduction. Turbulence mapping of the inlet has confirmed that the tone reductions are due to a reduction in turbulence, as the low frequency power spectra of the streamwise and transverse turbulence have been reduced by up to ten times and 100 times, respectively.

17 Key Words (Suggested by Author(s))	18 Distribution Statement
Aircraft Engine Noise Fan Noise Inlet Turbulence Inlet Cleanup	Unclassified - unlimited

19 Security Classif (of this report)	20 Security Classif (of this page)	21 No of Pages	22 Price*
Unclassified	Unclassified		

For sale by the National Technical Information Service, Springfield, Virginia 22161

TABLE OF CONTENTS

LIST OF FIGURES

LIST OF TABLES

FOREWORD

This report was prepared under Contract No. NAS3-17853 for NASA Lewis Research Center, under the technical direction of Dr. J. H. Dittmar. The work was conducted at the Power Generation and Propulsion Laboratory, General Electric Corporate Research and Development, in Schenectady, New York.

ABSTRACT

A widely recognized problem in the jet engine industry is the discrepancy between inflight measurements of fan noise as compared to static tests. This discrepancy consists of blade passing frequency tones, caused by ingested turbulence and flow distortions that appear in the static tests but do not appear in flight. This is significant not only to the problem of predicting the noise emission of a full scale engine, but also key to the area of further noise reduction. This excess rotor-turbulence interaction noise masks other noise sources in subsonic tip speed fans and has left many important acoustic design questions unanswered.

An intensive effort has been carried out to devise means by which an anechoic chamber could be employed to yield fan noise data (in a static facility) of the type that one obtains in flight. The means that were devised consist of·

1) a new inlet which would guide the flow into the inlet better than a standard bellmouth inlet;
2) provision for withdrawing or sucking away the boundary layer flow; and
3) conditioning the intake air by means of honeycomb and screen combination, hereafter to be called the turbulence control structure (TCS).

A modeling effort on a one-twelfth scale model of the anechoic chamber was carried out to sort out and verify these methods from a larger set of possible candidates.

The program has been very successful in reducing the ingested turbulence, to the point where reductions in the acoustic

power at blade passing frequency are as high as 18 dB for subsonic tip speeds. Even with this large subsonic tone suppression, the supersonic tip speed tonal content remains largely unchanged, indicating that the TCS did not appreciably attenuate the noise but effects the generation via turbulence reduction. Turbulence mapping of the inlet has confirmed that the tone reductions are due to a reduction in turbulence, as the low frequency power spectra of the streamwise and transverse turbulence have been reduced by up to ten times and 100 times, respectively.

This research program has convincingly demonstrated that it is possible to clean up the inlet flow of a static fan noise test facility to a point where the static acoustic data stimulates flight data.

1.0 INTRODUCTION

Static facilities for jet engine fan noise testing have consistently shown enhanced blade passing noise in comparison to flight data. Given the difficulties of flight tests, it is important to resolve the sources of this excess noise and affect reductions so that static facilities can accurately simulate the inflight fan noise emission. This excess noise has been generally attributed to rotor-turbulence interaction. The noise generation due to turbulence impinging on axial fans was first mentioned in the literature by Sofrin and McCann (Ref. 1) and by Filluel (Ref. 2). Temporal variations of both amplitude and phase of the blade passing frequency (BPF) signal were observed by Sofrin-McCann. Filluel was able to reduce the blade passing frequency sound pressure level by 5 to 6 dB by using a smooth bellmouth inlet rather than a sharp-edged cowl ring. Sofrin and McCann also noted that when inlet guide vanes were used, the BPF noise decreased with rotor-guide vane spacing only up to a certain point. Only when the guide vanes were removed did the noise drop to a lower level. Both of the effects were attributed to a reduction of inlet turbulence. The investigators had not, however, addressed the question of static to flight noise comparisons. One of the earliest investigators to establish the importance of turbulence on rotor noise and relate this to the flight-static noise discrepancy was Hanson (Ref. 3).

From a theoretical viewpoint, the turbulence interaction noise can be divided into two types: the first due to fluctuating lift on the rotor blades (dipole) and second the interaction of the turbulent eddies with the rotor-locked potential field (quadrupole). Mani (Ref. 4) and Pickett (Ref. 5) have made theoretical predictions of the noise due to fluctuating lift from subsonic lightly loaded rotors. Picket extended Mani's analysis to include transverse turbulent length scales

different from the axial length scale. Pickett was then able to show that the turbulent noise peaked at an intermediate transverse scale. For more highly loaded rotors, Mani (Ref. 6), in a more recent analysis, has included the quadrupole contributions. The existence of this quadrupole sound field was first pointed out by Ffowcs Williams and Hawkins (Ref. 7).

Attempts to control the rotor-turbulence noise from axial fans date back to Filluel's work, where the placement of radiators made up of honeycomb-like sections in front of the fan reduced the BPF noise. In an unreported experiment in 1973, Wells (Ref. 8) used a single fine meshed screen in a nearly spherical form to cover a conventional bellmouth. This screen produced a maximum reduction of 3 dB in the power level of the BPF tone. Boundary layer suction ahead of the rotor has been tried by Cumpsty and Lowrie (Ref. 9), Moore (Ref. 10), and Kazin, et al. (Ref. 11). In all of these suction cases, a slot was used to remove the boundary layer. Generally with no bleed flow, the BPF tone was enhanced. Application of suction did produce a reduced BPF tone level but the reduction was not sufficient to reduce the BPF tone (at subsonic tip speeds) to the broad band level. Considerable progress in tone noise reduction was reported by Lowrie (Ref. 12). A combination of boundary layer suction (via a slot) and a single hemispherical screen was used. Unfortunately, a high degree of variability of tone level occurred with suction and at no suction the BPF tone level was increased. In a further effort at Rolls-Royce, reported by Lowrie and Newby (Ref. 13) and Cocking and Ginder (Ref. 14), a hemispherical structure of self-supporting honeycomb was used to condition the flow to a subsonic rotor. Cocking and Ginder concluded that even though the reduction in the BPF tone protrusion above the broad band level was significant (up to 10 dB), further reductions of the tone were necessary. The peak angle BPF tones

were still protruding about 10 dB above the adjacent broad band level. Two other experimental studies have also been reported. Shaw et al. (Ref. 15) and Woodward et al. (Ref. 16) both used a nearly spherical flow conditioner consisting of an outer layer of honeycomb with a fine screen attached on the inner edge of the honeycomb. One study, by Shaw et al., tested a fan in a wind tunnel while the other, by Woodward et al., measured the fan noise in an anechoic chamber. Shaw found that the flow conditioner reduces the BPF tone by about 10 dB but the reduced level was still about 9 dB above what was obtained when the wind tunnel was used to simulate the flight condition. Likewise, Woodward found nearly identical results with a 10 dB reduction in the BPF tone being realized but the tone was not reduced to near broad band levels as had been observed in some flight measurements. As these prior investigations had not reduced the BPF tones of a subsonic rotor to near the broad band levels, a major effort was made in this program to identify and eliminate all the sources of ingested turbulence.

As a result of this effort, three inlet clean up methods were found to be effective and are described in this report. A flared reverse cone inlet is used to eliminate wakes from the fan casings and/or probe supports. Boundary layer suction is employed ahead of the fan rotor and as well on the outer flare of the cone to reduce the boundary layer turbulence and remove any residual wakes. To reduce the midstream turbulent intensity and length scales, a turbulence control structure, constructed with both a layer of honeycomb and a fine mesh screen, is also used.

To quantify the effects of these clean up methods, the far field noise is measured in an anechoic chamber, using a high speed fan (20 inch diameter) of the current high bypass type. The changes in the turbulent field impinging on this rotor are quantified by mapping the streamwise and transverse turbulent properties (spectra,

intensity and length scale) with crossed hot film probes. These tests are carried out at the General Electric Corporate Research and Development aeroacoustic facility in Schenectady, New York.

2.0 DESCRIPTION OF ORIGINAL FACILITY

A schematic diagram of the facility is shown in Figure 1 and a photograph showing an overview of the facility as it existed prior to this program is shown in Figure 2. The test vehicle used in this investigation was the NASA Lewis 0.504 m (20 in.) diameter fan model designated as Rotor 11. The fan design characteristics are given in Table 1. The stator set and casing were manufactured by General Electric. The anechoic chamber was designed to simulate a free field acoustic arena and provide adequate aerodynamic operation. It is approximately 10.7 m (35 ft.) wide by 7.6 m (25 ft.) long by 3.1 m (10 ft.) high as measured from the tips of the foam wedges. A free field acoustic environment was achieved by covering walls, ceiling, and floor with an array of 0.7 m (28 in.) long polyurethane foam wedges which provide less than $\pm$ 1 dB standing wave ratio at 200 Hz. Achieving adequate aerodynamic performance has become much more difficult with the recent recognition of the impact of inlet turbulence and flow distortions on fan acoustic emission. To achieve the lowest possible amount of inlet distortion and turbulence, in an effort to aerodynamically simulate the flight conditions, several methods were employed. One such feature of the aeroacoustic lab that existed prior to the onset of this program is that the sidewalls, ceiling and floor are porous. This porous box arrangement is achieved by a manifolding system whereby air flow is distributed from a filter house through 15.2 cm (6 in.) deep U-shaped channels surrounding the chamber. The array of foam wedges is secured to the channels so that the air flow enters the chamber by passing through small openings between the wedges. It has been demonstrated in a prior program (Ref. 17) that such an aspirating chamber arrangement reduces in-flow distortion to the fan.

3.0 TEST PROGRAM

3.1 Initial Tests with a Metal Conical Inlet

In this program, several approaches were studied in an effort to achieve flight-type acoustic data. One of the first of these was an inlet fairing that would eliminate wakes caused by return flow along a normal inlet such as in the typical configuration shown in Figure 2. As part of a prior contractual effort (Ref. 17), the wakes caused by probe actuators, etc., were identified as a possible cause of excess rotor-turbulence interaction noise. A preliminary version of this reverse cone inlet is shown in Figure 3. The acoustical results of using this metal cone, with the rest of the anechoic chamber left unaltered, are shown in Figure 4. With this configuration at best a 1 dB reduction in the acoustic power of blade passing frequency (BPF) is noted when compared to the standard bellmouth. This rather preliminary test while disappointing did identify the need for much more extensive efforts, which subsequently were modeled and tested in a one-twelfth scale model program which will be discussed in the following section.

3.2 One-Twelfth Scale Model Tests

3.2.1 Introduction

To determine the best possible combination of turbulence reduction schemes, a one-twelfth scale model of the anechoic chamber was used as a screening tool. The methods under consideration included: inlet boundary layer removal, revised chamber ventilation, backwall suction, more streamlined inlets, and turbulence control screens. Figure 5 shows the one-twelfth scale model with a portion of the ceiling removed for clarity. In this model, a reverse cone inlet with provisions for inner and outer boundary layer suction is used. The goal of this modeling phase was to sort out from the large number

of parameters the best possible combination for a low turbulence inlet flow. The turbulent intensity in the inlet is used as a figure of merit and was measured with a single hot film probe to quantify the effect of these approaches.

3.2.2 Model Testing

Discussion of the model test results will include the effects of backwall suction, chamber ventilation, turbulence control screens, and boundary layer suction in that approximate order.

Since the turbulent intensity is to be used as a figure of merit in this investigation, the distribution of that intensity across the inlet duct needed to be quantified. To determine the turbulent intensity distribution, vertical traverses were made across the flow duct at 2.5 inlet diameters downstream of the inlet face. A single wire hot film probe was used with the hot film perpendicular to the duct axis and along a circumferential line so that only the streamwise turbulent component is measured, that is assuming the radial component is negligible. Using this measuring scheme, the effects of the location of chamber ventilation and backwall suction were studied. Currently the full scale chamber is ventilated through a porous belt that is 12 feet wide and allows flow in through the ceiling, floor, and both sides. The centerline axis of the rotor passes through the belt with the inlet located so that 8 feet of the porous region is upstream and 4 feet downstream of the bellmouth inlet plane. This configuration will be referred to as side-vented. End ventilation is defined as allowing flow through the front end, the vertical wall facing the inlet, and closing the side ventilation area. End ventilation would hopefully eliminate any vortical patterns resulting from the opposing stream lines, as they currently occur with side ventilation. Backwall suction means that flow is removed at the vertical wall

behind (in a flow direction sense) the inlet. This in combination with the end ventilation is an effort to establish a slight "wind tunnel" effect in the chamber.

A very large number of tests were conducted with varying degrees of backwall suction. Backwall suction was applied with all the chamber ventilation schemes. Despite these efforts, backwall suction was seen to have little or no measurable effect on the inlet turbulent intensity, despite suction flows that equalled or exceeded the flow into the inlet.

To study the effect of screens and chamber ventilation on the midstream turbulence, a probe position of $r/a = 0.2$ was used. A nested set of three screens fabricated in the form of a "top hat" configuration was used as a turbulence control means. At all velocities for the side-vented case, the screens lowered the turbulent intensity, particularly at the lower velocities as seen in Figure 6. Turbulence intensity levels below 0.5% were recorded in the 75 to 120 fps velocity range. The variation, however, of the turbulent intensity with velocity is dramatic, especially around 130 fps. Because of this observed high sensitivity to velocity, a continuous plot of turbulent velocity versus the mean velocity was made on the x-y recorder, with the result illustrated in Figure 7. Clearly now we can see the nature of the problem: the step-like changes in the "RMS" hot film output occur when the cavities in the downstream piping (due to fittings, elbows, etc.) produce cavity resonance and hence a high acoustic output. These resonances appear when the velocity is in an acceptable band that excites the fundamental or higher modes of the cavity vortices.

Recognizing that elimination of the acoustical contamination would require a substantial redesign of the flow withdrawal system, it was decided to evaluate the effects of ventilation, inlet suction and back-wall suction in the region of flow velocity (50 to 150 fps) where the turbulence was found to be the dominant influence on the hot film output. Hot film traverses across the inlet duct were taken for the three different chamber venting schemes to determine radial distribution of turbulent velocity. At a point outside the boundary layer, $r/a = 0.2$, but nearer the far wall to minimize the effect of the probe access hole, the probe was stopped and the midchannel turbulence was measured with a long integration time. The result is shown in Figure 8, where it is quite clear that none of the ventilation schemes hold any distinct advantage, particularly in the region of 50 to 100 fps where a constant turbulence intensity of about 0.5% is realized.

Boundary layer suction tests were also carried out. An example of the change in the turbulent velocity profiles is shown in Figure 9. The reduction in the boundary layer thickness with suction flow rate is clearly seen while the midchannel is unaffected. The asymmetry of the plot is probably due to the effect of the probe access hole and all the data quoted for the midchannel have been taken between the centerline and the bottom boundary layer. To quantify the change in the boundary layer, the probe was fixed at the extreme end of its travel, 0.090" from the far wall. This point, $\Delta r/a = 0.11$, was then used for the remaining measurements. As the effect of chamber ventilation was found previously to be insignificant, the side-vented configuration, as it is presently done in the full scale chamber, was used for all these boundary layer suction tests. Without the turbulence reduction screens, and using both suction areas, it is seen on Figure 10 that it is necessary to provide a bleed flow of 25% of the inlet flow to begin to affect the boundary

layer turbulence at $\Delta r/a = 0.11$. To achieve a 50% reduction requires a bleed flow that is 40 to 45% of the inlet flow rate. Fortunately the use of the three turbulence reduction screens reduces the required bleed flow rates, as seen on Figure 11, with a bleed flow to inlet flow ratio of 30% required to achieve a 50% turbulence reduction. This is still a high rate of suction flow, so that the outer suction area was taped over and the inner suction area alone was used. With the inner suction alone, the suction to inlet flow ratio necessary to achieve a 50% reduction in turbulence was reduced to 15%. Since we are only measuring a fixed point in the boundary layer, the absolute numbers are not as important as the relative efficiencies of the various configurations. That is to say, it appears that the inner suction flow path requires only about one-half the suction flow as the combination, and that the turbulence control screens provide a further one-third reduction in suction requirements. This information then provides guidance as to the most efficient full scale system in advance of the actual full scale testing.

3.2.3 Summary of Model Testing

The model testing has demonstrated the reduction of inlet turbulence is possible with boundary layer suction and turbulence control screens. Because of these findings, the planned full scale tests of the reverse cone inlet will concentrate on using the inside suction path as the model testing has indicated that is the most effective approach. The turbulent control structure will be made from a combination of honeycomb and fine mesh turbulence reduction screens. This device is necessary to condition the inlet flow, that is outside the boundary layer, as none of the other methods, including inner and outer boundary layer suction, produced any reduction in this freestream turbulence.

The model testing has also demonstrated that the inlet turbulence does not depend greatly on the method of chamber ventilation and backwall suction so that the full scale tests of the reverse cone inlet will not require any extensive modifications to the anechoic chamber.

3.3 Full Scale Experiments in the Modified Anechoic Chamber

3.3.1 Introduction

This section will describe an intensive effort to devise means by which the anechoic chamber could be made to simulate inflight fan noise data. We are guided in methods of turbulence control by our one-twelfth scale model tests, but the success or failure of this effort must be judged on an acoustic basis and therefore we prepared several approaches to be tried in the anechoic chamber. These approaches consisted of:

1) a flared reverse cone inlet to better guide the flow into the fan than the standard bellmouth,
2) provision for withdrawing or sucking away the boundary layer flow, and
3) conditioning the intake air by means of a honeycomb-screen combination which will be referred to as the turbulence control structure, TCS.

The mechanical design of these devices and the test instrumentation are described in the following section.

3.3.2 Test Hardware

To reduce inlet distortion, a flared reverse cone inlet, as shown in Figure 12, was designed and fabricated. The reverse cone inlet acts as a shroud covering all of the "upstream" hardware associated with the inlet and other test instrumentation. This hardware has, in the past, been identified as a major source of inlet

distortion (Ref. 17). Along with the addition of the reverse cone inlet, great care was taken to aerodynamically clean up the chamber and remove all objects that protrude into the inlet flow field and therefore possibly generate flow distortions and turbulence. For example, the chamber back wall near the inlet was covered with smooth foam panels and the work platform (steel grate) was made removable. A comparison of before and after chamber clean up is seen in Figures 2 and 12. To further eliminate flow distortions and turbulence that reside in the boundary layer, the reverse cone inlet was equipped with both internal and external surface suction, as shown in Figure 13a.

The third inlet clean up method uses a turbulence control structure (TCS) to condition the inlet flow and is shown in Figures 13a, 13b, and 14. The TCS used for this program is very similar in size and shape to that used in the earlier work of Shaw et al. (Ref. 15) and Woodward et al. (Ref. 16). The major difference is that in this current design, the inner fine screen is displaced two inches downstream of the trailing edge of the honeycomb. This screen placement was based on the work of Morel (Ref. 18) who found that in contracting flows, the separation between the honeycomb and the screen was very beneficial in reducing the axial turbulent intensity. This TCS was designed and fabricated by General Electric's Aircraft Engine Business Group as part of a General Electric sponsored fan research program. The TCS is nearly spherical in shape, 2.10 m (82.5 in.) at its largest diameter, 1.31 m (51.38 in.) long and is of a two layer construction. The first or outermost layer consists of aluminum honeycomb plus a support screen under the honeycomb, as shown in Figure 13b. The honeycomb (the trade name is Flexcore, a product of Hexcell Corporation) is 5.08 cm (2 in.) thick with irregular shaped cells measuring approximately 0.95 cm (3/8 in.) in width with a wall

thickness of 0.063 mm (0.0025 in.). The second inner layer is a fine mesh (20 by 20) of .014 inch diameter wire. As can be seen in Figure 14, the TCS is divided into twelve sectors with 4 1/4 inch deep ribbing. The ribs are 1/8 inch thick and the screens are welded to the ribs. The complete structure was built and installed in such a way, see Figure 14, as to minimize the wakes from the support structure and therefore offer minimal flow distortion and self-generated turbulence.

3.3.3 Experimental Methods

The acoustic measurements were made in the anechoic chamber by the use of an array of twelve 0.935 cm (0.25 in.) microphones. The microphones (B&K Model 4135) were located every 10^{o} from 0^{o} (fan centerline) to 110^{o} at an arc radius of 5.2 m (17 ft.), as measured from the center of the inlet and one rotor diameter upstream from the rotor face (see Figure 1). The microphones were calibrated by a piston-phone (B&K Model 4220) prior to each run and measured spectra were corrected for the individual microphone frequency response. Atmosphere absorption is accounted for via the Society of Automotive Engineers Specification Number ARP866. No other acoustic corrections were applied to this data.

Circumferential inlet flow mapping was done at several radial immersions and at two speeds. Mean and unsteady components of both the streamwise and transverse velocities were measured via two crossed wire hot film probes (see Figures 15 and 16) mounted in the inlet just upstream of the rotor. The furthest upstream (movable) probe was mounted in a rotary actuator which was remotely controlled through a 180^{o} arc within an accuracy of ± 1%. By rotating the entire mechanism 180^{o}, a full 360^{o} inlet survey was provided. The fixed crossed hot film probe was placed at one of two locations, either 157.5^{o} or 337.5^{o} (forward looking aft and clockwise), depending

on which half of the inlet was being surveyed. For most of the tests, both fixed and rotating probes were set at one of two immersions either 63.5 mm (2.5 in.) or 12.7 mm (0.5 in.) as measured inward from the inner casing wall.

Calibration of the Thermal System, Inc., crossed hot film probes (Model 1240-20) was done on an air flow calibration stand that makes use of a clean air supply and a 17.78 mm (0.7 in.) diameter standard ASME nozzle. All of the crossed wires linearized voltage outputs were adjusted to yield the same amplitude at a given velocity, over a velocity range from zero to 500 fps. In addition to the above calibration, because inlet air temperatures depend solely on weather conditions, calibrations were done at three different air temperatures in an effort to minimize errors that may result from test conditions varying from those of the calibration. One of the three temperatures used was a best guess of the expected test conditions while the other two temperatures were used to develop a temperature correction factor to cover any nonseasonal excursions in temperature. With the data established in the temperature calibration, it was then possible to adjust each of the hot film's overheat temperatures to compensate for actual test conditions.

All acoustic and hot film data were recorded on a 28 channel FM tape recorder. Post test data reduction included turbulence spectrum and turbulent scales via the auto and cross correlations (see Figure 16). During the inlet mapping tests, on-line circumferential plots were made of the mean and turbulent velocities.

3.3.4 Aerodynamic Performance

Aerodynamic measurements were taken to determine the effects of the various inlet configurations on Rotor 11's performance. The instrumentation included: four total pressure/total temperature rakes, with five radial stations each, located downstream

of the rotor; and a 0.56 m (22 in.) diameter orifice located in the rotor discharge piping. With this information plus the chamber static pressure (the inlet was assumed to be loss-free), Rotor 11's fan performance map was established for various configurations and suction rates (see Figure 17). With the TCS in place, there is a slight reduction in the fan weight flow, particularly when the fan discharge is throttled (higher discharge valve setting).

3.3.5 Acoustic Results

Two basic inlet configurations were tested:

1) Reverse cone inlet, and
2) Reverse cone inlet with turbulence control structure.

Both configurations were tested without any suction, inside suction only and both inside and outside suction. Suction mass flow rates were set as a percentage of fan mass flow and ranged from 5% to 10% depending on the configuration. Three types of suction surface liners were used: 1) metal for hardwall or no suction; 2) feltmetal, and 3) perforated plate. The more porous perforated plate was used because of the difficulty of reaching the 10% suction rates at higher engine speeds with the feltmetal liner. Acoustic data was taken at seven corrected speeds (54%, 60%, 69%, 74%, 80%, 86%, and 100%) and one discharge valve setting, full open.

3.3.5.1 Flared Reverse Cone Inlet

With the reverse cone inlet installed, a series of tests with and without suction were conducted. The tests included far field acoustic measurements, inlet turbulence and mean velocity traverses. Our attention will be concentrated first on the acoustic results and the flow measurements will be taken up later in this report.

To clarify further discussion, let us digress for the moment and explain what the expected noise characteristics of this fan would be on an idealized basis. For this rotor-stator set operating with a completely turbulence free inlet flow, there would be two noise source mechanisms. These would be the rotor-stator interaction noise and the rotor alone noise. The rotor-stator interaction would be caused by the potential field interaction between the rotor and stator and by the rotor wakes impinging on the stator. The blade passing frequency (BPF) noise due to this rotor-stator interaction will not propagate in the inlet duct below a certain rotor speed; this speed is dependent on the rotor blade and stator vane numbers. For this particular rotor and stator, this phenomenon, called cut-off, occurs at about 74% speed. Likewise, the BPF noise caused by the supersonic rotor by itself is also governed by the same type of cut-off phenomenon only at a slightly higher rotational speed, about 77% speed. Therefore, it would be expected that with a completely turbulence-free inlet flow this fan would have very low BPF noise below 74% speed and above 74% speed, the rotor-stator interaction noise and the supersonic rotor alone noise would cut-on and produce high levels of BPF noise. In a non-ideal flow, that is one with large scale inlet turbulence, the BPF noise at high speed, above cut-off, would not be significantly affected due to the dominance of the rotor-stator and rotor alone noise. However, in a turbulent flow, the BPF noise at low speed, below cut-off, would be greatly increased due to the low levels of BPF noise below cut-off with a nonturbulent inlet flow.

The first tests were without suction flow and with hard walls replacing the suction surfaces. The acoustic results of these tests are shown in Figures 18, 19, 20, 21, 22, and 23. In this condition, the flared reverse cone did not offer any major reduction in BPF

noise, in either power level, PWL, or sound pressure level, SPL, at 60^{o} to the inlet as seen on Figures 18 and 19, respectively. When the suction surfaces are exposed and high rates of suction used to remove both the inner and outer boundary layers, still only a modest reduction in the PWL at BPF of 2.6 dB is achieved, as seen in Figure 20. At the peak angle, $\theta = 60^{o}$, for 69% speed, a slightly larger reduction (3.3 dB) in SPL at BPF is shown in Figure 21. For these suction runs, both the inner and outer suction surfaces were made from a feltmetal material called Brunsacoustic. Due to the difference in suction surface areas, the majority of the suction flow passes through the outer surface. The scale model test program had also indicated that the outer surface was very inefficient in reducing the inlet boundary layer thickness and therefore in agreement with the implication of these acoustic results. With this confirmation of the one-twelfth scale model test conclusions, it was decided to proceed with the most effective suction scheme as determined by those model tests.

These one-twelfth scale model tests indicated that the inner suction surface was more effective in reducing the boundary layer thickness incident on the rotor. To determine the acoustic benefits of this thinner boundary layer, the outer suction surface was covered with a metallic tape and the inner suction surface was used by itself. For some of these tests, at high suction flows, a perforated plate of 40% porosity replaced the inner feltmetal suction surface. In Figure 22, the inner suction alone is seen to be more efficient in reducing the BPF tone and its immediate surrounding broad band content. The broad band level here is defined as the average of the two bands adjacent to the tone. The tone reduction for this subsonic speed is, however, still small, about 4 dB, indicating that the rotor-turbulence

interaction noise is only slightly reduced. At higher speeds, as shown in Figure 23, the BPF tone reduction decreases to 1.5 dB as would be expected, since in this speed range the rotor alone and rotor-stator interaction noise are cut-on and dominant. Going back and comparing these results to those obtained with a standard bell-mouth, a maximum BPF tone reduction of about 5 dB is seen at the lower speeds for a 10% inner suction rate, as shown in Figure 24. In summary then, the combination of a flared reverse cone inlet and a suction rate of 5 to 10% of the main flow will result in only a modest 5 dB reduction in BPF tone for this subsonic cut-off fan. This level of reduction is not enough to achieve flight simulation and therefore a turbulence control structure must be employed.

3.3.5.2 Flared Reverse Cone Inlet with Turbulence Control Structure

As the combination of the reverse cone inlet and boundary layer suction did not provide sufficient inlet clean up, it was necessary to use the TCS to condition the inlet flow. This device is shown in Figure 5 in its installed position. The effect of the TCS on BPF tone is dramatically illustrated in Figure 25. Not only are the BPF tones greatly reduced below cut-off (about 74% for Rotor 11) but at supersonic rotor Mach numbers well above cut-off, the BPF noise is not greatly affected by the TCS as one would hope. This indicates that the TCS is not greatly attenuating the fan noise and that agrees with the calibration of the TCS as given in Appendix I. To briefly summarize the results given in that appendix, it may be stated that on a power level basis, the attenuation is less than 1 dB for frequencies less than 16,000 Hz. Above 16,000 Hz, the power level is attenuated by about 1 1/2 dB. The sound pressure level shows a somewhat greater attenuation at the shallow angles, between 20^{o} to 50^{o} from the inlet centerline. At the fundamental (3150 Hz) and fifth harmonic (16,000 Hz) of the one-half wave length resonance

of the honeycomb, attenuation levels of 3 dB are reached at 30° to the inlet centerline. Most important is that at BPF, the acoustic power level would be attenuated by less than 1 dB by the TCS.

These results give good confidence that the TCS has reduced the inlet turbulence and hence the rotor turbulence interaction noise generation and not just suppressed the overall noise emission. The BPF tone reduction due to the TCS is as high as 12 dB at 69% speed. This large reduction in BPF tones due to the TCS compared to the effect of boundary layer suction points to the existence of disturbed flow that is well outside the boundary layer. However, the boundary layer reforms downstream of the TCS and it is possible to bleed off this developed boundary layer to gain a further reduction in BPF tone levels. This effect is shown in Figure 26 where an additional 4 to 5 dB reduction, at rotor speeds below cut-off, is achieved with 5 to 8% suction using the feltmetal inner suction surface. As can also be noted in Figure 26, the BPF tone reduction is somewhat dependent on the inner suction surface used. Generally the feltmetal surface provides a greater reduction in BPF tone levels than the perforated plate surface. When compared to the bare bellmouth results shown in Figure 18, the maximum BPF tone reductions range from 12 dB at 54% speed to almost 18 dB at 69% speed. Further evidence that these BPF noise reductions are due to rotor-turbulence noise source reductions and not any acoustic attenuation due to TCS is provided by the power spectra data.

The power spectra shown in Figures 27 to 33 illustrate the comparative effects of the TCS on the flared reverse cone inlet and the effect of inner suction in conjunction with the TCS. In this case, the feltmetal suction surface is used with metallic tape covering the outer suction surface. To study the change in acoustic emission, the power spectra is used as it will not be affected by any redirec-

tion of the acoustic waves that might be caused by the TCS. For the lower speeds (below or near cut-off, Figures 27, 28, 29, and 30), the installation of the TCS produces a substantial reduction in the BPF tone while a much smaller reduction is seen in the second harmonic of BPF. This is reasonable as the second harmonic is cut on at these low fan speeds and any potential interaction of the rotor and stator can then produce a tonal sound. When suction is applied, it produces an additional reduction in the BPF tone protrusion.

To further clarify the effect the suction and the suction surface liner have on the acoustic emission of the fan, the changes in the power spectra caused by the feltmetal liner (with and without suction) with respect to a hardwall inlet are shown on Figures 34a and 34b. Without suction, the feltmetal liner provides about a 1 to 2 dB broad frequency band reduction in acoustic power level. This is apparently a "treatment" effect, with the feltmetal liner backed by the suction plenum acting like a short acoustic liner. When suction is applied, the reduction is selective with the BPF tone and its harmonics being reduced more than the broad band level. The broad band reduction is also increased as well as one might expect, since the removal of the fine structure turbulence in the boundary layer should cause a broad band noise reduction. There is some slight evidence in this data to suggest that the suction surface and its plenum are damping out some of the turbulent eddies before they impinge on the rotor, in particular at 60% and 69% speed where the zero suction case shows higher selective reductions of the BPF tones then the surrounding broad band levels. In all of the cases of suction effects discussed in this paragraph, the fan speeds are subsonic and cut-off.

At the higher speeds, 80%, 86%, and 100%, the fundamental BPF tone due to rotor alone and rotor-stator interation noise domi-

nates, as one would expect. The effect of the TCS and suction have a lesser effect as speed increases, until at 100% speed only a 1 1/2 dB reduction occurs with the use of the TCS. This is a very gratifying result as the supersonic rotor alone noise should dominate at these speeds and should not be affected by inlet turbulence and hopefully not attenuated by the TCS. Similar trends are exhibited by the sound pressure, SPL, spectra, as shown in Figures 35 to 41, where the same cases as the previous series on power spectra are shown. In some instances, two sets of suction data are shown: the first with the feltmetal suction surface and the second with a perforated plate suction surface. These two different suction techniques produce slightly different results. The feltmetal suction surface produces more reduction than the perforated plate, particularly at 69% (Figure 37) and 74% (Figure 38). However, at 80% speed, the effect at BPF is reversed. At this speed, however, the BPF frequency is not centered on a one-third octave band and some band splitting may have occurred. In general, the effects of the TCS and suction are right in line with what was seen in the PWL data, Figures 27 to 33, except for the persistence of BPF tone at 69% speed. Only when suction is applied through the feltmetal surface is the 69% speed BPF tone effectively reduced. This is perhaps understandable when the SPL directivity effects are studied.

To study the directivity effects, we will restrict our attention to those speeds where the BPF tone is centered in a one-third octave band. Figures 42 to 45 display the SPL at BPF for 54%, 69%, 86% and 100% speed. Now at 69% speed, the SPL is seen to be peaked at $\theta_i = 60^o$. This speed is also very close to cut on for the rotor-stator spinning modes and 60^o is very close to the peak angle for the first cut on mode. So the relative persistence of the BPF tone, as

seen in Figure 37, is due to the concentration of the SPL at this angle. As the speeds become higher, the TCS and suction cause changes in directivity patterns, with the exception of the SPL at $\theta_i = 60^o$, which is relatively unaffected by the TCS or suction. This indicates that the BPF level at 60^o is dominated by the cut-on spinning modes due to rotor-alone and rotor-stator interaction noise. When suction and the TCS are applied, the net result is sharply lobed BPF directivity patterns as one would expect from a fan that is producing relatively pure tone noise.

As stated in the Introduction, the goal of this effort was to simulate flight noise in a static facility. To measure how well we have done, let us summarize the general affects of flight on the measured noise signal. One of the most subjective parts of this comparison is what has been removed from the measured flight noise to account for all the other engine and airframe-related noise sources. The intent here is not to provide an exhaustive review of this comparison as that falls well outside of the scope of this program, but rather to use readily available flight-to-static noise comparisons. Perhaps one of the most complete studies in this area is that published by Blankenship (Ref. 19). Of the data presented in that paper, we will concentrate only on the forward arc noise from fans running at subsonic cut-off conditions. This is necessary to avoid turbine tones that appear in the sideline noise and cut-on rotor alone and rotor-stator interaction noise. Restricted to these measurements, the fundamental BPF tone reductions for the DC-10-10 airplane, with the CF6-6D engine, are 7.5 dB at 60^o from the inlet centerline, at about a rotor tip Mach number of 0.73. For the same rotor Mach number and emission angle, the second harmonic is also reduced by 5 dB. The higher harmonics are likewise reduced, for example at a slightly higher rotor tip Mach number of 0.83, the third and fourth harmonics were reduced by 3.5 and 5.5 dB, respectively.

Unfortunately, Blankenship (Ref. 19) did not include the higher harmonic tone reductions at the lower rotor Mach number (0.73); however, the second harmonic tone reduction went from 5 dB to 2.5 dB when the rotor tip Mach number increased from 0.73 to 0.83, indicating that the other higher harmonics may have behaved in the same manner and shown lower flight reductions at a higher tip Mach number.

Similar reductions in the fundamental BPF tone and its harmonics in flight data with respect to static data, as reported by Blankenship, have been reported by Lowrie (Ref. 12) (for the Rolls-Royce RB211) and by Feiler and Merriman (Ref. 20)(for the General Electric CF6-6). These flight measurements seem then in general agreement, in that the fundamental of the blade passing tone, of subsonic cut-off fans, is barely visible (0 to 2 dB) above the surrounding broad band level and the higher harmonics also protrude only slightly (2-3 dB) above the surrounding levels. This is observed only in the forward arc and with one-third octave band filtering. Wind tunnel fan noise measurements reported by Feiler and Groeneweg (Ref. 21) and Shaw et al. (Ref. 15) show a somewhat different result. Here again with the wind on the fundamental tone of BPF is reduced to the broad band level. However, in these tests, the second harmonic and in Shaw's data, the higher tone levels also remained unchanged with the presence of flow. In both cases, the second harmonic tone level was about equal to the fundamental without tunnel flow and while the fundamental reduced by 15 to 20 dB with the tunnel's flow, the second harmonic levels did not change appreciably. It should be noted that these wind tunnel tests used constant band width filters which tend to make the tones protrude more. Both of the fans used in the wind tunnel experiments had low blade number rotors in contrast to the actual engines used in the flight data. It is beyond the scope of this report to try to explain these differences in the reduction of the

higher harmonics as seen in flight and in the flight simulation in the wind tunnel.

Has simulation of in-flight fan noise data been achieved in this facility? With respect to the protrusion of BPF fundamental tones, it would appear so. For the higher harmonics of BPF, the earlier discussion indicates that in-flight data and wind-tunnel flight simulation are in substantial disagreement and that makes a clear cut answer difficult. However, it is informative to compare results from this effort, Figure 46, with the previously reported static flight comparisons of Feiler and Merriman (Ref. 20), Figure 47. At the harmonics of BPF, there is reasonable agreement of magnitude of tone reductions. For the in-flight data shown on Figure 47, it appears that a turbine blade passage tone harmonic is appearing at 5 kHz, midway between the fan second and third BPF harmonic. This turbine noise is pointed out by Blankenship (Ref. 19) and indeed comparing to Figure 24a of Blankenship's paper will reveal a remarkable similarity to the results shown on Figure 47.

To further quantify the reduction in tonal content of the far field acoustic signal, a series of narrow band spectra are presented in Figures 48, 49, and 50. Three different test conditions are shown on these sets of figures: first a hardwall inlet without the TCS; second a hardwall inlet with the TCS; and third, the feltmetal suction inlet with the TCS. For each inlet configuration, the narrow band spectra for each of seven fan speeds are shown. In Figures 48a, b, c and d, where neither the TCS nor suction are employed, strong tones at BPF and multiples of BPF are seen for all these subsonic tip speed conditions. When the TCS is attached to the reverse cone inlet, the fundamental of the BPF is reduced (8 to 17 dB) for the cut-off rotor speeds, as seen in Figures 49a, b, c and d. Not only

is the peak reduced but the tones are also substantially narrower; in particular, compare the narrowness of the tone in Figure 49d to Figure 48d. These tones are reduced further when the TCS is employed along with an 8% inner suction rate, as seen in Figures 50a, b, c and d. At the lowest speed, 54%, the total reduction in the BPF tone is 19 dB while the surrounding broad band is reduced only 5 dB.

Reductions in the broad band levels immediately adjacent to the BPF tones were determined by overlaying of the narrowband spectra and the results are shown on Figure 51. For the hardwall inlet, with the TCS, at a 54% corrected speed, the broad band level did not appreciably change. This is in agreement with the notion that the TCS reduces mainly the large scale turbulence causing a reduction in the tonal content but the small scale turbulence is relatively unaffected and hence the broad band noise content should remain nearly unchanged. This also confirms that the calibration of TCS is reasonably accurate as that calibration indicated that for $\theta = 60^{\circ}$ and 6300 Hz, about a 0.5 dB of attenuation is expected. According to Pickett's analytical results (Ref. 5), for sufficiently large transverse turbulent integral scale to blade spacing ratio (L/S) of greater than 0.2, the noise centered around BPF will rise more quickly with rotor speed than with smaller transverse scales. It then seems reasonable to assume that with the reduction in transverse scale caused by the TCS the broad band level difference between the two cases would grow with rotor speed as shown in Figure 51. However, this picture is clouded by the fact that Pickett's analysis takes in noise in a wide band centered around the BPF. Without an estimate of the spectral shape near BPF, it is then difficult to know what the broad band level will do. Unfortunately then, the cause of the increase in the difference in broad band level with speed cannot be pinpointed. Another important aspect

of the data shown in Figure 51 is the sudden drop in difference in broad band level when the rotor-stator interaction and rotor alone spinning modes cut-on, between 74% and 80% of corrected speed. Here it is apparent what is happening from the comparison of Figures 48 and 49. Broadening of the base of the spectral peaks at BPF, or commonly called "haystacking," progressively occurs above cut-off when the TCS is employed. At 100% speed, the total spectra is very similar for both hardwall cases, with and without the TCS. The high frequency differences seen in comparing Figures 49g and 50g are near the 1 1/2 dB attenuation levels caused by the TCS.

When suction is applied along with the TCS, the broad band levels near BPF are reduced by about 4-5 dB more than the hardwall case over the whole speed range. As explained earlier, in regard to Figures 34a and 34b, approximately 1 to 2 dB of this added reduction is probably due to treatment effect of the suction liner. The remaining 2 to 4 dB is most likely due to the thinning of the boundary layer and subsequent reduction in the wide band noise of the rotor tip interacting with the boundary layer flow.

Substantial reductions of the other harmonics of BPF also occur when the TCS and inner suction are employed. For the supersonic tip speeds, 80% and above, the supersonic rotor alone noise dominates and the tone levels are increasingly independent of the presence of the TCS and suction as the rotor approaches 100% speed. This can be seen by comparing Figures 48e, f, and g to Figures 46e, f, and g, and Figure 50 e, f, and g. The main effect of the TCS and suction is to reduce the broad band noise levels and not the tonal content. This is in complete agreement with the viewpoint that with a supersonic rotor tip speed, the tonal content is governed by the rotor bow shock pattern and its subsequent upstream distortion and the broad band content is primarily due to the inter-

action of the rotor tip with the turbulent boundary layer. The fact that this inlet clean up method greatly reduces the tonal content below cut-off and does not substantially alter it above cut-off proves that the flight quality fan noise data can be simulated in a static test facility.

3.3.6 Hot Film Results

In order to determine the state of the flow impinging on the rotor, hot film surveys of the inlet were taken. A rotary actuator was used to traverse a crossed film probe around the circumference at a given radial immersion. The fan speeds were restricted to less than 69% speed; in fact the majority were taken at 54% speed. There are three reasons for this. The first is that the higher level acoustic signals at the high speeds could cause acoustic contamination of the turbulence measurements and secondly that probe life decreases dramatically at high velocity. Thirdly, since in this effort we are trying to characterize the turbulent state of air ingested by the fan, it was felt that fan speed should not have a large effect on the turbulent intensity and length scales. Of very definitive interest are, however, the effects of the TCS and the amount and method of boundary layer removal on the turbulent condition of the inlet flow. From the twelfth scale model tests, the best combination for cleaning up the inlet flow was found to be the inner suction alone with some sort of turbulent control structure. For this reason, relatively little effort was expended in measuring the inlet flow with both suction surfaces operating and without the turbulence control structure. These measurements, although limited, do form a basis of comparison and will be discussed first.

3.3.6.1 Turbulence Intensity and Mean Velocity with Inner and Outer Suction

On-line plots of turbulent intensities and mean velocity will be discussed. Since the main stream conditions are of primary interest and the effects of suction on boundary layer flow are rather well known, it was decided to use an immersion (15% of the radius) that would survey just beyond the outer edge of the wall boundary layer. Circumferential distributions of the mean and turbulent velocity are shown in Figure 52 for the streamwise component and in Figure 53 for the transverse component. Both cases of with and without suction are shown. At a 69% rotor corrected speed, the circumferentially averaged axial turbulent intensity was 2.7% with a variation from 1% to 4% with angular location. Likewise, the circumferentially averaged transverse turbulent intensity was 2.8% with a variation from 0.9% to 4.8% with angular location. Boundary suction flow rates on the order of 19% of the main flow lower the axial turbulence level by about 10% and the average transverse intensity by about 40%. The mean axial velocity plot shown in Figure 52 indicates a velocity defect in the $\psi = 0^{o}$ to $\psi = 90^{o}$ quadrant (in the forward looking aft, FLA, mode). This defect persists even in the presence of a high suction flow rate. The turbulence levels measured with both suction surfaces open are higher than with the standard bellmouth, (Ref. 17). Two possible explanations exist for this: one that the boundary layer is thicker due to the build up that occurs on the outer flare; second, that the cross flow through the suction plenum from the outer surface and through the inner surface causes a mixing of the two streams and creates an excess turbulence. This turbulence would then impinge on the hot film probe which is downstream of the inner suction surface. As a result of this last possibility, the remainder of the turbulence measurements will be conducted with only the inner suction permeable and therefore only flow moving through the suction

surface in the radially outward direction will be possible. Also to insure that the freestream measurements are outside the wall boundary layer, a greater immersion depth, equal to one-quarter of the fan tip radius, will be used.

3.3.6.2 Turbulence Intensity and Mean Velocity with Inner Suction

For these remaining hot film traverses, a rotor corrected speed of 54% of design speed was used. The outer suction surface was covered with metallic tape and the feltmetal inner suction surface was employed. Table 2 illustrates the test matrix. For the freestream immersion, $\frac{\Delta r}{R_o} = 0.25$, two crossed wire hot film sensors were used so that circumferential length scales could be determined. A twelve minute time record was taken to allow spectral resolution below 1 Hz and determination of large eddy sizes. In the boundary layer, $\frac{\Delta r}{R_o} = 0.05$, only a single probe was used so that only axial length scale, turbulent spectra and turbulent intensity could be determined. When these data were taken, on-line x-y plots of circumferential distributions of the mean and fluctuating velocities for both the streamwise and transverse directions were taken. A presentation of these on-line measurements will be discussed before going into the more detailed spectral and length scale data.

As a starting point, let us consider the case of midstream turbulence, $\frac{\Delta r}{R_o} = 0.25$, when the TCS was not used. The flow, in this situation, is characterized by very uneven, but repeatable, distribution of the streamwise and transverse turbulent intensities, as seen in Figure 54. These intensity distributions are "locked" to the inlet casing and do not change with time. A 4 kHz low pass filter is used to suppress any BPF acoustic perturbations and probe vibration effects that might show up on these x-y plots.

For analog tape recording to be used in spectral and correlation measurements, this low pass filter was not used. With the large eddy length scales expected in this situation, a 10 second integration time was used, the RMS meter (TSI Model No. 1076) then has a 0.6 Hz minimum frequency. The levels of the circumferentially averaged streamwise intensity reach 1.4% with a range from 0.63% to 2.86%. Likewise, the transverse intensity averages 2.1% with a range from 0.89% to 3.4%. The peak levels of turbulent intensity are the major concern as they are the major sources of rotor-turbulence interaction noise. With the addition of suction (w_s/w_{in} = 8% using the inner surface only), a very small decrease in the turbulent intensity was noted, with the streamwise average dropping only by about 5% and very little change in the relative distribution of intensity around the circumference. Similarly, the transverse shows a slight improvement with the average dropping about 10%. While suction had only a minimal effect on the free-stream ($\frac{\Delta r}{R_o}$ = 0.25) turbulence, as was found also in our one-twelfth scale model tests, the use of the TCS produces major changes.

These changes in the turbulent structure are seen in Figures 55 and 56. On the bottom half of each of these figures, the data taken without the TCS in place is displayed. When the TCS is used, a very dramatic change is seen. Indeed now the turbulent intensities are very uniform and of low level. Streamwise intensity ranges from 0.37% to 0.6% over the circumference with an average of 0.41%; likewise the transverse intensity ranges from 0.33% to 0.48% with an average of 0.35%. These averages represent a 3 to 1 and 4 to 1 improvement, respectively, in the streamwise and transverse turbulent intensities over the case when the TCS

is not used. Perhaps even more important is the reduction in the peak intensities where an improvement of 4 to 1 and 6.5 to 1 are seen in the streamwise and transverse intensities, respectively. The turbulence levels are so low that the small wakes due to the TCS support structure can be seen in the transverse turbulence plots, Figure 56. There are twelve ribs, every 30°, in the TCS and in the top half of the inlet their wakes are easily seen. The mean transverse velocity also is not quite uniform. The level of this transverse velocity is also very low, on the order of 3% of the axial component. It is interesting to note that the axial velocity defect, between $\psi = 0^{\circ}$ and $\psi = 90^{\circ}$, persists even in the presence of the TCS (Figure 55). With the TCS in place, removing the boundary layer with the inner feltmetal suction surface had almost no measurable effect on these intensity measurements at this freestream location, $\frac{\Delta r}{R_o} = 0.25$. The only effect was to lower the mean circumferential velocity slightly to a level of 2% of mean axial velocity. The axial velocity defect, between $\psi = 0^{\circ}$ and $\psi = 90^{\circ}$, remained at about 5% of the mean. These results agree with the one-twelfth scale model results which indicated that suction would have minimal effect on the measurements of the freestream. Suction will, however, affect the measurements near the wall in the boundary layer, at $\frac{\Delta r}{R_o} = 0.05$, as will be discussed in the following.

To evaluate what effects the wall suction and the TCS will have on the boundary layer properties, a series of single probe measurements were made. As a starting point, the flared reverse conical inlet without the TCS will be discussed. The turbulent intensities in this situation are quite high, as seen in the top portions of Figures 57 and 58. The streamwise turbulences vary from 0.6%

to 6% with an average of 2%; likewise, the transverse intensity varies from 0.75% to 3.1%, with an average of 1.7%. Particularly high levels are seen at $\psi = 270^{o}$ and $\psi = 30^{o}$. These are two of the three locations (the other being $\psi = 150^{o}$) where the three pieces of the inner suction surface have a parting line. The mating pieces at these points have some irregularities and also there is some end gap. The turbulence caused by these end gap regions is limited to very narrow strips and there are other rather extensive regions of high turbulence that may contain turbulence of large length scales. Due to the large scale turbulence, a 10 second integration time constant (lower frequency limit of 0.6 Hz) was used to replot the lower half of the inlet, as seen in Figure 59. In general, the levels are increased indicating spectral content below 6 Hz, which is the "RMS" meter's minimum frequency at the 1 second time constant. In contrast to the results at $\frac{\Delta r}{R_o} = 0.25$, suction does have a large effect on the turbulence at $\frac{\Delta r}{R_o} = 0.05$, as seen in the bottom portion of Figures 57 and 58. In particular, the streamwise component is roughly reduced by a factor of two, with a reduced average of 0.84% and a range from 0.54% to 2.9%. A major difference is the absence of the large levels at $\psi = 30^{o}$ and $\psi = 270^{o}$. The suction has removed the disturbed flow at these points and generally quieted the whole inlet boundary layer. The transverse turbulence intensity component remains basically unchanged by suction with an average of 1.6% and a range from 0.11% to 2.7%. Both turbulence components are affected when the TCS is used, however.

Placing the TCS on the inlet produces marked changes in the measurements at $\frac{\Delta r}{R_o} = 0.05$ clearly indicating that the freestream flow unsteadiness is perturbing the boundary layer. The disturbed flow seen without the TCS at $\psi = 270^{o}$, 30^{o}, and even 150^{o} now shows up clearly in upper traces in Figures 60 and 61. This is due to the fact that the turbulence intensity levels are less than 0.5%

except for these isolated regions. The streamwise intensity now has an average of 0.59% with a range from 0.41% to 3.6% while the transverse intensity has an average of 0.46% with a range from 0.35% to 2.9%. The axial velocity defect, between $\psi = 0^{\circ}$ and $\psi = 90^{\circ}$, is practically unchanged and remains centered at $\psi = 30^{\circ}$.

When suction is applied to inlet with TCS in place, these localized regions of high turbulence, due to the end regions of the suction surface segments, disappear as seen in the bottom portions of Figures 60 and 61. The only troublesome region remaining is from $\psi = 340^{\circ}$ to $\psi = 60^{\circ}$, see Figure 60. This coincides with a nonuniformity in both the mean axial and transverse velocities. In the bottom half of the inlet, the flow is cleaned up to the extent that the wakes from the TCS support structure appear, as in the measurement at $\frac{\Delta r}{R_o} = 0.25$ (Figures 55 and 56). This indicates that perhaps there exists some defect in the cone or the suction surface in that azimuthal location. This combination of TCS and 8% inner suction produces levels of turbulence in the boundary layer that are quite low. The streamwise intensity averages 0.48% with a range from 0.38% to 1.1% while the transverse intensity averages 0.39% with a range from 0.34% to 0.48%.

In summary, the combination of TCS and inner suction can produce an inlet flow that contains turbulent intensities on the order of 0.5% or less. The effect of these controls on the turbulent spectra and length scales will be taken up next.

3.3.6.3 Turbulent Length Scales

Two crossed film sensors with an angular separation were used to measure the transverse cross correlation of the transverse velocities. These measurements were made at an immersion of $\frac{\Delta r}{R} = 0.25$ and at the same time as the on-line intensity plots.

Without the TCS in place, the decay of the normalized cross correlation with probe separation is seen in Figure 62. Two locations of the reference sensor, $\psi_f = 157.5^o$ and 337.5^o, were used and produced essentially equivalent results as can be seen in Figure 62. The data was fitted to functional relations shown in Figure 62 and integrated to yield a transverse integral length scale of 0.47 inches. Measurements were also made with the TCS in place but due to the extremely small transverse scale, discernible levels of cross correlation were not possible even at the smallest probe separation of $\Delta\psi = 5^o$. Probe separations of much less than 5^o can cause the downstream probe to be in the wake of the fixed upstream reference probe and therefore were not attempted.

To determine the streamwise or axial length scales, the autocorrelation of a single cross film sensor was integrated over time and eddy convection assumed to be equal to the streamwise velocity. Figure 63 illustrates the distribution of the axial length scales around the inlet circumference. Without the TCS, the axial length scales are on the same order as measured previously in this facility, Ref. 17. When the TCS is in place, a rather large reduction in the length of the eddies occurs. This reduction does not appear to be as large as occurs with the transverse scale. In comparing this data with that found in Ref. 17, it is seen that without the TCS, the data reported herein indicates that the turbulent intensities and axial length scales are nearly equal. The acoustic results seen in Figure 18 confirm this also as only about a 1 dB reduction in the BPF tone occurs with the reverse cone inlet, as compared to the standard bellmouth. The most interesting result is that in spite of the substantial streamwise turbulent length scales, up to 8 feet, the TCS produces a large reduction in the BPF tones. This can be explained by briefly reviewing the theoretical aspects of rotor-turbulence interaction noise.

To generate significant tone noise, the ingested turbulence has to have certain characteristics. A long axial integral scale is necessary to allow the rotor to cut the eddy many times, as pointed out by Ffowcs Williams and Hawkings (Ref. 7). For the range of axial scales measured here, without the TCS (5 to 20 feet), the rotor blades will chop the typical eddy from 200 to 800 times as it passes through the rotor. Clearly the eddies are sufficiently long; even with the TCS the typical eddy will be chopped from 20 to 300 times. The transverse scale also has an effect on the noise generation, as pointed out by Mani (Ref. 4). In particular, the ratio of the integral length scale to the transverse blade spacing is very important. For large values (above 2), the turbulence acts like a low lobe number inlet distortion that produces relatively coherent interactions that are spinning too slowly to propagate effectively. As the scale to spacing ratio goes down, the spectra broadens and the resulting higher order modes propagate more effectively. For very low transverse scale to spacing ratios, below 0.5, the spectral peak is no longer apparent and the signal at BPF drops with a decreasing ratio. The overall acoustic power level increases, however, but now is of a broad band nature. Pickett has given an example of this effect on the noise centered around the BPF signal and found that the noise was a maximum at a ratio of transverse scale to blade spacing of 0.2. The ratio of the transverse scale to blade pitch (at the tip) for the experiments reported herein, without the TCS, is 0.33. This is quite close to the point of maximum turbulence-rotor interaction noise generation as predicted by Pickett. To reduce the BPF tone level by 10 dB by the use of the TCS would require about a 10 to 1 reduction in transverse scale. Unfortunately, the transverse scale could not be measured when the TCS was used so that the effect of reducing transverse scale cannot be quantified. It then remains to determine if the large reductions in intensity are more responsible for this acoustic benefit. To more thoroughly

assess this effect of the TCS on the turbulent intensities, the turbulent spectra have to be examined.

3.3.6.4 Turbulent Spectra

To determine the effect of the TCS on the spectra of the turbulent velocity components, the inlet was measured at $\frac{\Delta r}{R_o} = 0.25$ in four different circumferential locations: $\psi = 0^o$, 90^o, 180^o, and 270^o. To allow for adequate resolution of the very low frequencies, a 12 minute data record was taken. For ease in data reduction, a 7 1/2 ips tape speed was used. The tape recorder at this speed in the FM mode has an upper frequency limit of 5000 Hz. This means any acoustic perturbations (of BPF or higher harmonics) will be considerably attenuated. Two spectra for every combination of angle, ψ, velocity component and with or without TCS are presented. A Hewlett-Packard Fourier Analyzer was used to measure a constant band width velocity squared spectra. The high frequency plots, Figures 64a through 64d and 65a through 65d, illustrate that most of the turbulent spectra content is below 1.25 kHz and that acoustic perturbations do occur at BPF. The TCS causes a sharp reduction in these BPF perturbations for the transverse component, in particular. This correlates well with the reductions seen in the acoustic far field. The axial spectra, unlike the transverse spectra, show much less BPF reduction with the use of the TCS indicating that these may be due to cut-off modes that are attenuated as they propagate forward away from the rotor inlet plane. A signal that is at a higher frequency than the BPF acoustic contamination is also seen. This particular tone may be due to vibration of the probe support or wake shedding from the cluster of probe supports, as it does not depend on the TCS. However, since this signal is beyond the frequency range of interest, it can be ignored.

The principal effect of the TCS is to reduce the spectral content at the low frequency end for both velocity components, with the reduction in the transverse turbulent velocity being particularly evident on Figures 65a through 65d. To quantify the reduction in turbulent velocity at the low frequencies, it is necessary to examine the second set of spectra which have a 6.25 Hz upper frequency.

The low frequency turbulent spectra, as shown in Figures 66a through 66d and Figures 67a through 67d, are concentrated below 5 Hz and in some cases a peak is seen between 0.2 to 0.8 Hz. The turbulence data at frequencies below 0.2 Hz are very difficult to separate from such effects as slight speed variations of the fan which occur in the twelve minute data record. What is apparent though is the large reduction in the spectra content below 1.25 Hz when the TCS is in place. The square of the streamwise turbulent velocity is reduced by eight to ten times (depending on circumferential position) and in the transverse direction it is reduced by 60 to 100 times (depending on circumferential position) when the TCS is placed on the reverse cone inlet. These reductions are in substantial agreement with those determined from the on-line plots of the "RMS" values of the turbulent velocities. This indicates that the turbulence reduction is also occurring below the low frequency cut-off of the "RMS" meter which is 6 Hz when a one second integration time is used. Since this low frequency end of the spectra is of primary concern, the TCS is seen to be remarkably effective in reducing the inlet turbulence.

To estimate the possible BPF tone reduction due to a drop in turbulent intensities, the well known dependence of the rotor-turbulence interaction noise on the square of the turbulence intensity can be used. If we assume that the total intensity dropped by 10 to 1 when the TCS was employed, then a drop in the BPF sound power level of 20 dB would be expected. This number is not at all

unreasonable and suggests that a substantial portion of the noise reduction is due to the reduction of the turbulence intensity with the transverse scale reduction contribution being somewhat less.

4.0 CONCLUSIONS

This program has been very successful in demonstrating the type of inlet turbulence control techniques that are necessary to obtain "flight" quality data from a static fan anechoic test facility. A flared reverse cone inlet that eliminates wakes from probe supports and actuators is used along with a turbulence control structure to condition the inlet flow. With this inlet configuration for a subsonic, cut-off fan, blade passing frequency tone reductions as high as 12 dB were obtained. By applying boundary layer suction ahead of the rotor, further tone reductions of 4 to 5 dB, for the subsonic rotor tip speeds, are realized. These reductions in PWL at BPF (in one-third octave bands) then range from 12 to 18 dB for this subsonic tip speed range. Equally important is the observed steep rise in the BPF acoustic power as the rotor tip speed becomes supersonic and the first spinning modes cut-on. The fan noise BPF noise levels become nearly independent of the TCS and boundary layer suction indicating that the TCS is not an attenuator of the fan noise but is effecting the subsonic noise generation and the inlet clean up scheme doesn't alter the supersonic rotor-alone noise.

Turbulence mapping of the inlet confirmed the conclusions from the far field acoustic data. In the freestream at an immersion of a quarter of the fan radius, the employment of the TCS reduced the squares of the low frequency streamwise and transverse turbulent velocities by up to ten times and 100 times, respectively. The streamwise and transverse turbulent length scales were also correspondingly reduced.

This research program has convincingly demonstrated that it is possible to clean up the inlet flow of a static fan noise test facility to a point where the static acoustic data simulates flight data.

REFERENCES

1. T. G. Sofrin and J. C. McCann, 1966, Paper presented at the 72nd Meeting of the Acoustical Society of America, "Pratt and Whitney Experience in Compressor Noise Reduction."

2. N. Les Filleul, 1966, J. Sound and Vibration, 3, 147, "An Investigation of Axial Flow Fan Noise."

3. D. B. Hanson, 1974, J. Acoust. Soc. Am., Vol. 56, No. 1, 110, "Spectrum of Rotor Noise Caused by Atmospheric Turbulence."

4. R. Mani, 1971, J. Sound and Vibration, 17, No. 2, 250, "Noise due to Interaction of Inlet Turbulence with Isolated Stators and Rotors."

5. G. F. Pickett, 1974, Paper presented at the 87th Meeting of The Acoustical Society of America, "Effects of Nonuniform Inflow on Fan Noise."

6. R. Mani, "Isolated Rotor Noise Due to Inlet Distortion or Turbulence," NASA Report No. NASA CR-2479, October 1974.

7. J. E. Ffowcs Williams and D. L. Hawkings, 1969, J. of Sound and Vibration, Vol. 10, 10, "Theory Relating to the Noise of Rotating Machinery."

8. R. J. Wells, personal communication.

9. N. A. Cumpsty and B. W. Lowrie, 1973, ASME Paper 73-WA/GT-4, "The Cause of Tone Generation by Aero Engine Fans at High Subsonic Tips and the Effect of Forward Speed."

10. C. J. Moore, 1975, J. of Sound and Vibration, Vol. 43, No. 4, "Reduction of Fan Noise by Annulus Boundary Layer Removal."

11. S. B. Kazin, W. R. Minzner, and J. E. Paas, "Acoustic Testing of a 1.5 Pressure-Ratio Low Tip Speed Fan with Casing Tip Bleed," NASA Report No. NASA CR-120827.

12. B. W. Lowrie, 1975, AIAA Paper No. 75-463, "Simulation of Flight Effects on Aero Engine Fan Noise."

13. B. W. Lowrie and D. R. Newby, 1977 AIAA Paper No. 77-1323, "The Design and Calibration of a Distortion-Reducing Screen for Fan Noise Testing."

14. B. J. Cocking and R. B. Ginder, 1977 AIAA Paper No. 77-1324, "The Effect of an Inlet Flow Conditioner on Fan Distortion Tones."

15. L. M. Shaw, R. P. Woodward, F. W. Glaser, and B. J. Pastoli, 1977 AIAA Paper No. 77-1345, "Inlet Turbulence and Fan Noise Measured in an Anechoic Wind Tunnel and Statically with an Inlet Flow Control Device."

16. R. P. Woodward, J. A. Wazyniak, L. M. Shaw, and M. J. MacKinnon, 1977 NASA TM-73855, "Effectiveness of an Inlet Flow Turbulence Control Device to Simulate Flight Fan Noise in an Anechoic Chamber."

17. K. L. Bekofske, R. E. Sheer, Jr. and J. C. F. Wang, NASA Report No. CR-135177, "Basic Noise Research Program -- Fan Noise -- Effect of Inlet Disturbances on Fan Inlet Noise During a Static Test.

18. T. Morel, J. of Fluids Engineering, September 1976, Discussion of a Paper by Loehrke and Nagib, "Control of Free-Stream Turbulence by Means of Honeycombs: A Balance Between Suppression and Generation."

19. G. L. Blankenship, 1977 AIAA Paper No. 77-1346, "Effect of Forward Motion on Turbomachinery Noise."

20. C. E. Feiler and J. E. Merriman, NASA Report No. NASA TMX-71591, "Effects of Forward Velocity and Acoustic Treatment on Inlet Fan Noise."

21. C. E. Feiler and J. F. Groeneweg, NASA Report No. NASA TM-73722, "Summary of Forward Velocity Effects on Fan Noise."

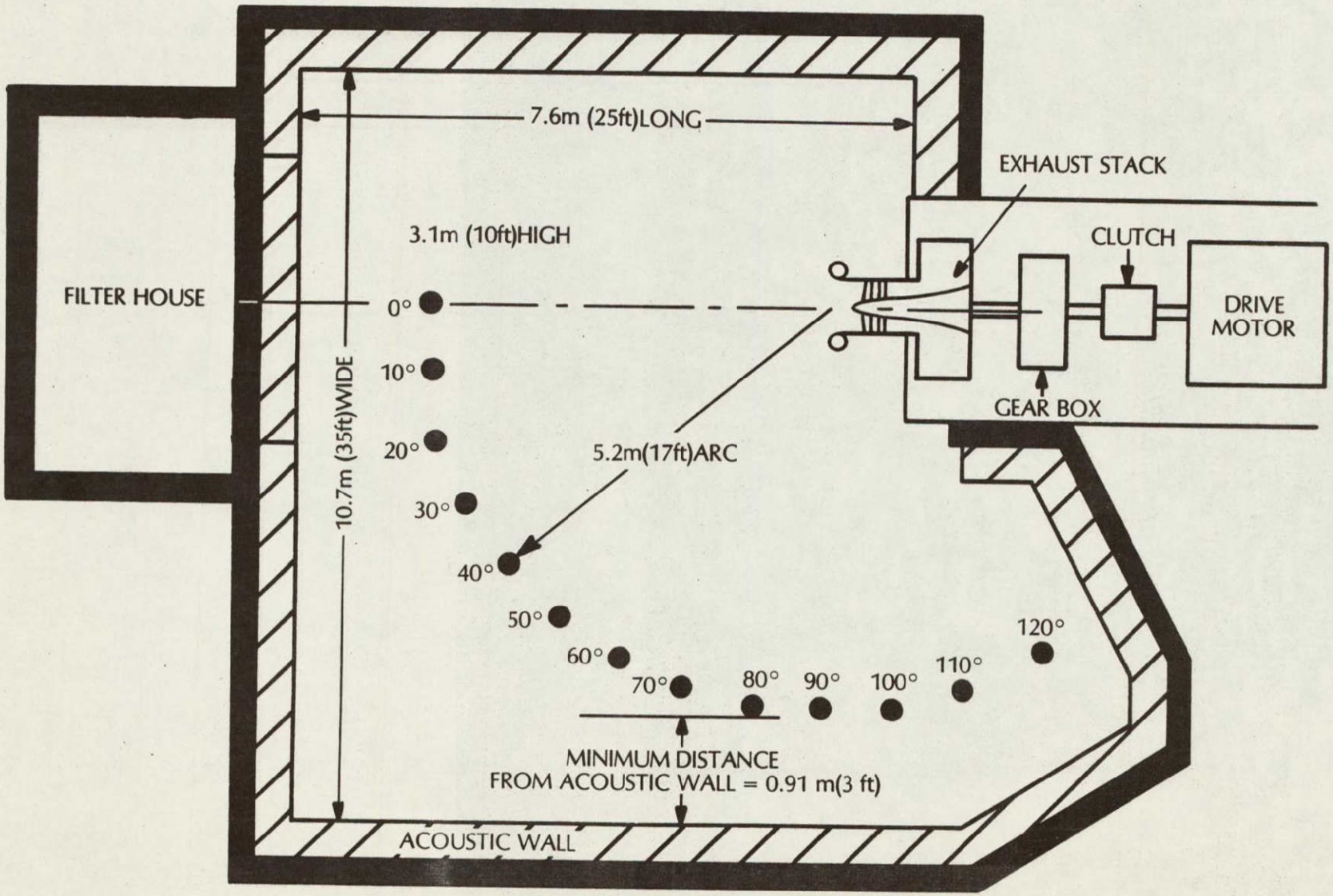

Figure 1: Schematic of Aeroacoustic Laboratory

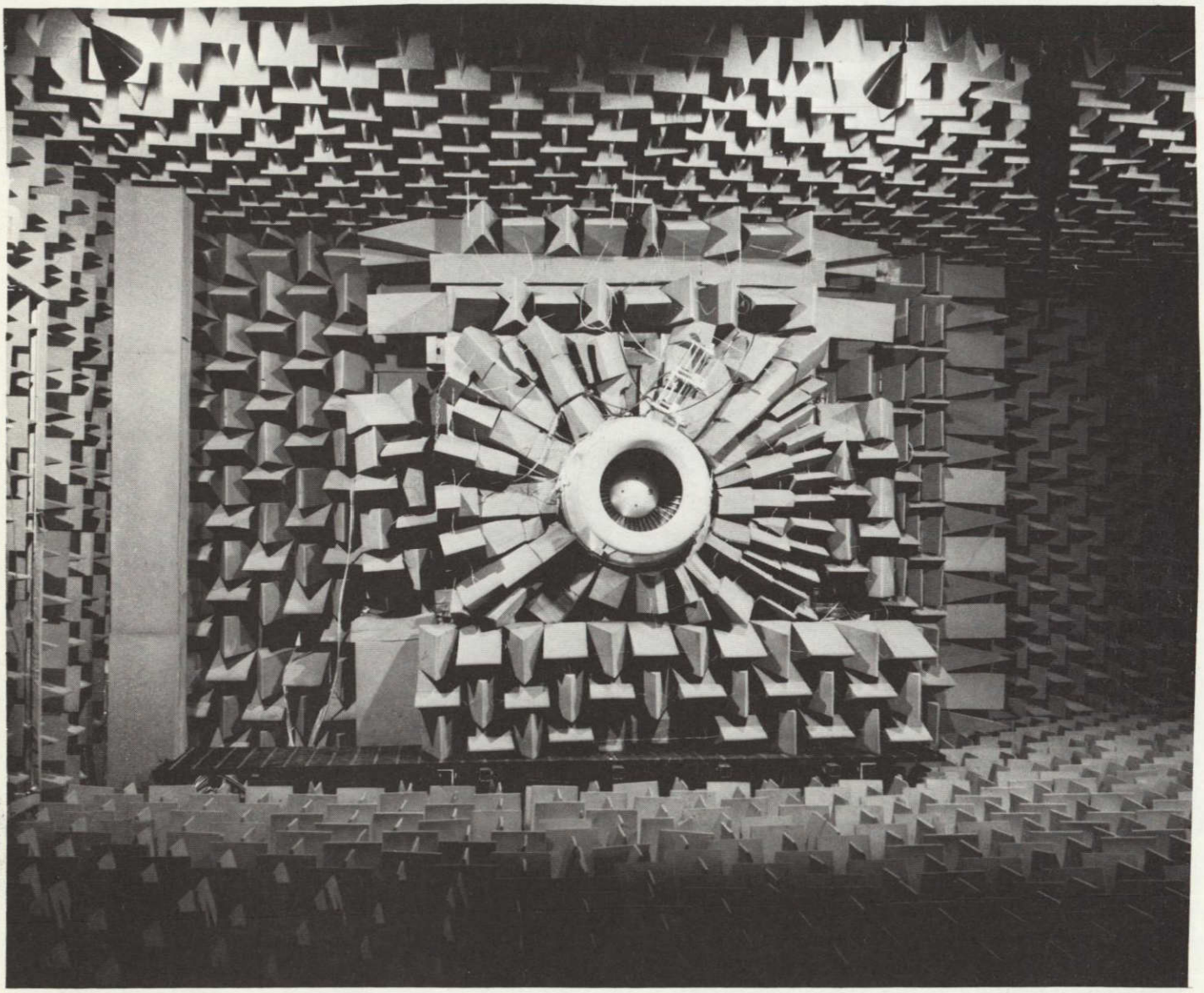

Figure 2 Aero-Acoustic Chamber - Before Inlet Cleanup

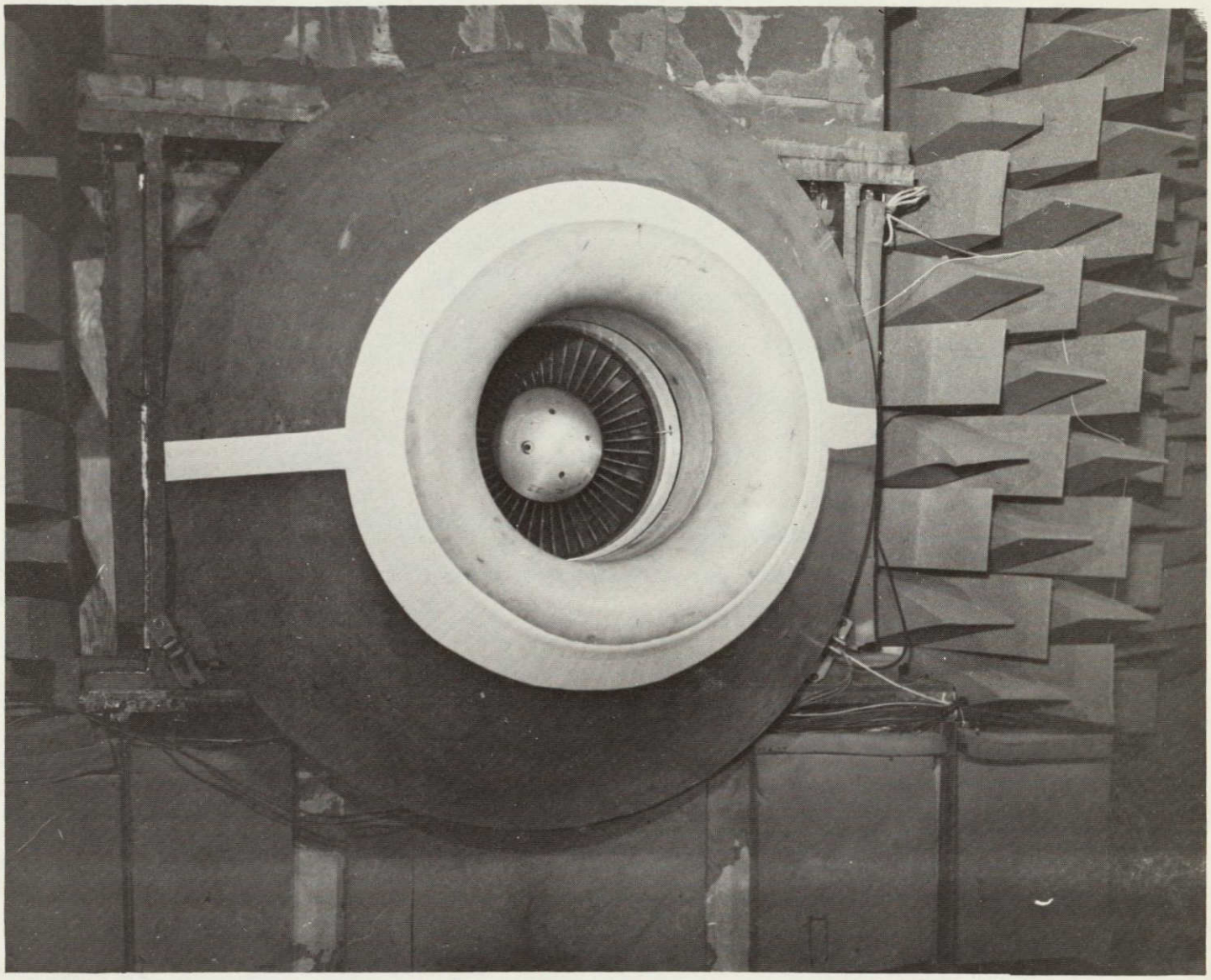

Figure 3 Metal Cone Installed on Standard Bellmouth

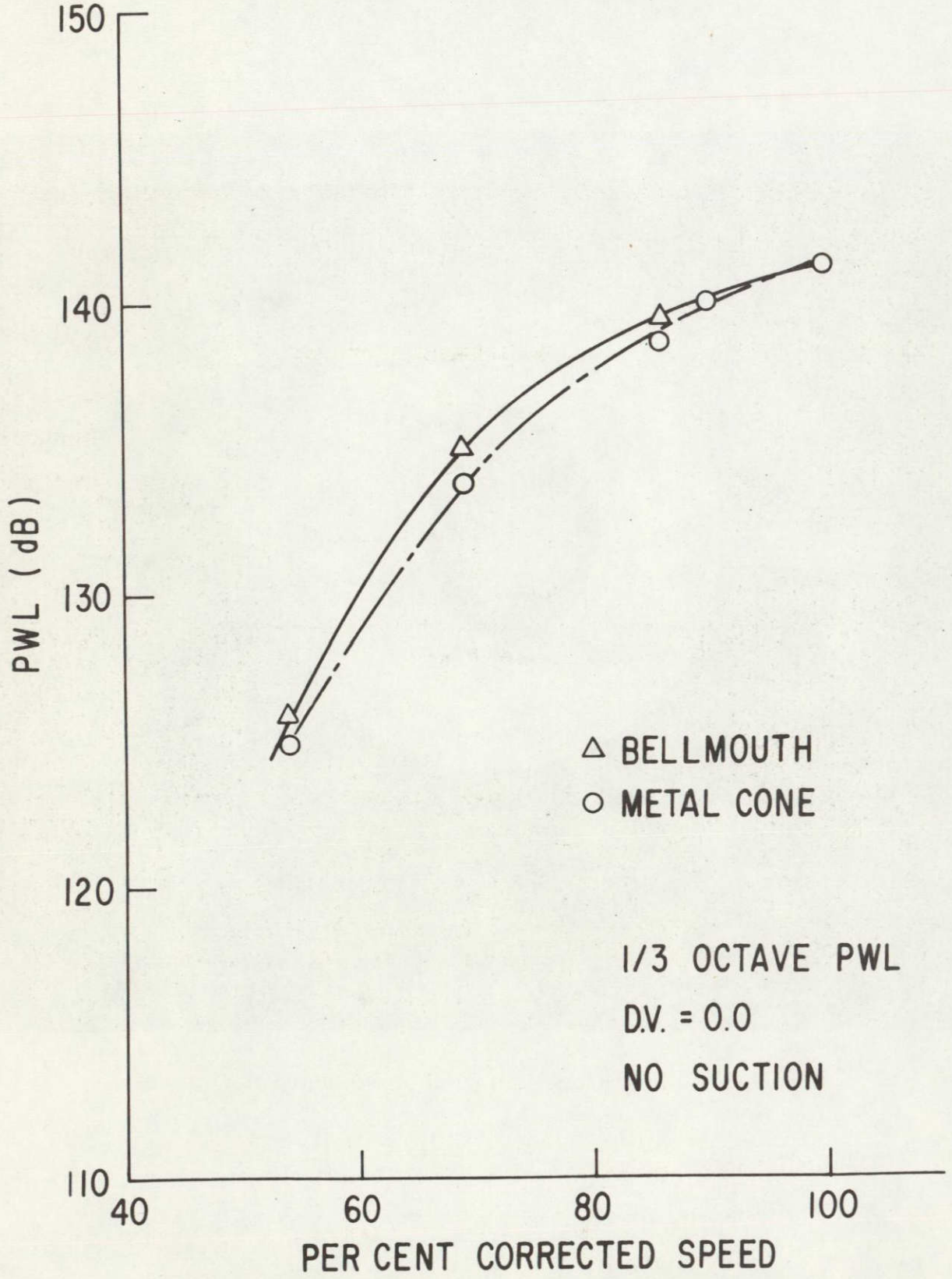

FIG. 4 EFFECT OF METAL CONE ON ACOUSTIC POWER AT BPF, NO TCS

Figure 5 One-Twelfth Scale Model Simulation of Aero-Acoustic Chamber with Reverse Cone Suction Inlet

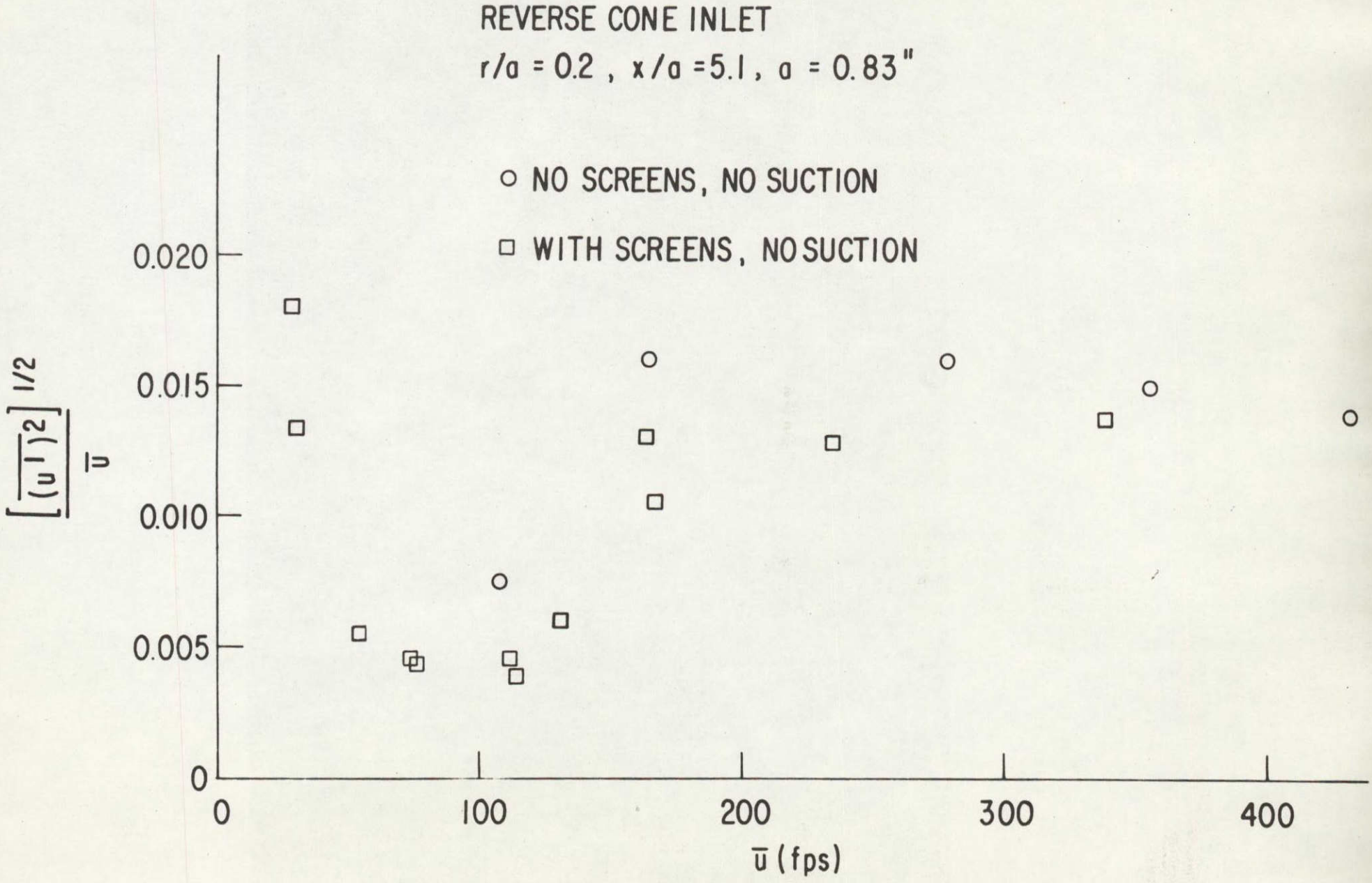

FIG. 6 EFFECT OF SCREENS ON MID-CHANNEL TURBULENCE, SIDE VENTED

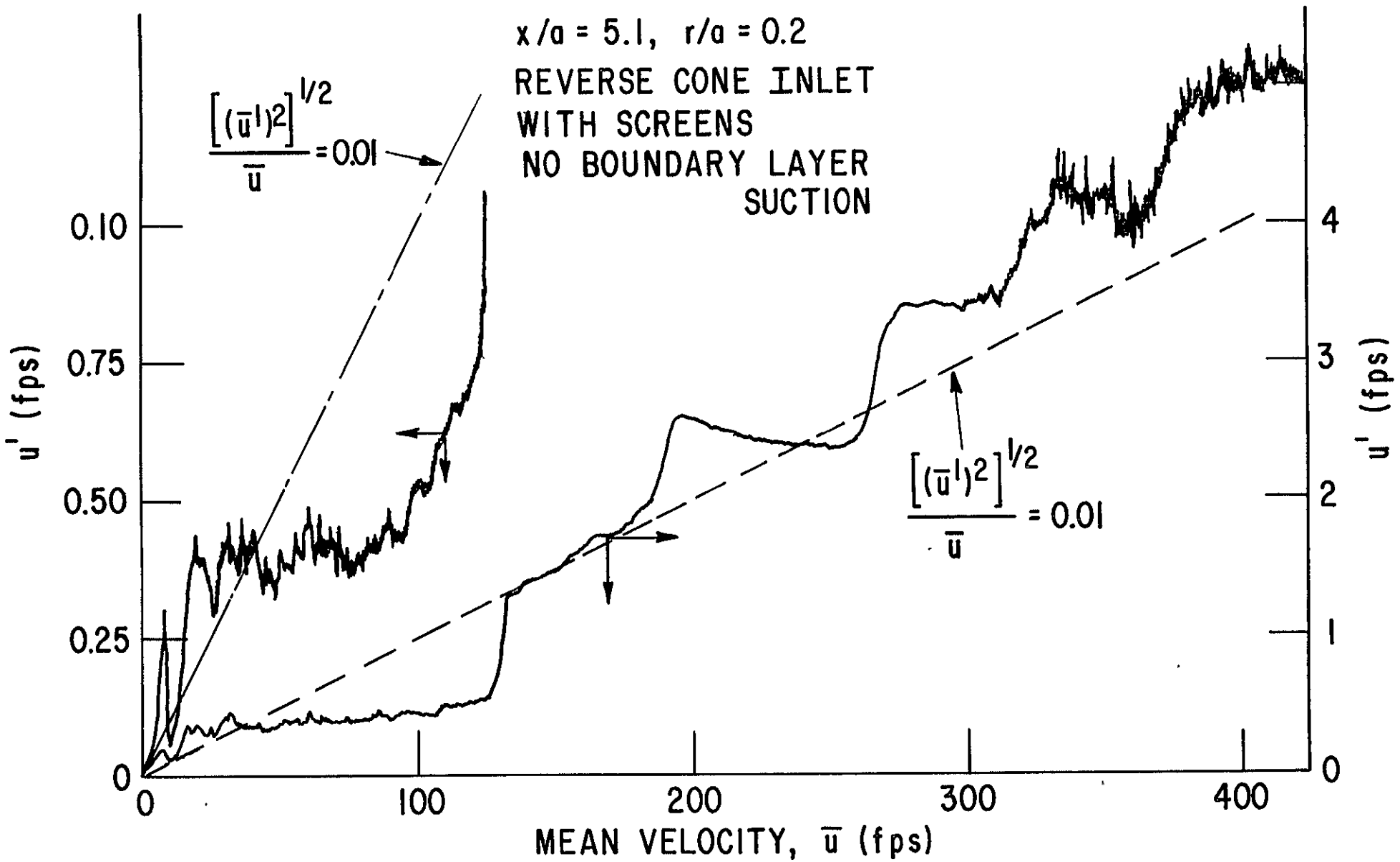

FIG. 7 TURBULENT VELOCITY vs MEAN VELOCITY, SIDE VENTED

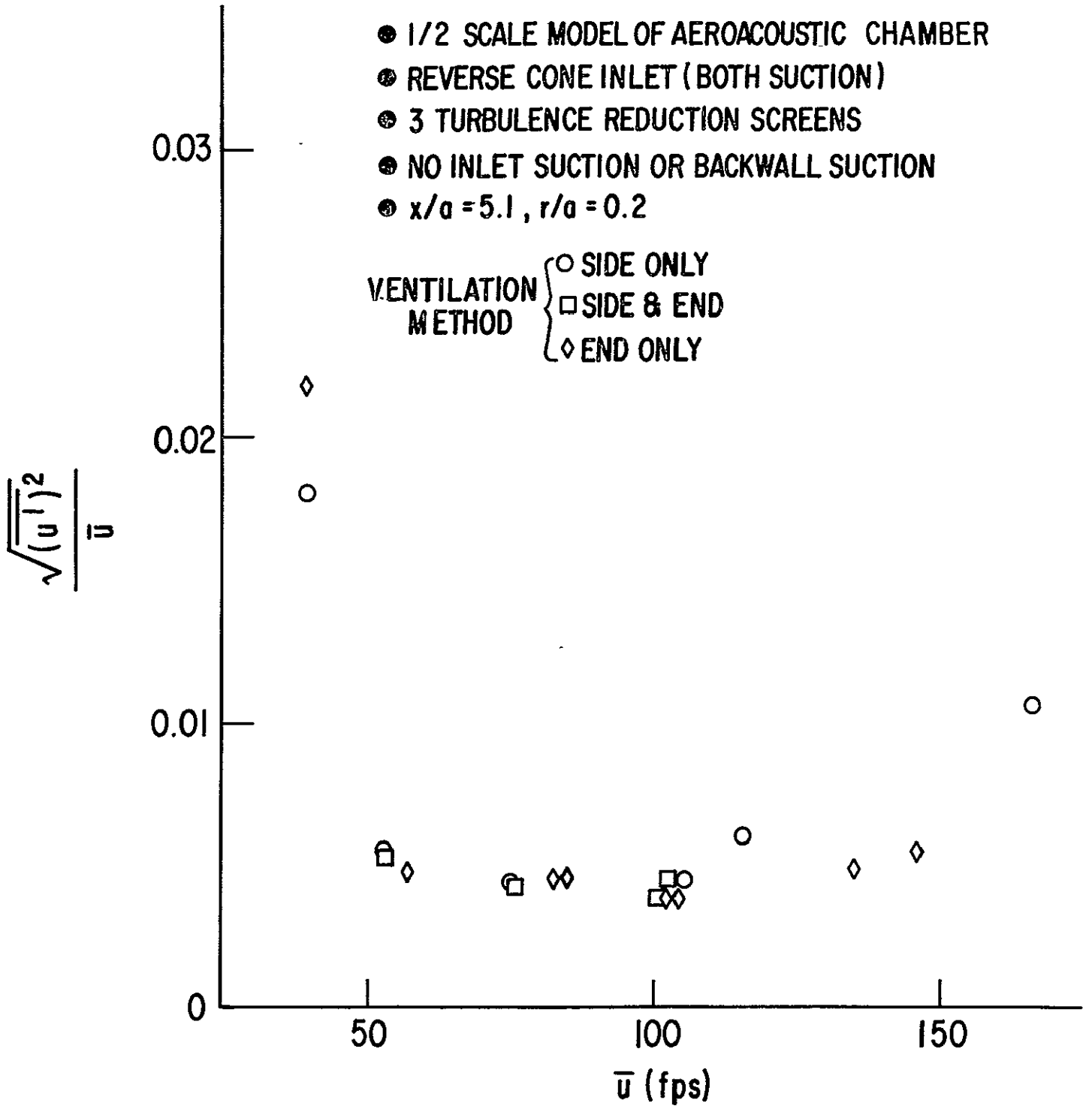

FIG. 8 EFFECT OF CHAMBER VENTILATION ON MID-STREAM AXIAL TURBULENCE

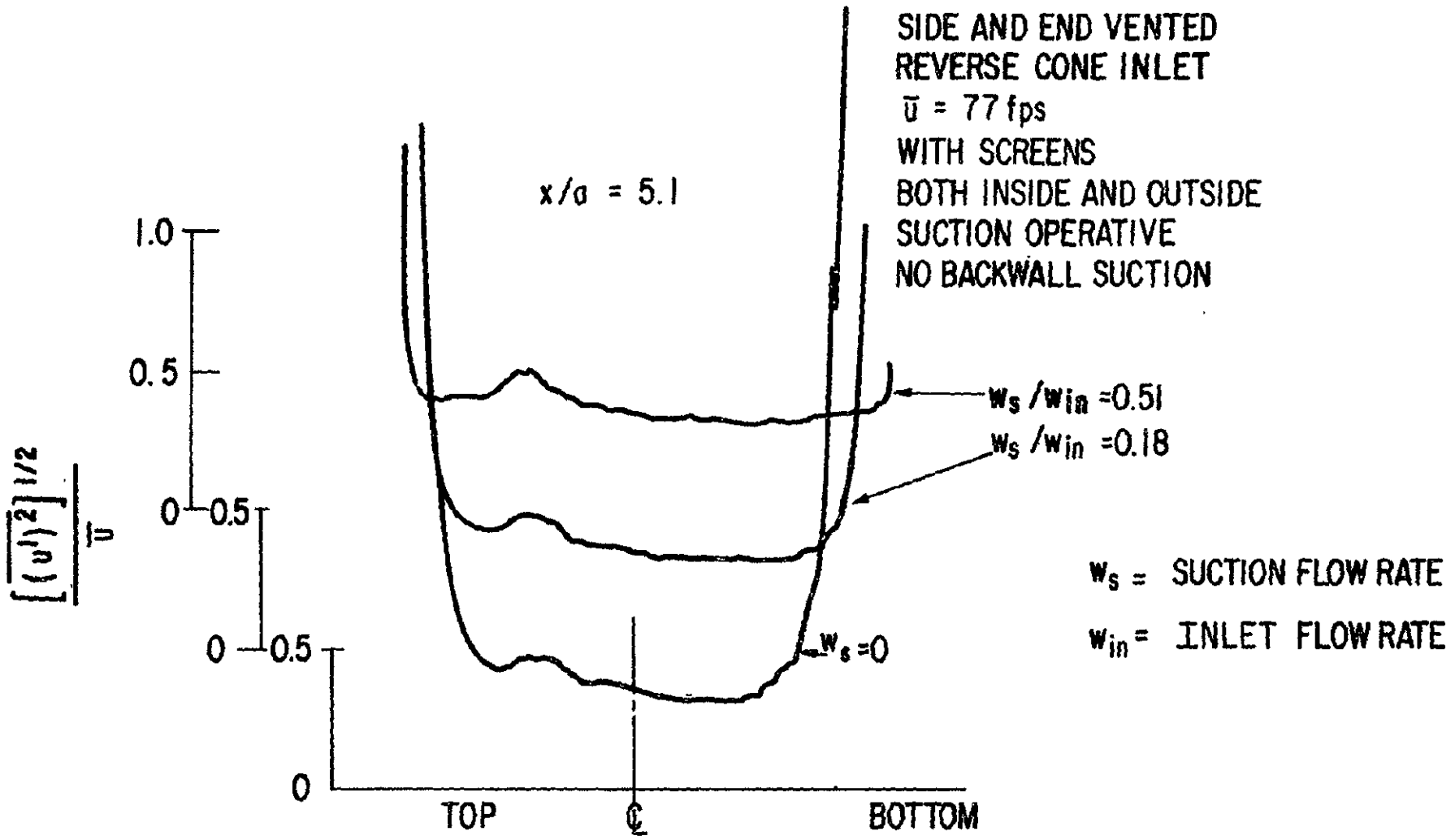

FIG. 9 TURBULENT VELOCITY TRAVERSE AT DIFFERENT SUCTION FLOWS

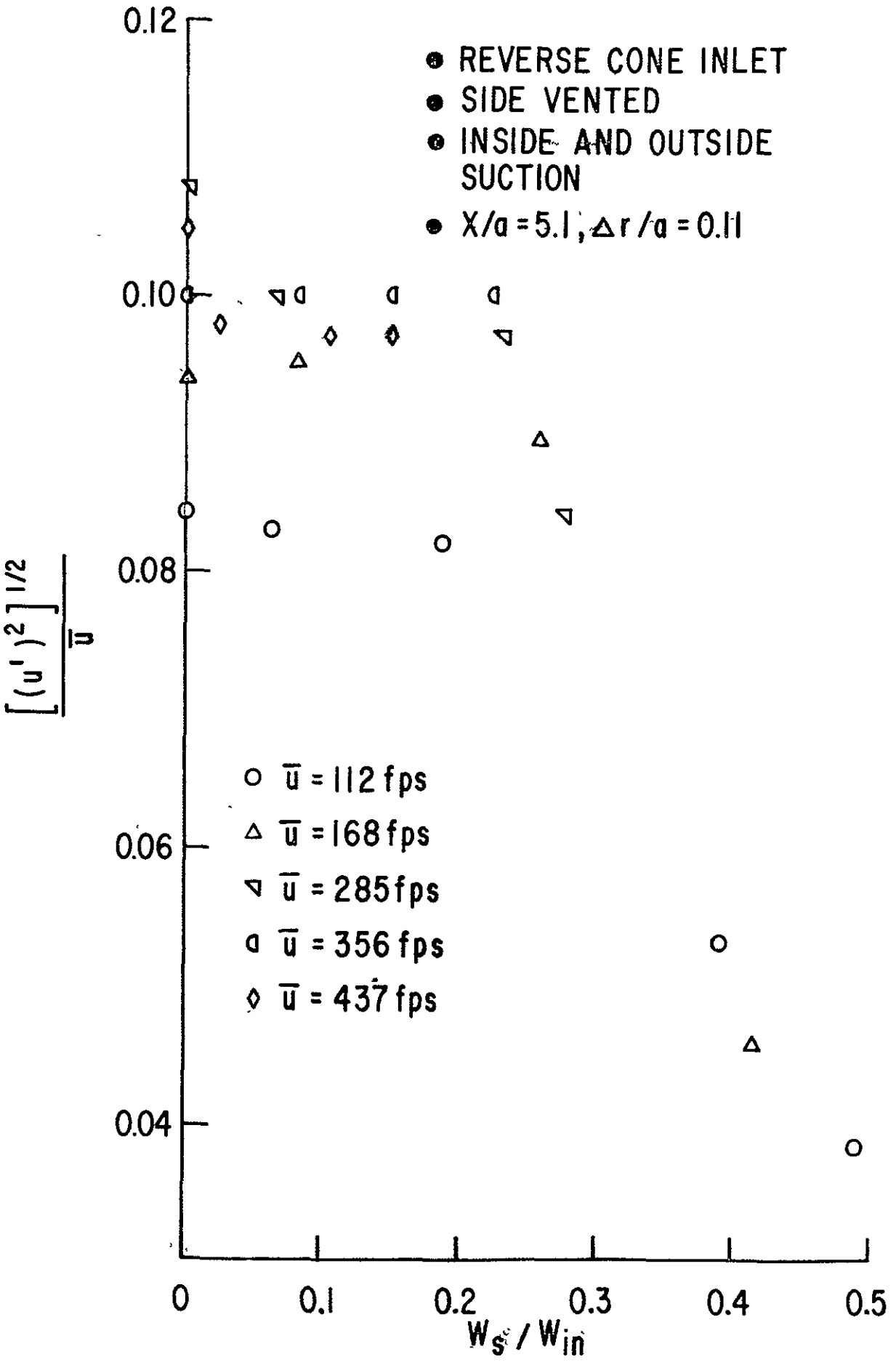

FIG. 10 BOUNDARY LAYER TURBULENCE REDUCTION WITH SUCTION FLOW, WITHOUT SCREEN

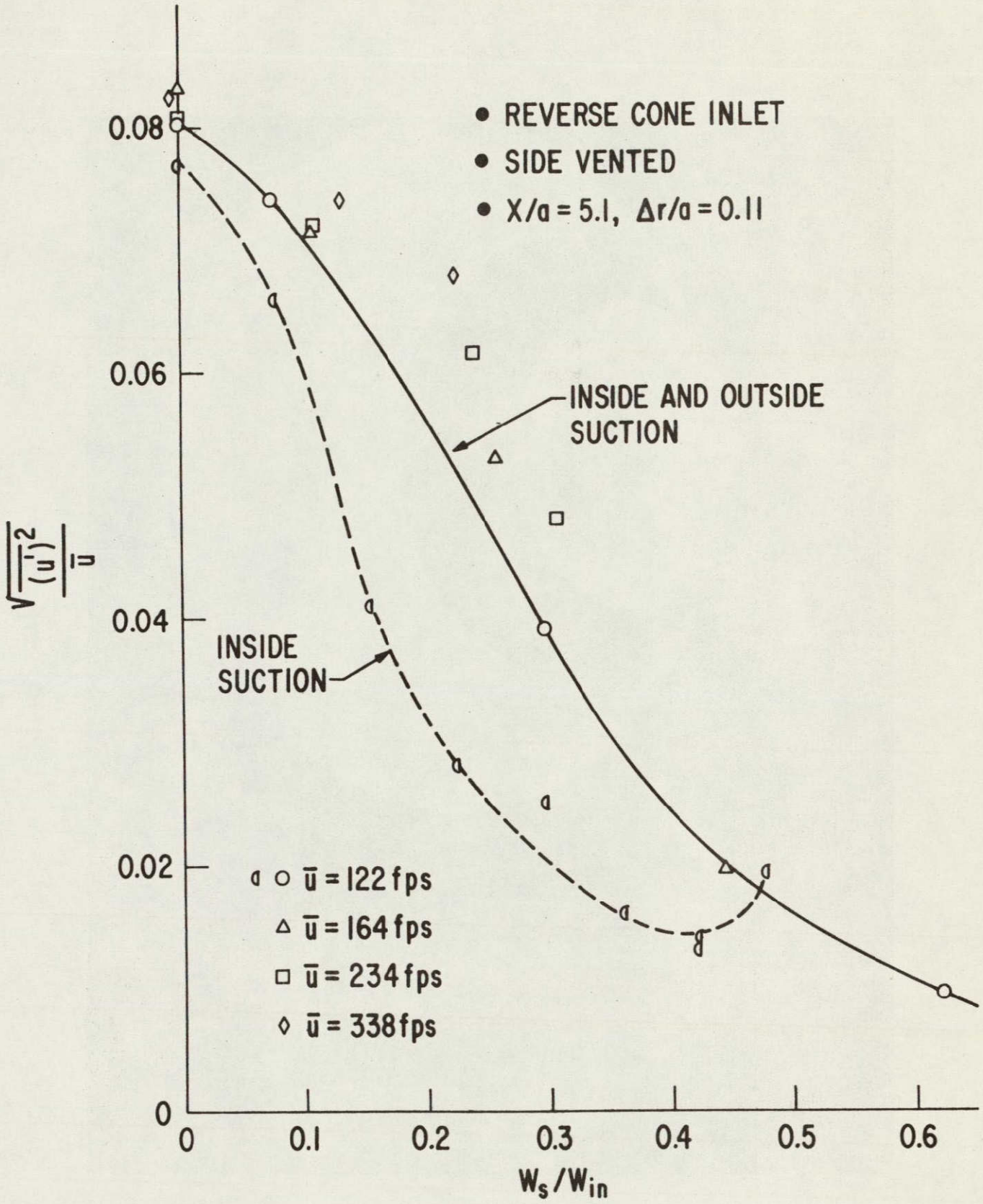

FIG. 11 BOUNDARY LAYER TURBULENCE REDUCTION WITH SUCTION FLOW, WITH SCREENS

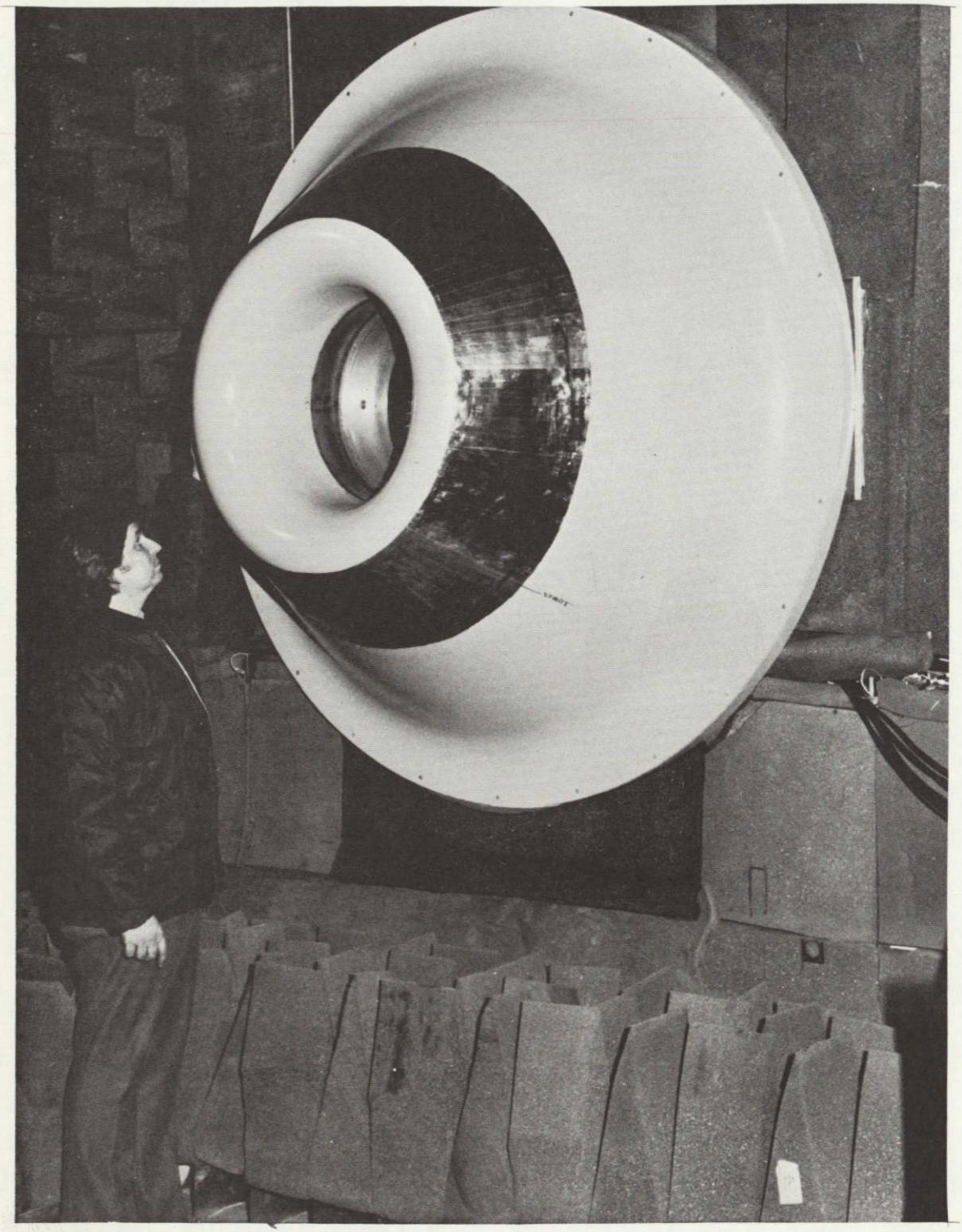

Figure 12 Reverse Cone Inlet Installed

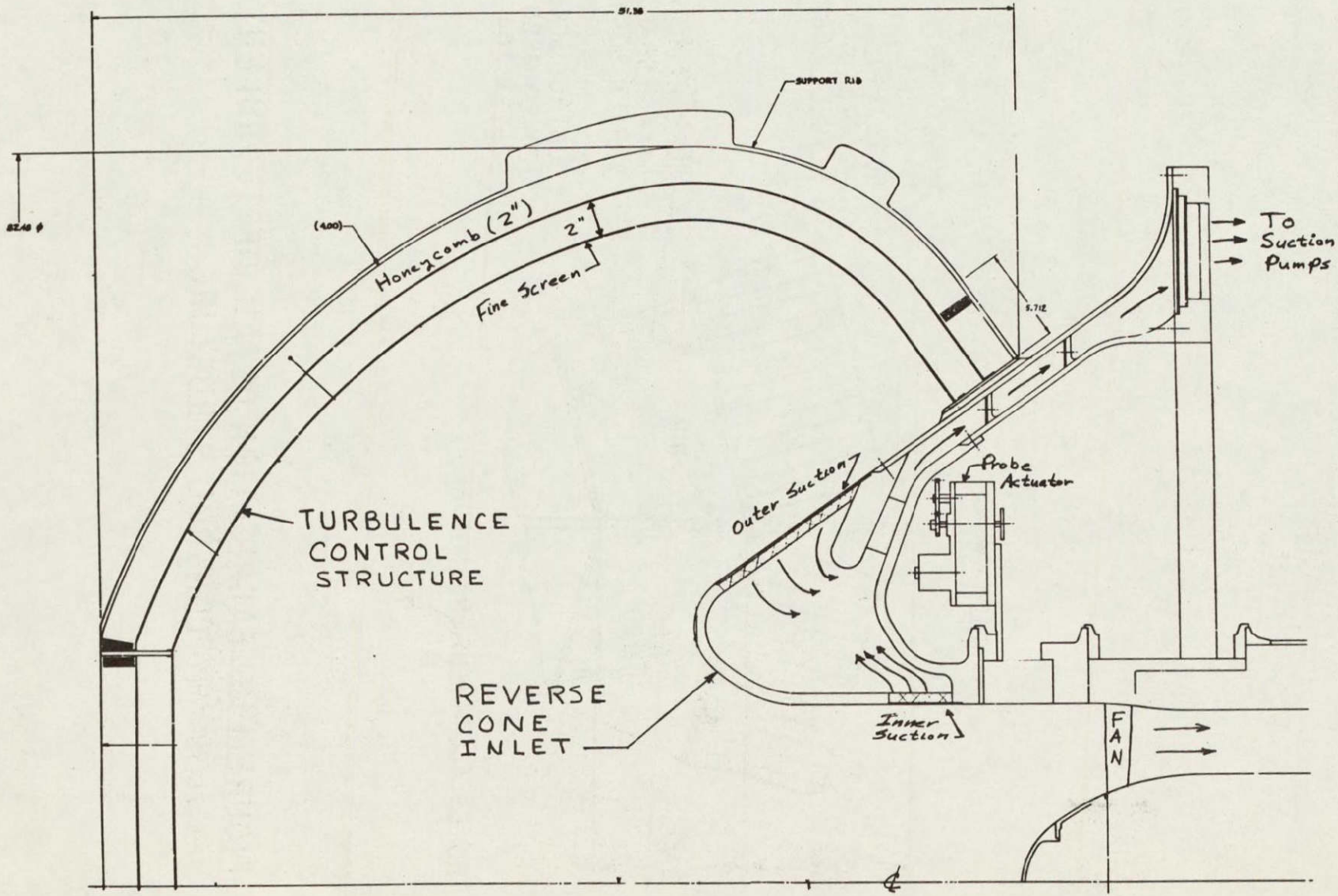

Figure 13a Assembly Sketch of Reverse Cone Inlet and the Turbulence Control Structure

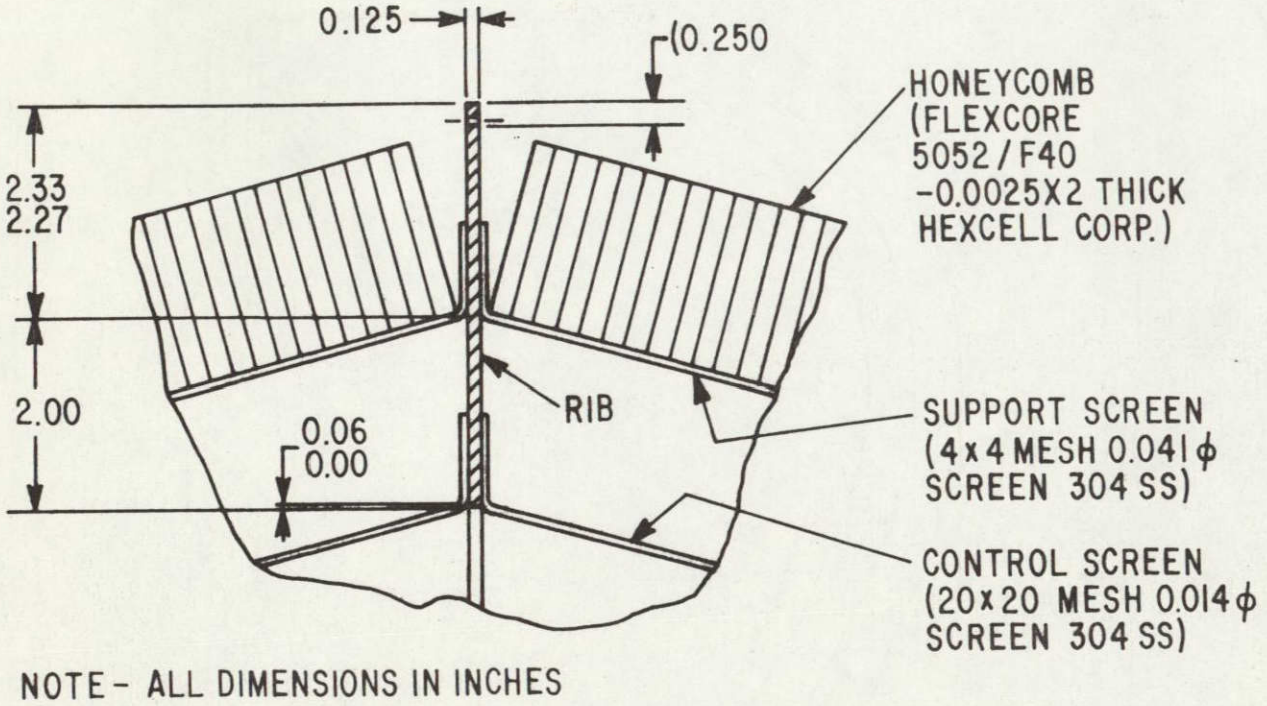

FIGURE 13b. FABRICATION DETAIL OF TURBULENT CONTROL STRUCTURE

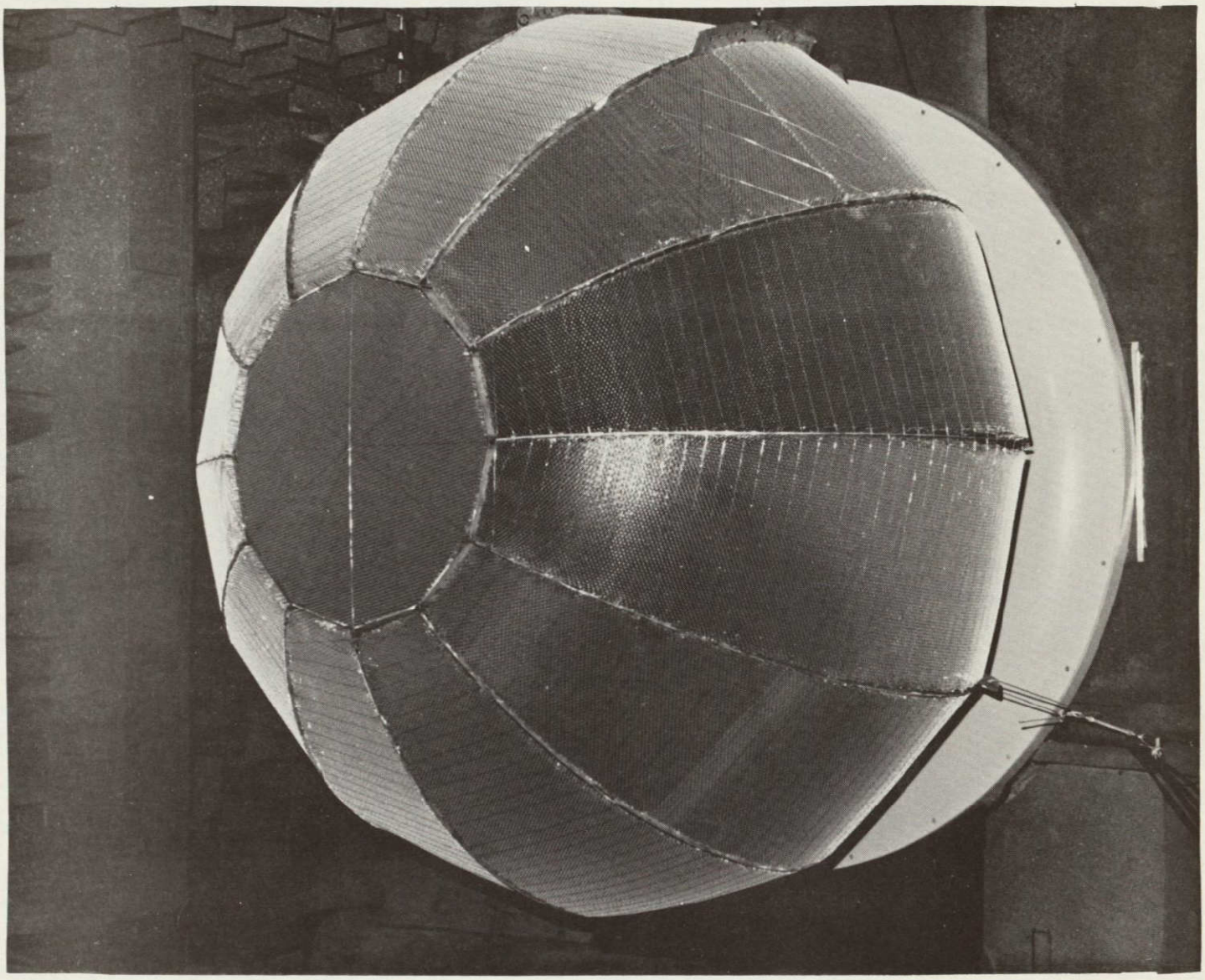

Figure 14 Reverse Cone Inlet with Turbulence Control Structure Installed

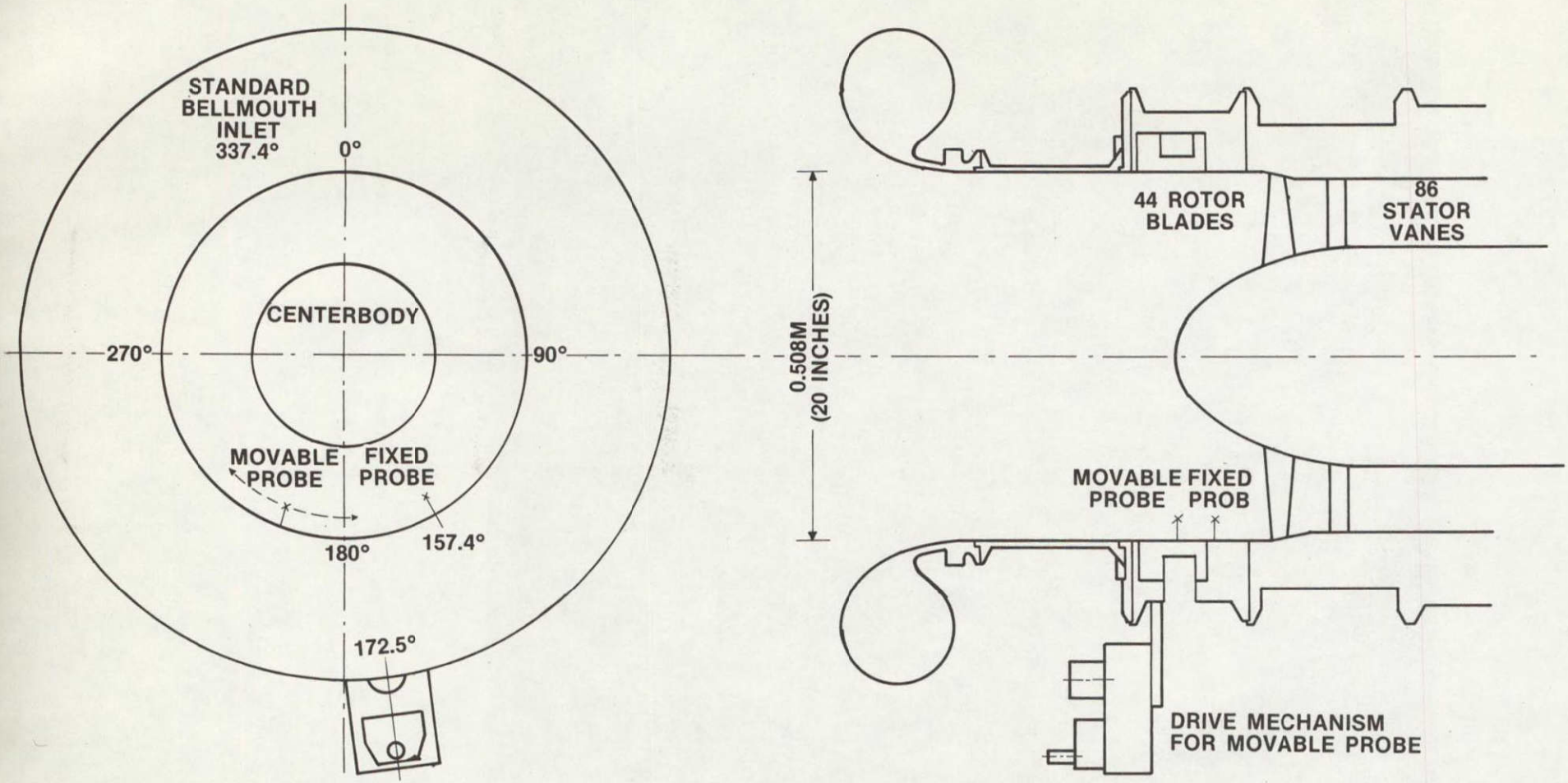

FIGURE 15 HOT-FILM TRAVERSING MECHANISM

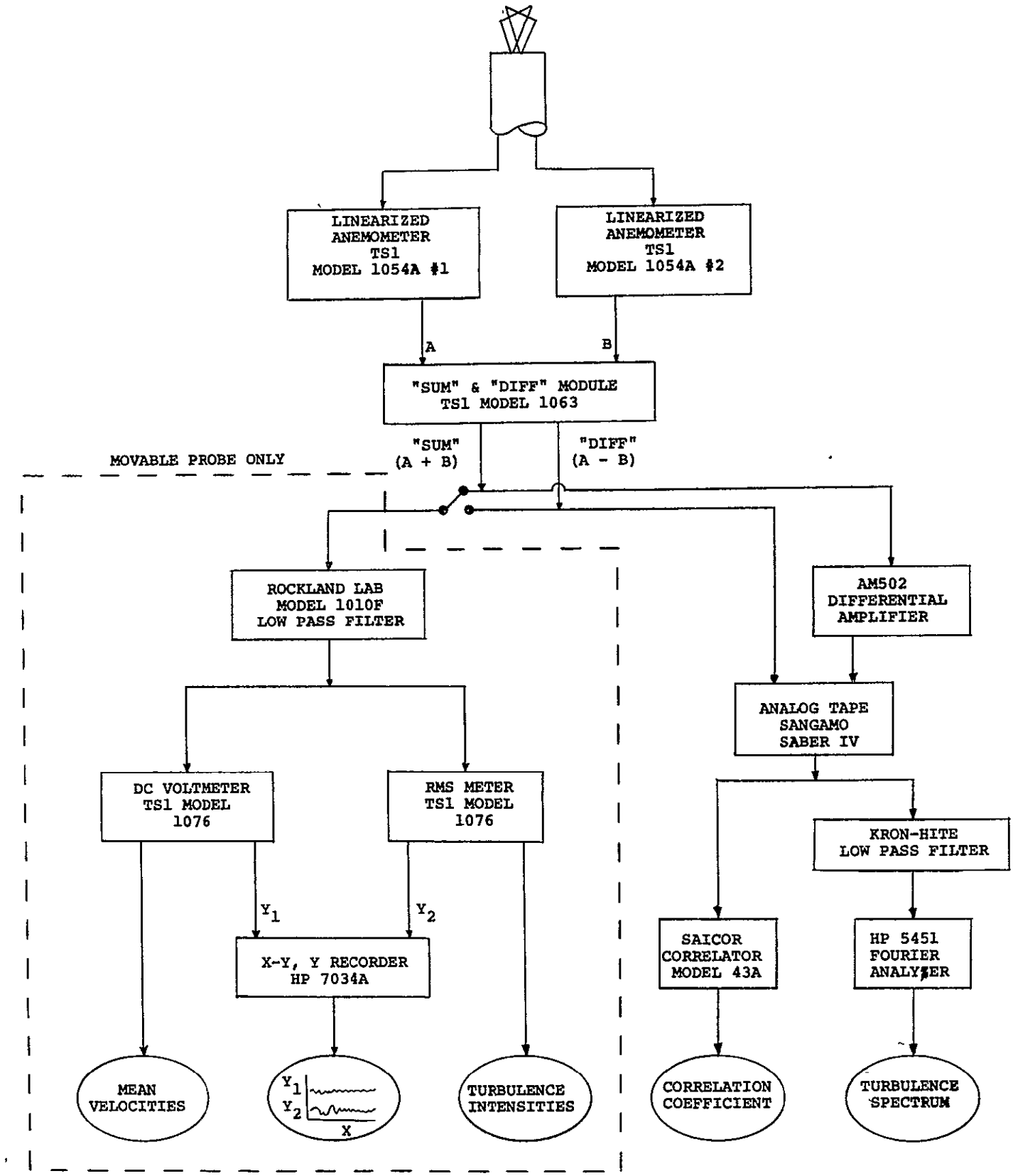

Figure 16: Hot Film Equipment Schematic

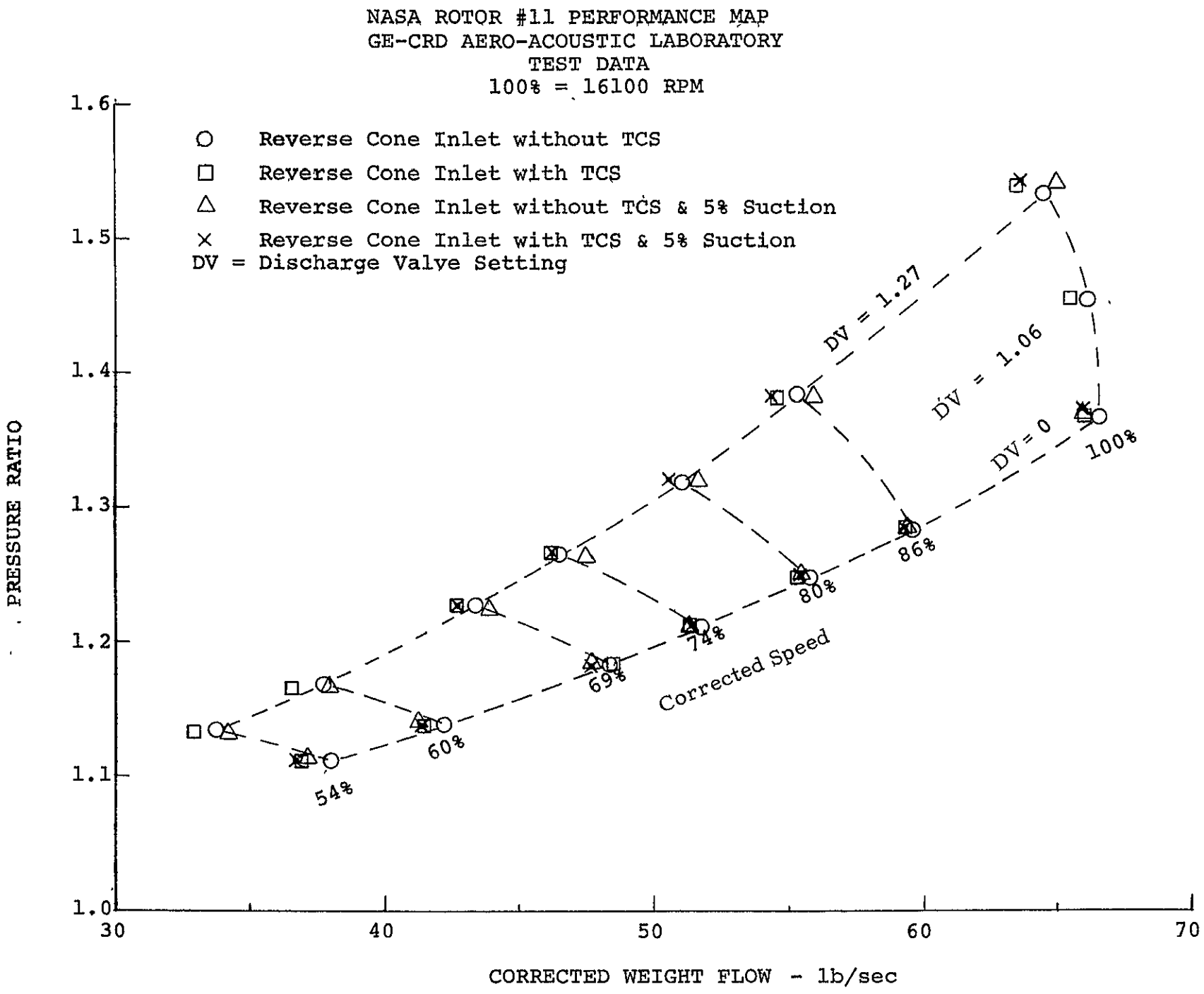

FIGURE 17 TEST VEHICLE FAN PERFORMANCE MAP

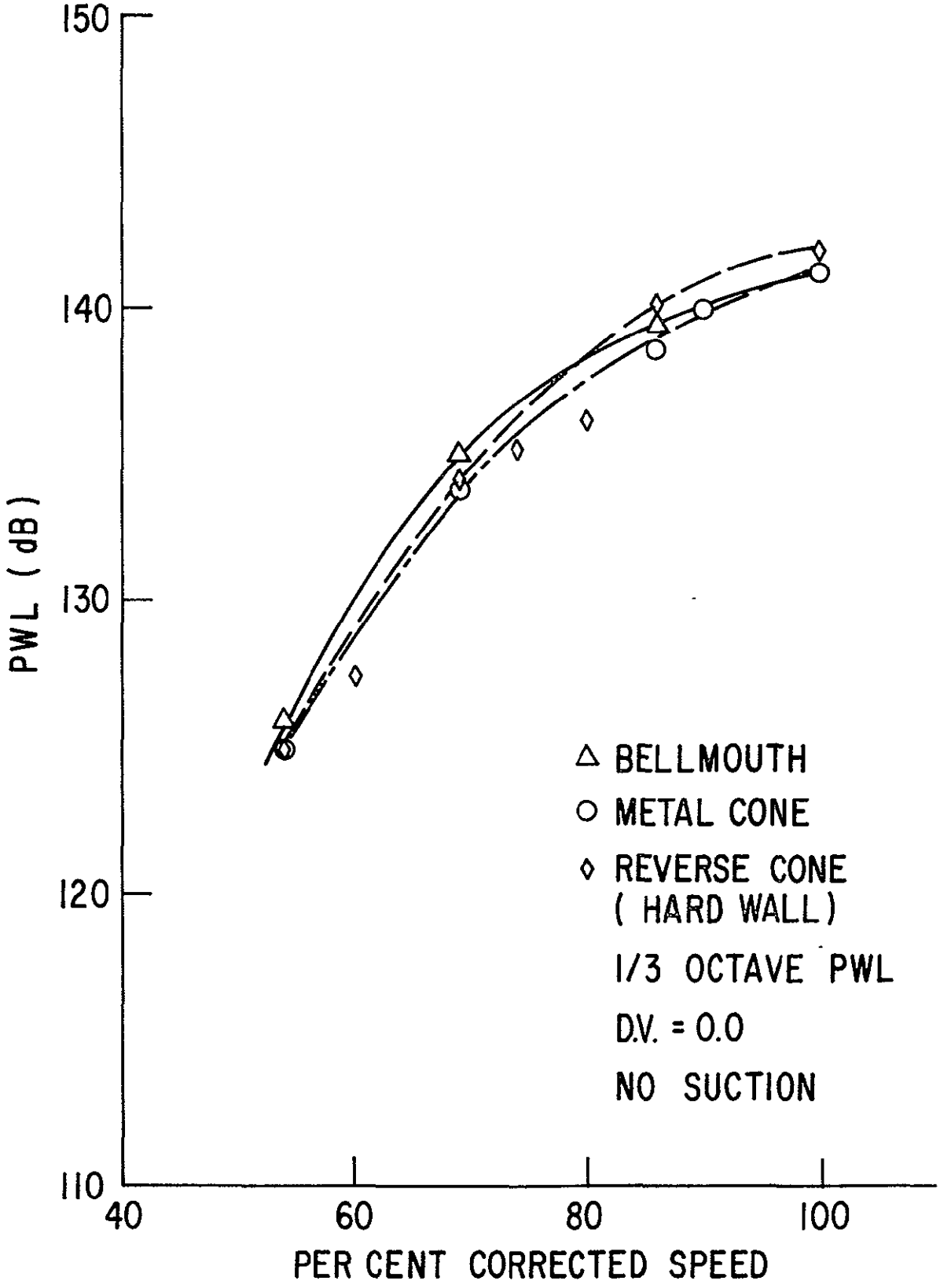

FIG. 18 EFFECT OF INLET SHAPE ON ACOUSTIC POWER AT BPF, NO TCS

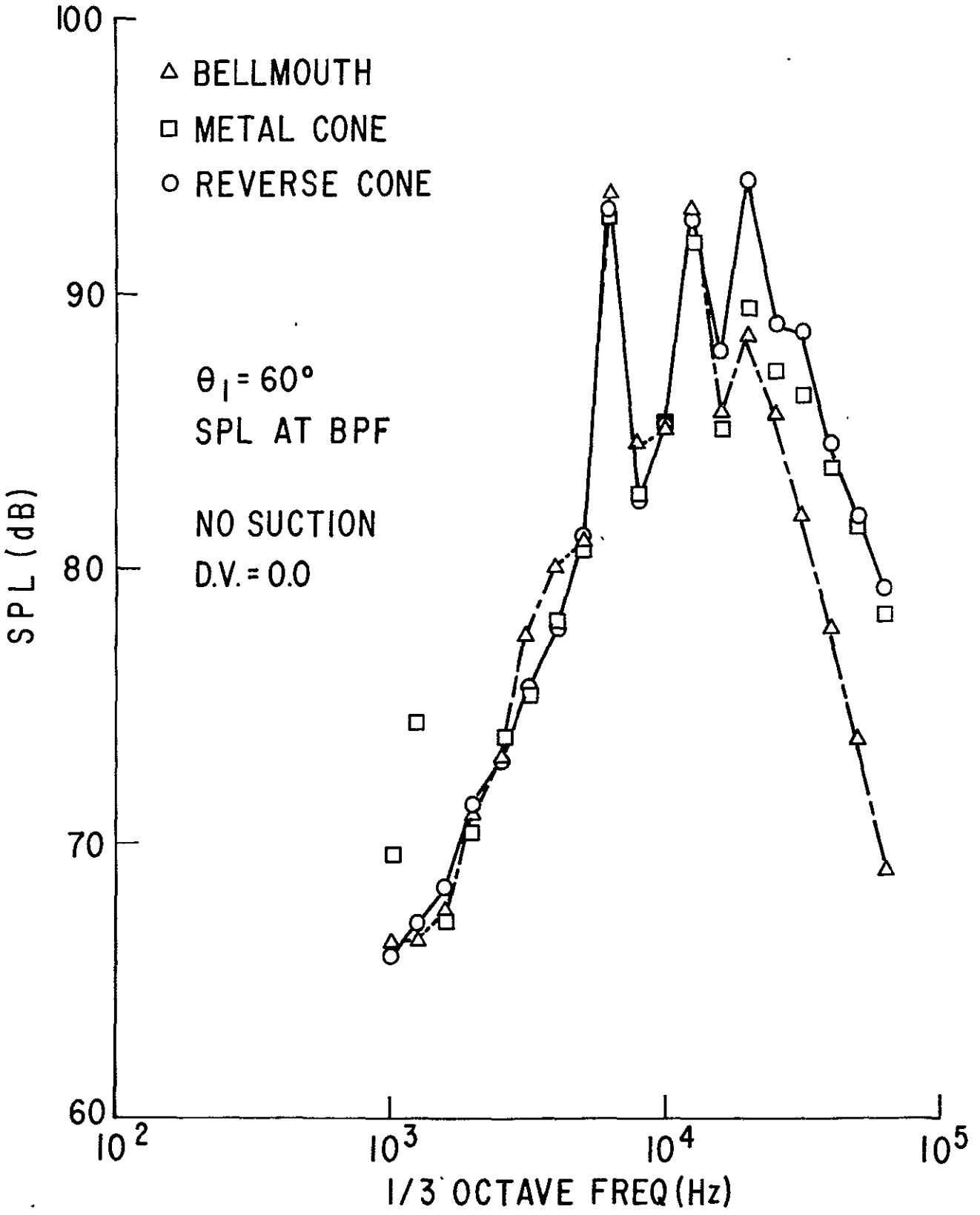

FIG. 19 SPL SPECTRUM, EFFECT OF INLET SHAPE, 54% SPEED, NO TCS

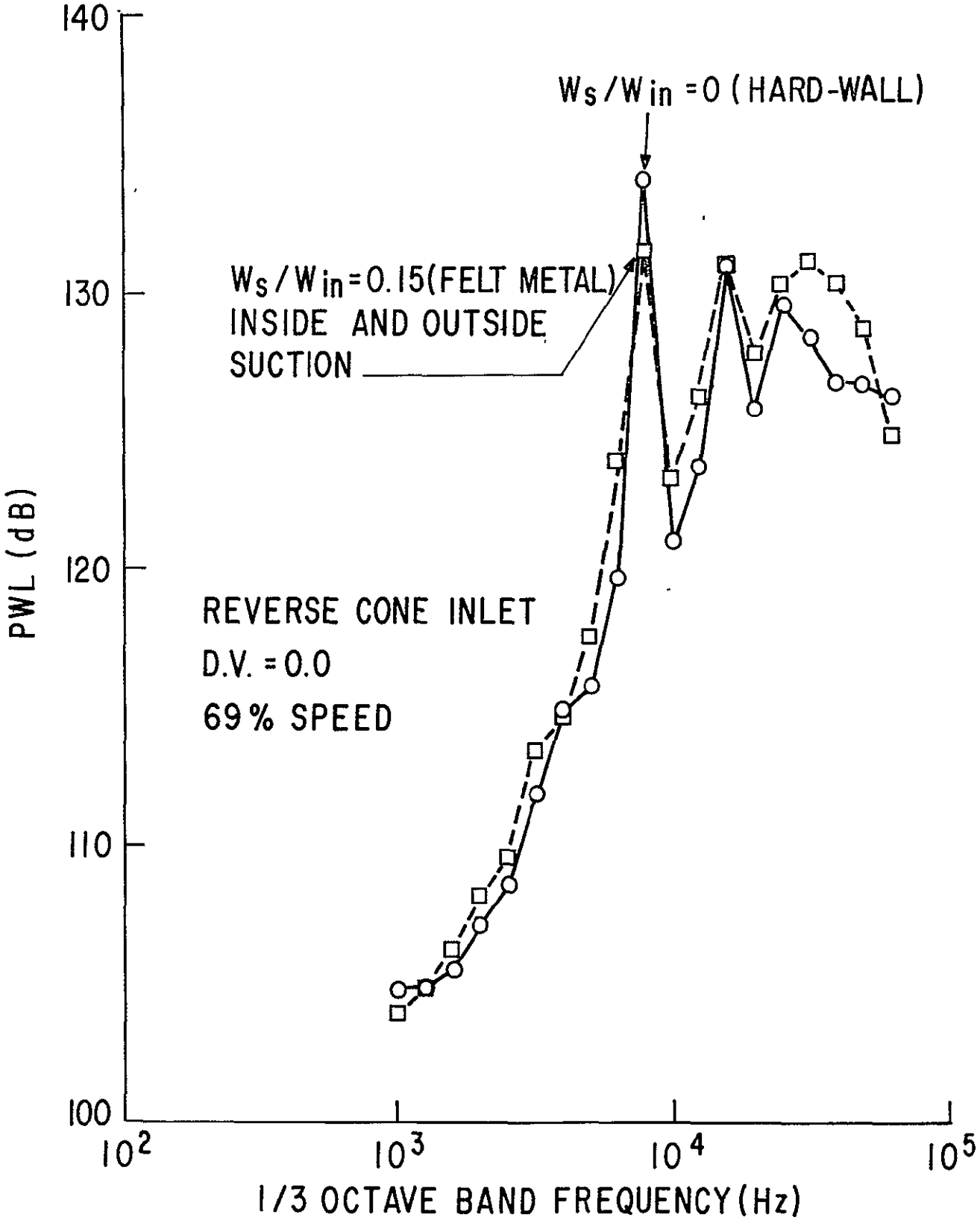

FIG. 20 EFFECT OF INNER AND OUTER SUCTION ON PWL SPECTRUM, NO TCS

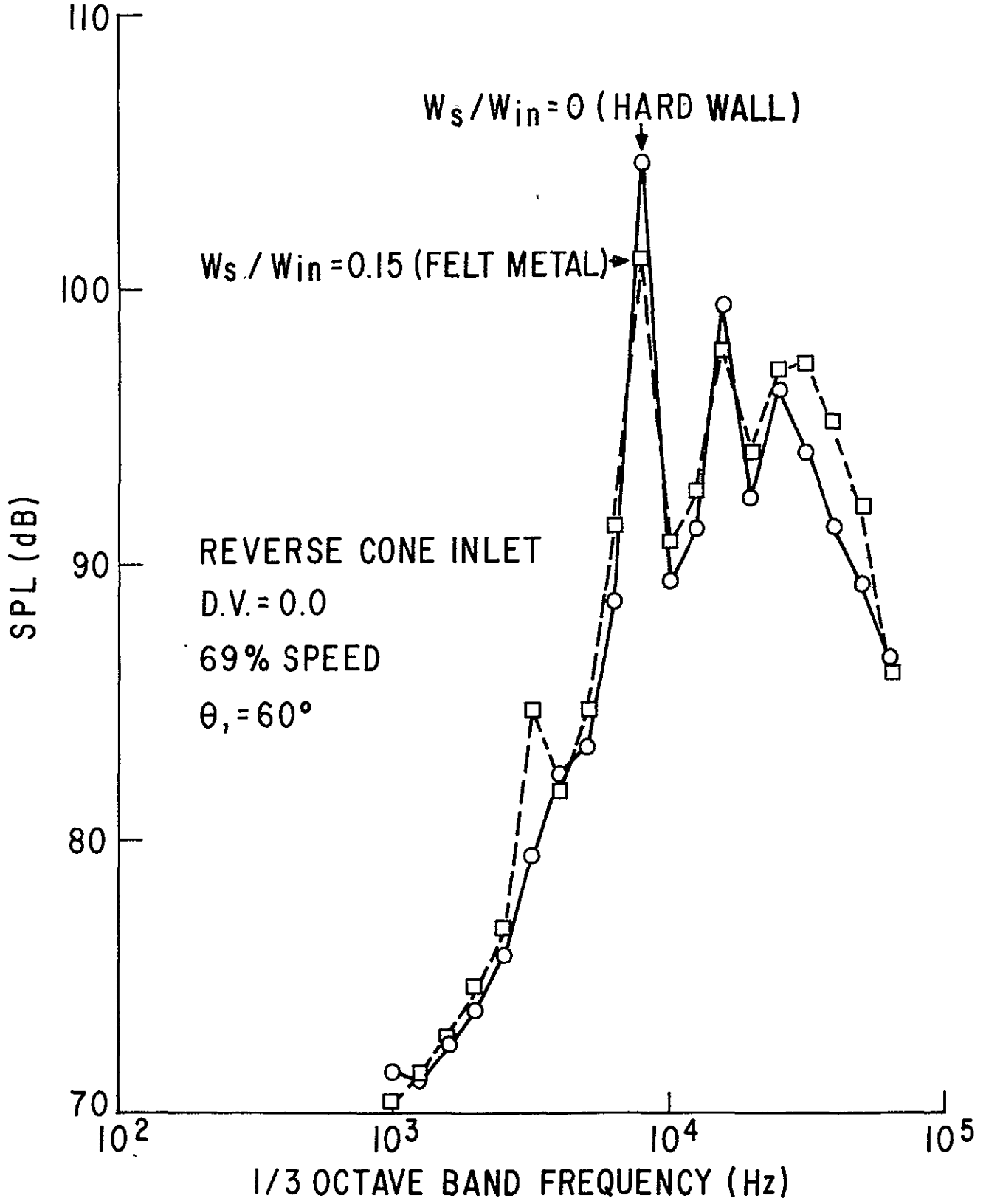

FIG. 21 EFFECT OF INNER AND OUTER SUCTION ON SPL SPECTRUM, NO TCS

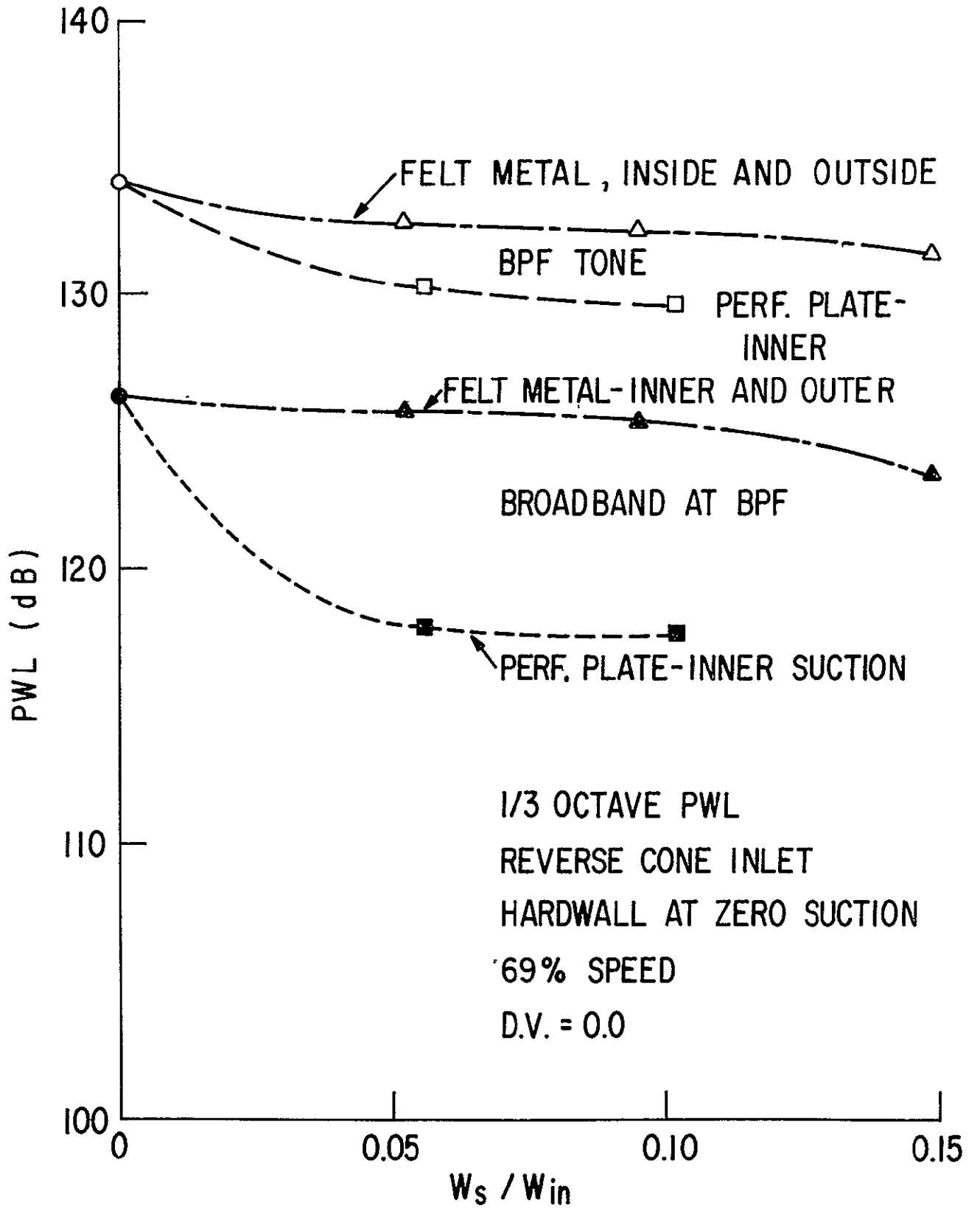

FIG. 22 EFFECT OF SUCTION METHODS ON ACOUSTIC POWER AT BLADE PASSING FREQUENCY, NO TCS

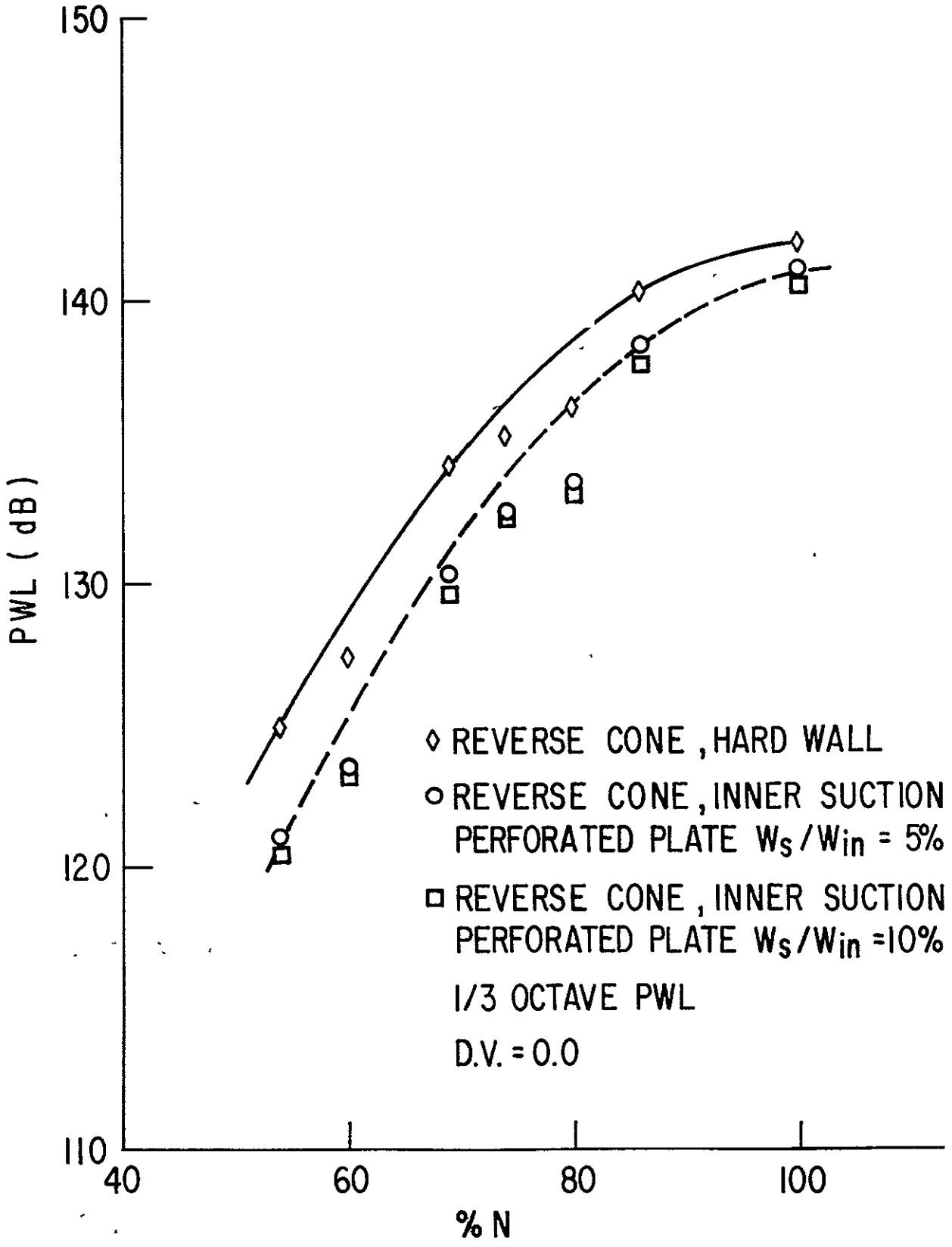

FIG. 23 EFFECT OF CORRECTED FAN SPEED AND SUCTION ON ACOUSTIC POWER AT BPF, NO TCS

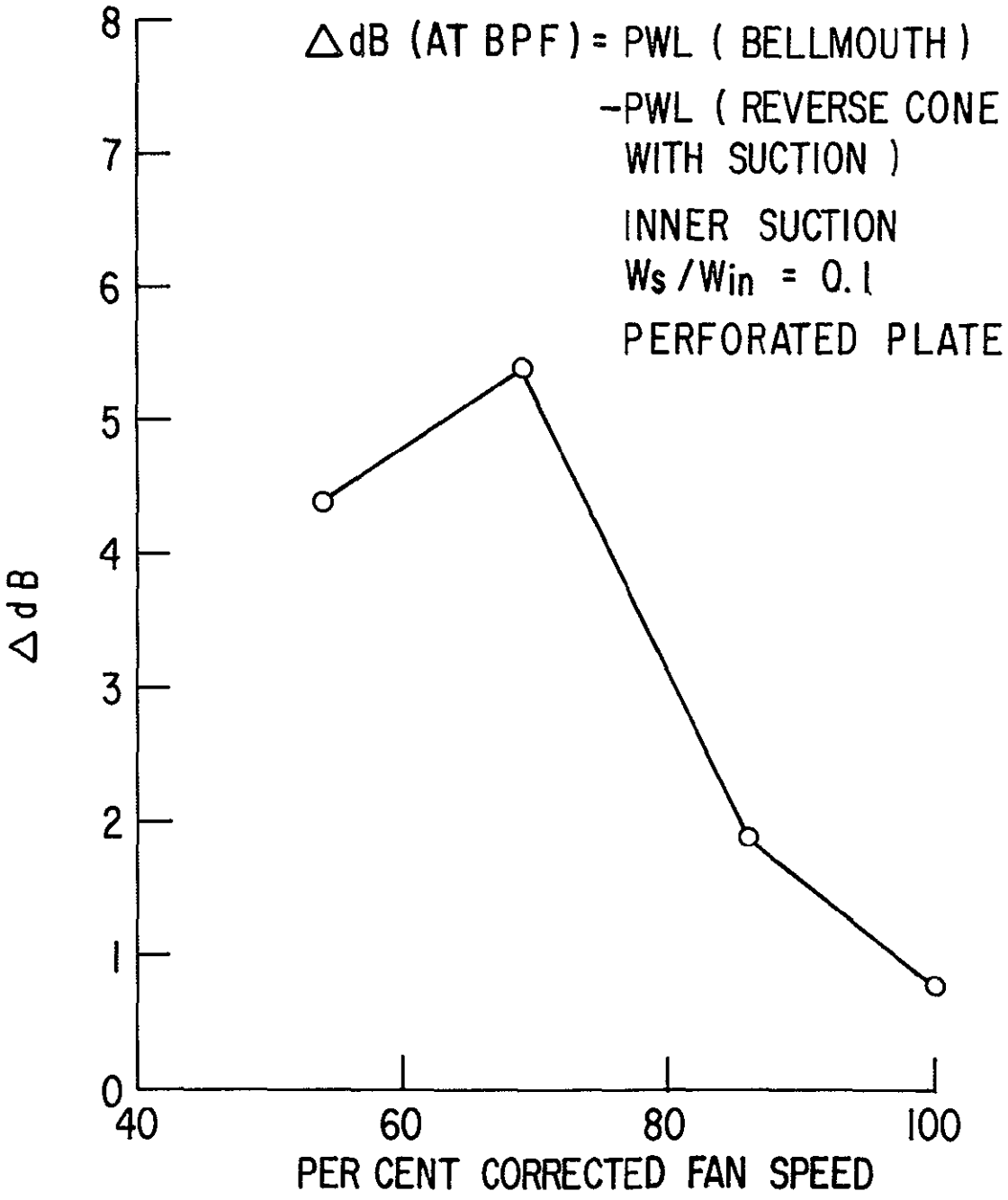

FIG. 24 ACOUSTIC POWER REDUCTION DUE TO REVERSE CONE INLET AND SUCTION , NO TCS

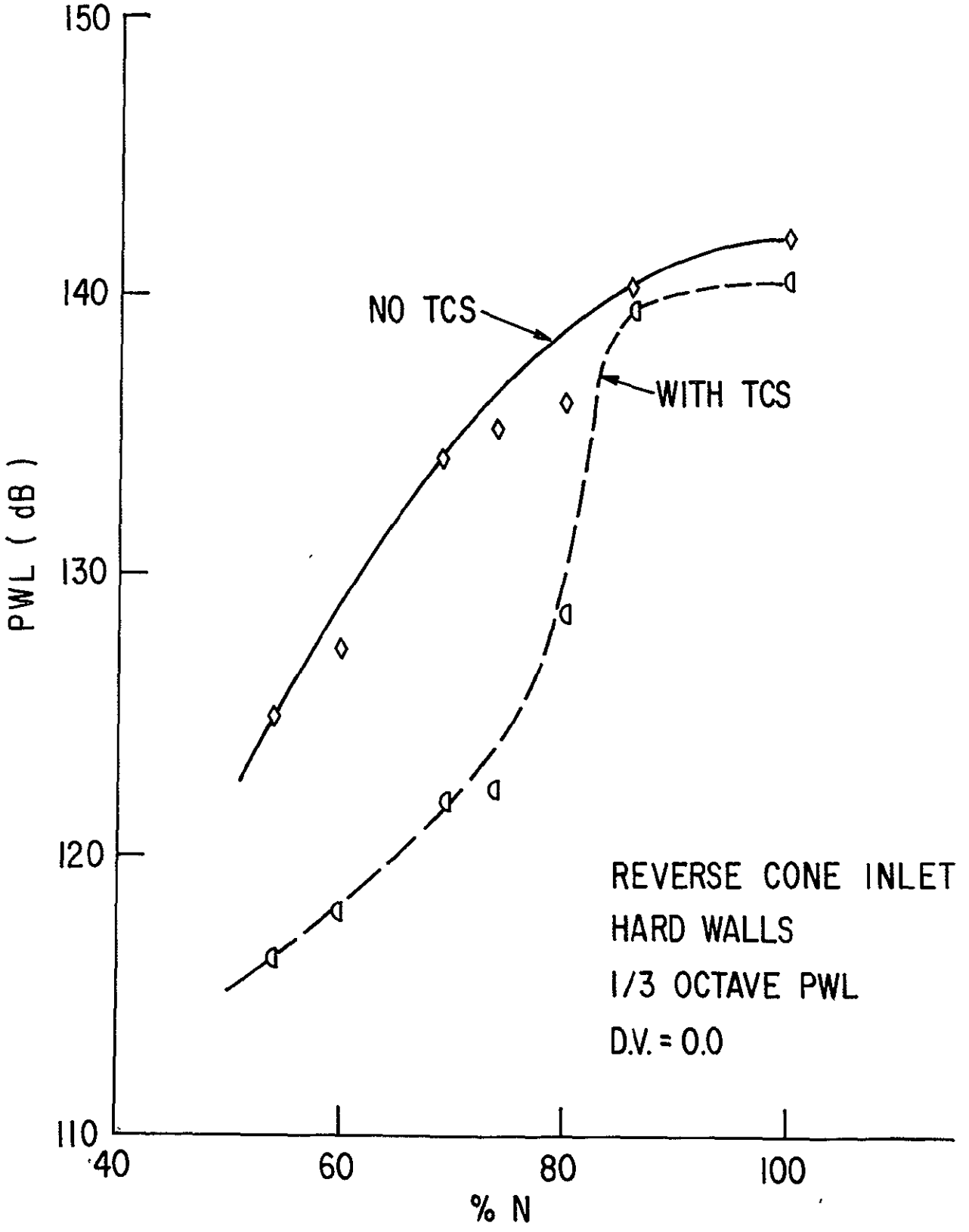

FIG. 25 EFFECT OF TCS ON PWL AT BPF VERSUS FAN SPEED

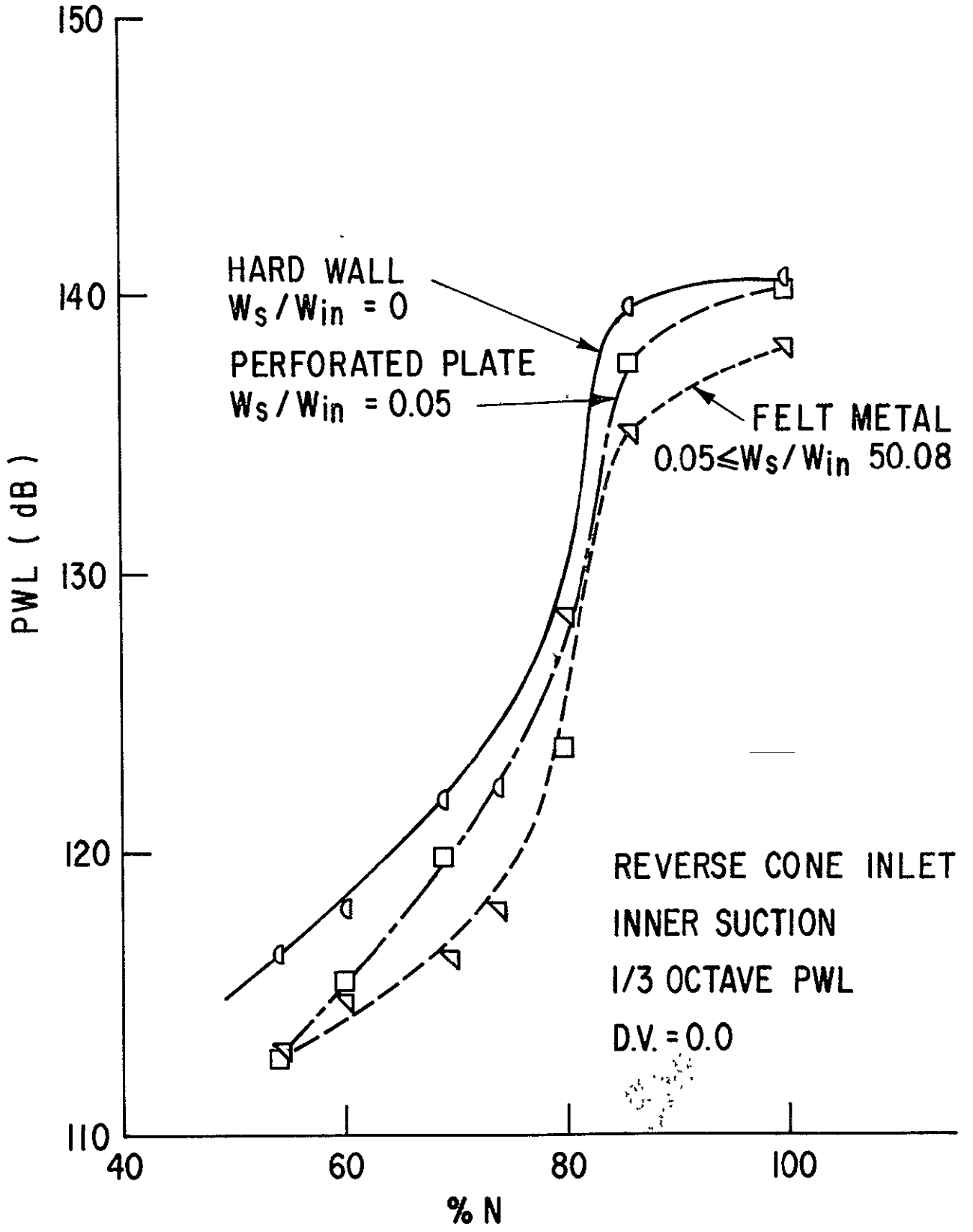

FIG. 26 EFFECT OF SUCTION ON PWL AT BPF, WITH TCS

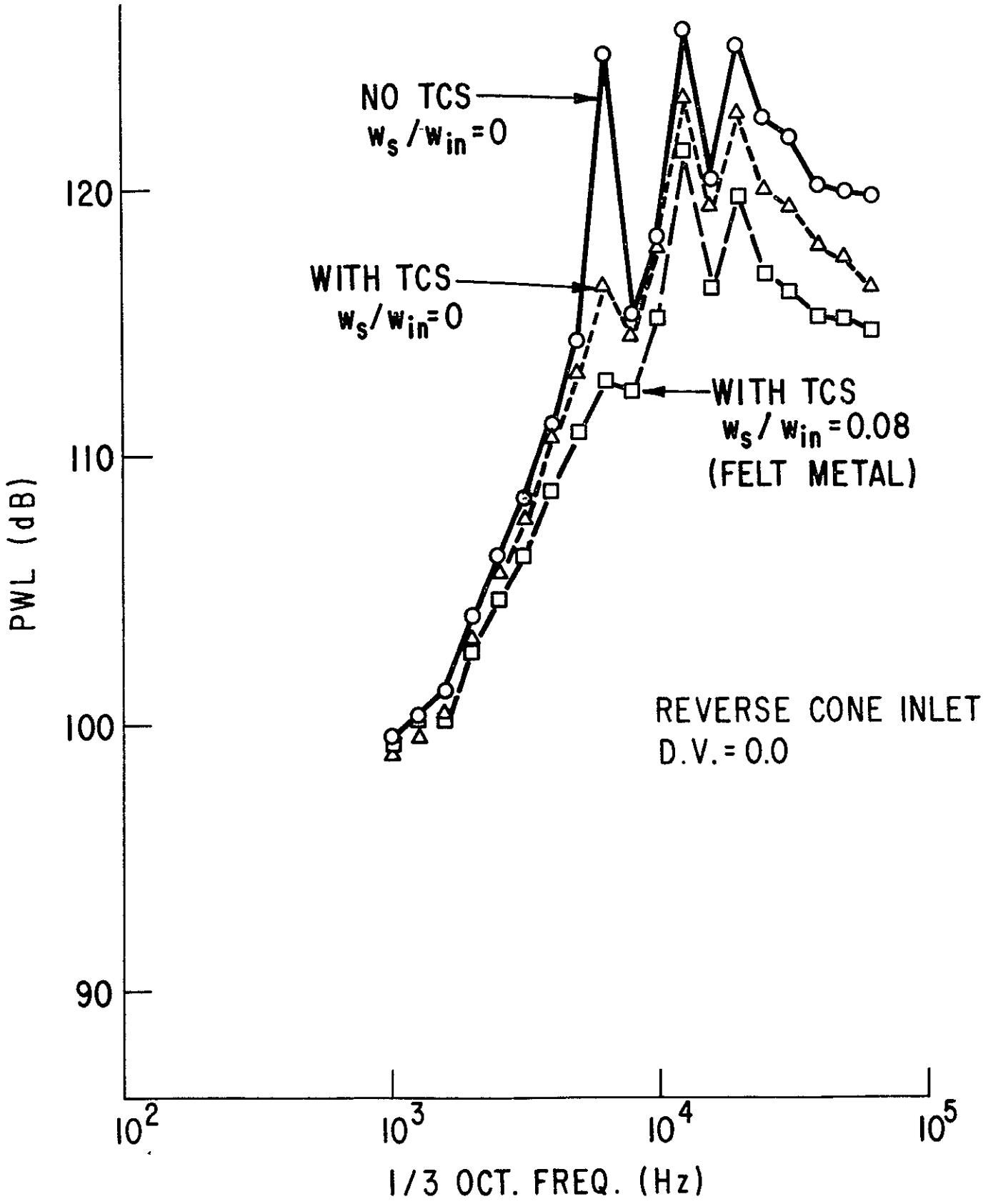

FIG. 27 ACOUSTIC POWER SPECTRA, EFFECT OF TCS AND INNER SUCTION, 54% SPEED

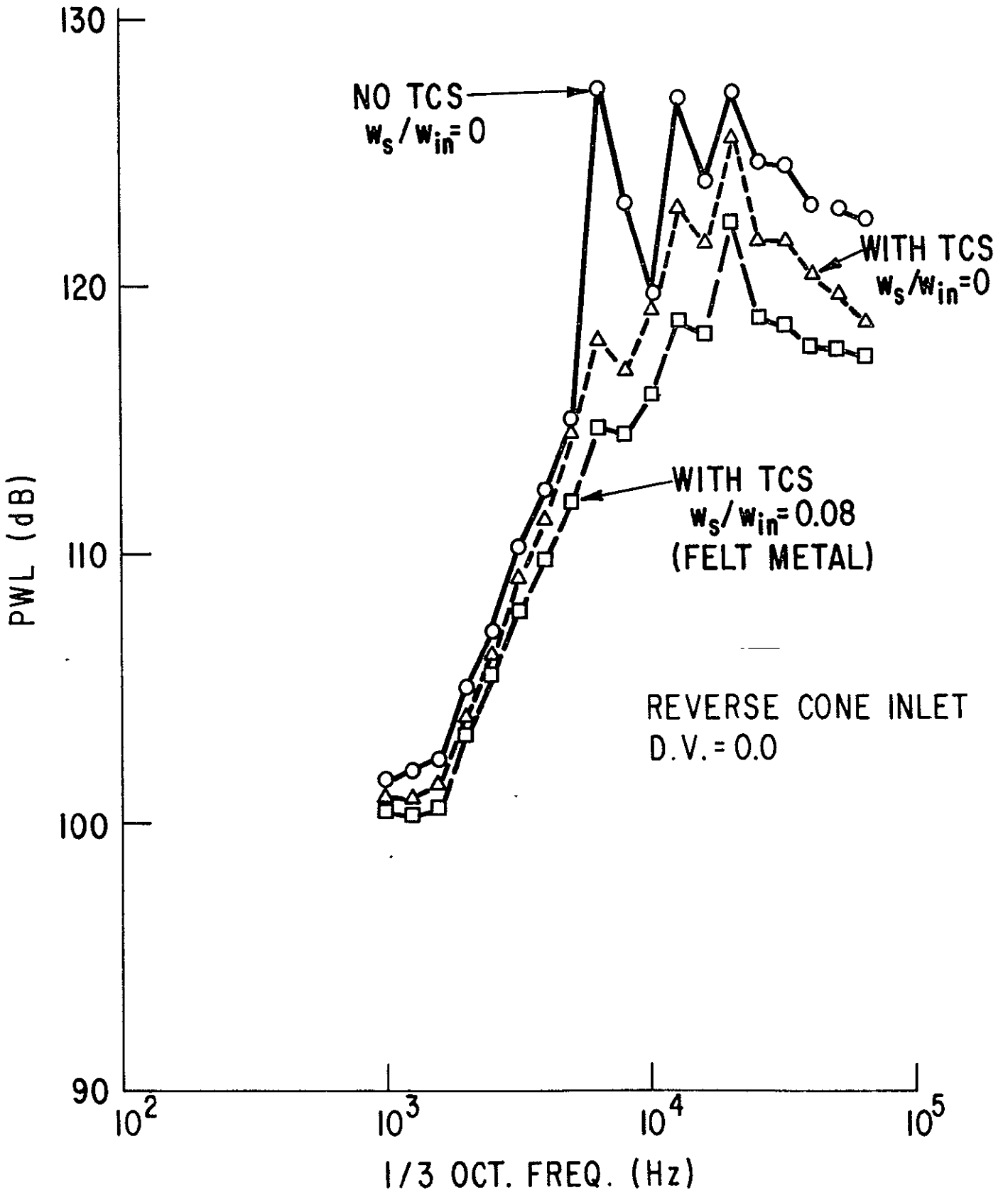

FIG. 28 ACOUSTIC POWER SPECTRA, EFFECT OF TCS AND INNER SUCTION, 60% SPEED

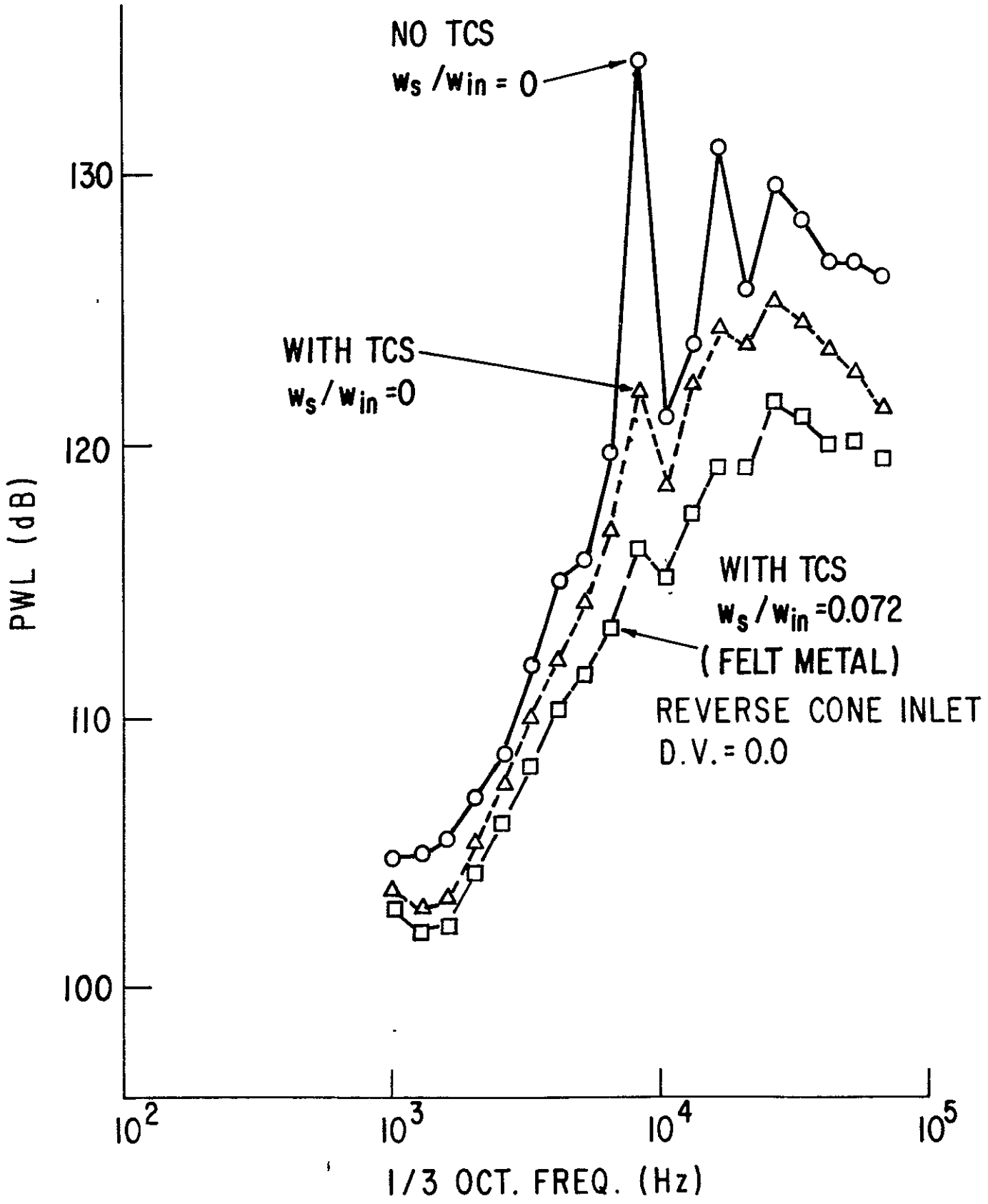

FIG. 29 ACOUSTIC POWER SPECTRA, EFFECT OF TCS AND INNER SUCTION, 69% SPEED.

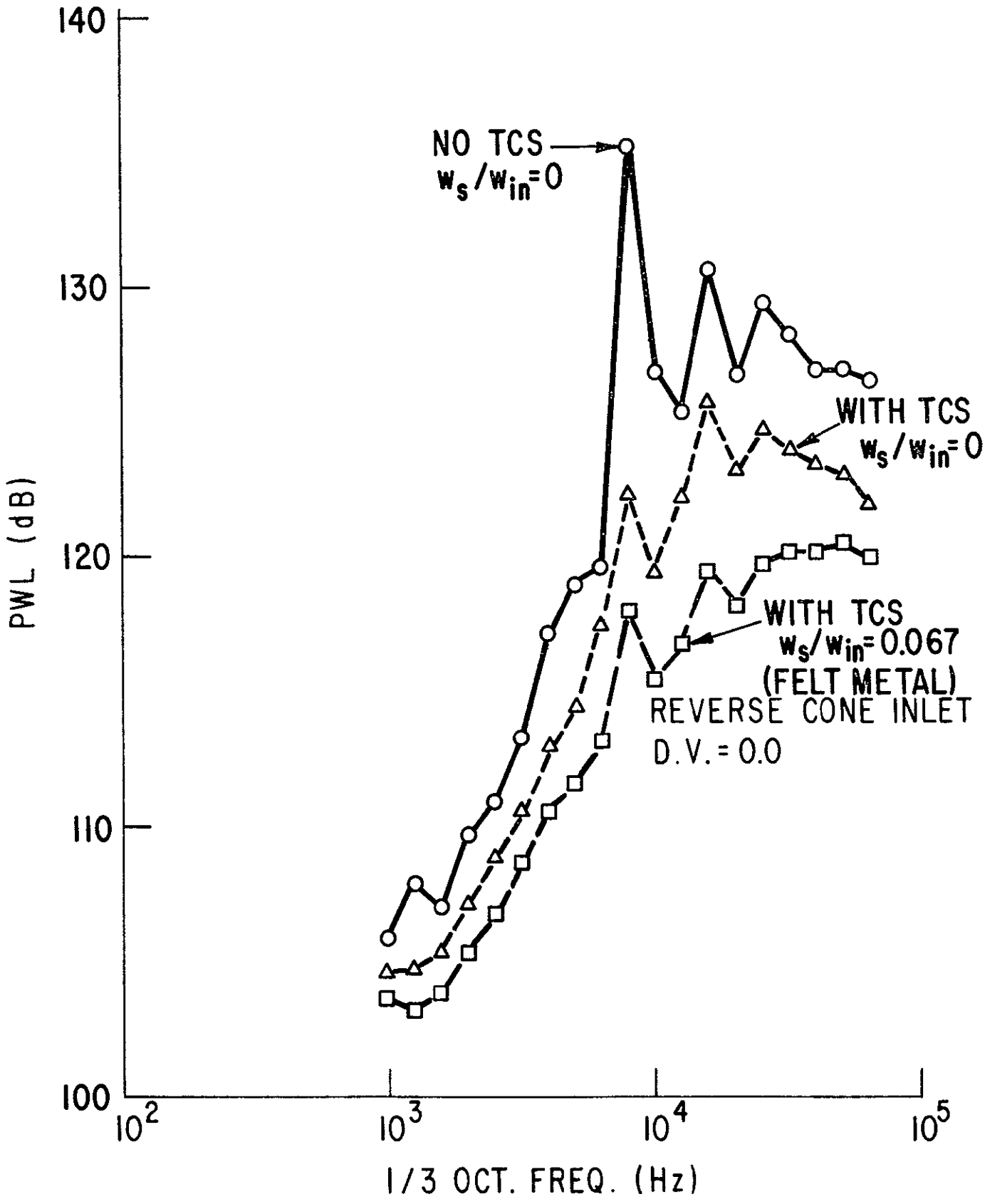

FIG. 30 ACOUSTIC POWER SPECTRA, EFFECT OF TCS AND INNER SUCTION, 74% SPEED

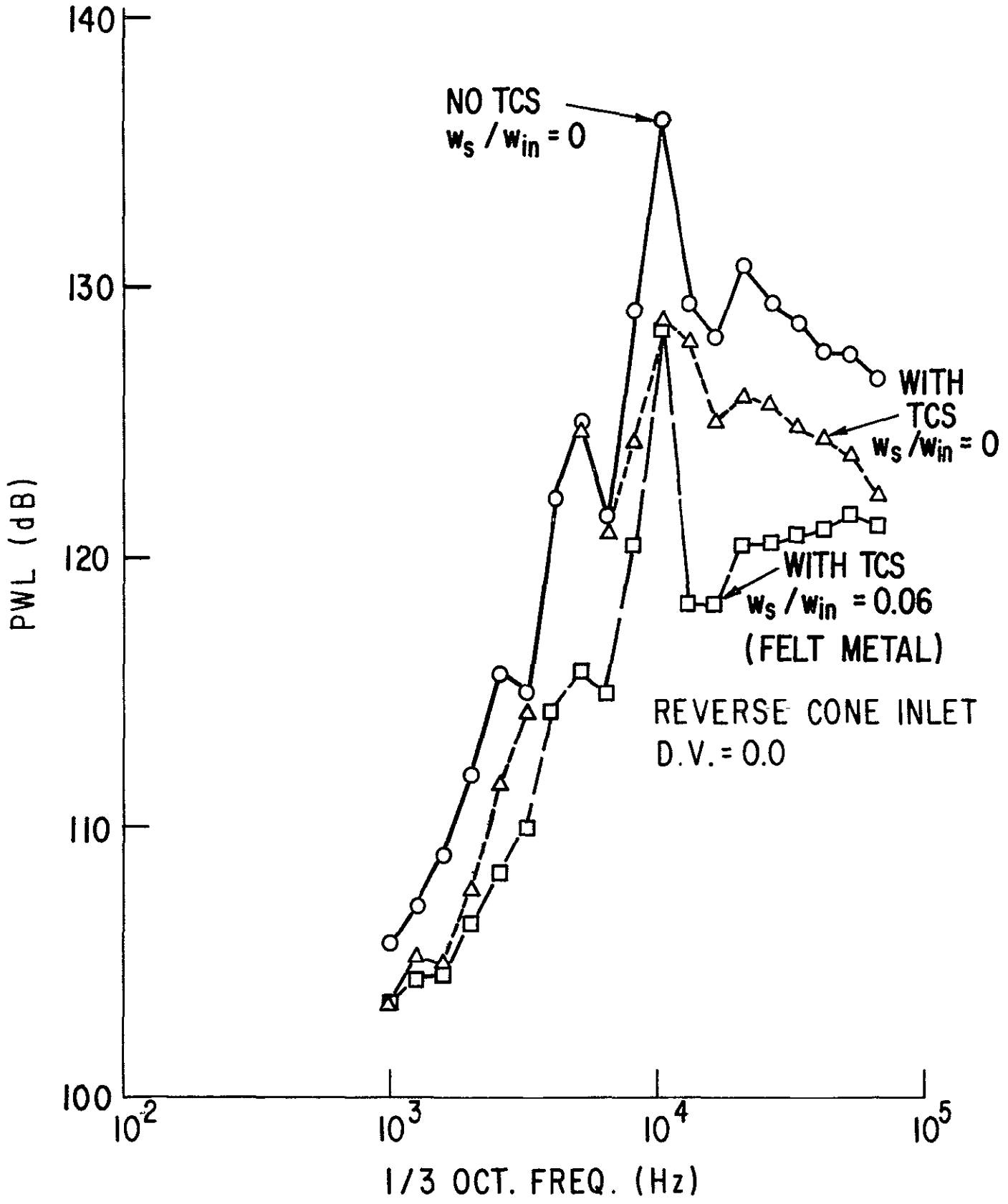

FIG. 31 ACOUSTIC POWER SPECTRA, EFFECT OF TCS AND INNER SUCTION, 80% SPEED

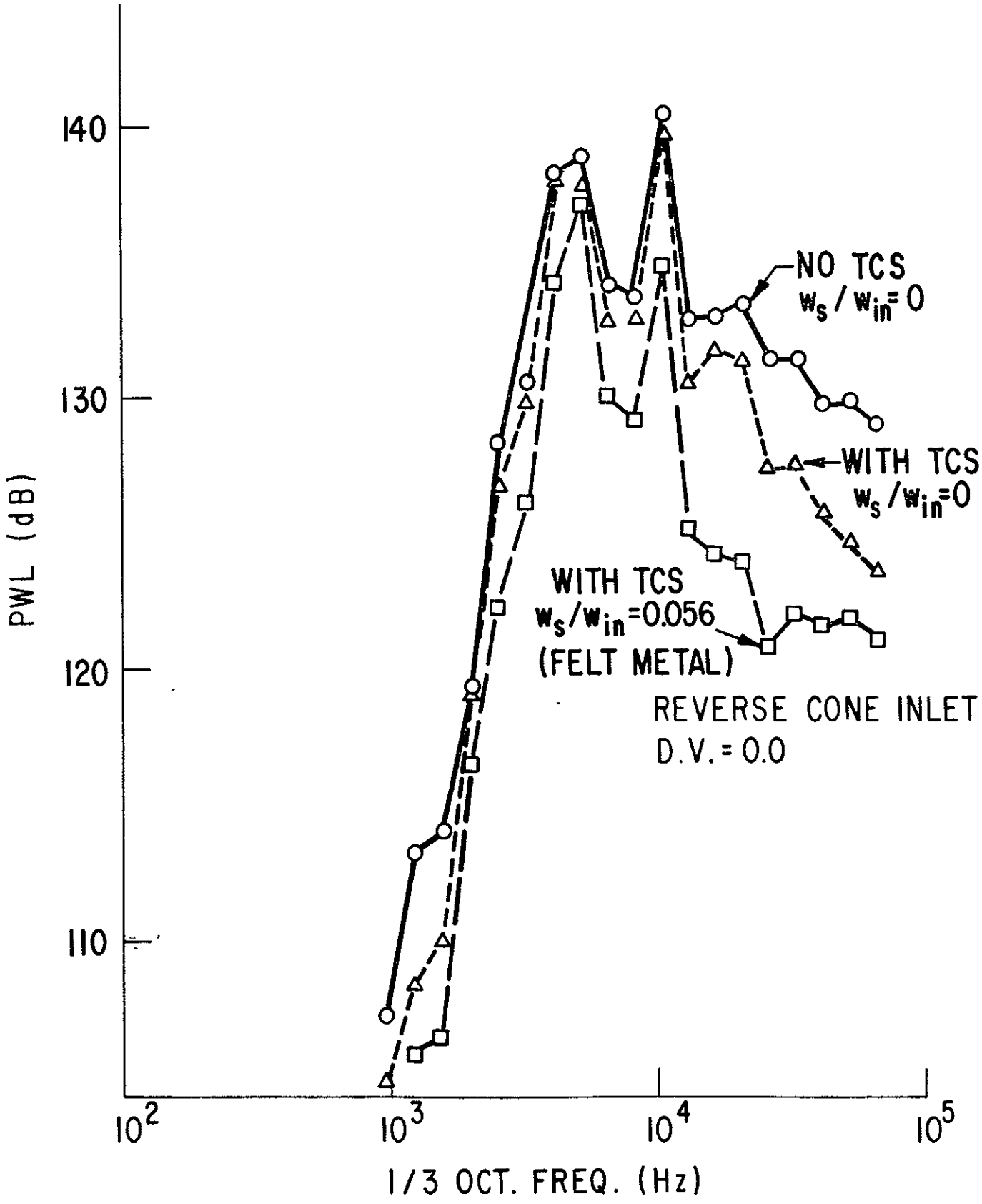

FIG. 32 ACOUSTIC POWER SPECTRA , EFFECT OF TCS AND INNER SUCTION , 86% SPEED

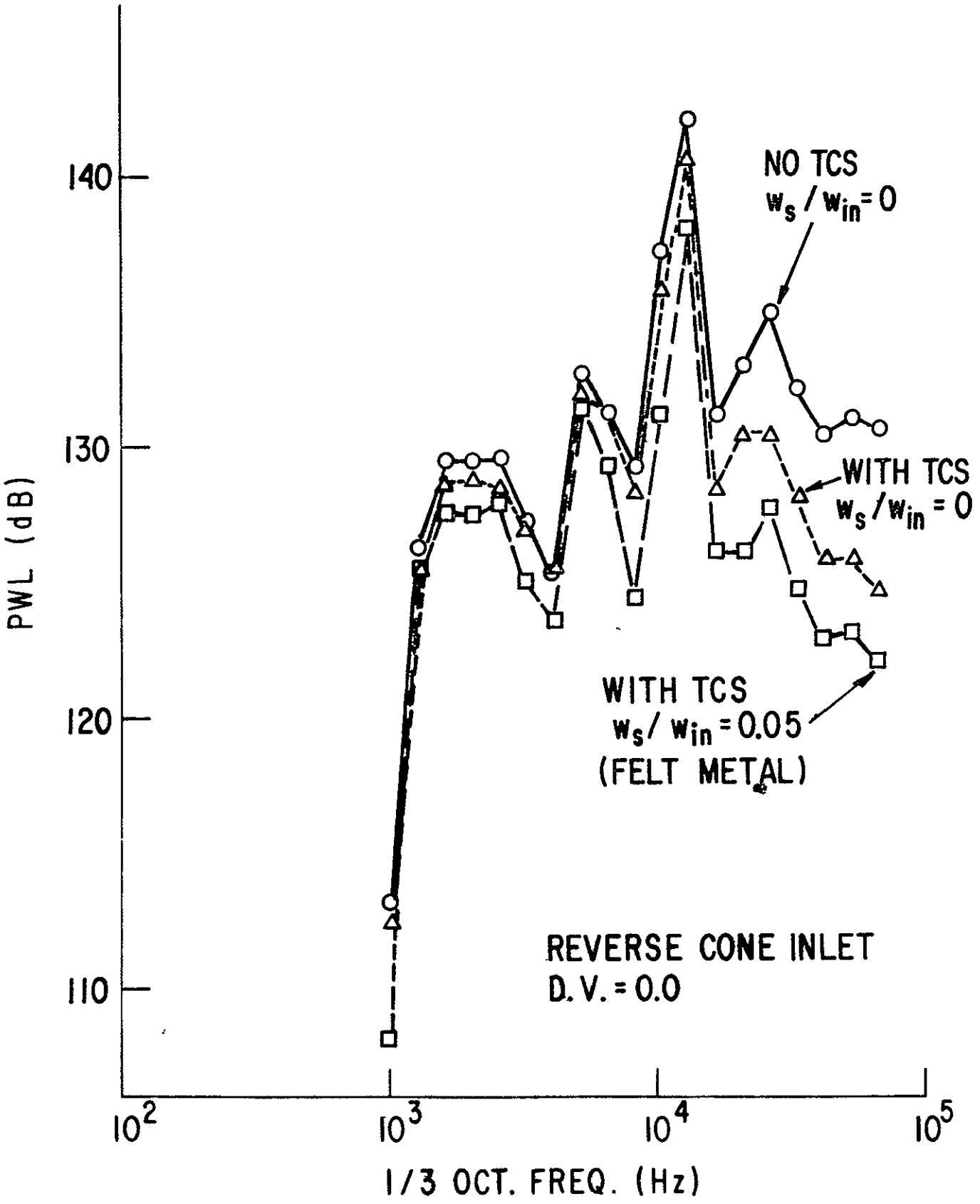

FIG. 33 ACOUSTIC POWER SPECTRA , EFFECT OF TCS AND INNER SUCTION , 100% SPEED

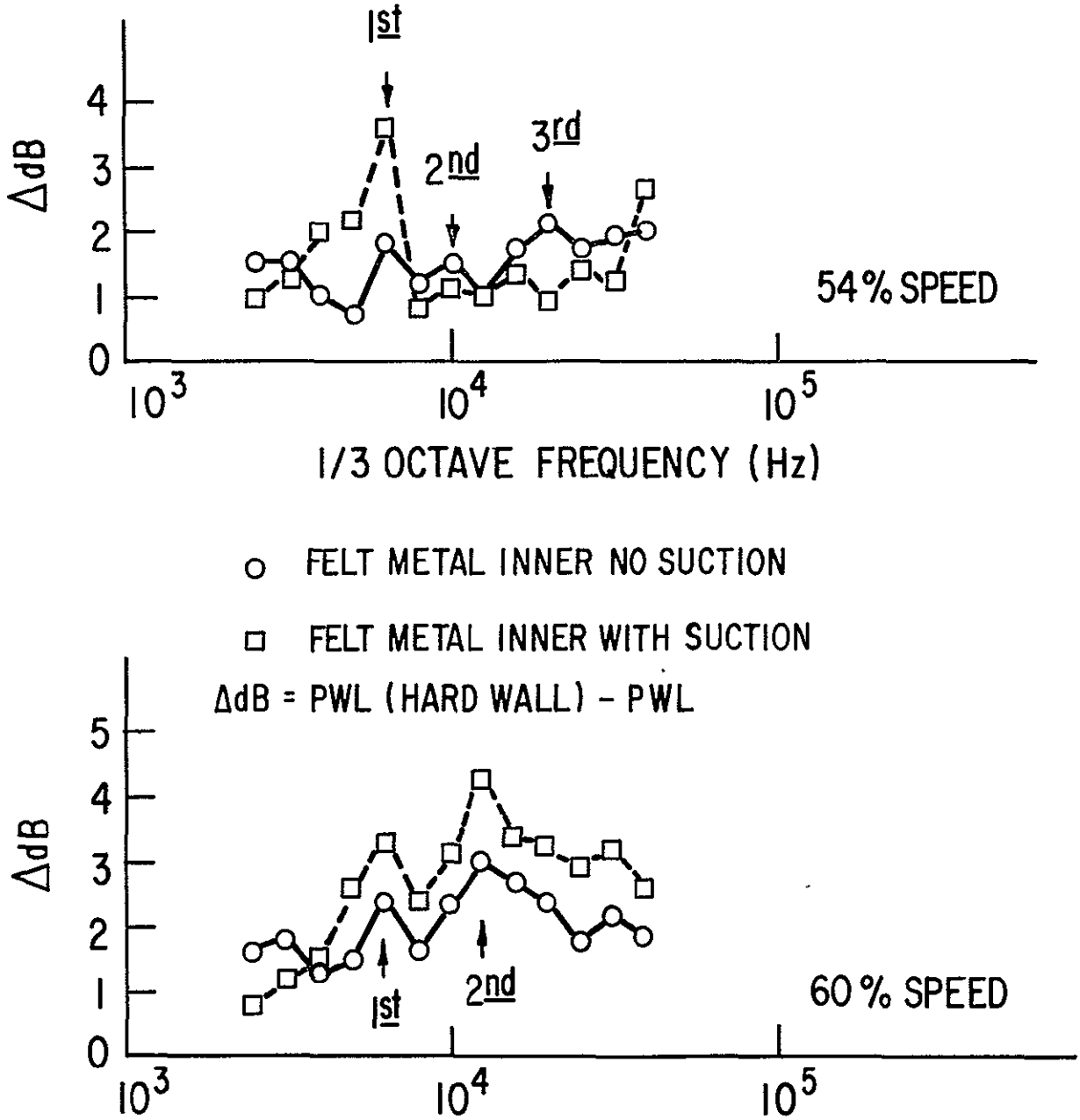

ROTOR II, REVERSE INLET, TCS, D.V. = 0

34a CHANGE IN POWER SPECTRA, DUE THE TCS AND SUCTION, SUBSONIC

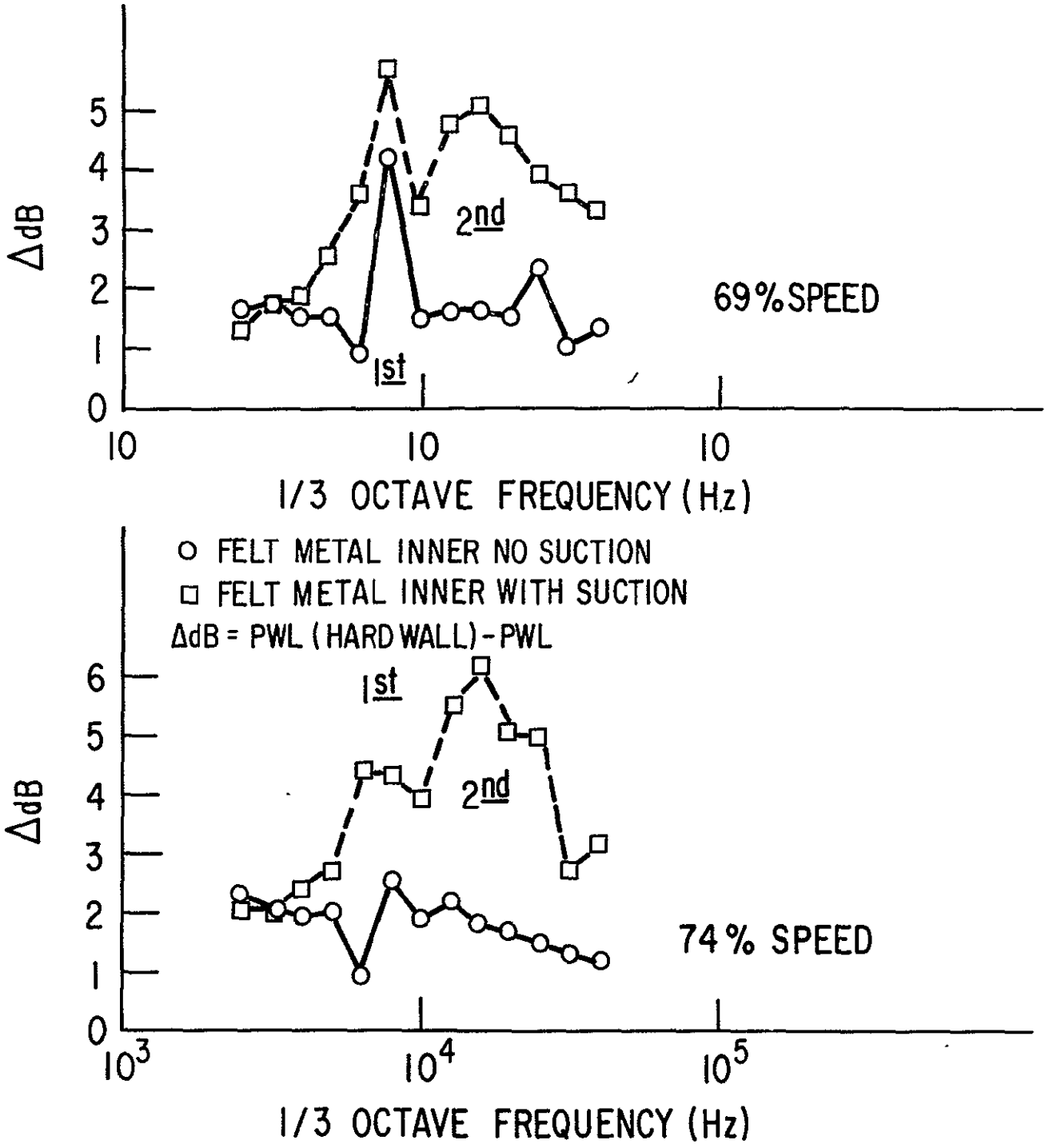

ROTOR 11, REVERSE CONE INLET, TCS, D.V. = 0

34b CHANGE IN POWER SPECTRA, DUE THE TCS AND SUCTION, HIGH SUBSONIC

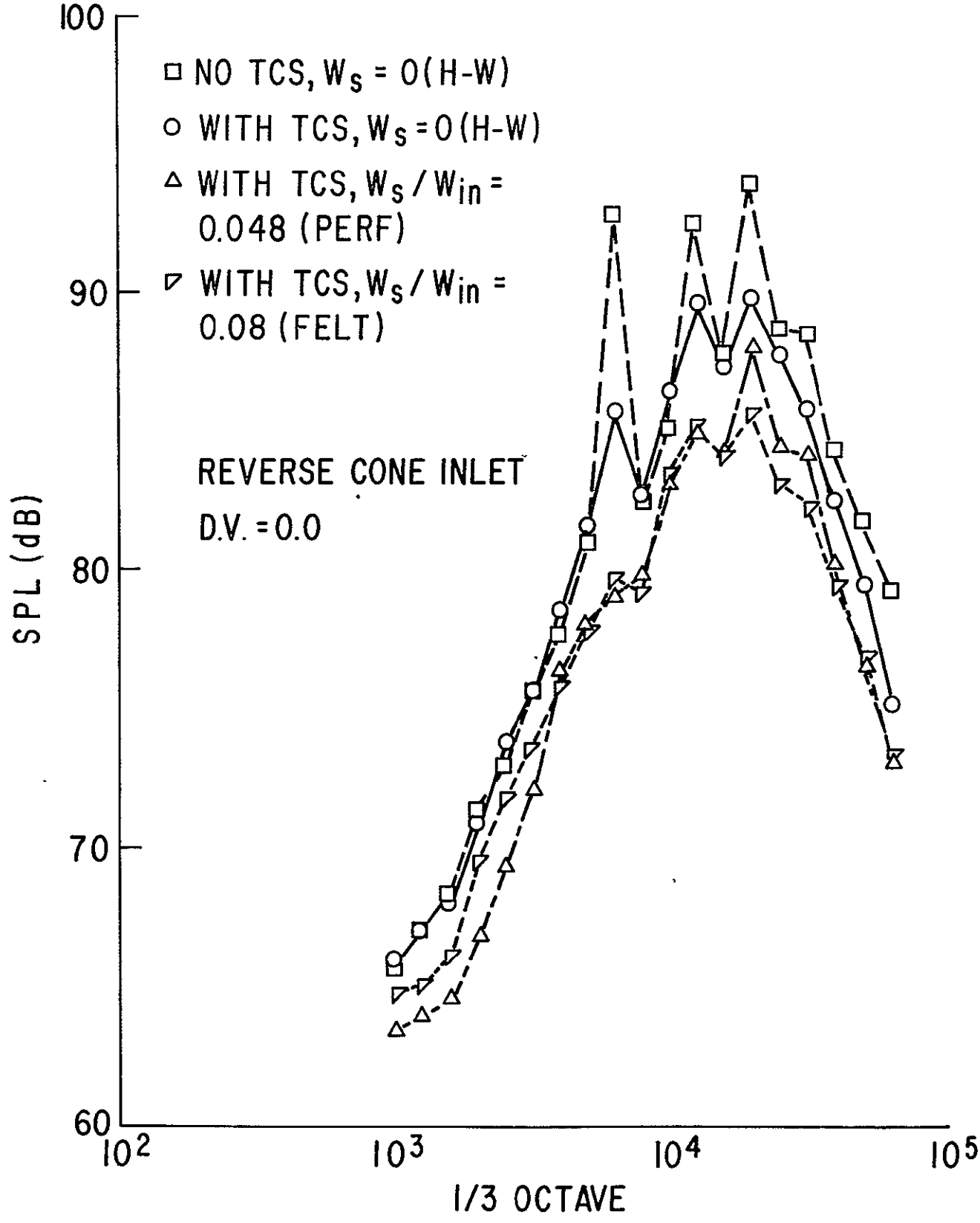

FIG. 35 SOUND PRESSURE SPECTRA AT θ=60, EFFECT OF TCS AND INNER SUCTION, 54% SPEED

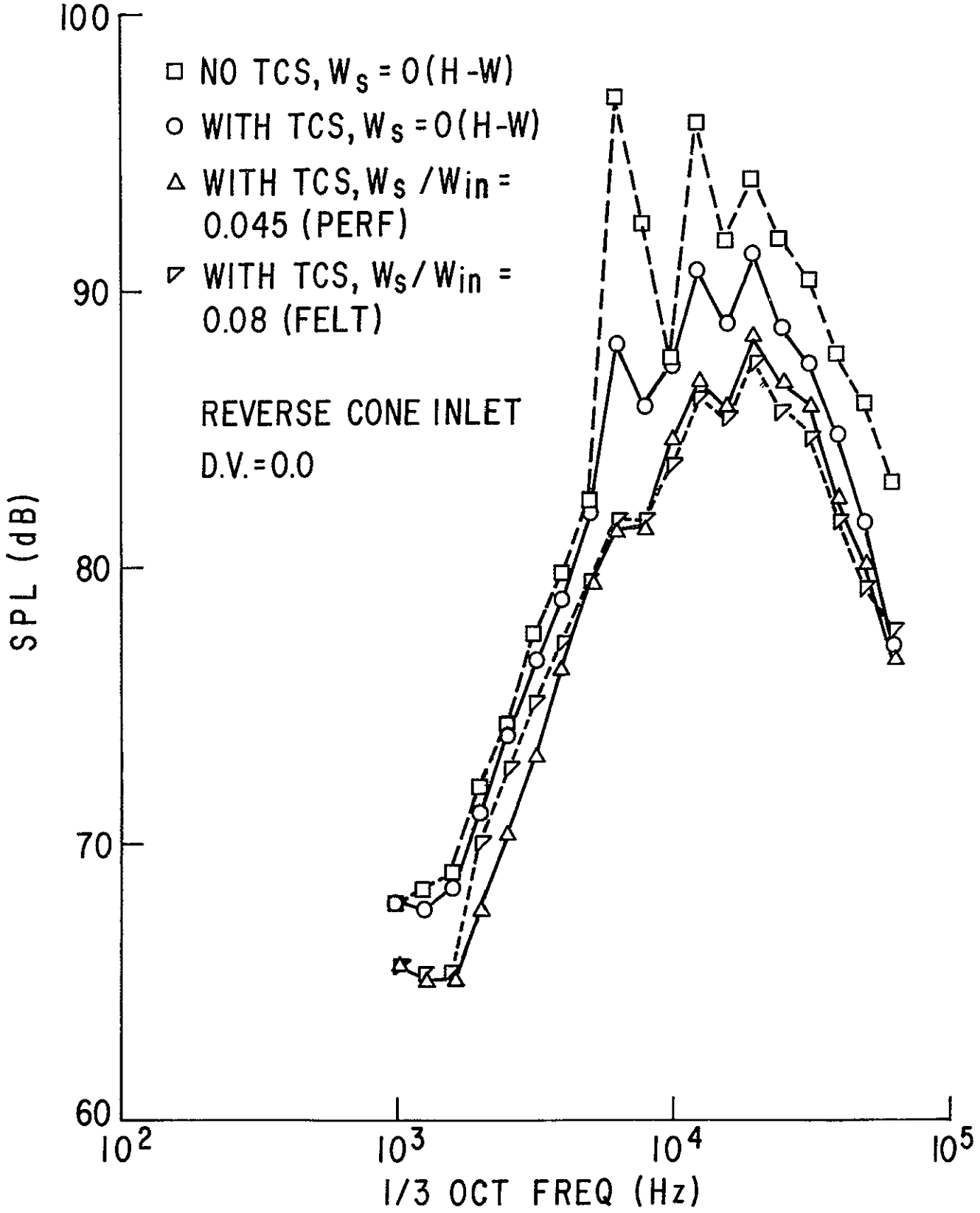

FIG. 36 SOUND PRESSURE SPECTRA AT θ = 60°, EFFECT OF TCS AND INNER SUCTION, 60% SPEED

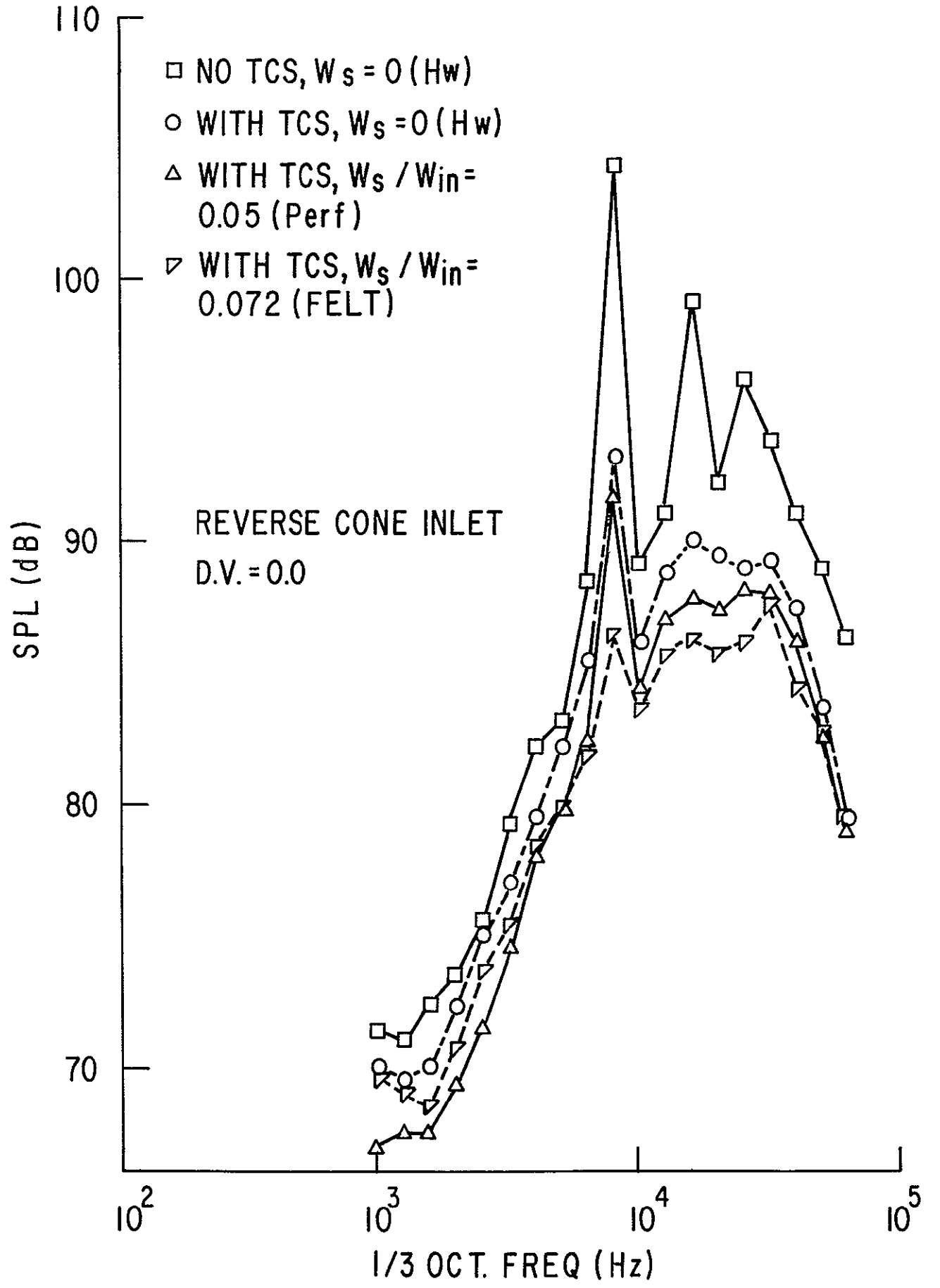

FIG. 37 SOUND PRESSURE SPECTRA AT θ=60°, EFFECT OF TCS AND INNER SUCTION, 69% SPEED

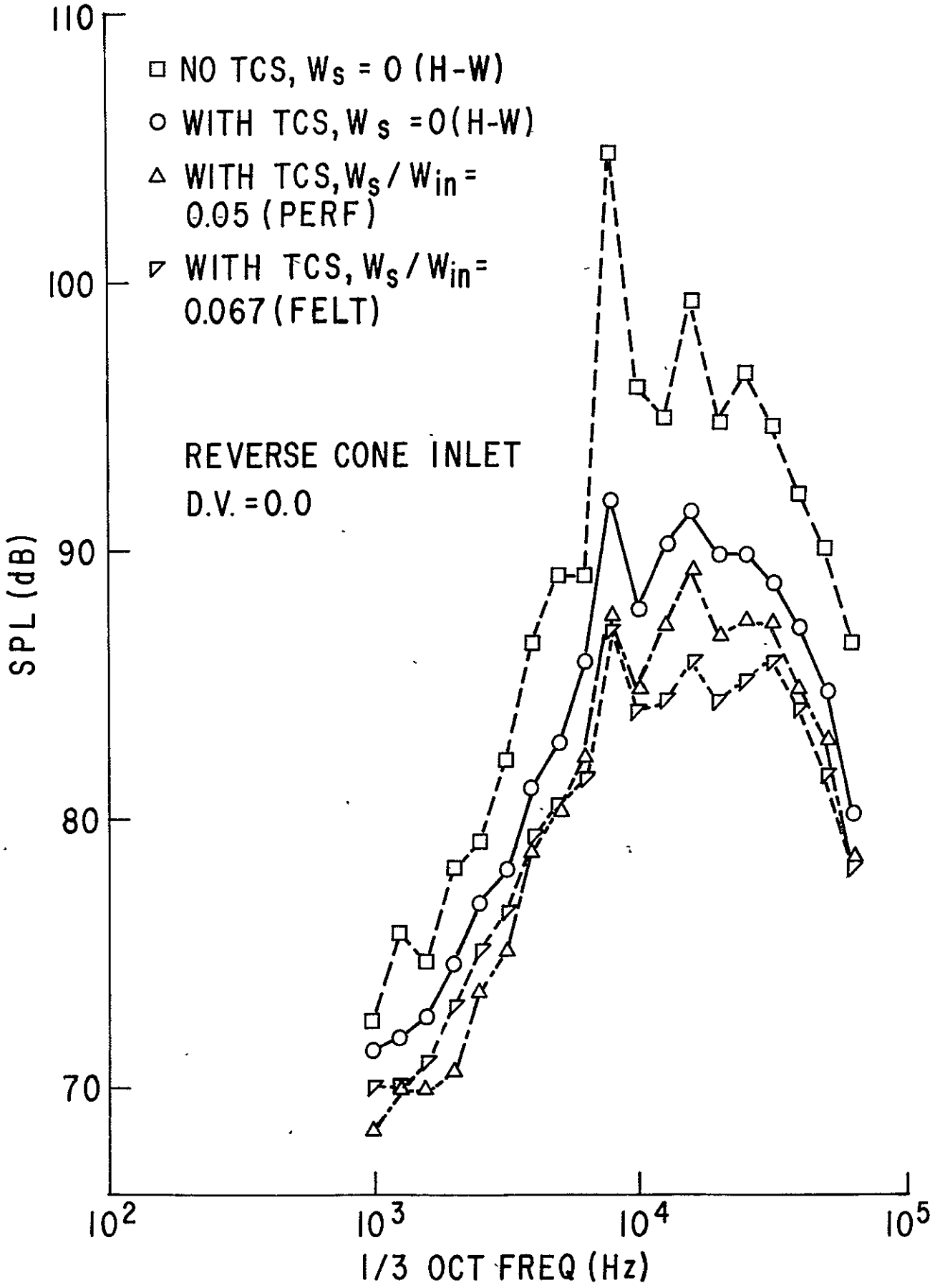

FIG. 38 SOUND PRESSURE SPECTRA AT θ = 60°, EFFECT OF TCS AND INNER SUCTION, 74% SPEED

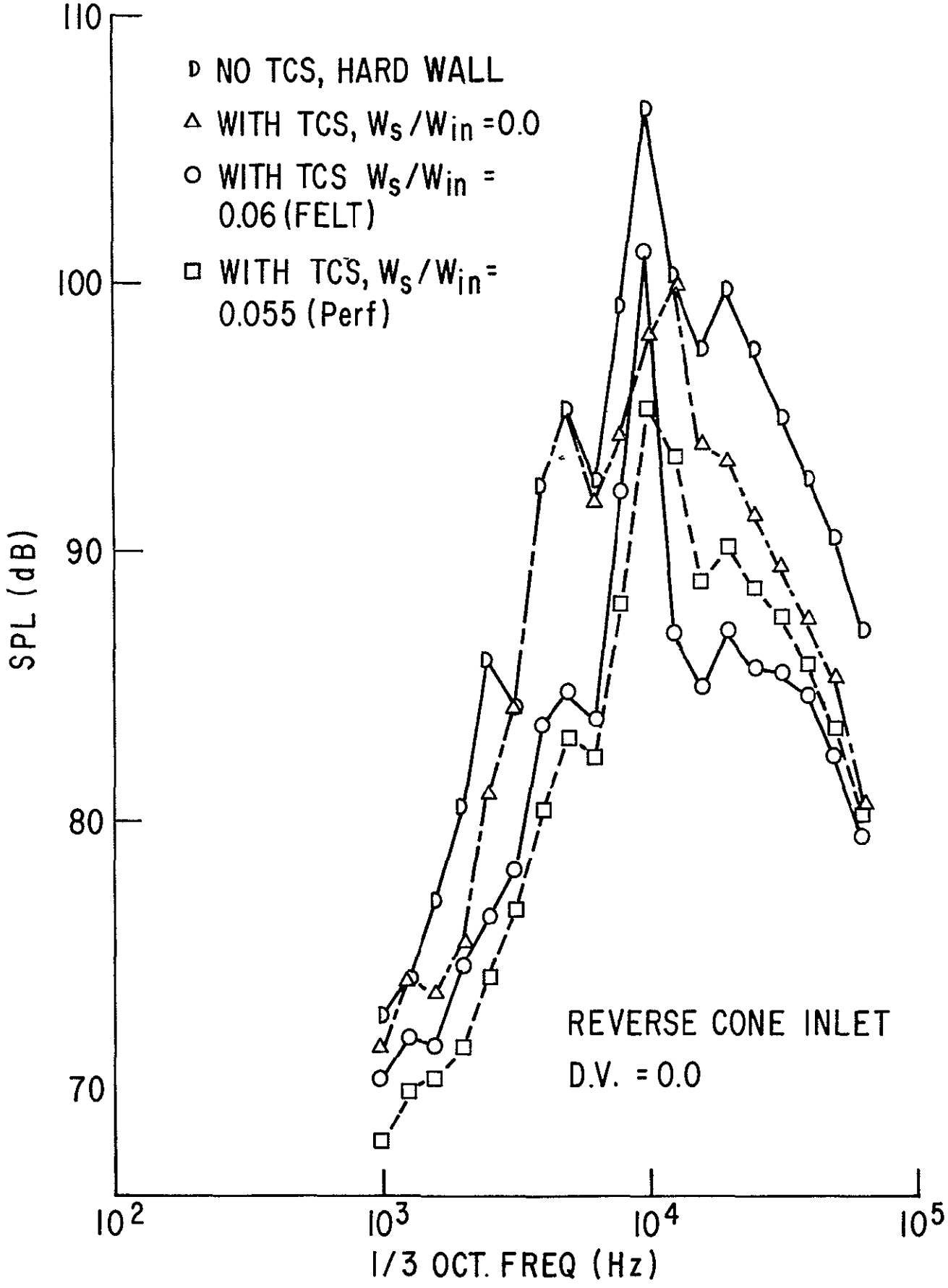

FIG. 39 SOUND PRESSURE SPECTRA AT θ=60°, EFFECT OF TCS AND INNER SUCTION, 80% SPEED

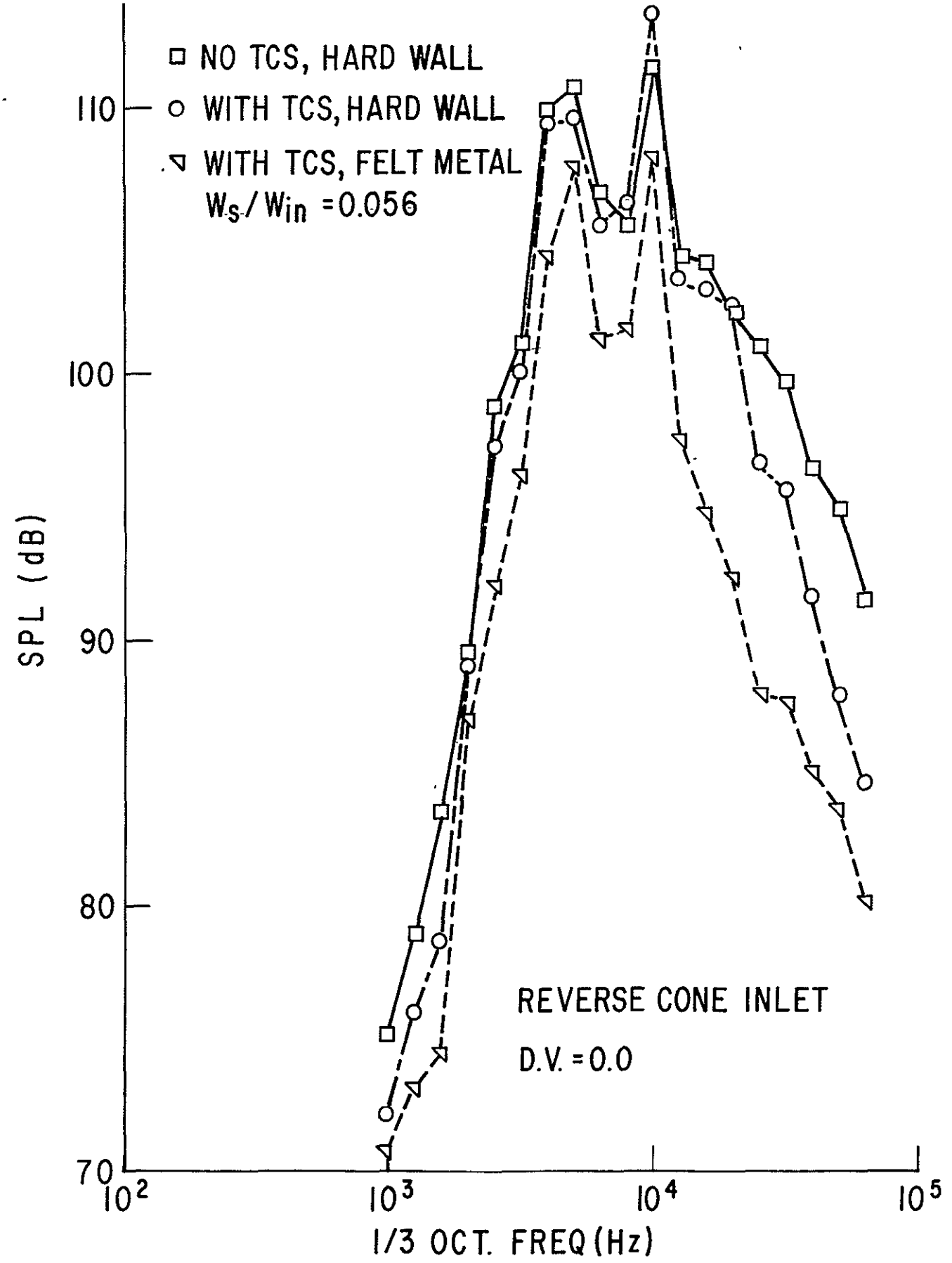

FIG. 40 SOUND PRESSURE SPECTRA AT θ = 60°, EFFECT OF TCS AND INNER SUCTION, 86% SPEED

C2

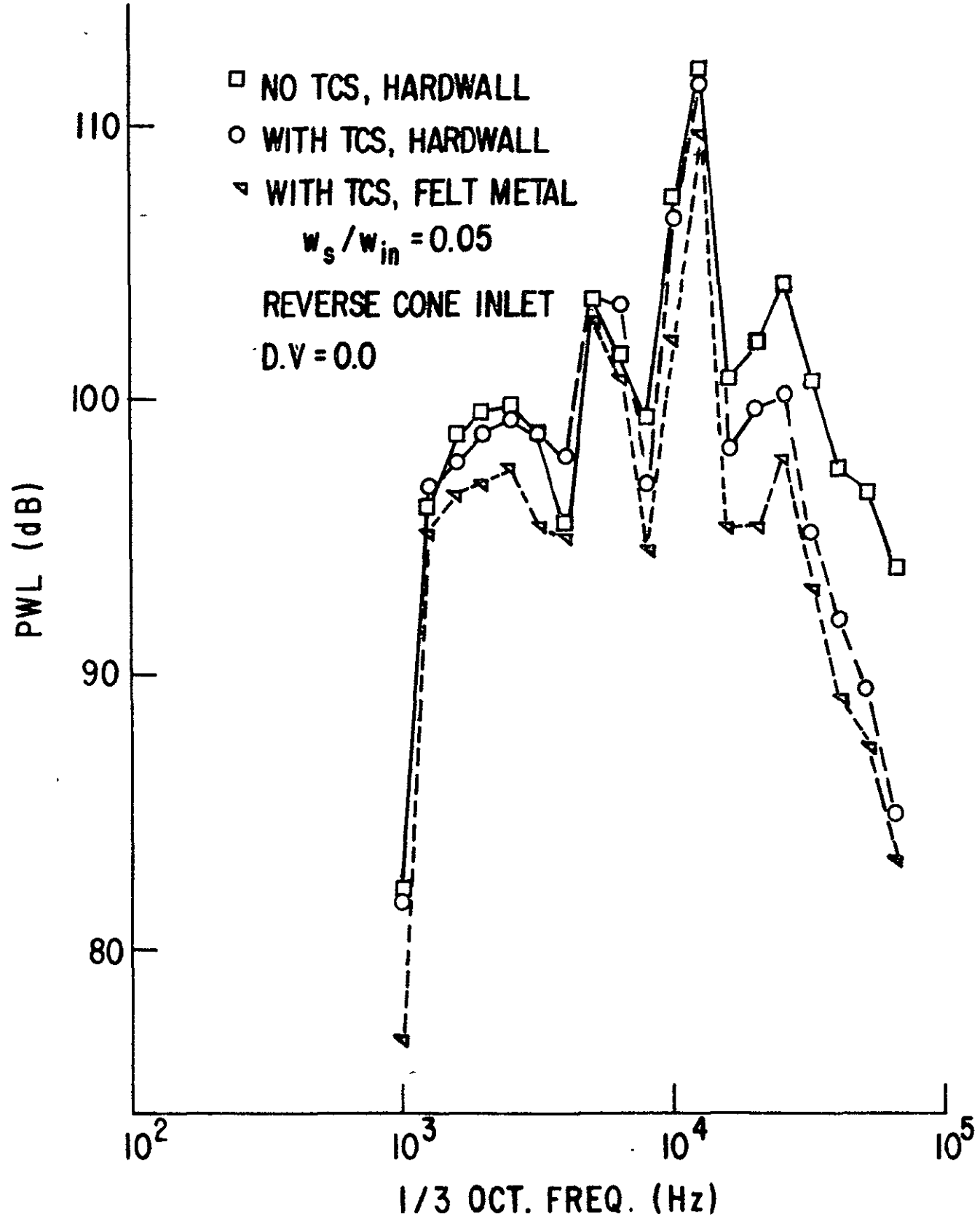

FIG. 41 SOUND PRESSURE SPECTRA AT $\theta = 60°$, EFFECT OF TCS AND INNER SUCTION, 100% SPEED

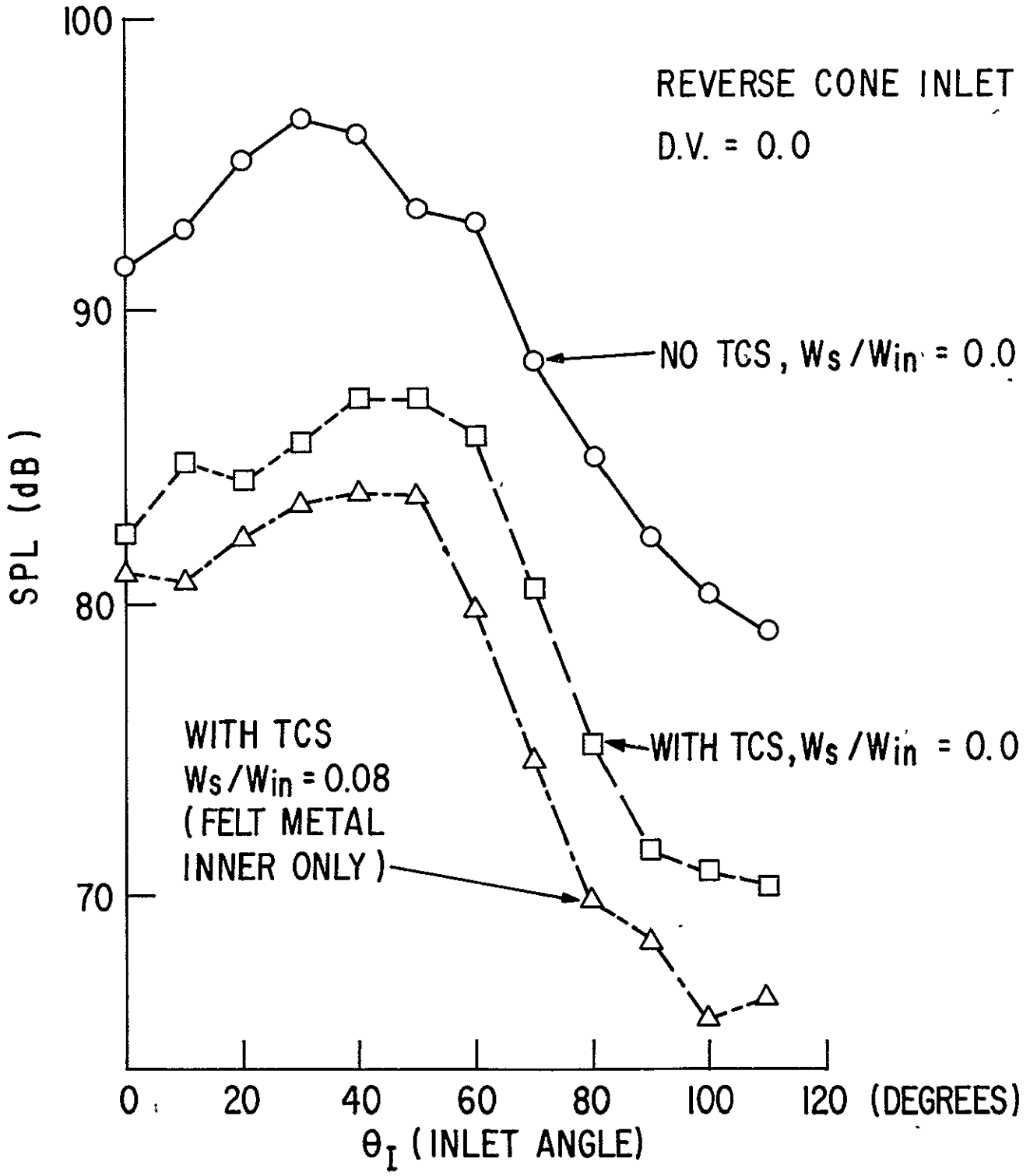

FIG. 42 1/3 OCTAVE SPL DIRECTIVITY AT BLADE PASSING FREQUENCY, 54% SPEED

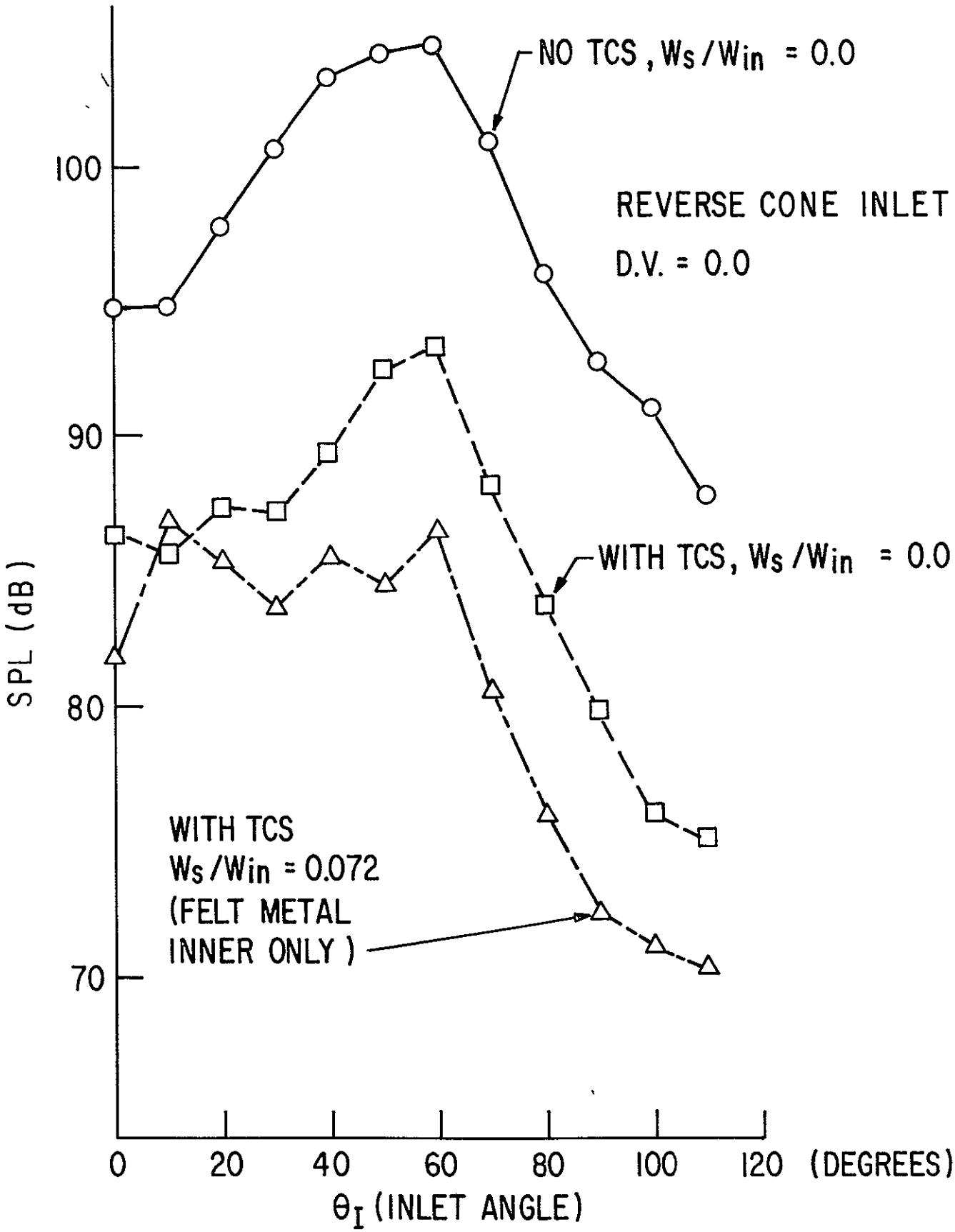

FIG. 43 1/3 OCTAVE SPL DIRECTIVITY AT BLADE PASSING FREQUENCY, 69% SPEED

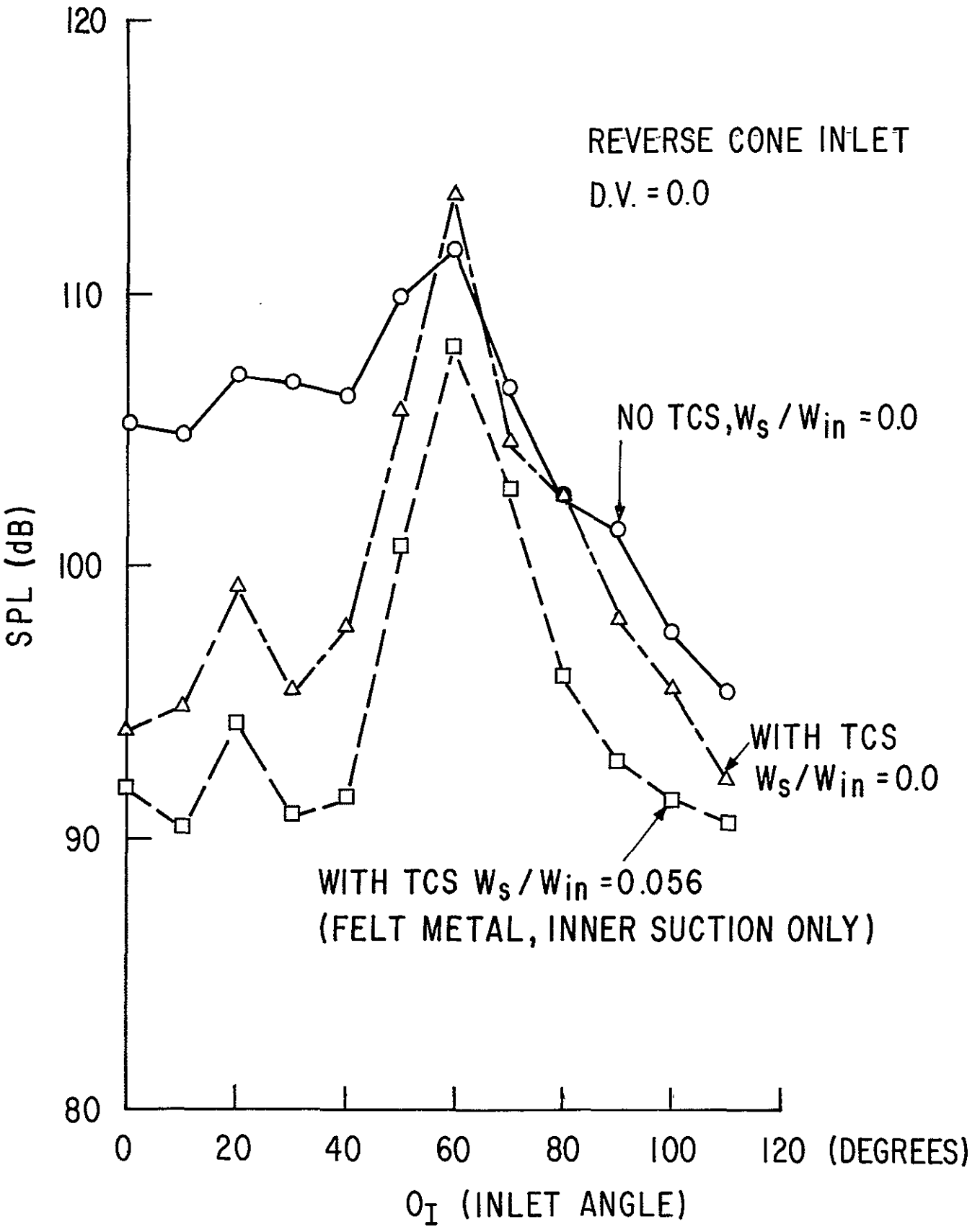

FIG. 44 1/3 OCTAVE SPL DIRECTIVITY AT BLADE PASSING FREQUENCY, 86% SPEED

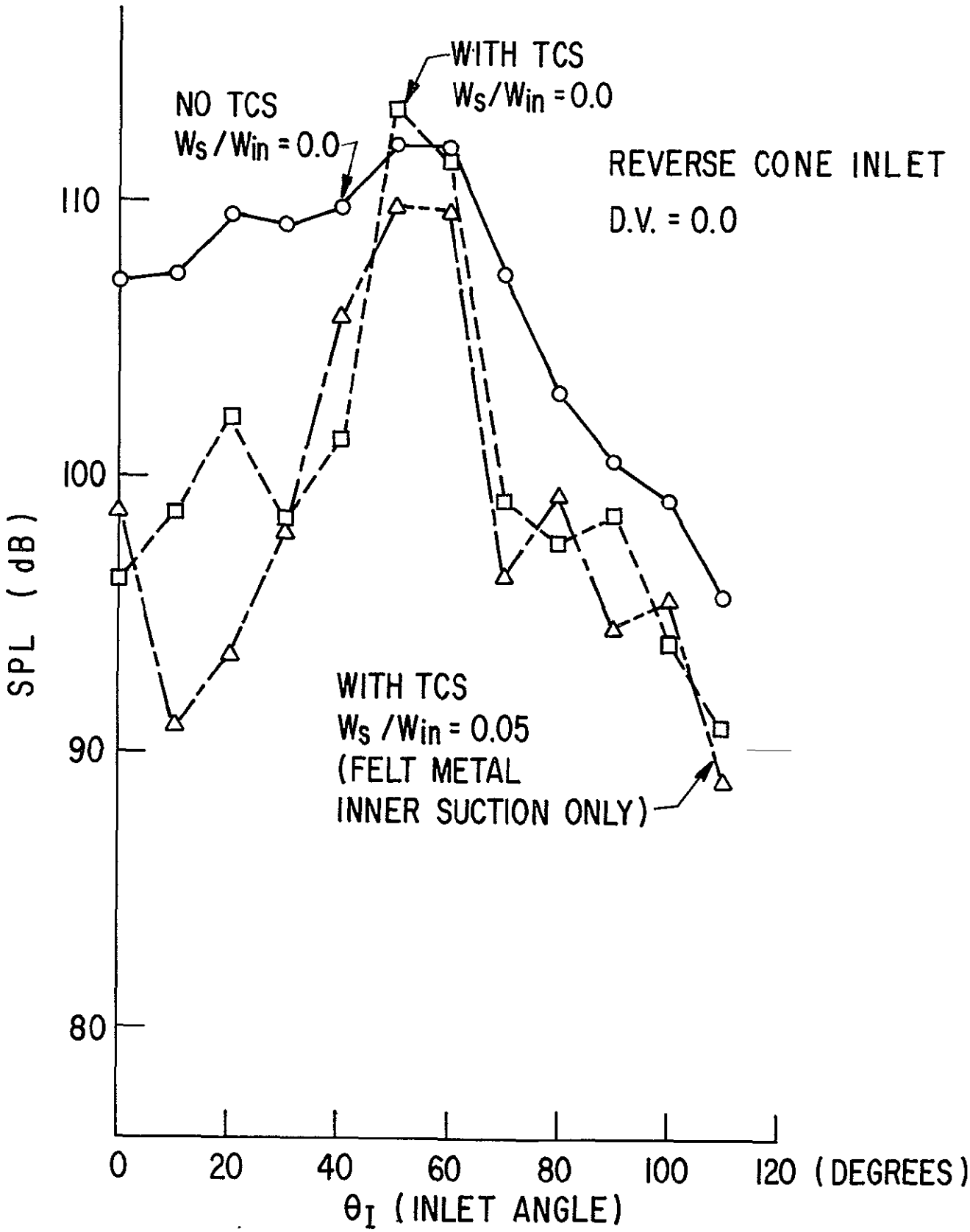

FIG. 45 1/3 OCTAVE SPL DIRECTIVITY AT BLADE PASSING FREQUENCY, 100% SPEED

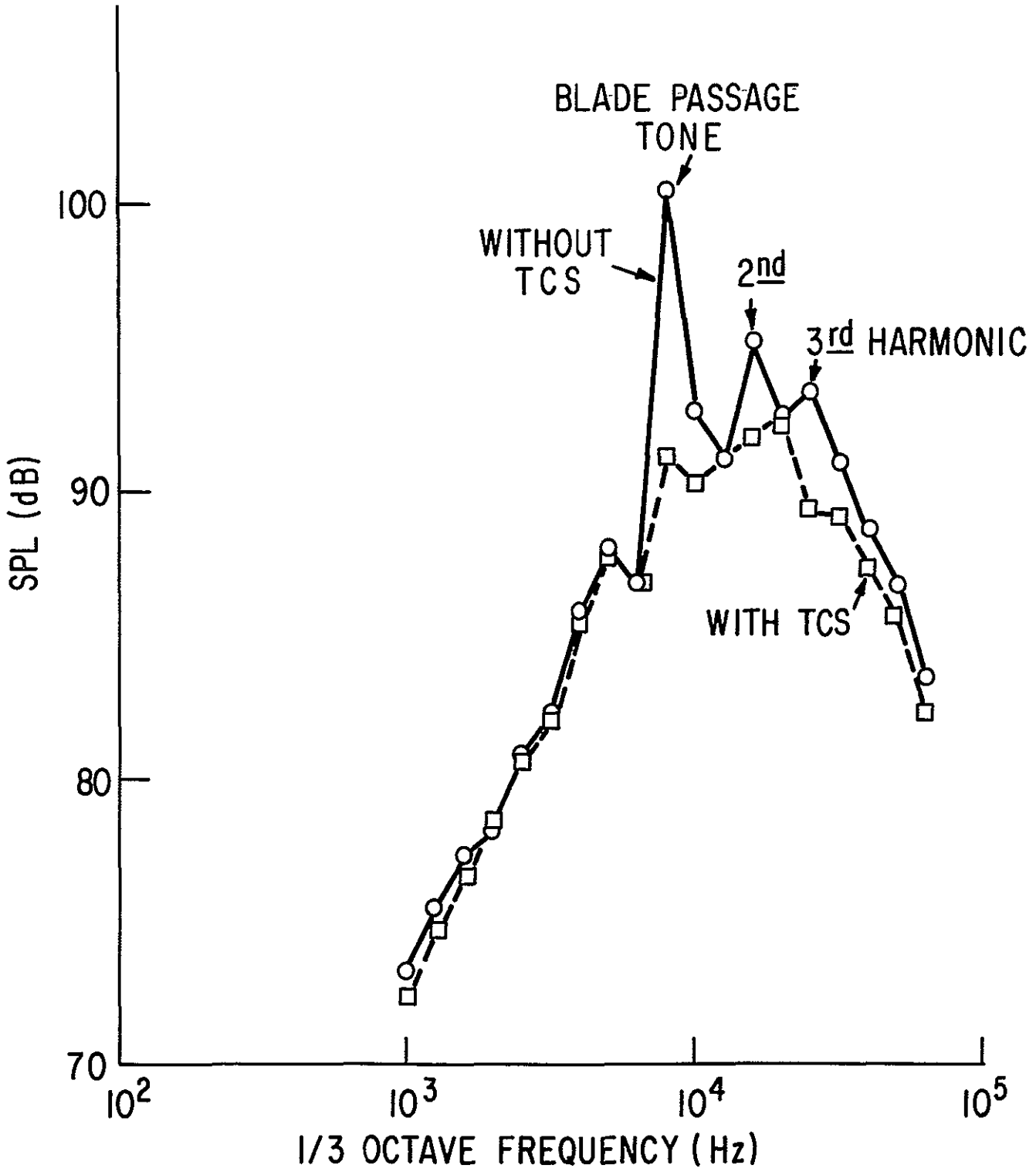

FIGURE 46 SOUND PRESSURE SPECTRA AT θ = 70°, EFFORT OF TCS AT D.V. = 1.27, 74% SPEED

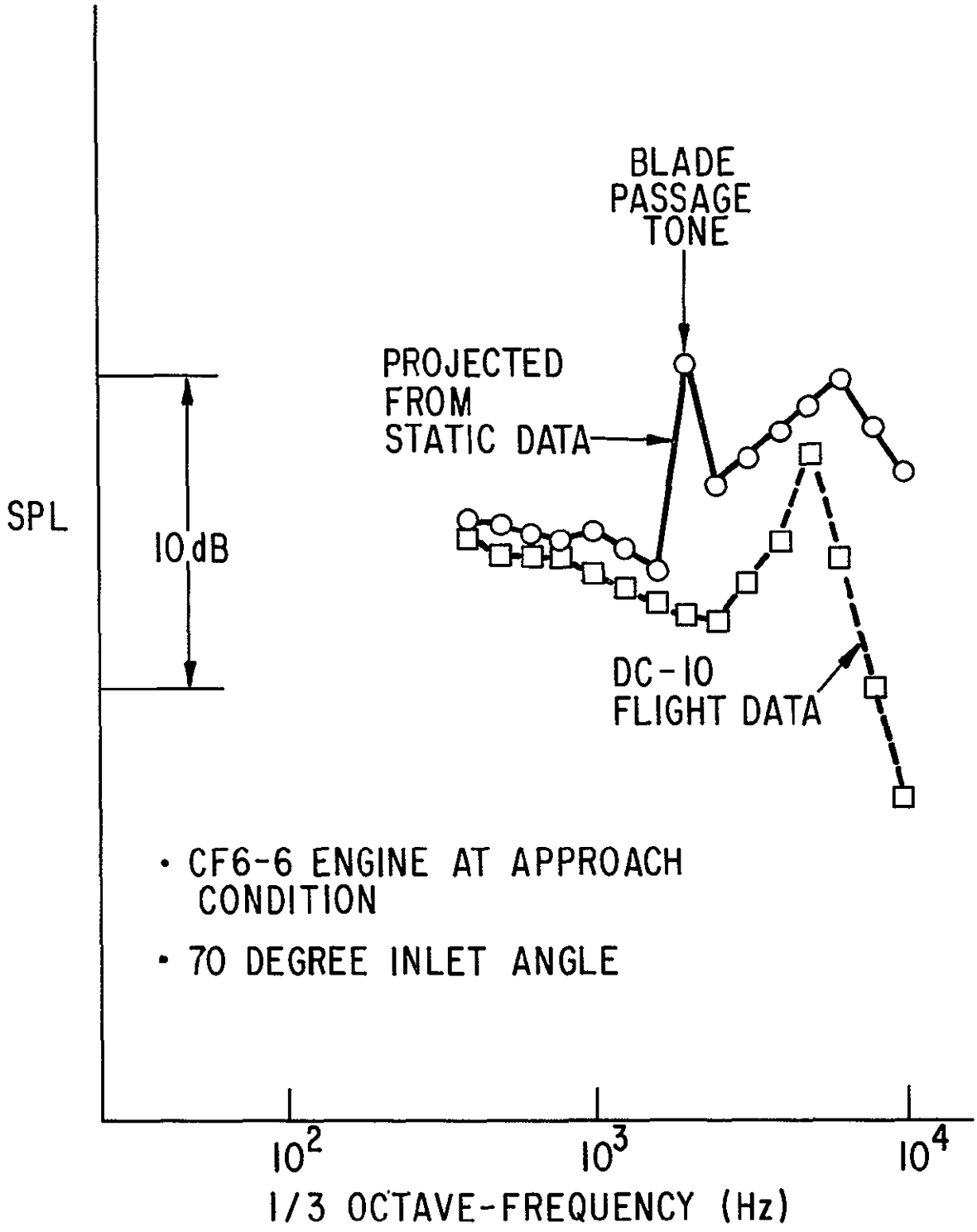

FIG. 47 NOISE COMPARISON FLIGHT TO STATIC

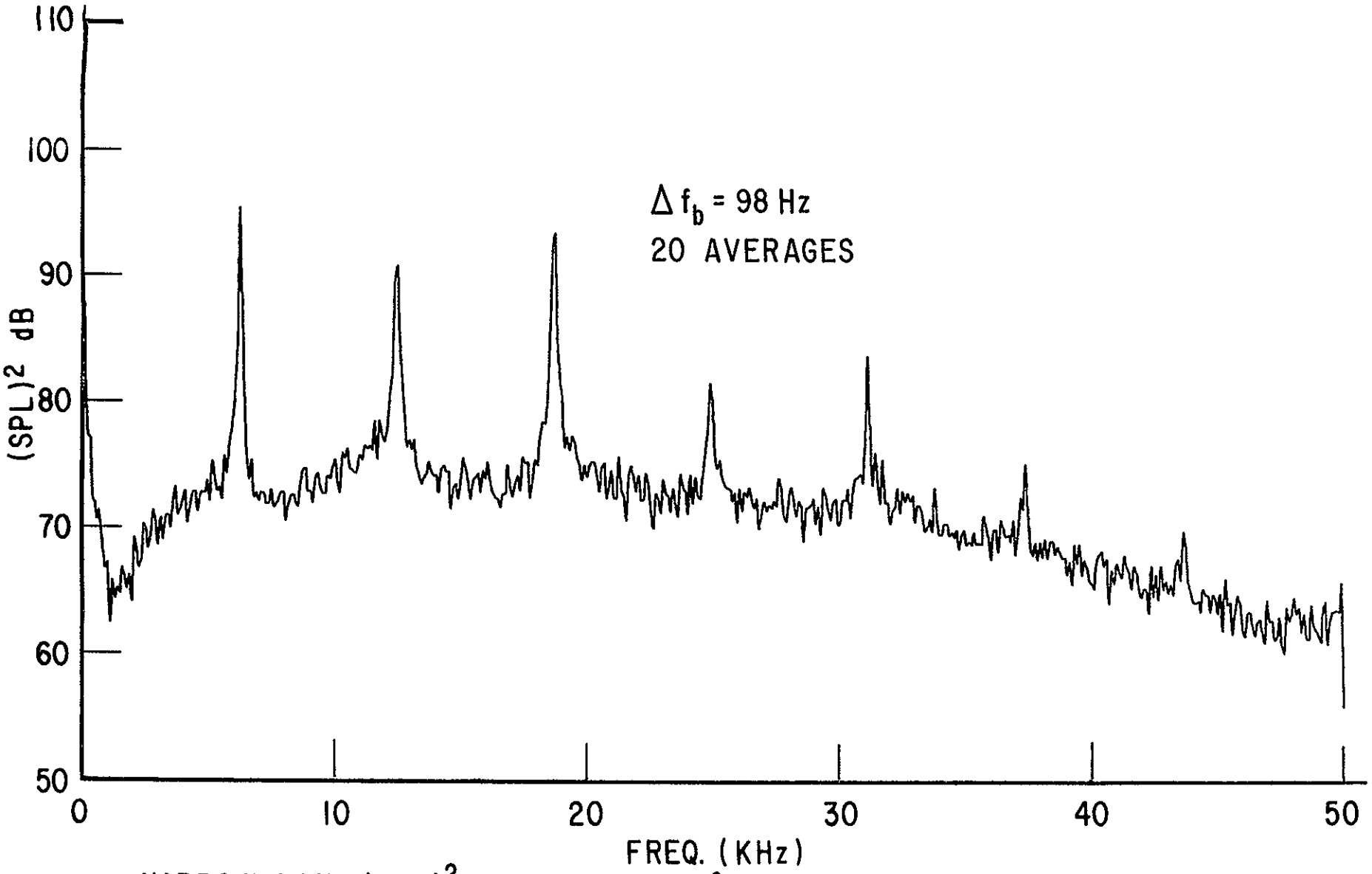

NARROW BAND $(SPL)^2$ SPECTRUM AT θ = 60°, OUTER HARDWALL, HARDWALL INNER SUCTION SURFACE, NO SUCTION, NO TCS, 54% SPEED

FIG. 48a

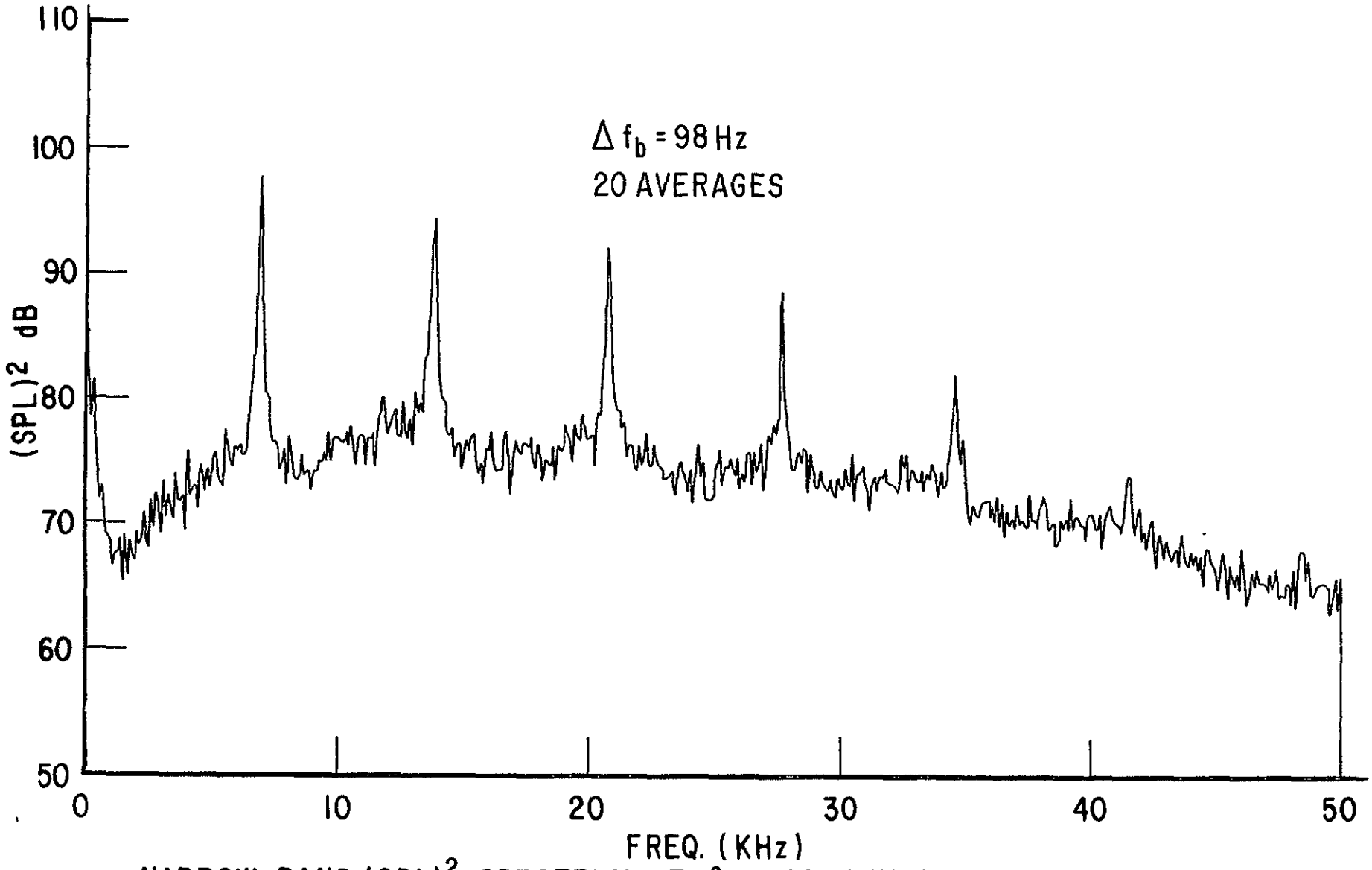

NARROW BAND $(SPL)^2$ SPECTRUM AT $\theta = 60°$, OUTER HARDWALL, HARDWALL INNER SUCTION SURFACE, NO SUCTION, NO TCS, 60% SPEED

FIG. 48b

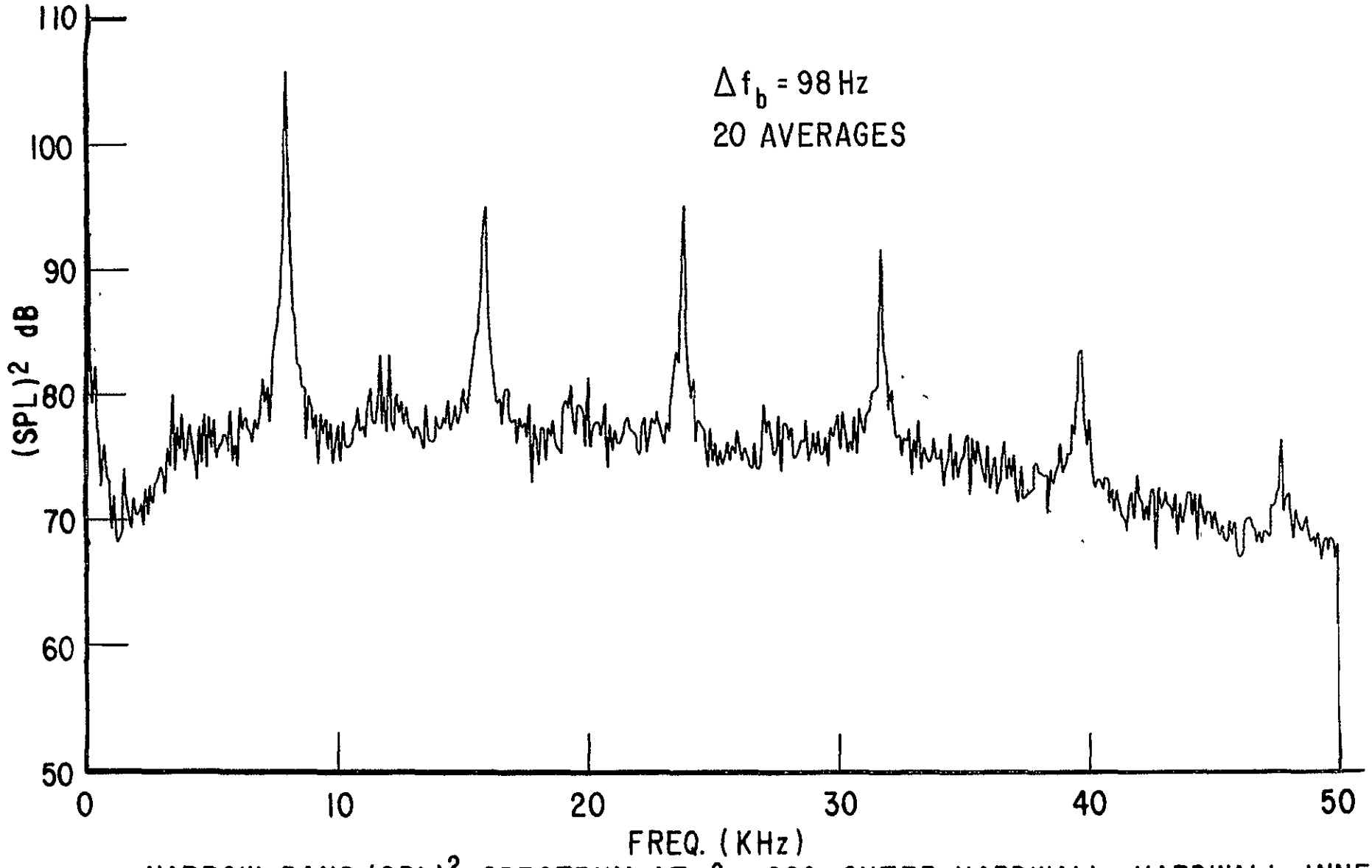

NARROW BAND $(SPL)^2$ SPECTRUM AT $\theta = 60°$, OUTER HARDWALL, HARDWALL INNER SUCTION SURFACE, NO SUCTION, NO TCS, 69% SPEED

FIG. 48c

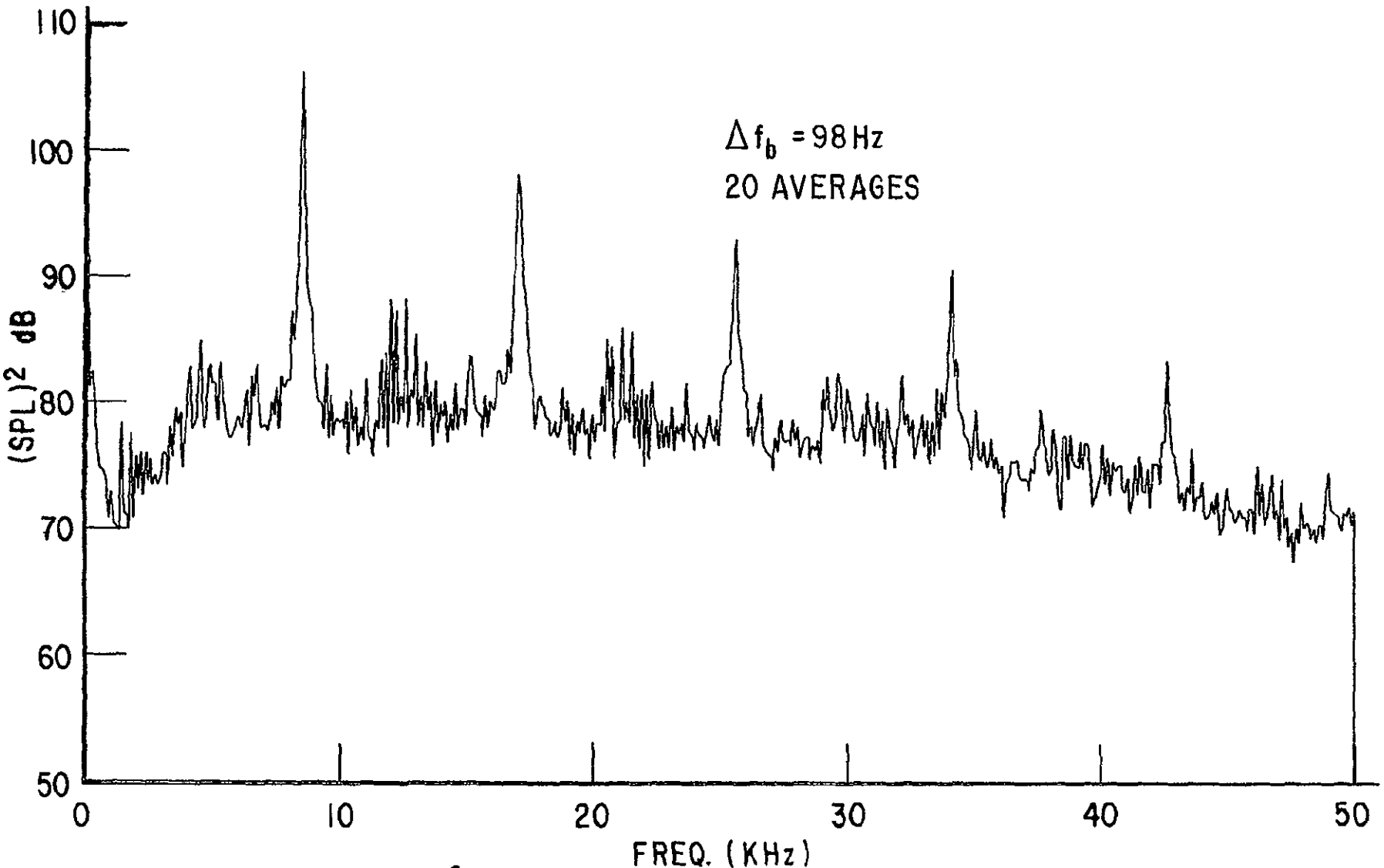

NARROW BAND $(SPL)^2$ SPECTRUM AT $\theta = 60°$, OUTER HARDWALL, HARDWALL INNER SUCTION SURFACE, NO SUCTION, NO TCS, 74% SPEED

FIG. 48 d

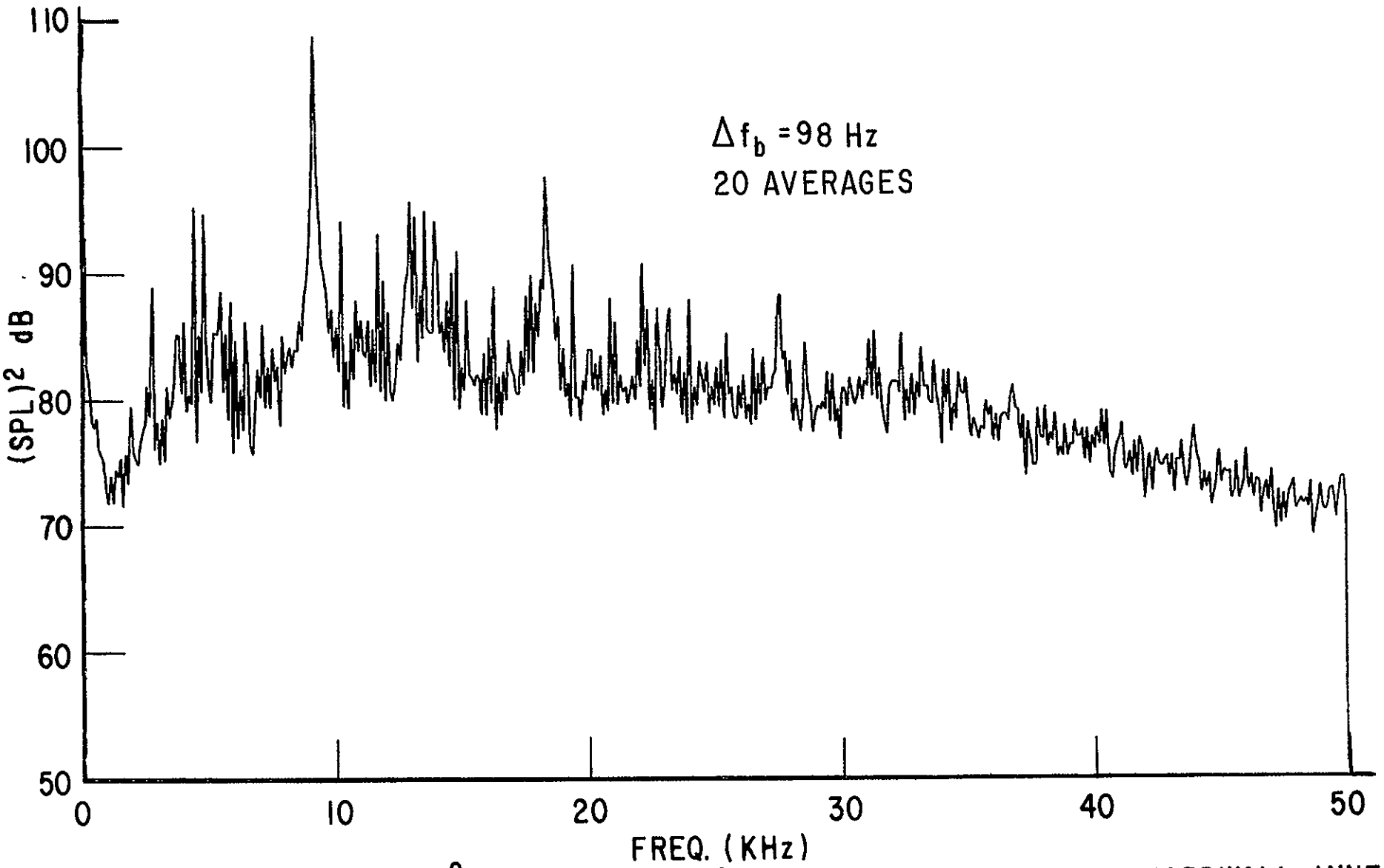

NARROW BAND $(SPL)^2$ SPECTRUM AT $\theta = 60°$, OUTER HARDWALL, HARDWALL INNER SUCTION SURFACE, NO SUCTION, NO TCS, 80% SPEED

FIG. 48e

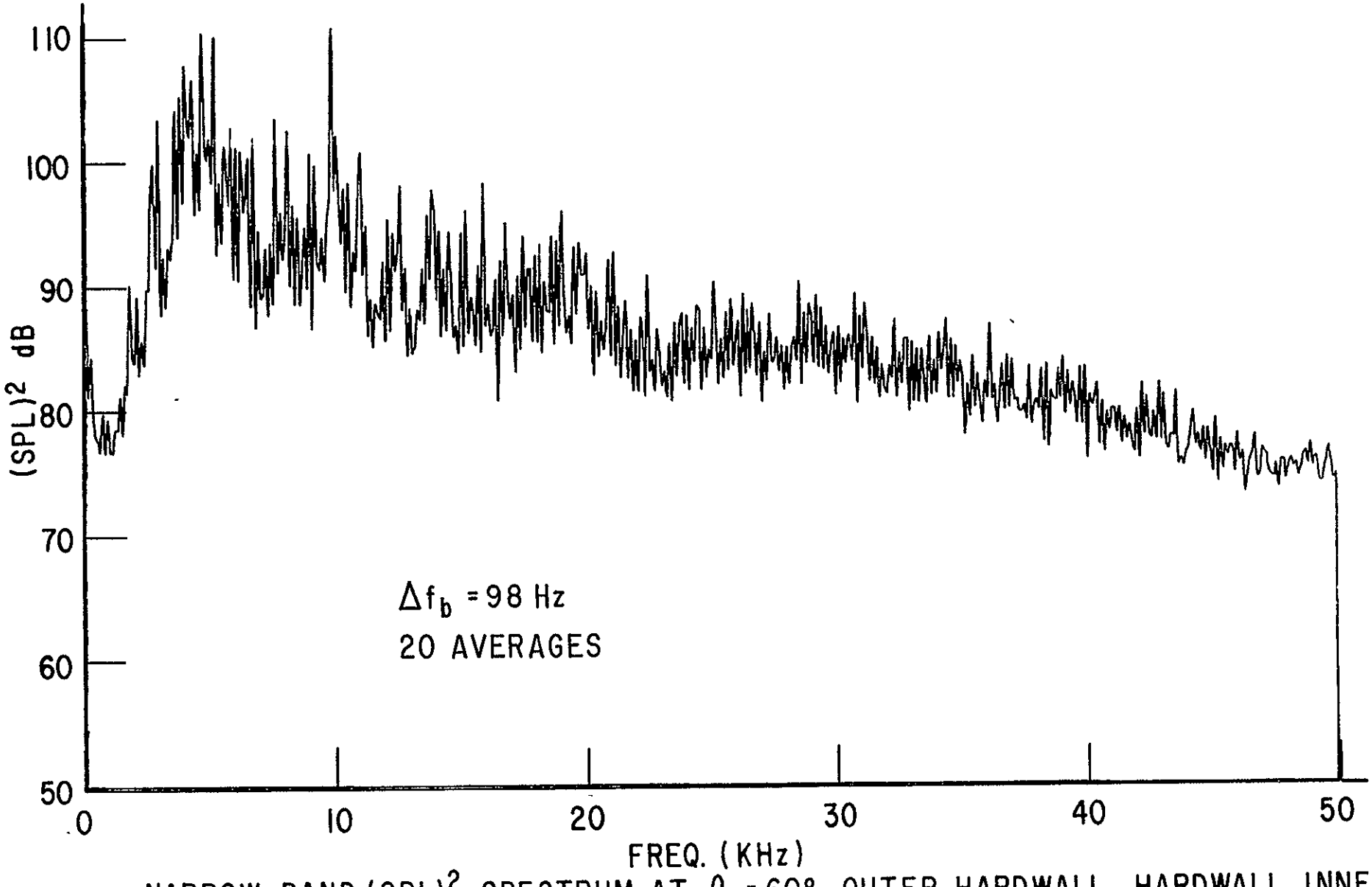

NARROW BAND $(SPL)^2$ SPECTRUM AT θ = 60°, OUTER HARDWALL, HARDWALL INNER SUCTION SURFACE, NO SUCTION, NO TCS, 86% SPEED

FIG. 48 f

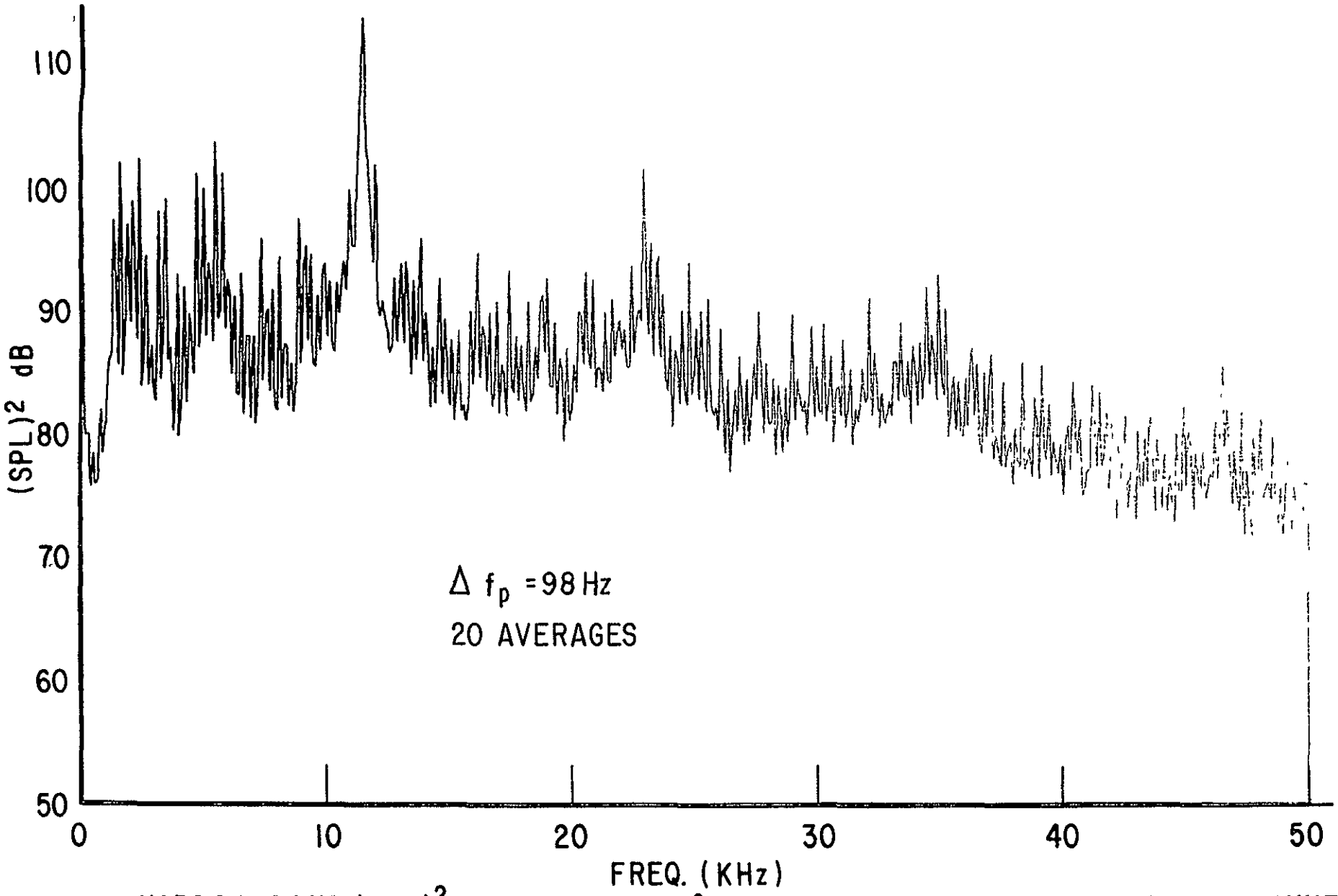

NARROW BAND $(SPL)^2$ SPECTRUM AT $\theta = 60°$, OUTER HARDWALL, HARDWALL INNER SUCTION SURFACE, NO SUCTION, NO TCS, 100% SPEED

FIG. 48g

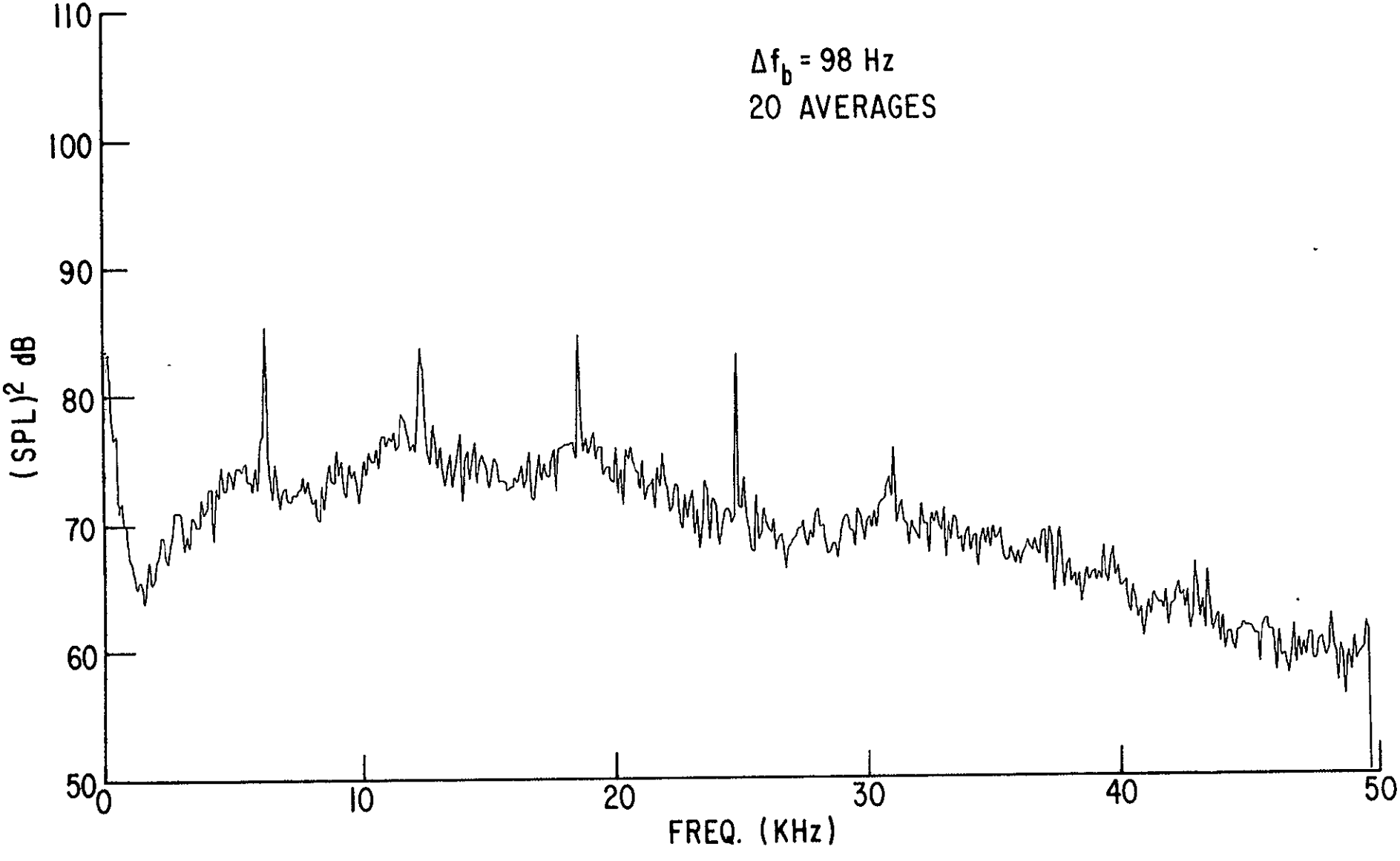

NARROW BAND $(SPL)^2$ SPECTRUM AT θ=60°, OUTER HARDWALL, HARDWALL INNER SUCTION SURFACE, NO SUCTION, WITH TCS, 54% SPEED

FIG. 49 a

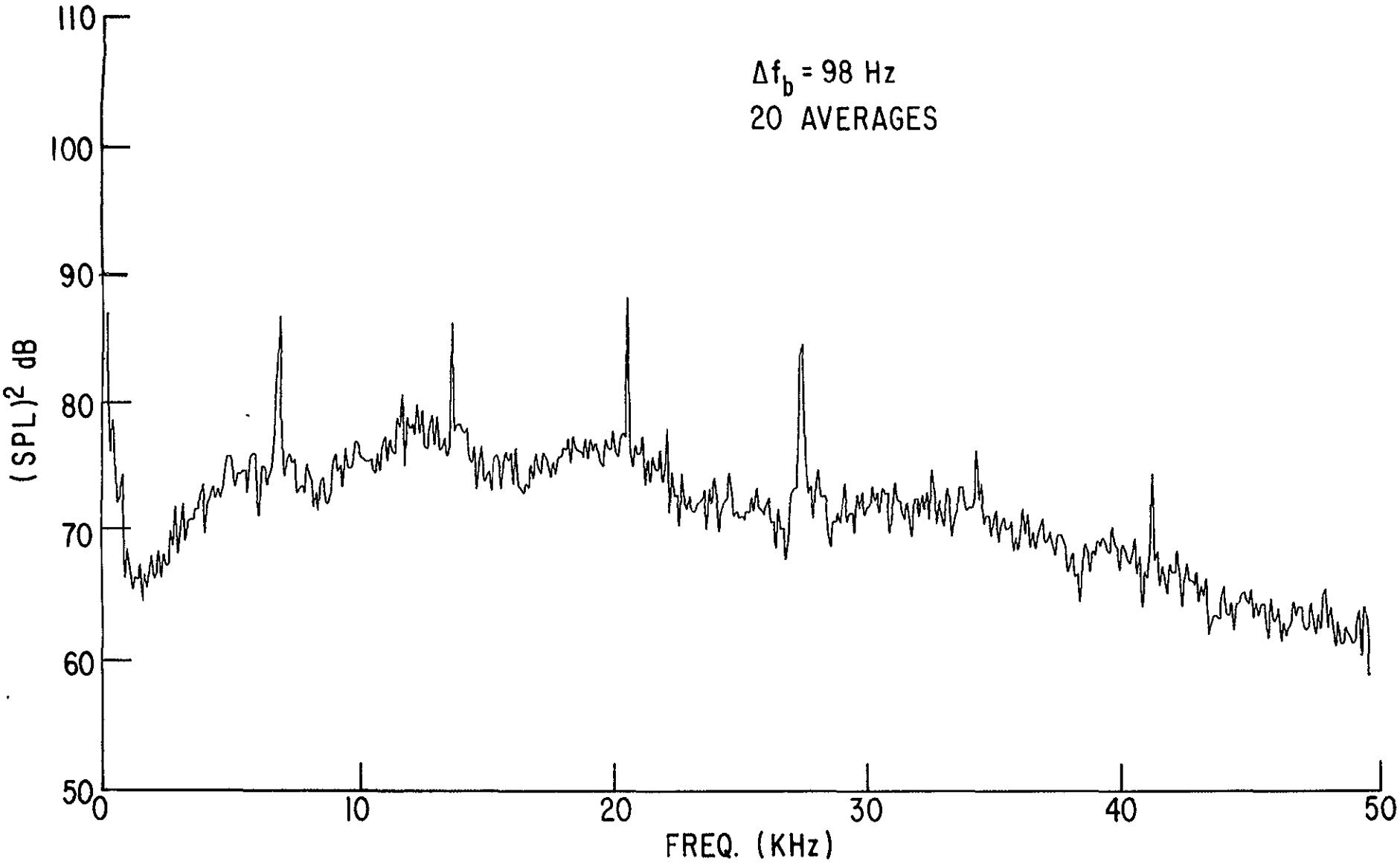

NARROW BAND $(SPL)^2$ SPECTRUM AT θ=60°, OUTER HARDWALL, HARDWALL INNER SUCTION SURFACE, NO SUCTION, WITH TCS, 60% SPEED

FIG. 49b

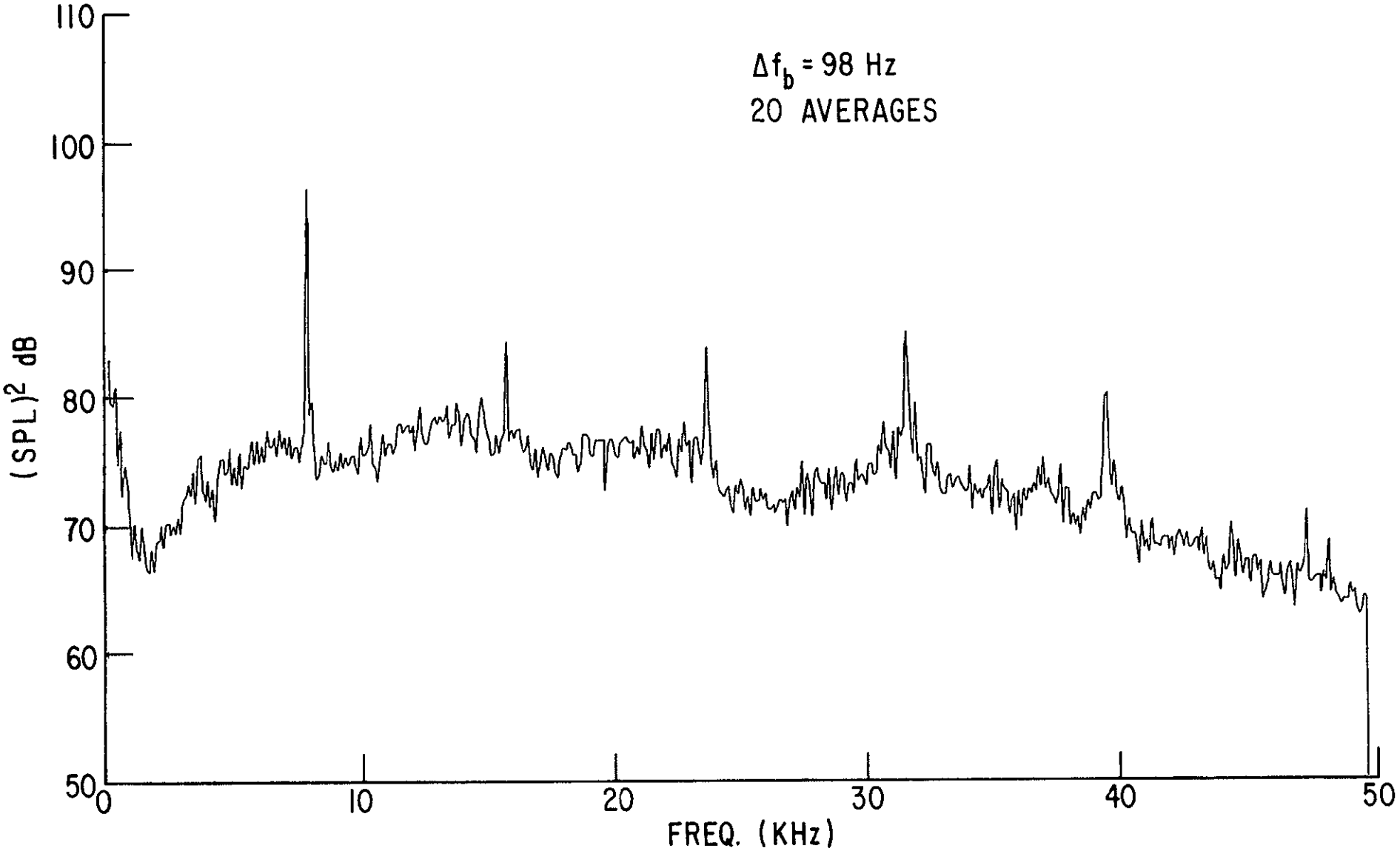

NARROW BAND $(SPL)^2$ SPECTRUM AT θ=60°, OUTER HARDWALL, HARDWALL INNER SUCTION SURFACE, NO SUCTION, WITH TCS, 69% SPEED

FIG. 49 c

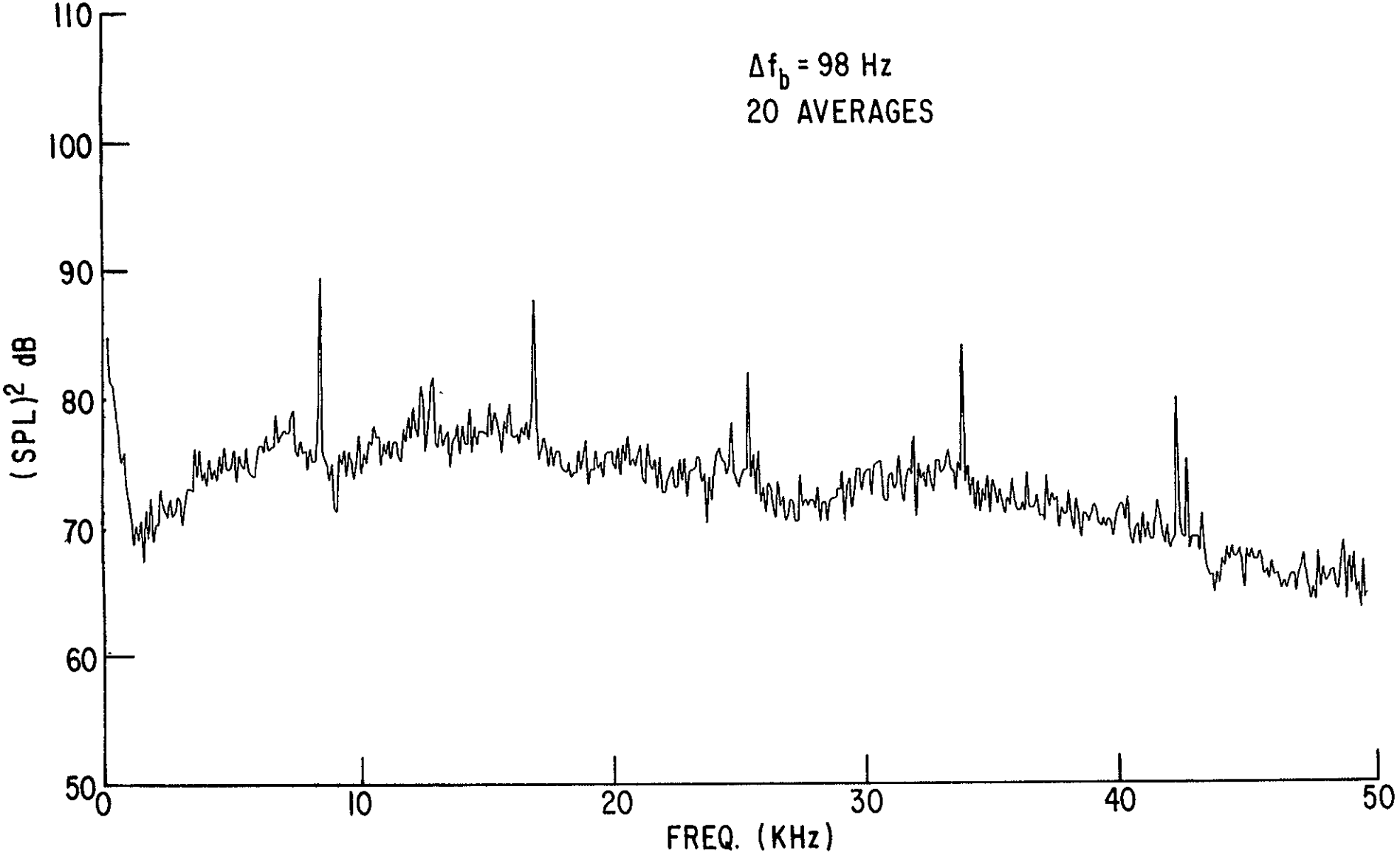

NARROW BAND $(SPL)^2$ SPECTRUM AT θ=60°, OUTER HARDWALL, HARDWALL INNER SUCTION SURFACE, NO SUCTION, WITH TCS, 74% SPEED

FIG. 49 d

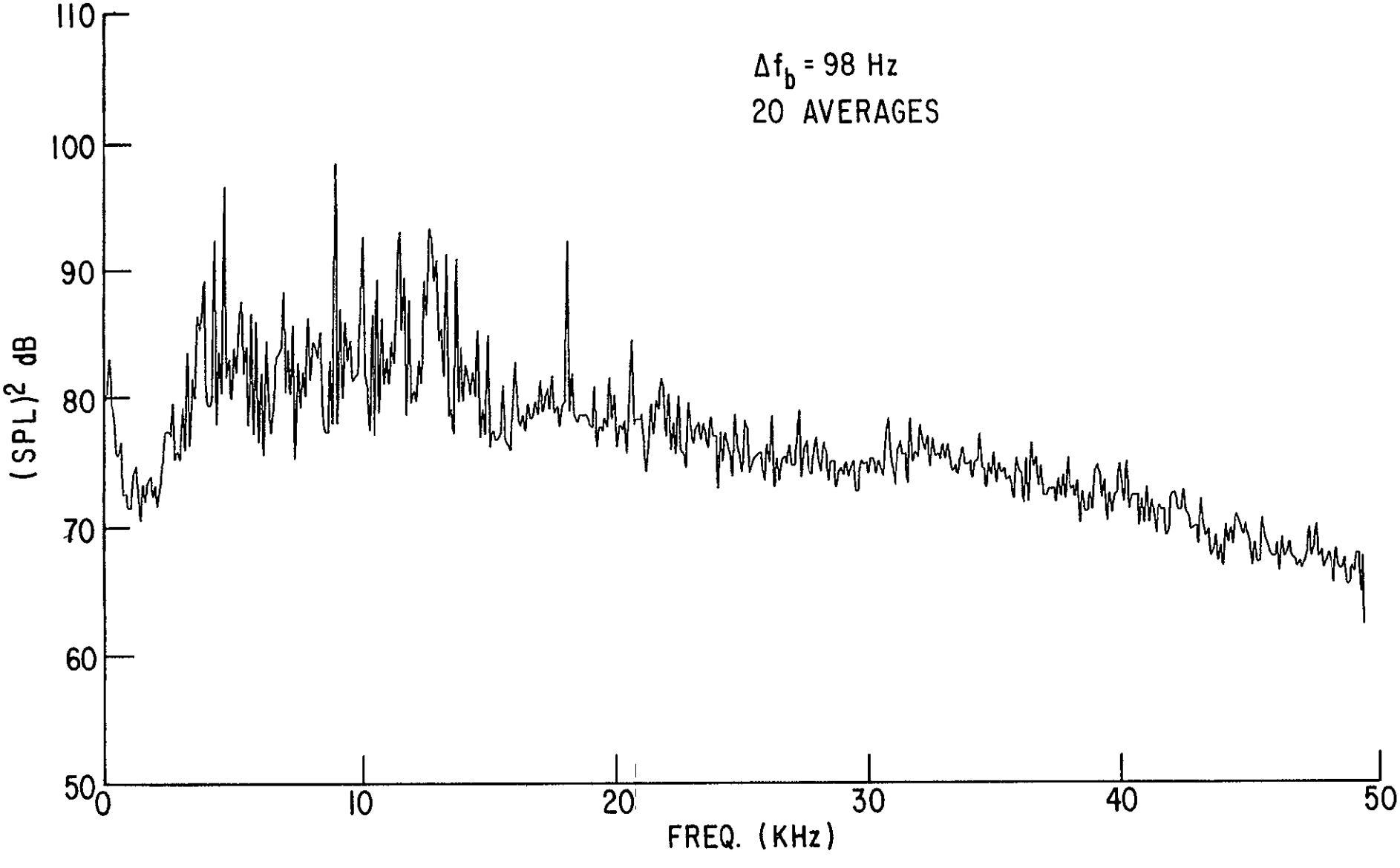

NARROW BAND $(SPL)^2$ SPECTRUM AT θ=60°, OUTER HARDWALL, HARDWALL INNER SUCTION SURFACE, NO SUCTION, WITH TCS, 80% SPEED

FIG. 49 e

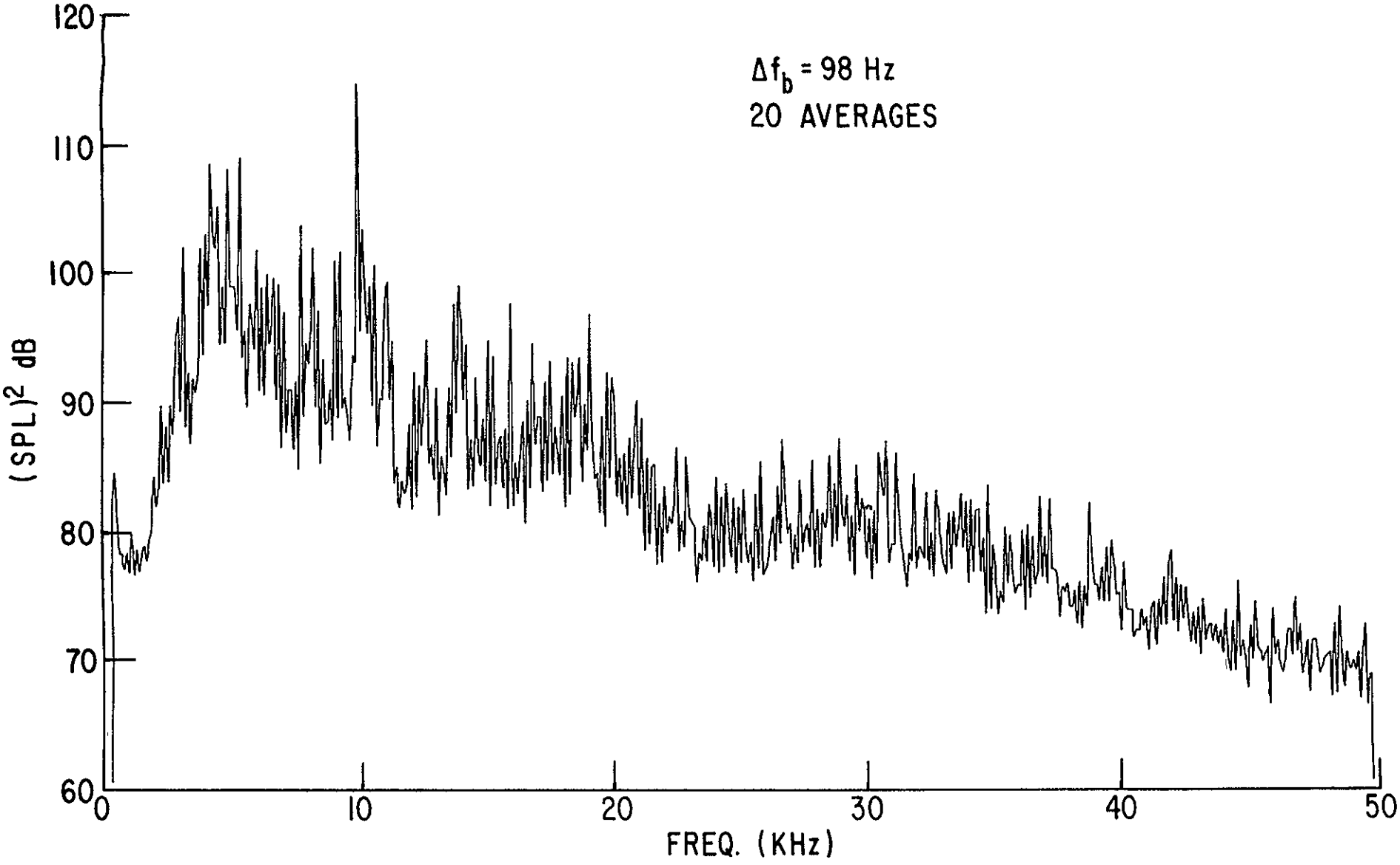

NARROW BAND $(SPL)^2$ SPECTRUM AT $\theta = 60°$, OUTER HARDWALL, HARDWALL INNER SUCTION SURFACE, NO SUCTION, WITH TCS, 86% SPEED

FIG. 49 f

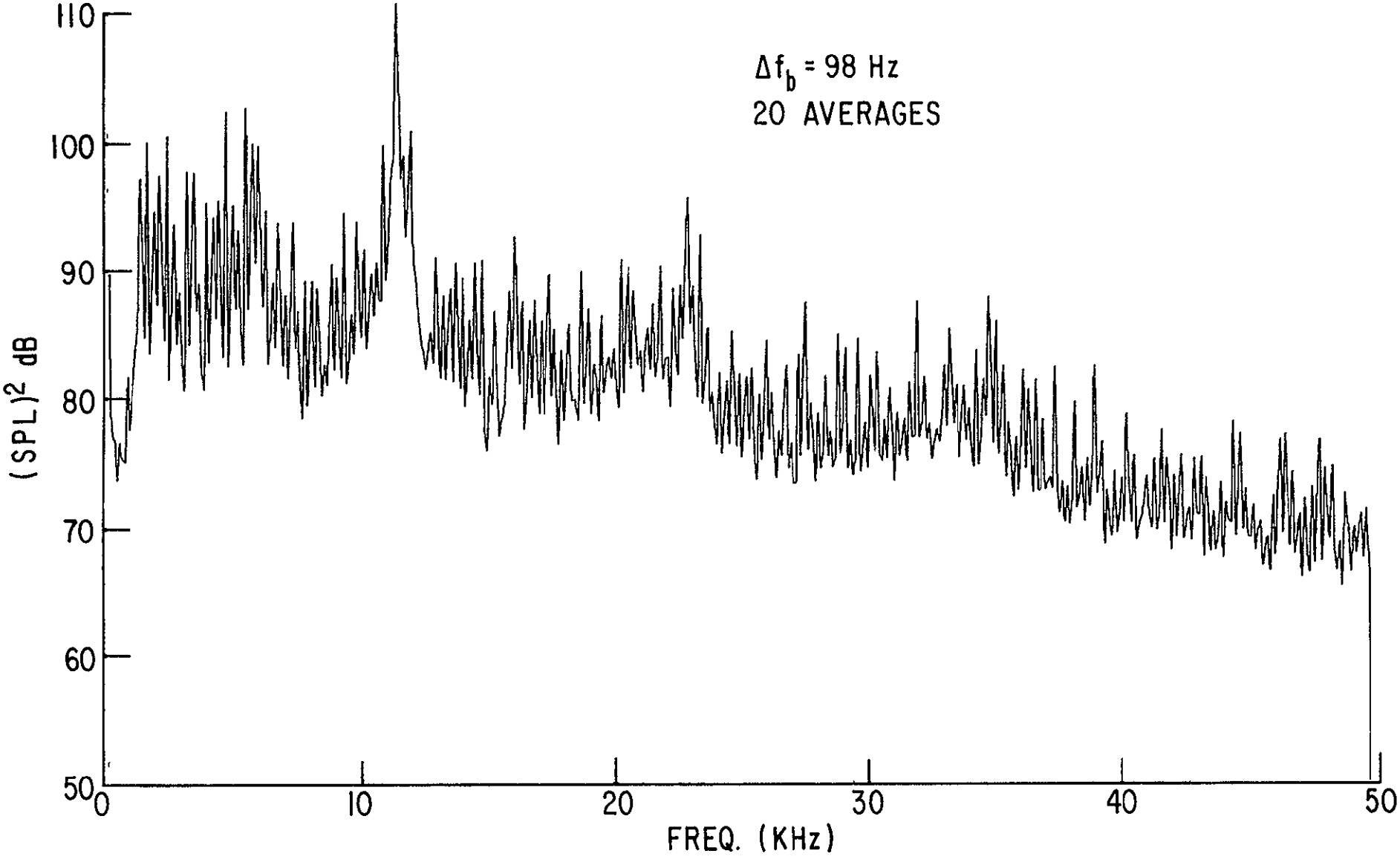

NARROW BAND $(SPL)^2$ SPECTRUM AT θ=60°, OUTER HARDWALL, HARDWALL INNER SUCTION SURFACE, NO SUCTION, WITH TCS, 100% SPEED

FIG. 49g

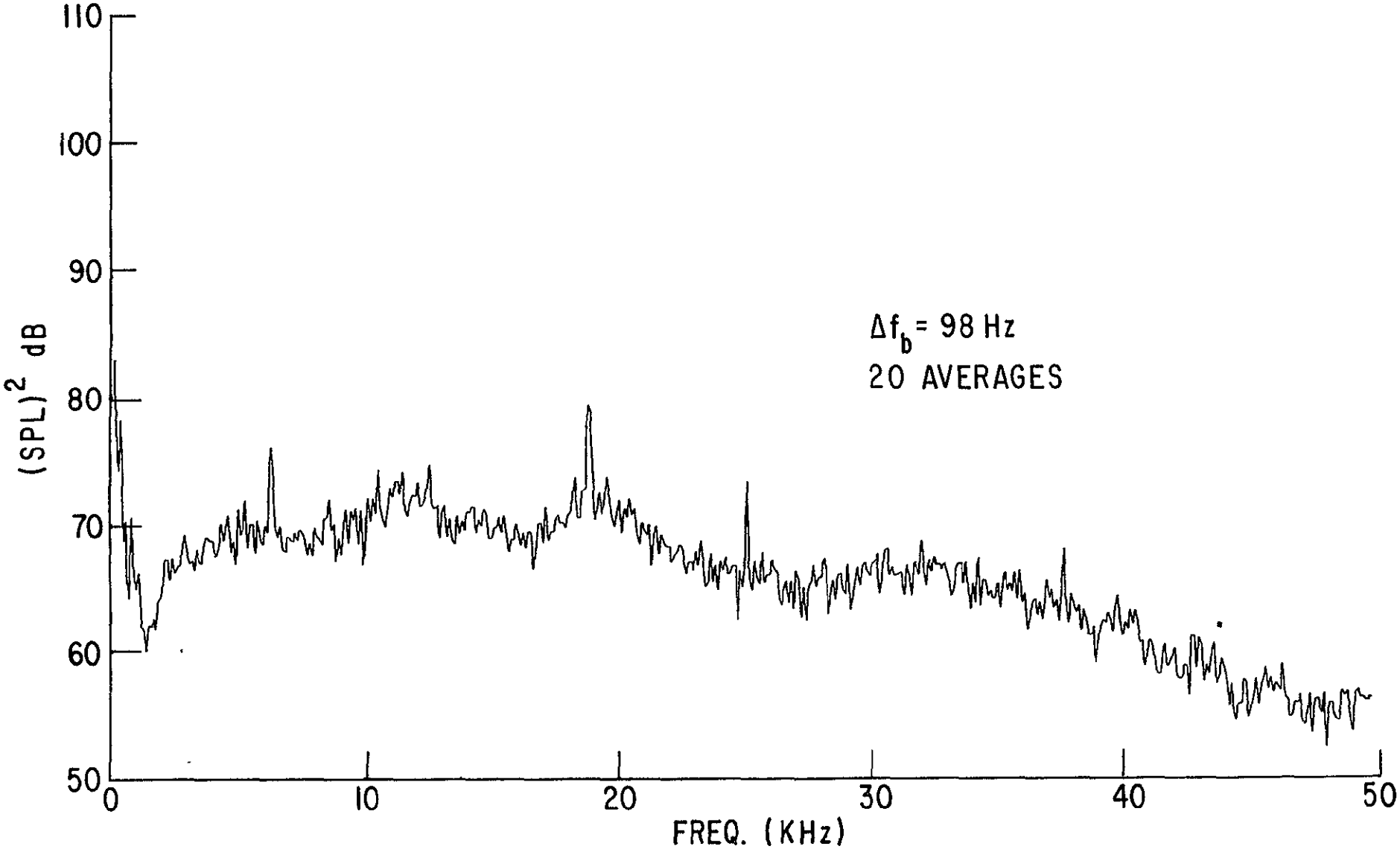

NARROW BAND $(SPL)^2$ SPECTRUM AT $\theta = 60°$, OUTER HARDWALL, FELT METAL INNER SUCTION SURFACE, 8% SUCTION, WITH TCS, 54% SPEED

FIG. 50a

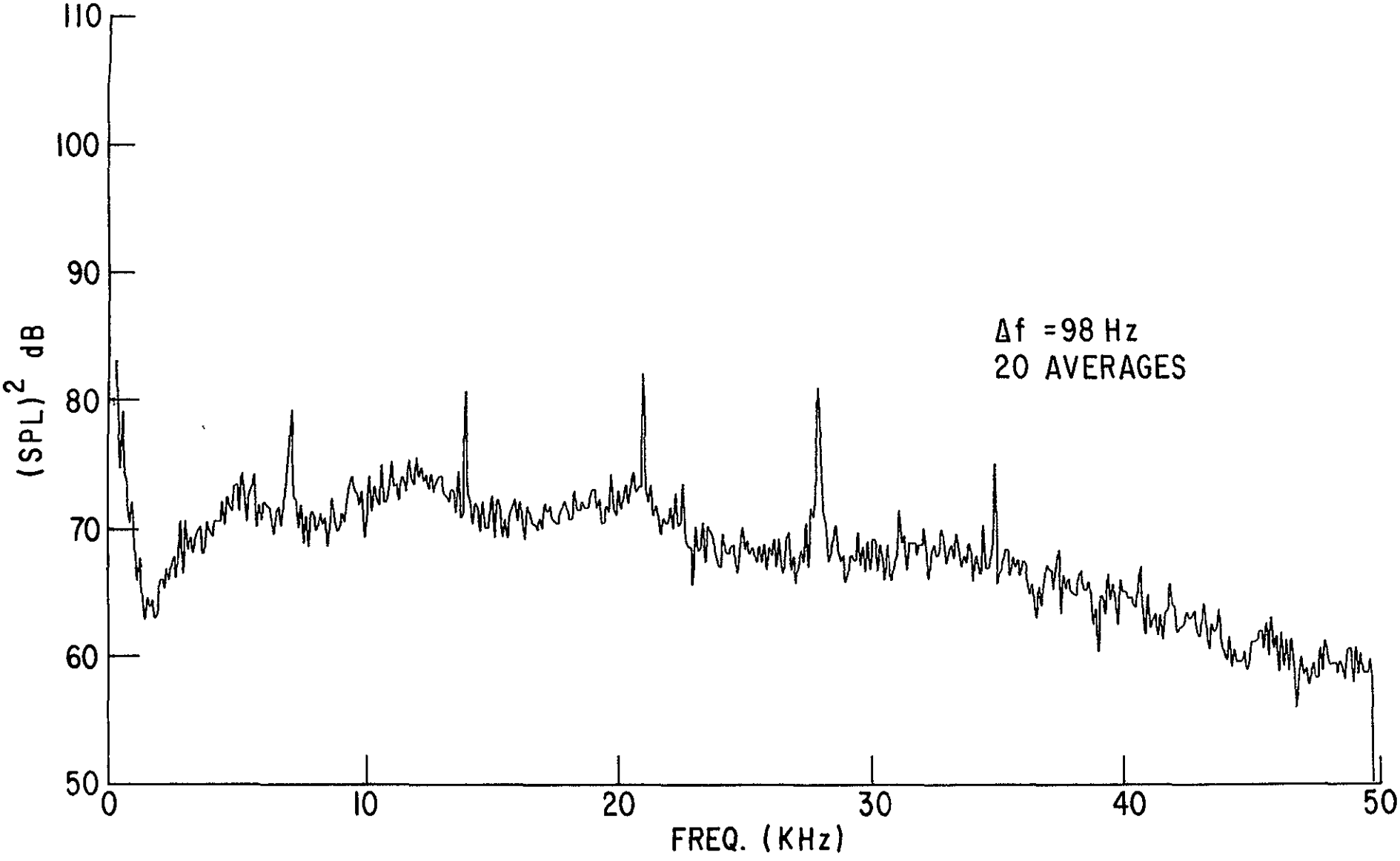

NARROW BAND $(SPL)^2$ SPECTRUM AT $\theta = 60°$, OUTER HARDWALL, FELT METAL INNER SUCTION SURFACE, 8% SUCTION, WITH TCS, 60% SPEED

FIG. 50b

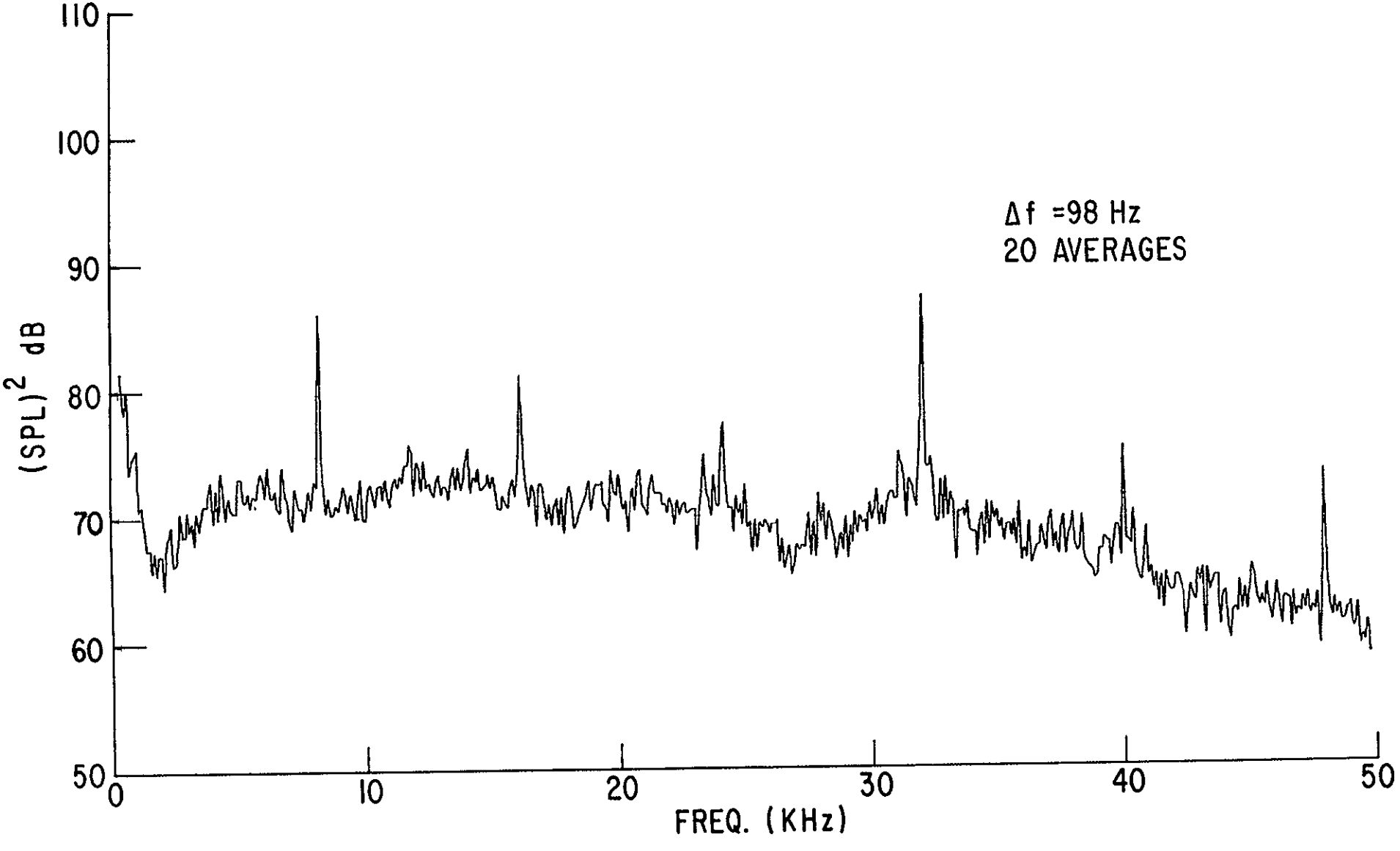

NARROW BAND $(SPL)^2$ SPECTRUM AT $\theta = 60°$, OUTER HARDWALL, FELT METAL INNER SUCTION SURFACE, 7.2% SUCTION, WITH TCS, 69% SPEED

FIG. 50 c

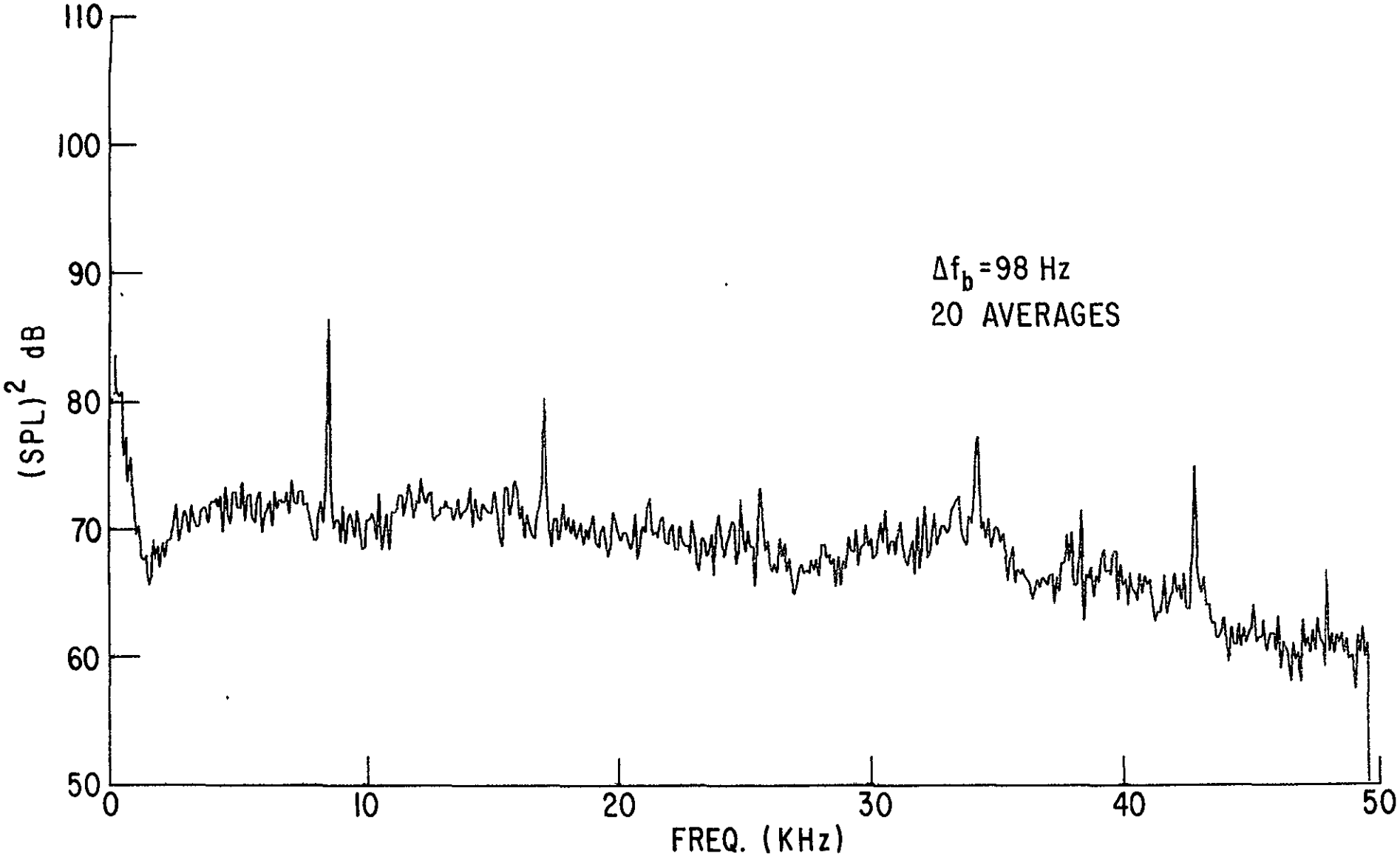

NARROW BAND $(SPL)^2$ SPECTRUM AT $\theta = 60°$, OUTER HARDWALL, FELT METAL INNER SUCTION SURFACE, 6.7% SUCTION, WITH TCS, 74% SPEED

FIG. 50 d

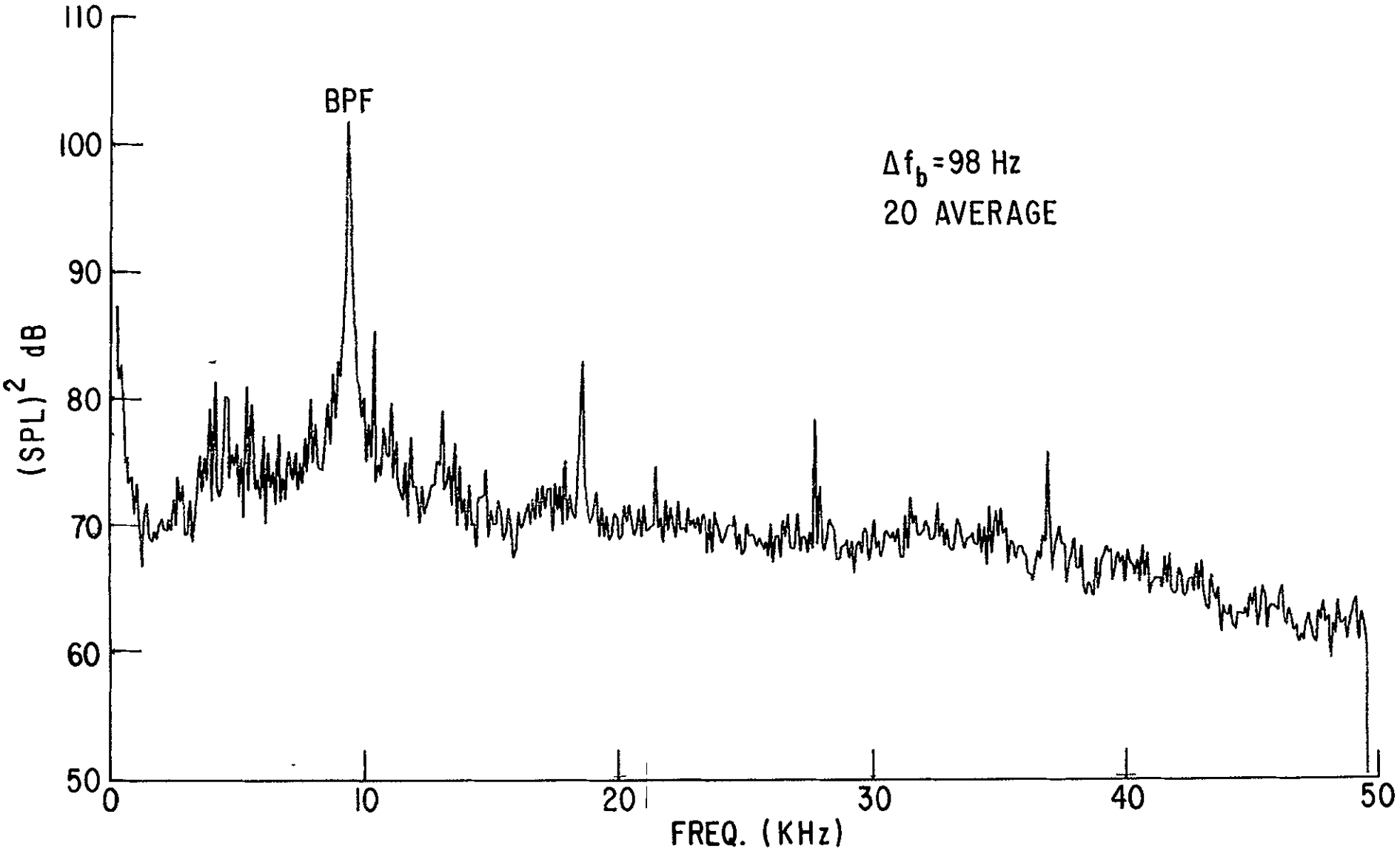

NARROW BAND $(SPL)^2$ SPECTRUM AT $\theta = 60°$, OUTER HARDWALL, FELT METAL INNER SUCTION SURFACE, 6% SUCTION, WITH TCS, 80% SPEED

FIG. 50e

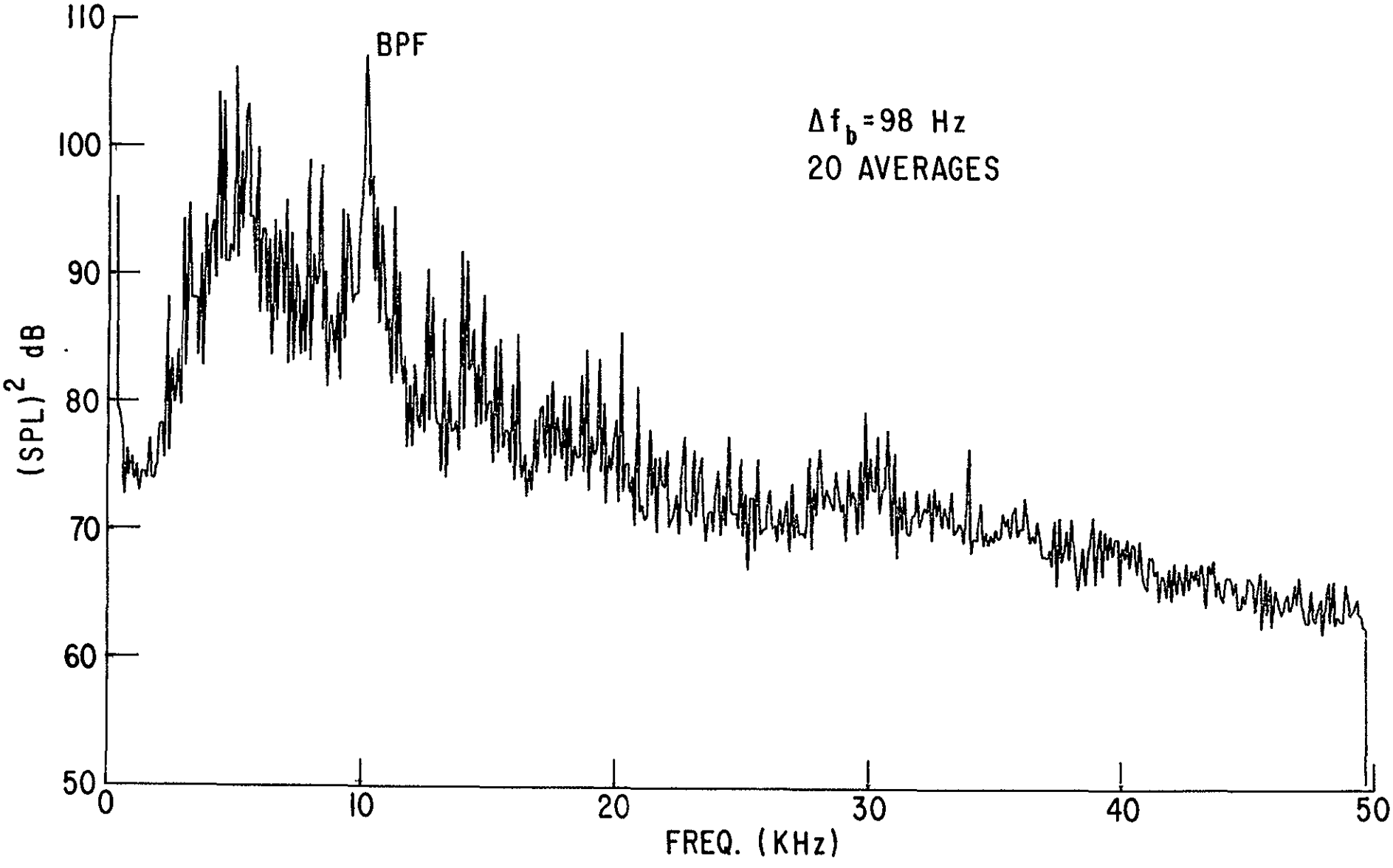

NARROW BAND $(SPL)^2$ SPECTRUM AT $\theta = 60°$, OUTER HARDWALL, FELT METAL INNER SUCTION SURFACE, 5.6% SUCTION, WITH TCS, 86% SPEED

FIG. 50f

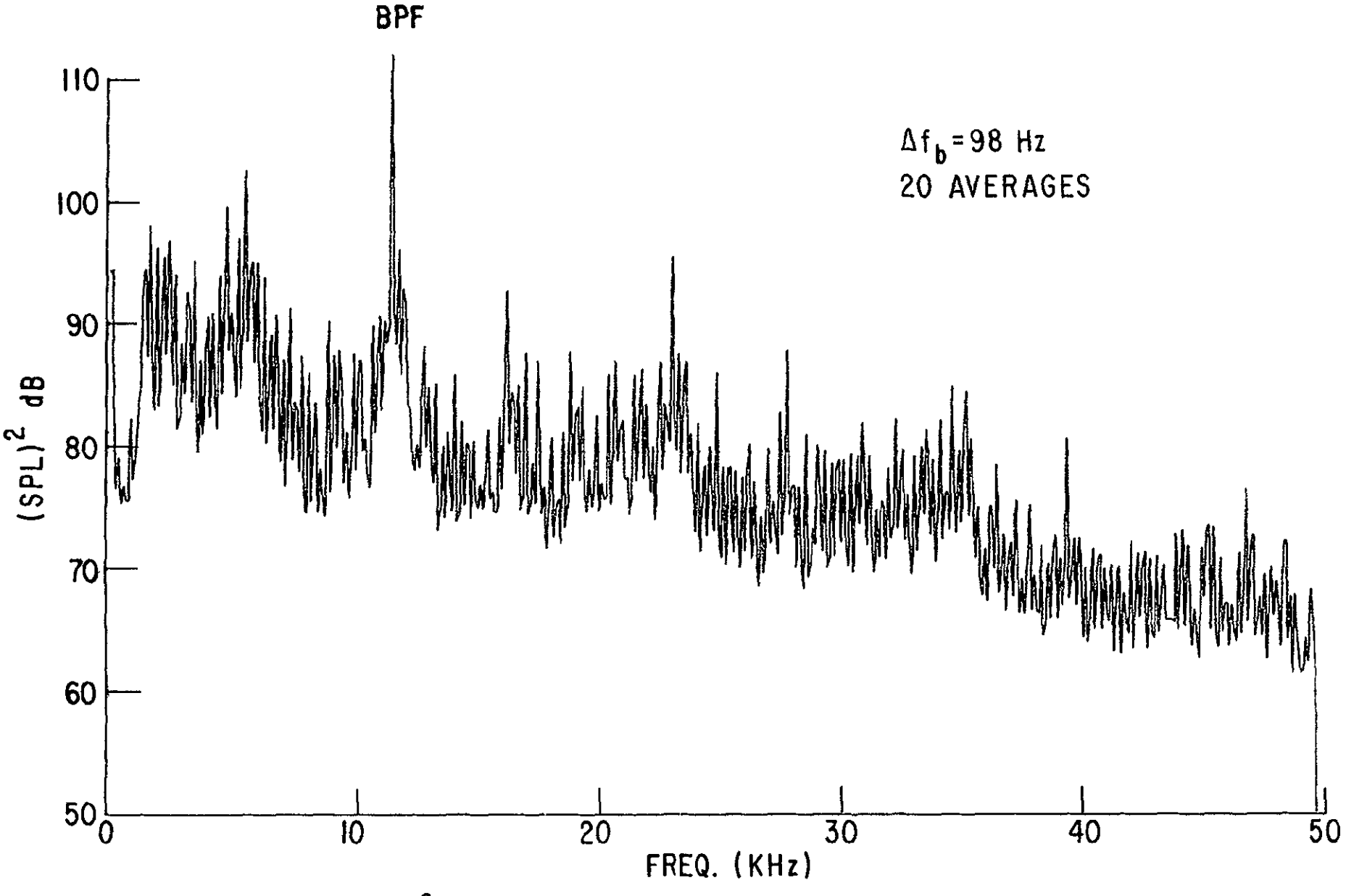

NARROW BAND $(SPL)^2$ SPECTRUM AT $\theta = 60°$, OUTER HARDWALL, FELT METAL INNER SUCTION SURFACE, 5% SUCTION, WITH TCS, 100% SPEED

FIG. 50g

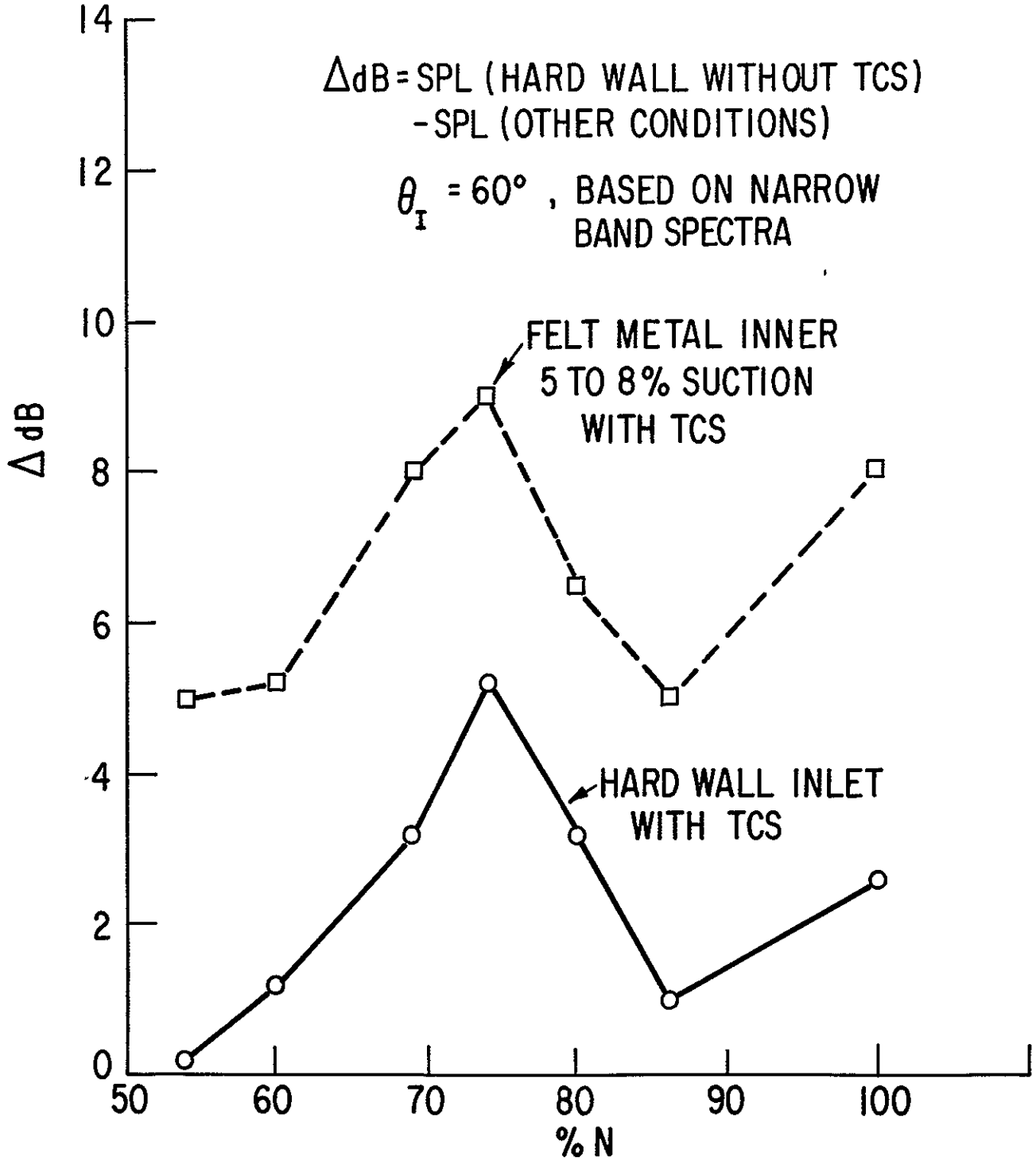

FIGURE 51 REDUCTION OF BROAD BAND SPL AT BPF DUE TO TCS AND SUCTION

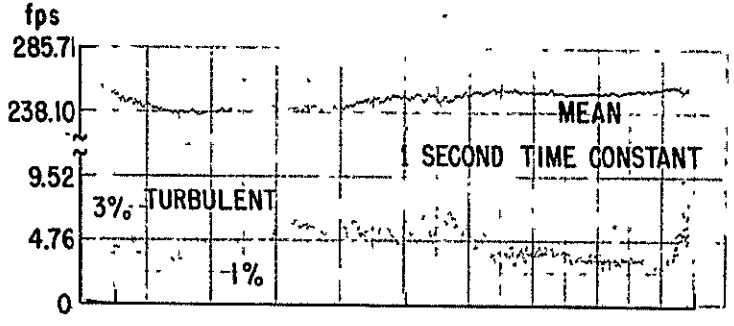

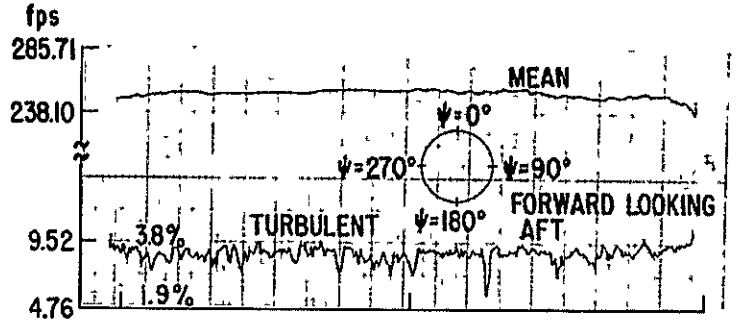

NO SUCTION

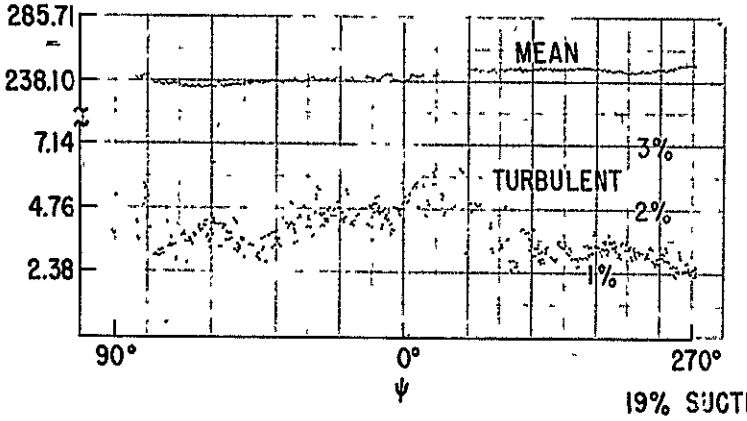

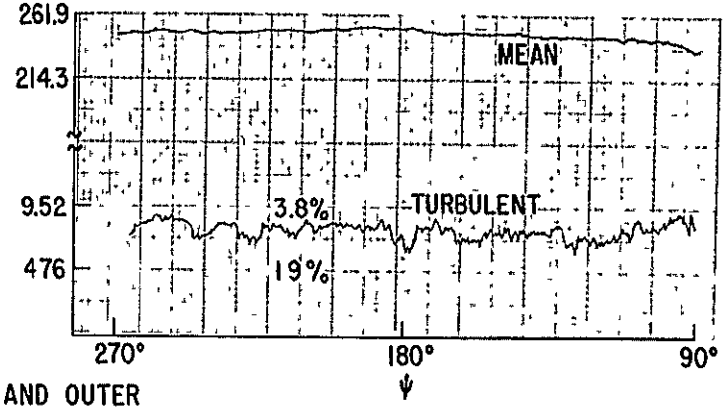

19% SUCTION, INNER AND OUTER

CIRCUMFERENTIAL DISTRIBUTION OF MEAN AND FLUCTUATING VELOCITIES, 69% SPEED, AXIAL VELOCITY, $\Delta r/R_0 = 0.15$, NO TURBULENCE CONTROL STRUCTURE

Figure 52

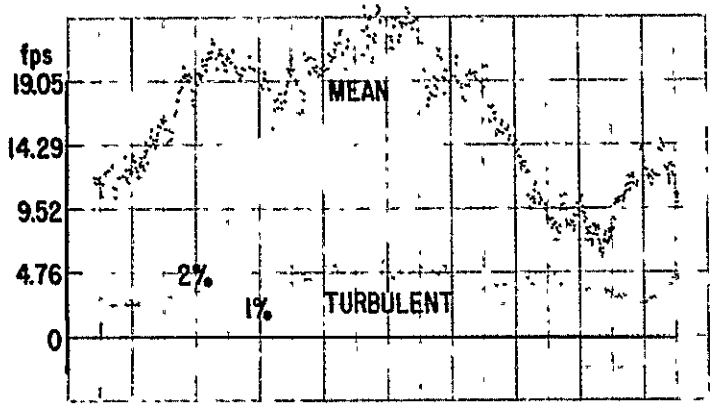

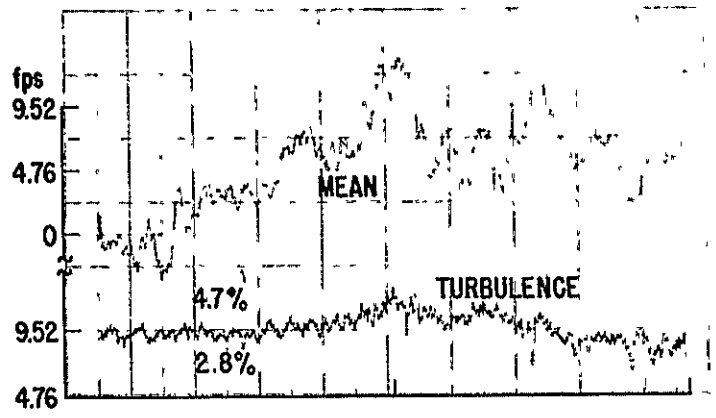

NO SUCTION

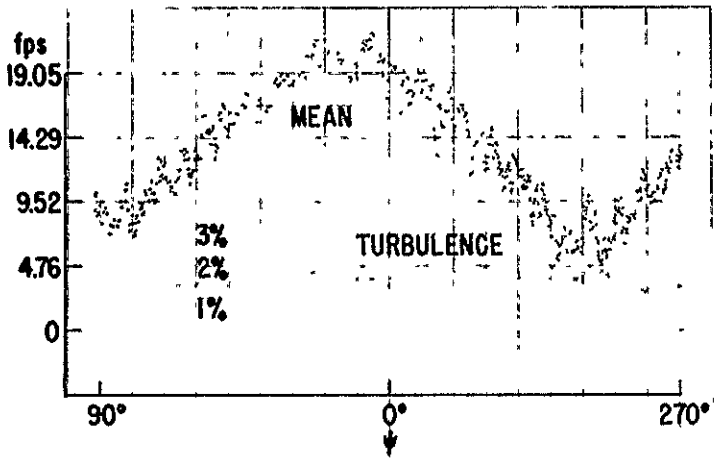

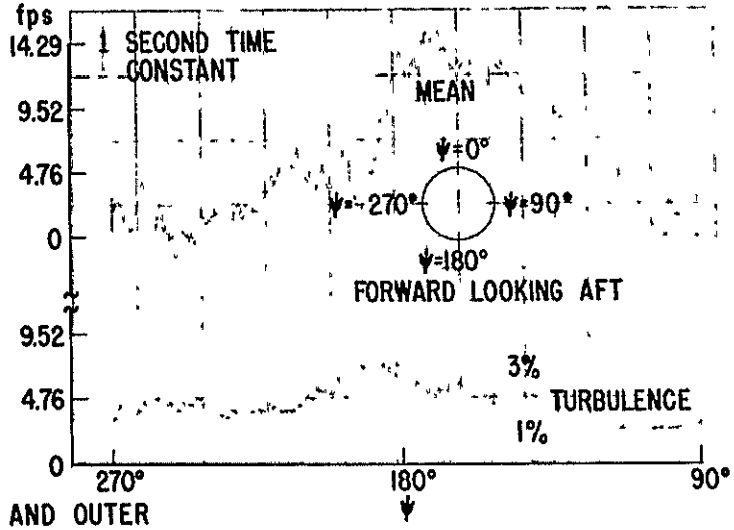

19% SUCTION, INNER AND OUTER

CIRCUMFERENTIAL DISTRIBUTION OF MEAN AND FLUCTUATING VELOCITIES, 69% SPEED, TRANSVERSE VELOCITY, $\Delta r/R_0 = 0.15$, NO TURBULENCE CONTROL STRUCTURE

Figure 53

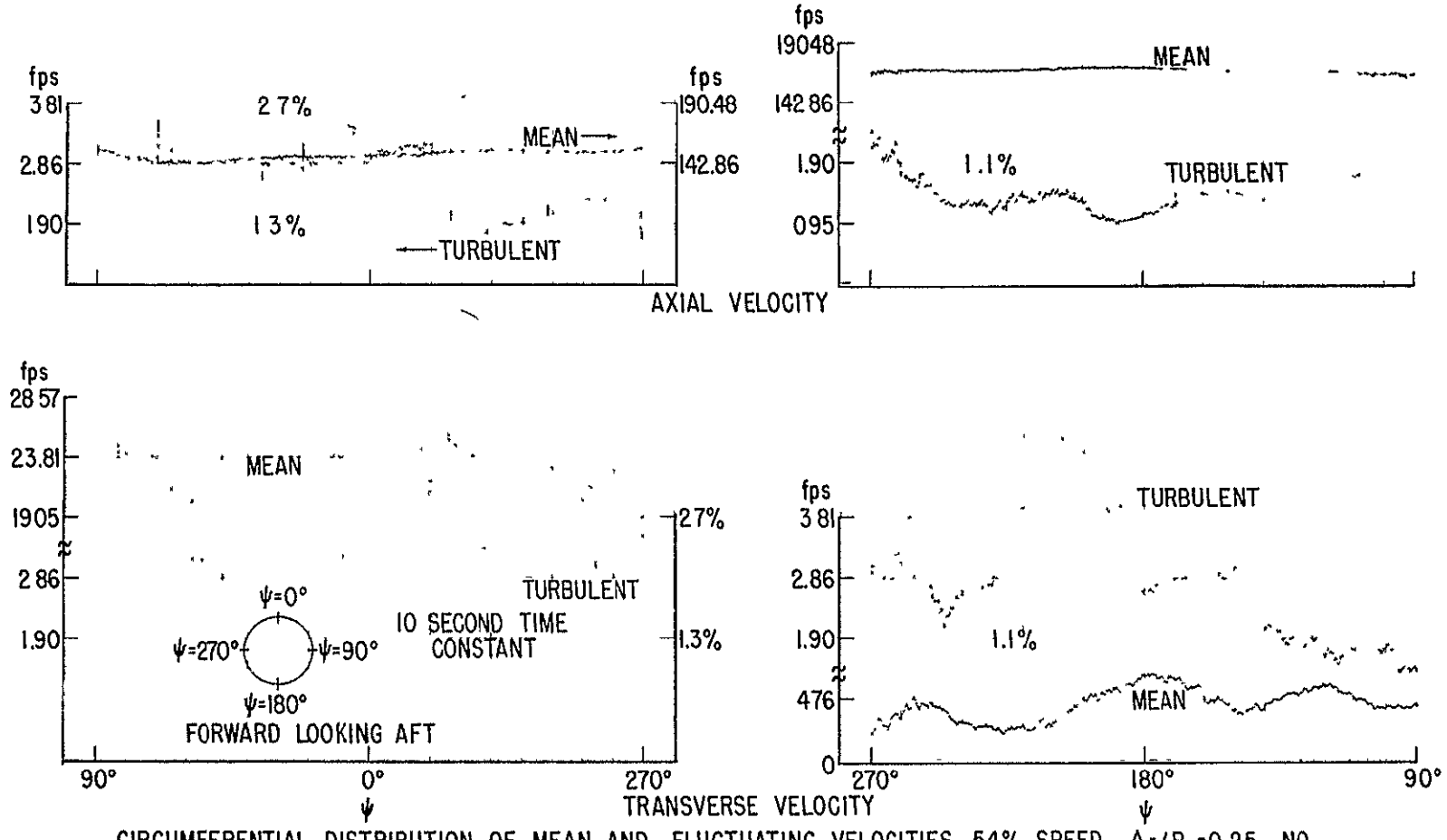

CIRCUMFERENTIAL DISTRIBUTION OF MEAN AND FLUCTUATING VELOCITIES, 54% SPEED, $\Delta r/R_0$=0.25, NO TURBULENCE CONTROL STRUCTURE, NO SUCTION

Figure 54

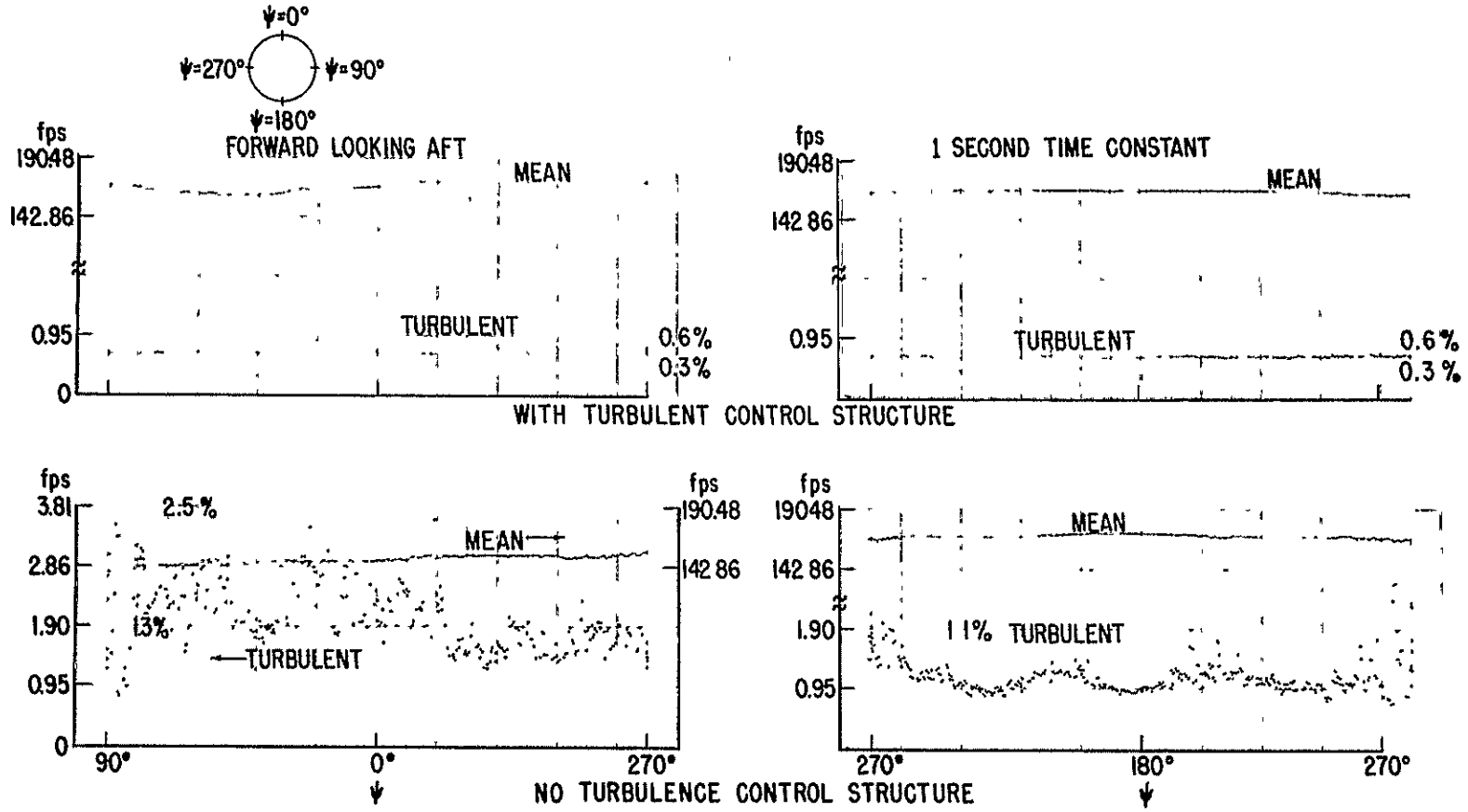

CIRCUMFERENTIAL DISTRIBUTION OF MEAN AND FLUCTUATING VELOCITIES 54% SPEED, AXIAL VELOCITY, $\Delta r/R_0$=0.25, NO SUCTION

Figure 55

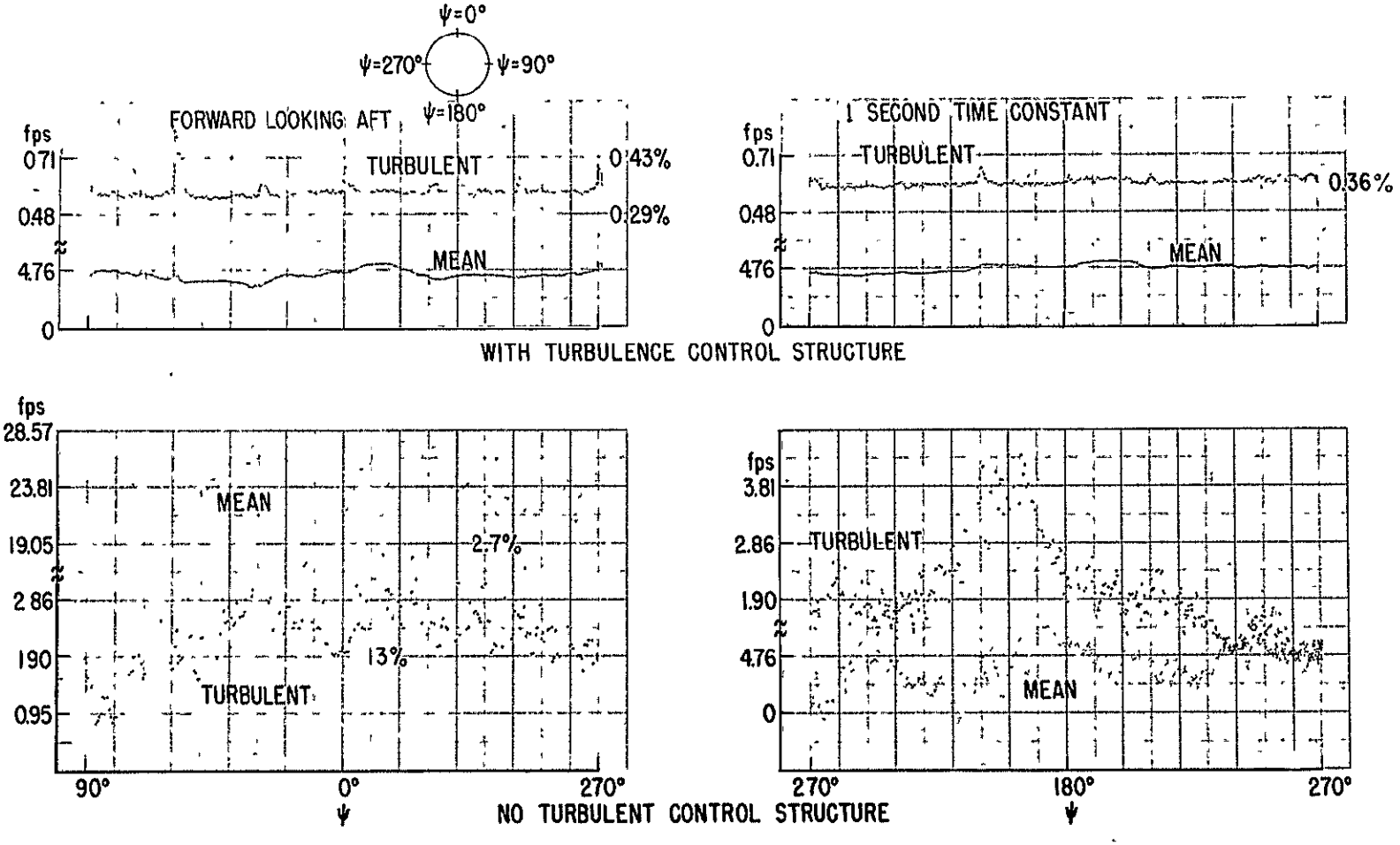

CIRCUMFERENTIAL DISTRIBUTION OF MEAN AND FLUCTUATING VELOCITIES, 54% SPEED, TRANSVERSE VELOCITY, $\Delta r/R_0 = 0.25$, NO SUCTION

Figure 56

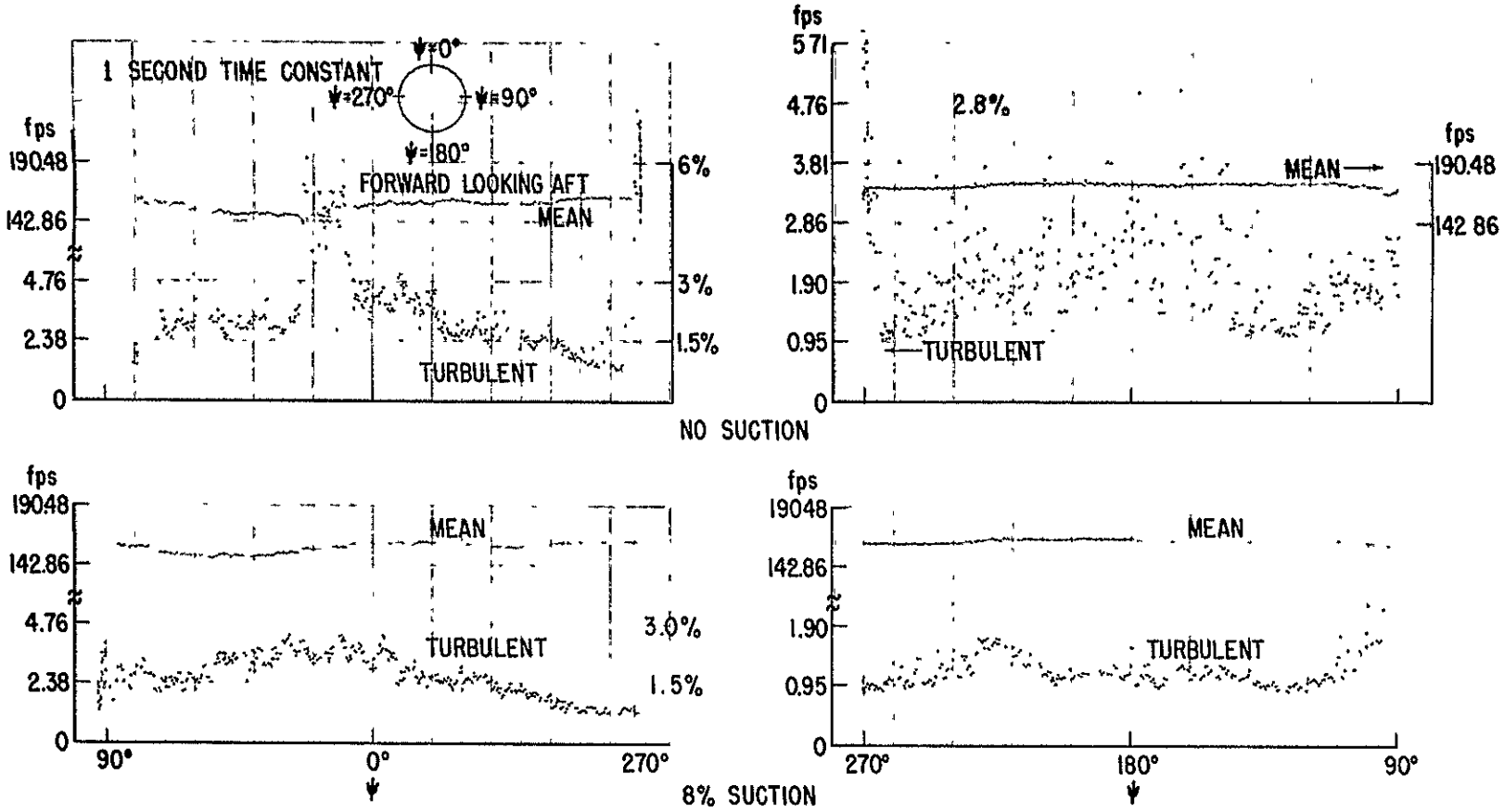

CIRCUMFERENTIAL DISTRIBUTION OF MEAN AND FLUCTUATING VELOCITIES, 54% SPEED, AXIAL VELOCITY, $\Delta r/R_0 = 0.05$, NO TURBULENCE CONTROL STRUCTURE

Figure 57

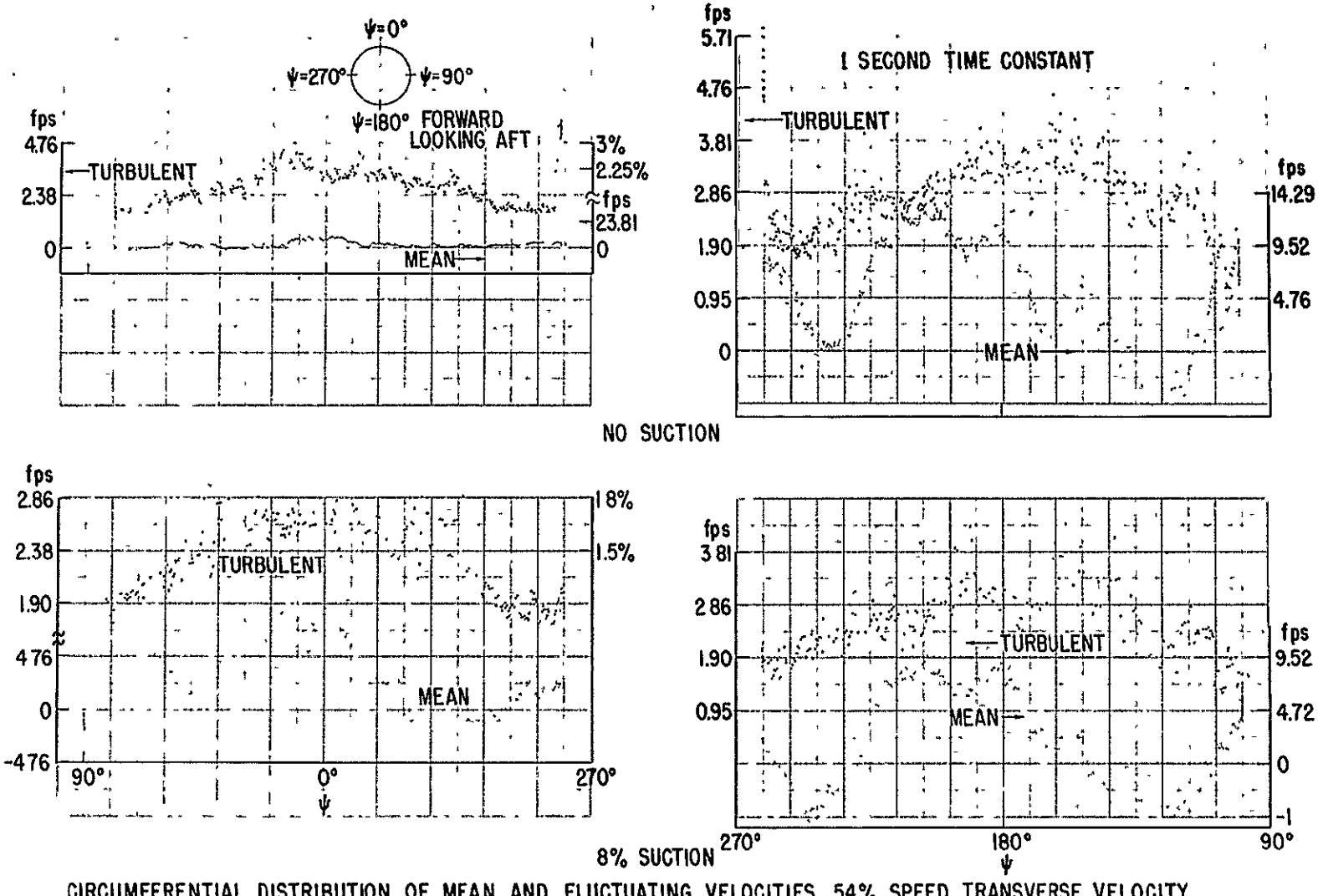

CIRCUMFERENTIAL DISTRIBUTION OF MEAN AND FLUCTUATING VELOCITIES, 54% SPEED, TRANSVERSE VELOCITY, $\Delta r/R_0 = 0.05$, NO TURBULENCE CONTROL STRUCTURE

Figure 58

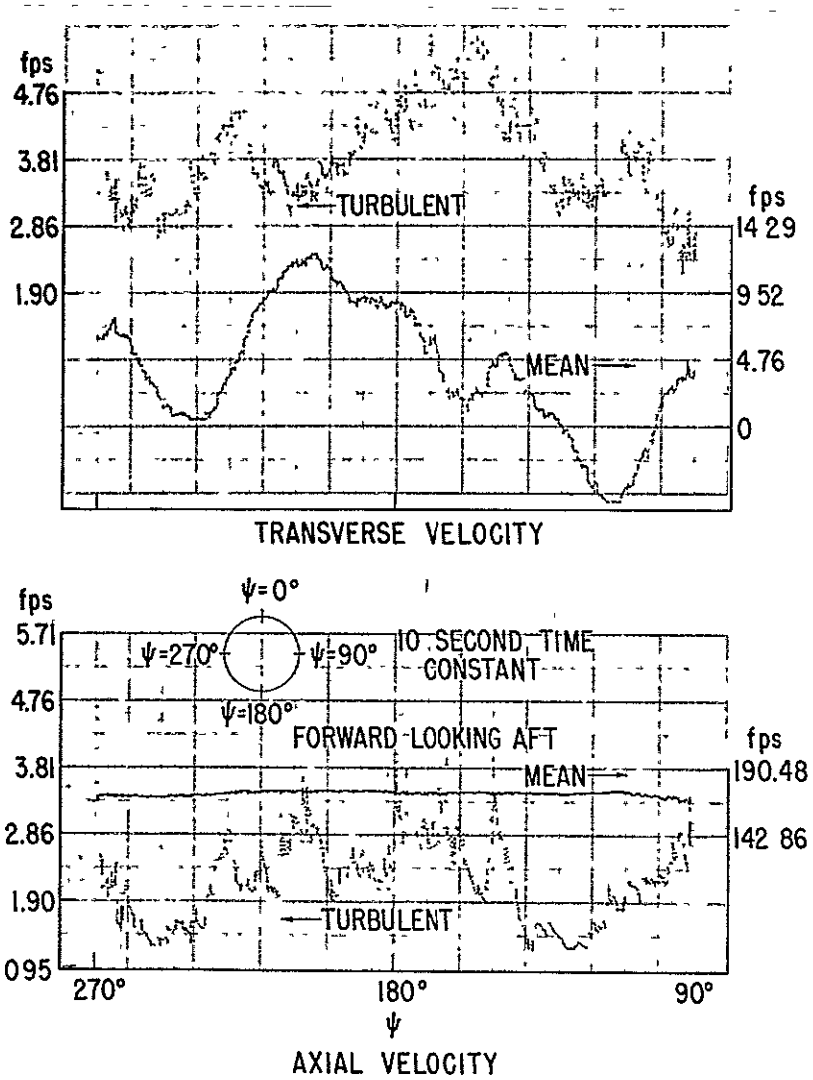

CIRCUMFERENTIAL DISTRIBUTION OF MEAN AND FLUCTUATING VELOCITIES, 54% SPEED, $\Delta r/R_0 = 0.05$, NO TURBULENCE CONTROL STRUCTURE, NO SUCTION

Figure 59

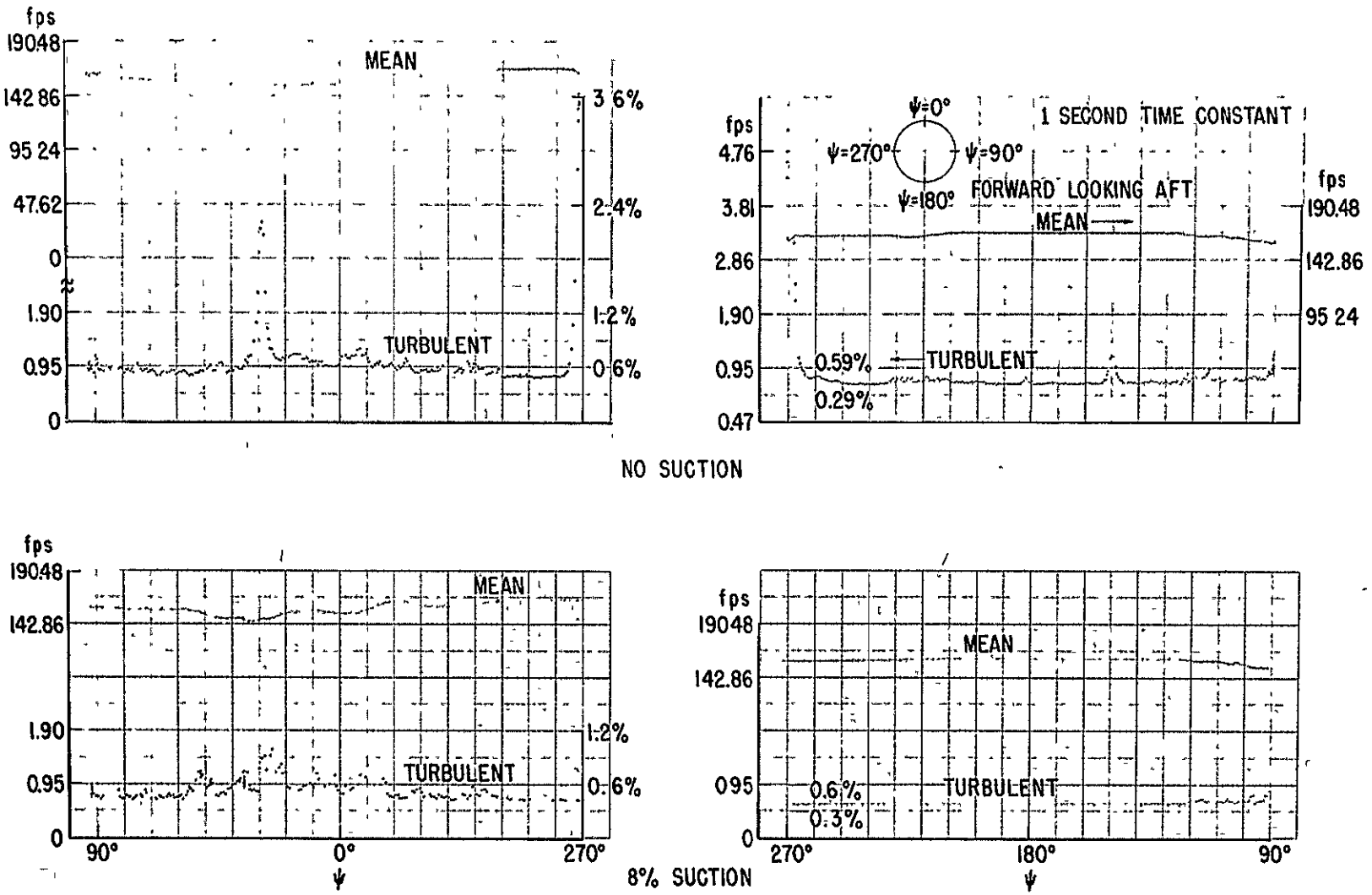

CIRCUMFERENTIAL DISTRIBUTION OF MEAN AND FLUCTUATING VELOCITIES, 54% SPEED, AXIAL VELOCITY, $\Delta r / R_0 = 0.05$, WITH TURBULENCE CONTROL STRUCTURE

Figure 60

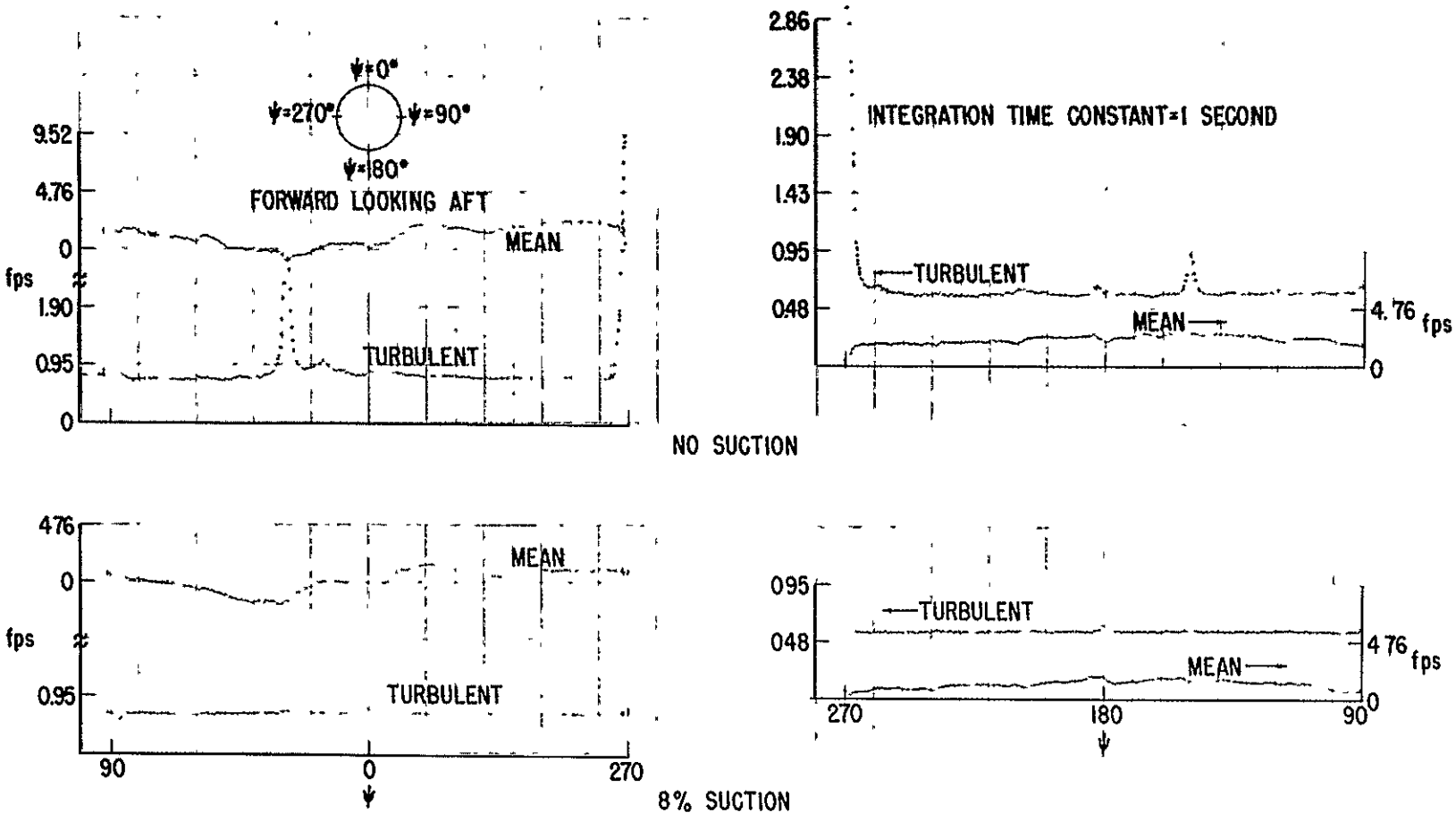

CIRCUMFERENTIAL DISTRIBUTION OF MEAN AND FLUCTUATING VELOCITIES, 54% SPEED, TRANSVERSE VELOCITY, $\Delta r/R_\delta$=0.05, WITH TURBULENCE CONTROL STRUCTURE

Figure 61

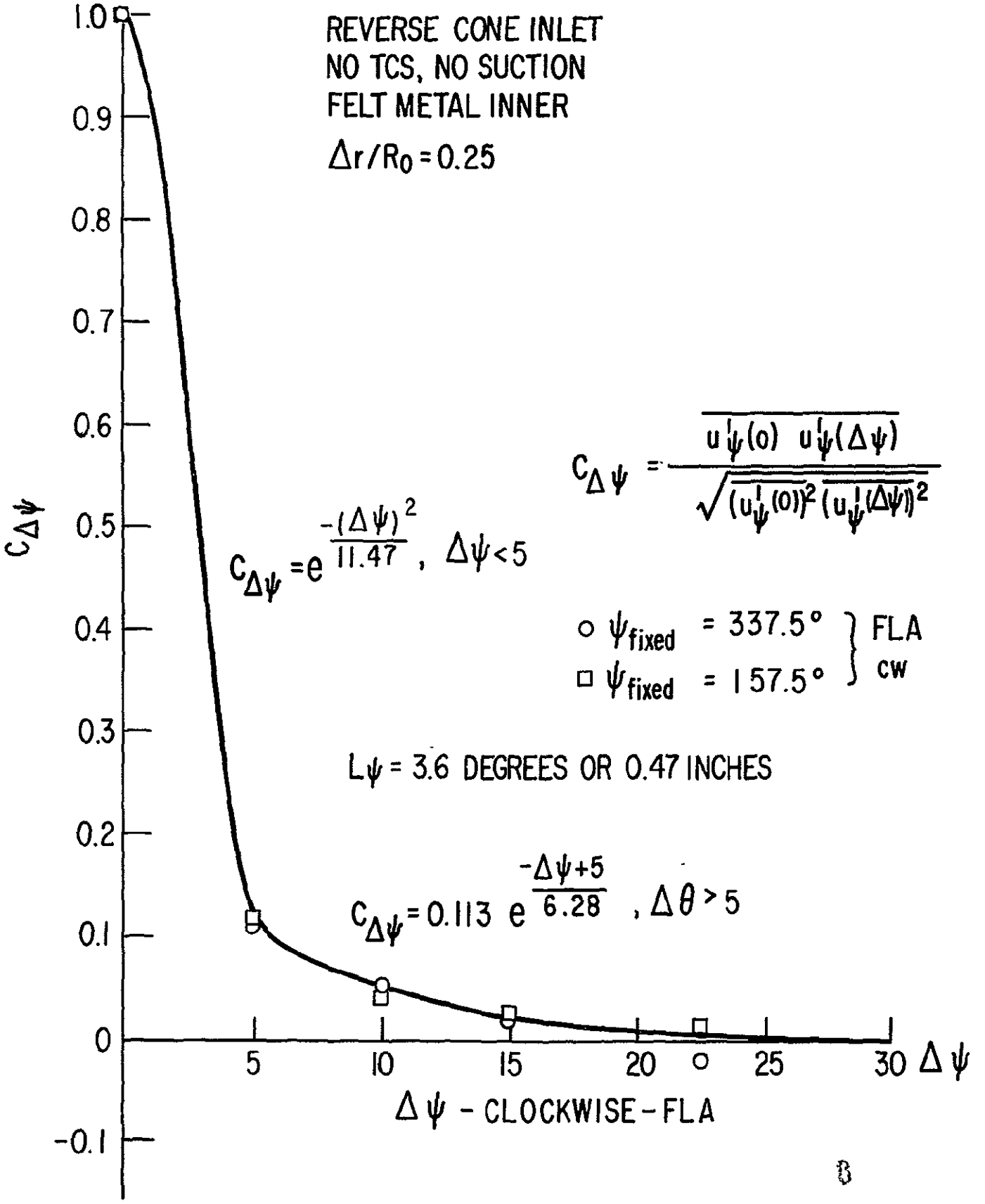

FIG. 62 NORMALIZED CROSS-CORRELATION OF TRANSVERSE VELOCITIES

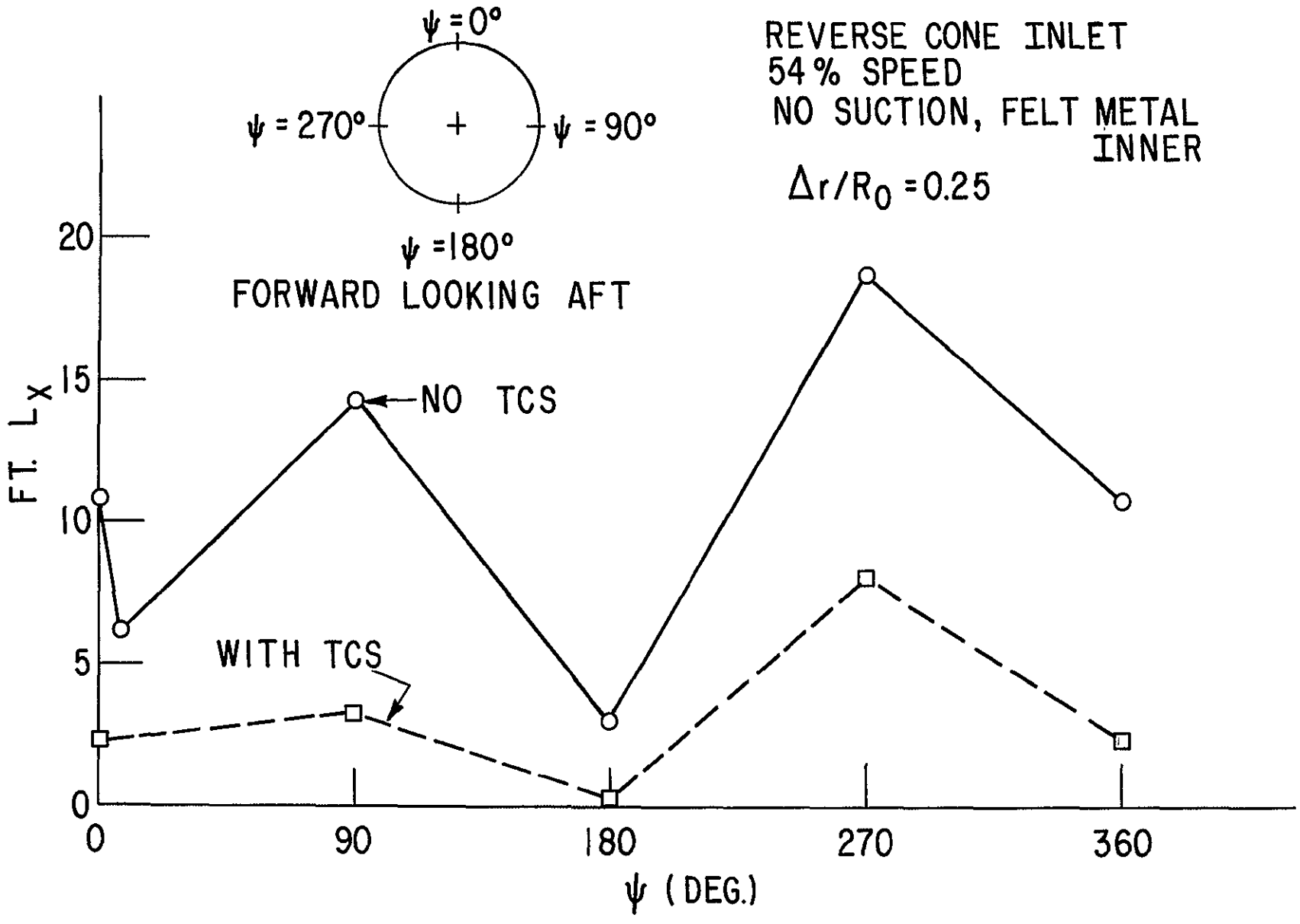

FIG.63 STREAMWISE TURBULENT LENGTH SCALE

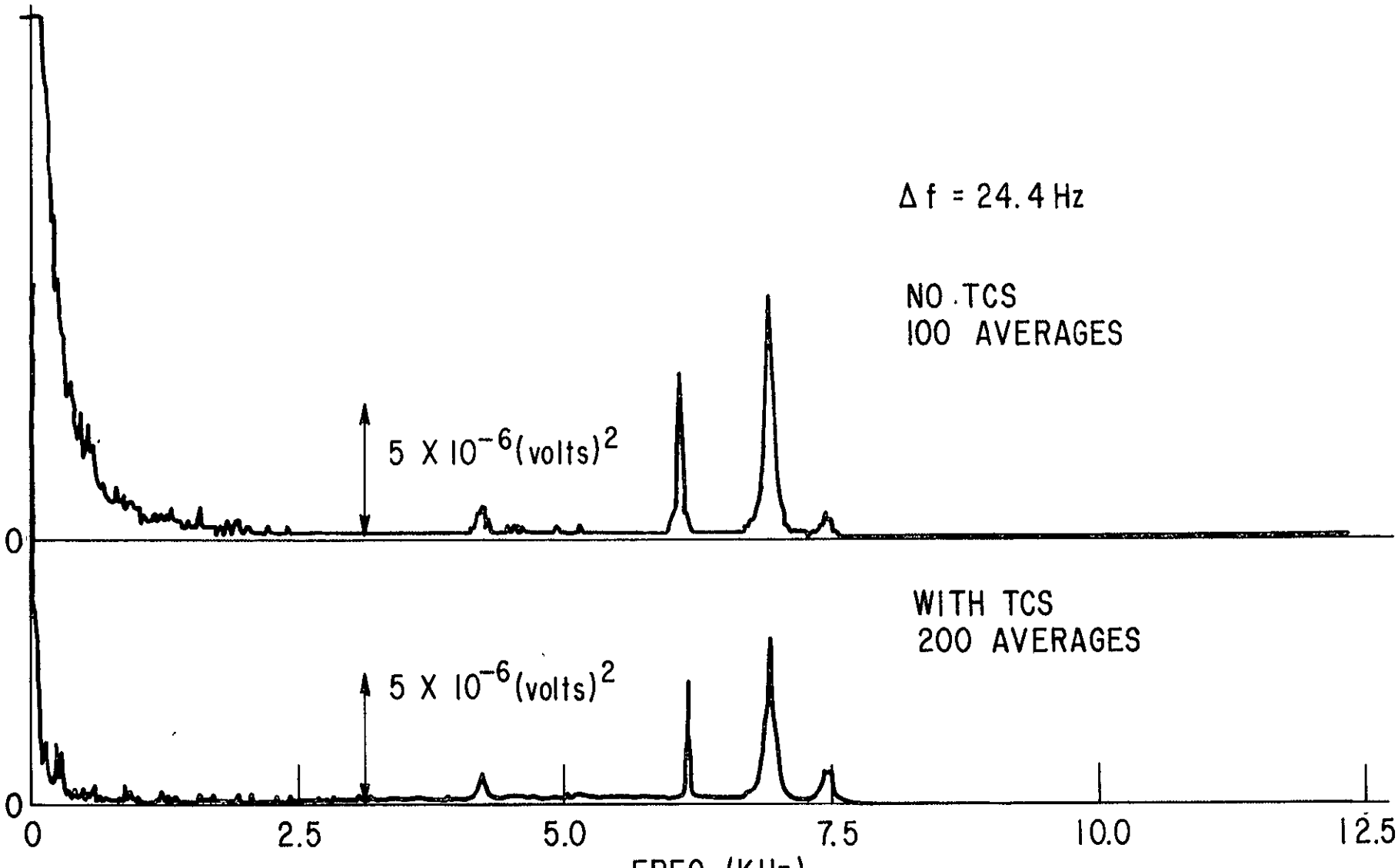

TURBULENT (VELOCITY)^2 SPECTRA, REVERSE CONE INLET, NO SUCTION, EFFECT OF TCS, HIGH FREQUENCY, $\theta = 0°$, $\Delta r/R = 0.25$, AXIAL VELOCITY

FIG.64a

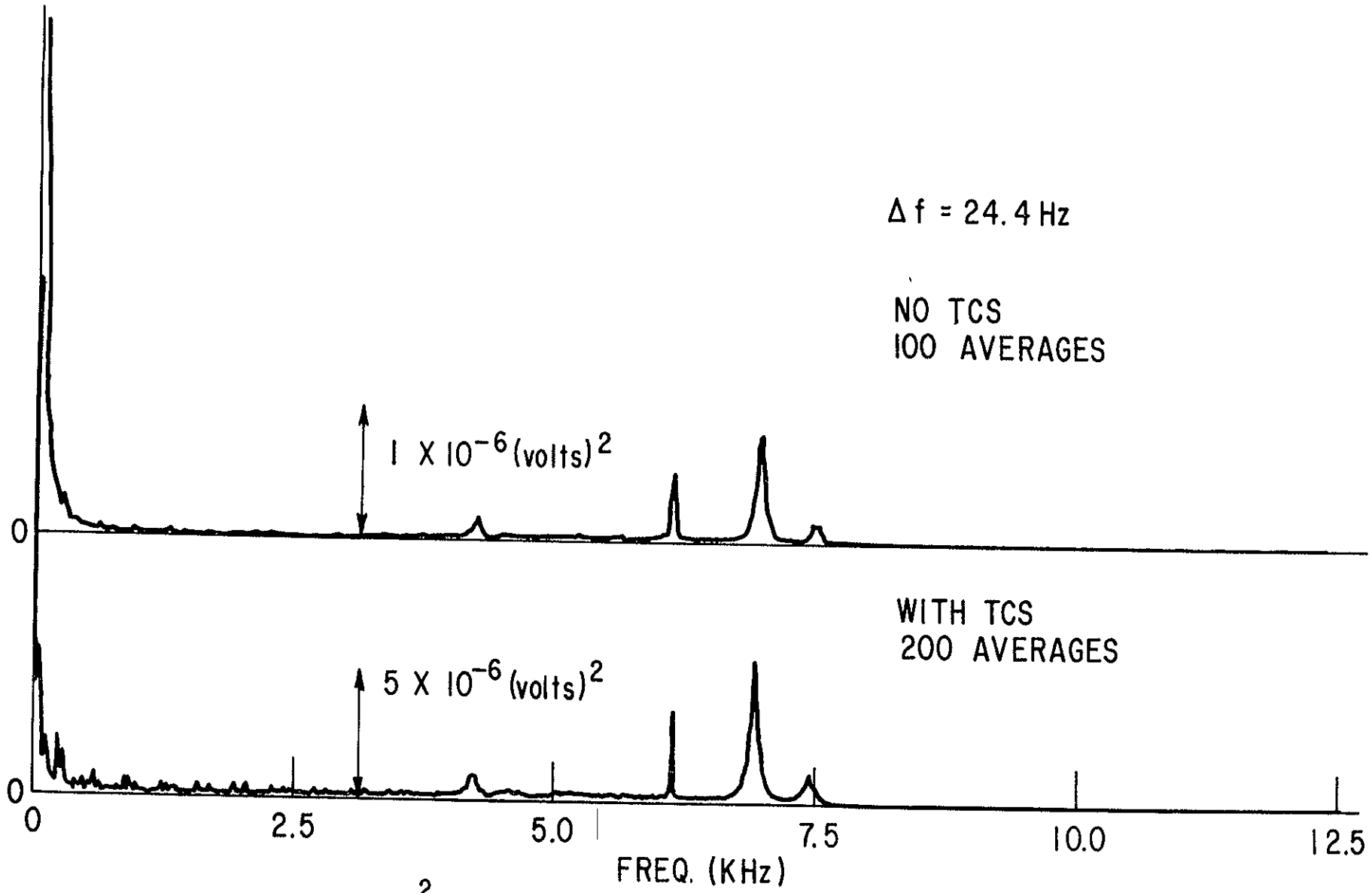

TURBULENT (VELOCITY)^2 SPECTRA, REVERSE CONE INLET, NO SUCTION, EFFECT OF TCS, $\Delta r/R_0 = 0.25$, HIGH FREQUENCY, $\theta = 90°$, AXIAL VELOCITY

FIG. 64b

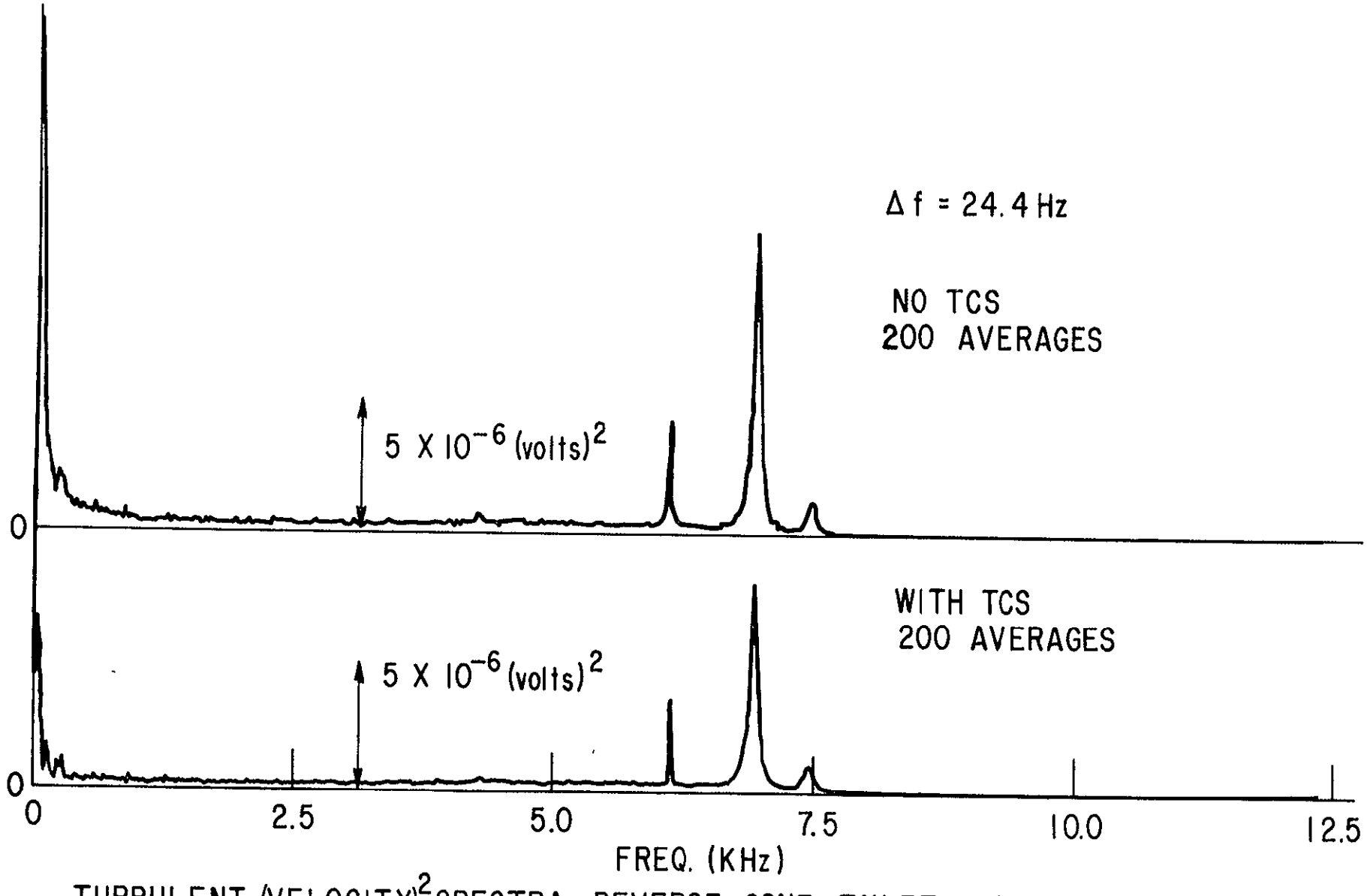

TURBULENT (VELOCITY)^2 SPECTRA, REVERSE CONE INLET, NO SUCTION, EFFECT OF TCS, $\Delta r/R_0 = 0.25$, HIGH FREQUENCY, $\theta = 180°$; AXIAL VELOCITY

FIG. 64c

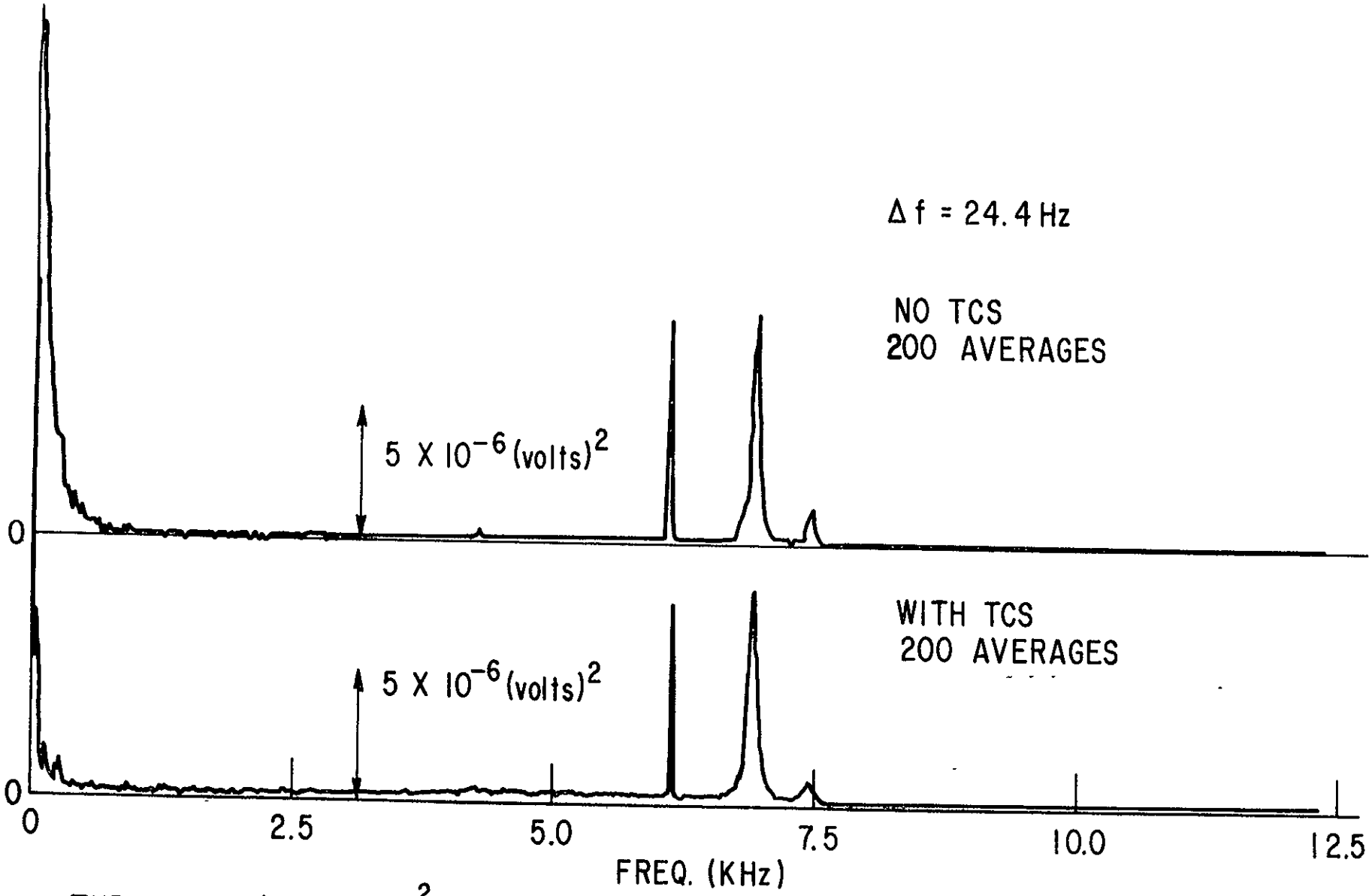

TURBULENT (VELOCITY)^2 SPECTRA, REVERSE CONE INLET, NO SUCTION, EFFECT OF TCS, $\Delta r/R_0 = 0.25$, HIGH FREQUENCY, $\theta = 270°$, AXIAL VELOCITY

FIG. 64 d

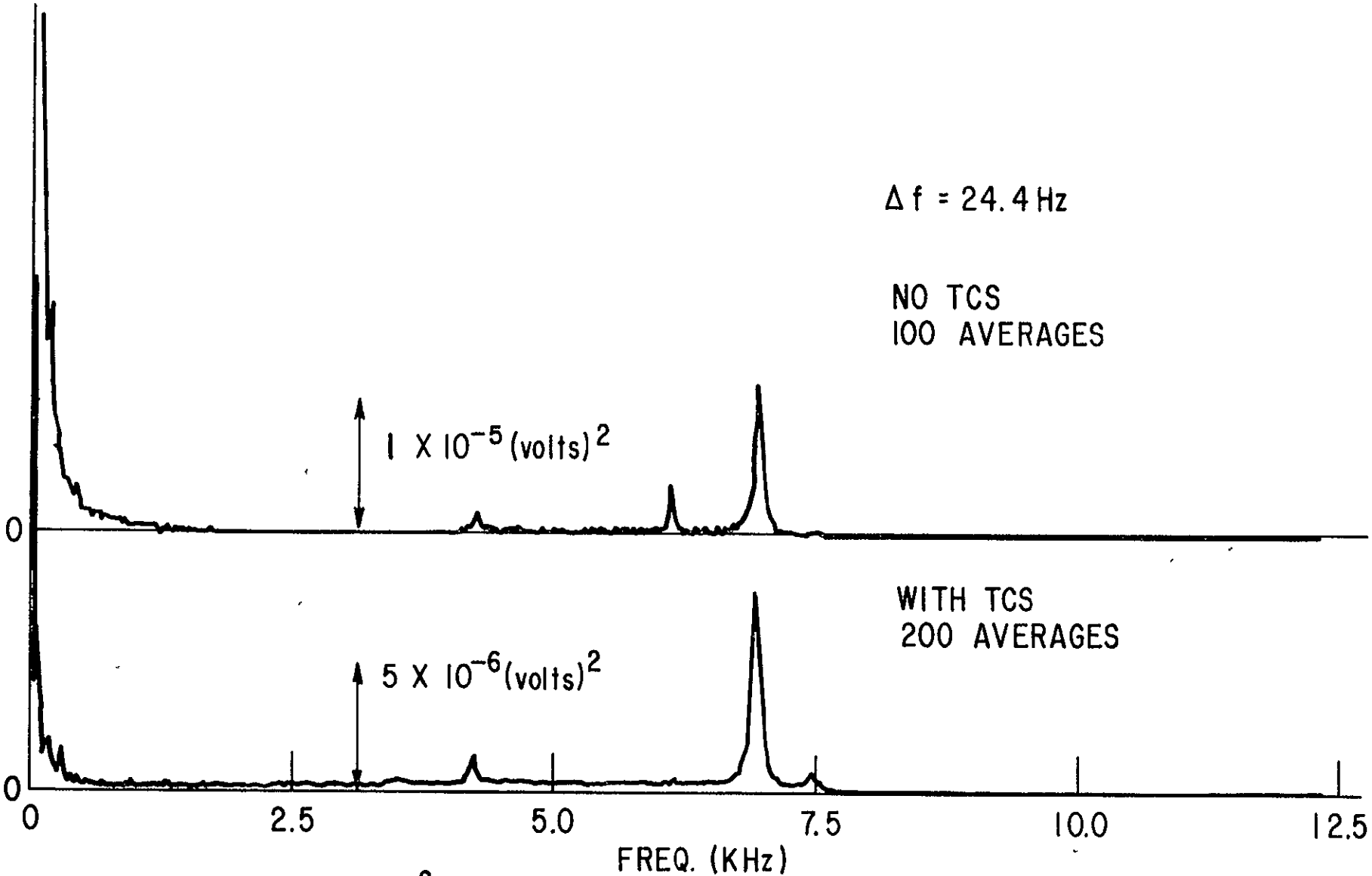

TURBULENT (VELOCITY)^2 SPECTRA, REVERSE CONE INLET, NO SUCTION, EFFECT OF TCS, $\Delta r/R_0 = 0.25$, HIGH FREQUENCY, $\theta = 0°$, CIRCUMFERENTIAL VELOCITY

FIG. 65a

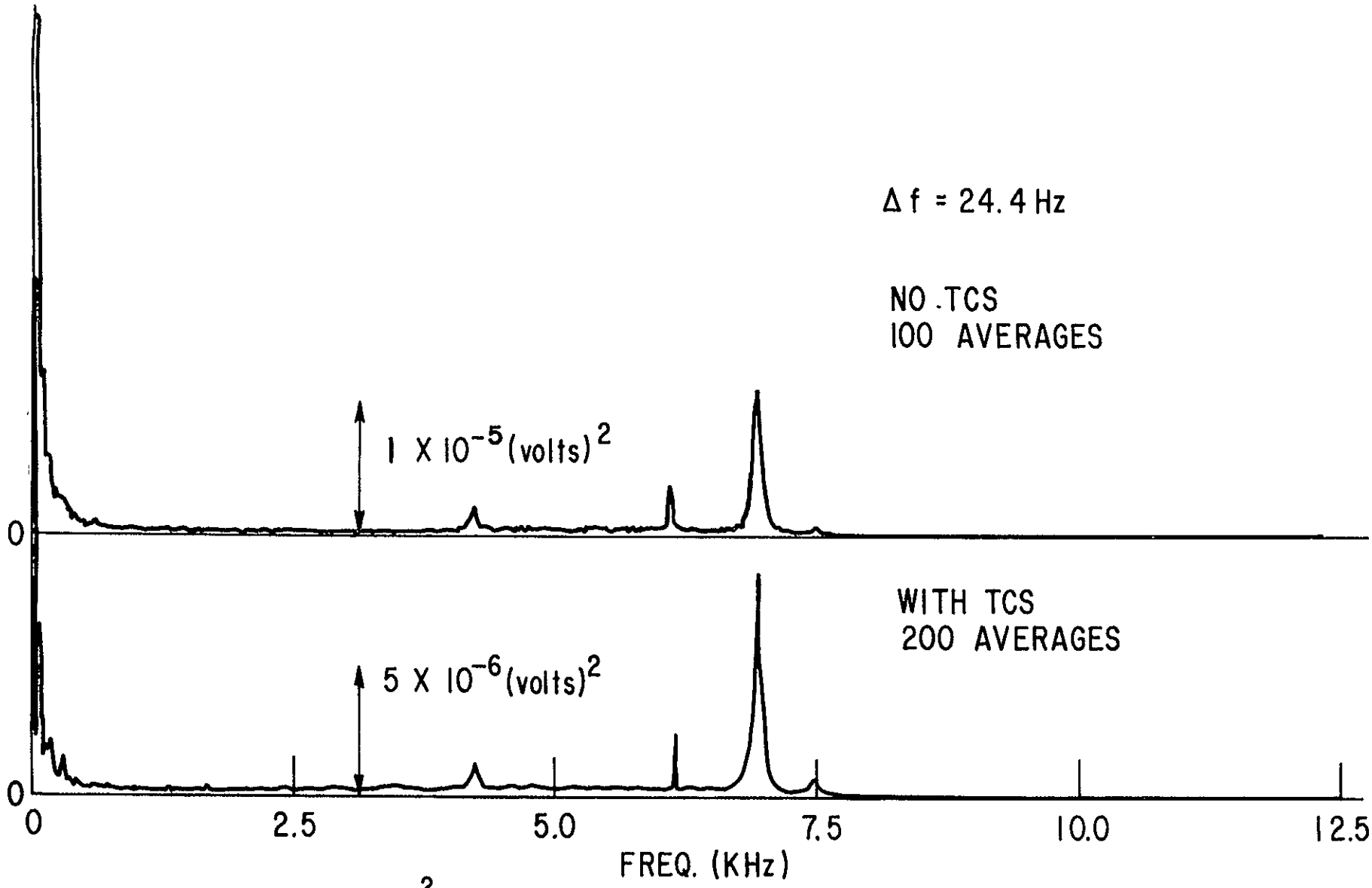

TURBULENT (VELOCITY)^2 SPECTRA, REVERSE CONE INLET, NO SUCTION, EFFECT OF TCS, $\Delta r/R_0 = 0.25$, HIGH FREQUENCY, $\theta = 90°$, CIRCUMFERENTIAL VELOCITY

FIG. 65b

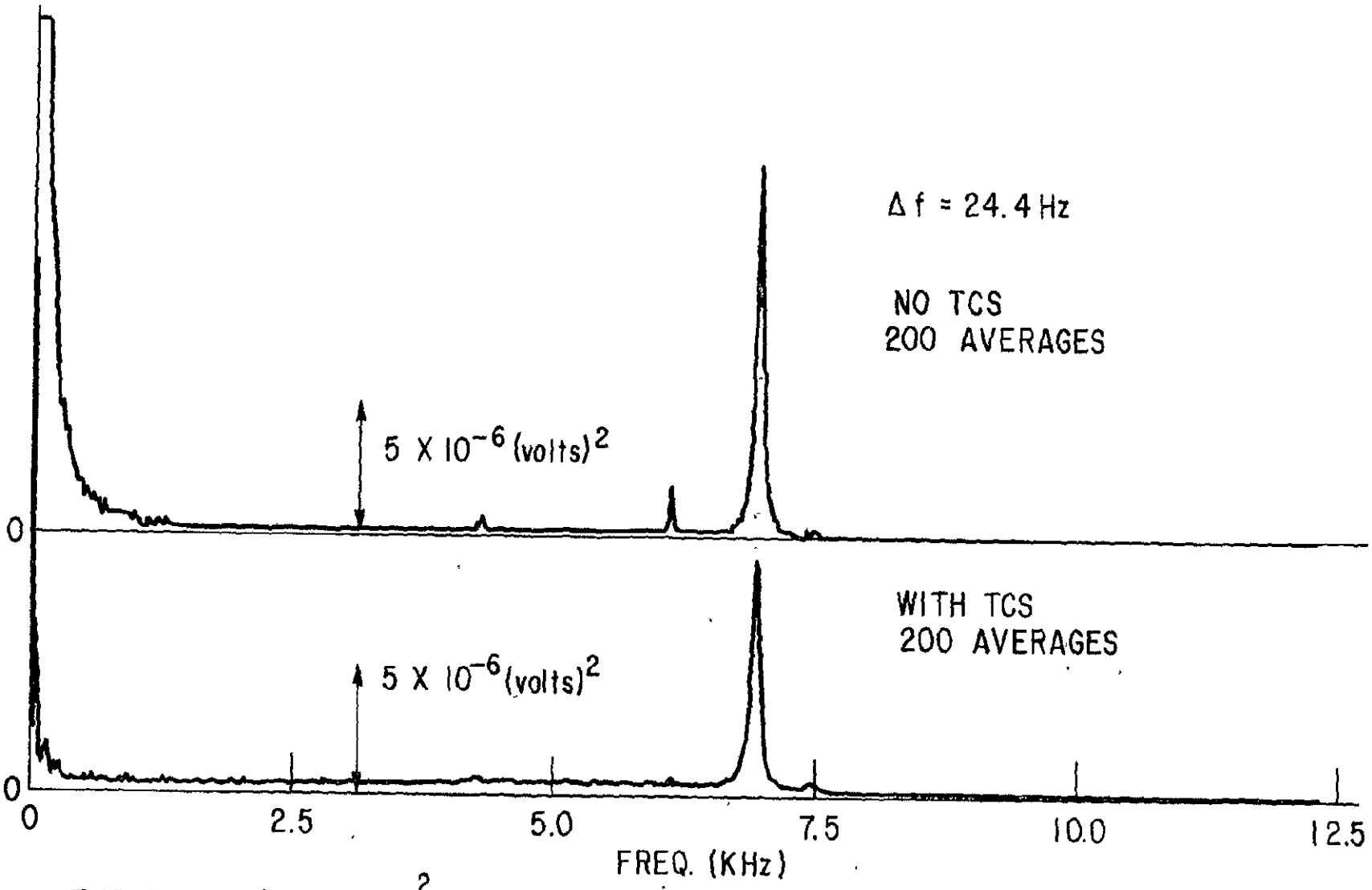

TURBULENT (VELOCITY)^2 SPECTRA, REVERSE CONE INLET, NO SUCTION, EFFECT OF TCS, $\Delta r/R_0 = 0.25$, HIGH FREQUENCY, $\theta = 180°$; CIRCUMFERENTIAL VELOCITY

FIG. 65c

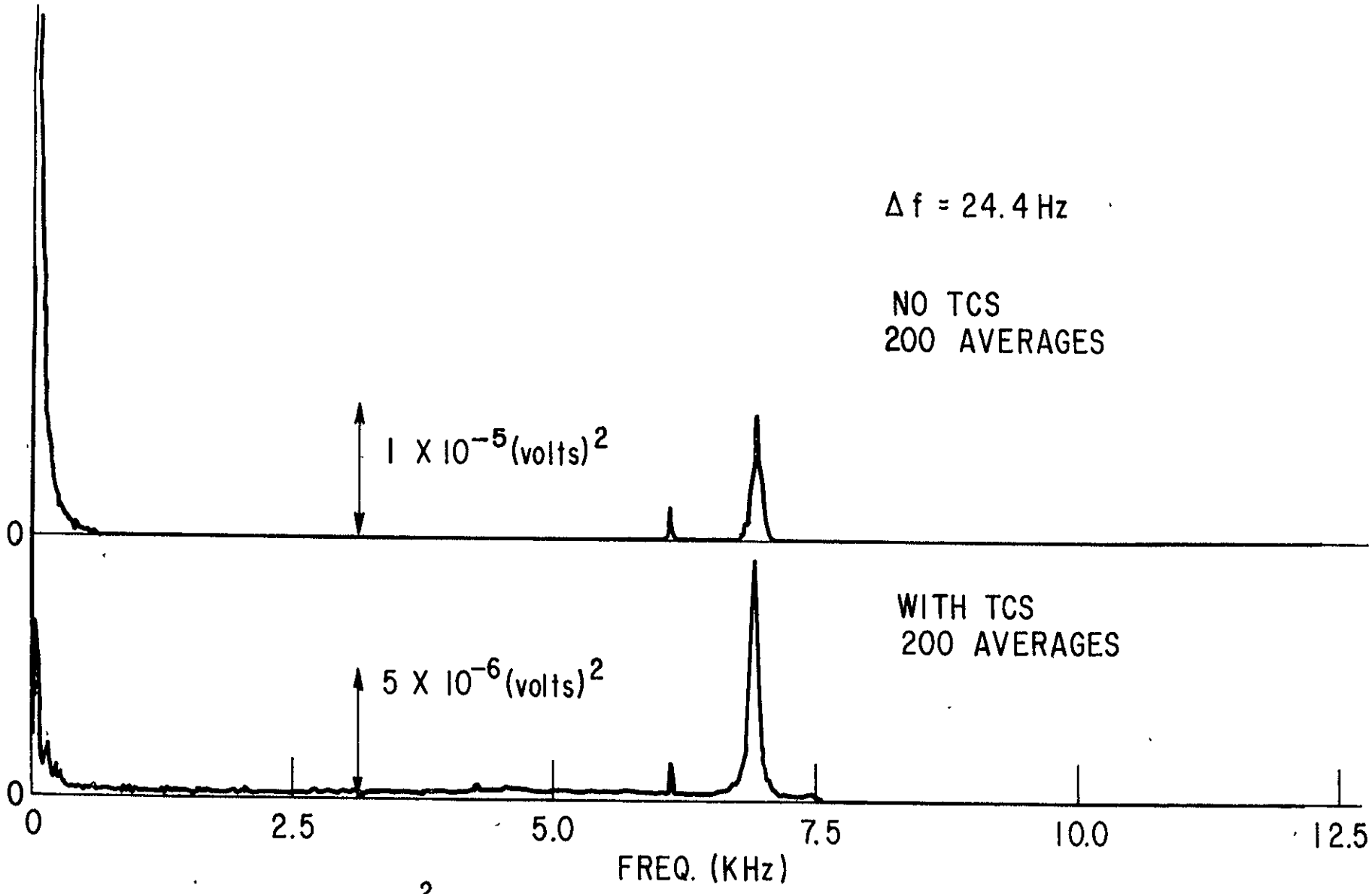

TURBULENT (VELOCITY)^2 SPECTRA, REVERSE CONE INLET, NO SUCTION, EFFECT OF TCS, $\Delta r/R_0 = 0.25$, HIGH FREQUENCY, $\theta = 270°$, CIRCUMFERENTIAL VELOCITY

FIG. 65d

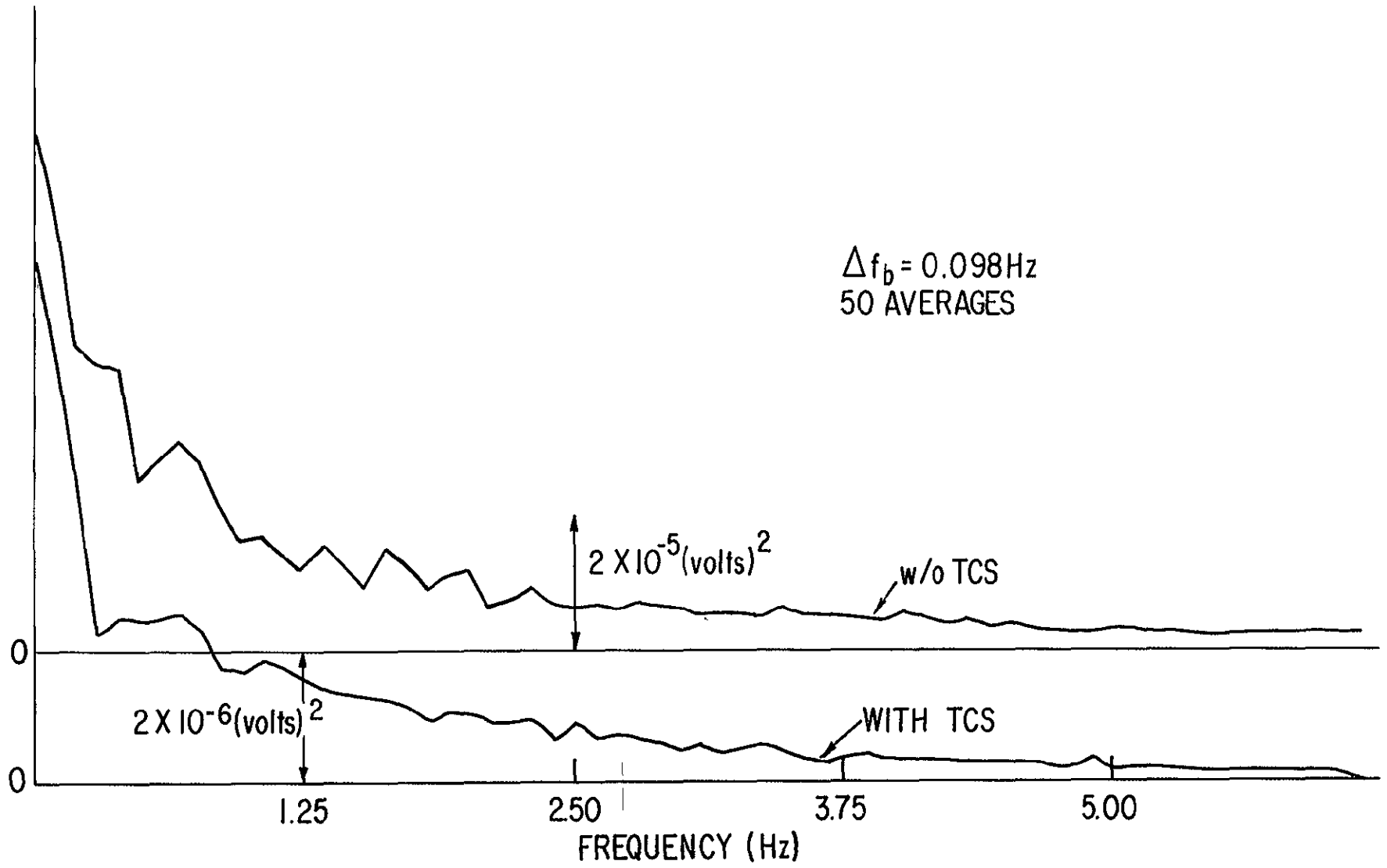

TURBULENT (VELOCITY)^2 SPECTRA, REVERSE CONE INLET, NO SUCTION, EFFECT OF TCS, $\Delta r/R_0 = 0.25$, LOW FREQUENCY, $\theta = 0°$, AXIAL VELOCITY

FIG. 66a

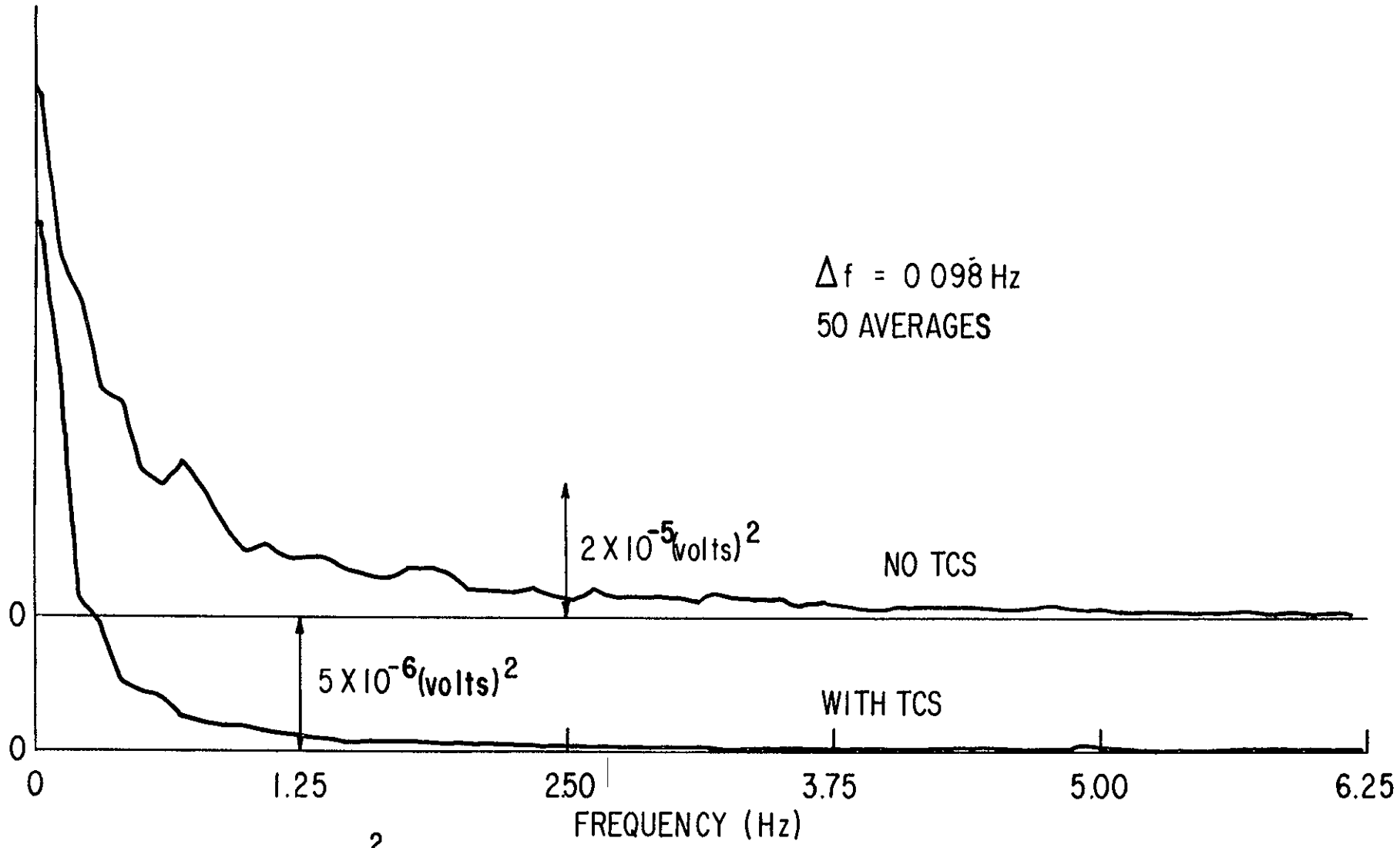

TURBULENT (VELOCITY)^2 SPECTRA, REVERSE CONE INLET, NO SUCTION, EFFECT OF TCS, $\Delta r/R_0 = 0.25$, LOW FREQUENCY, $\theta = 90°$, AXIAL VELOCITY

FIG. 66b

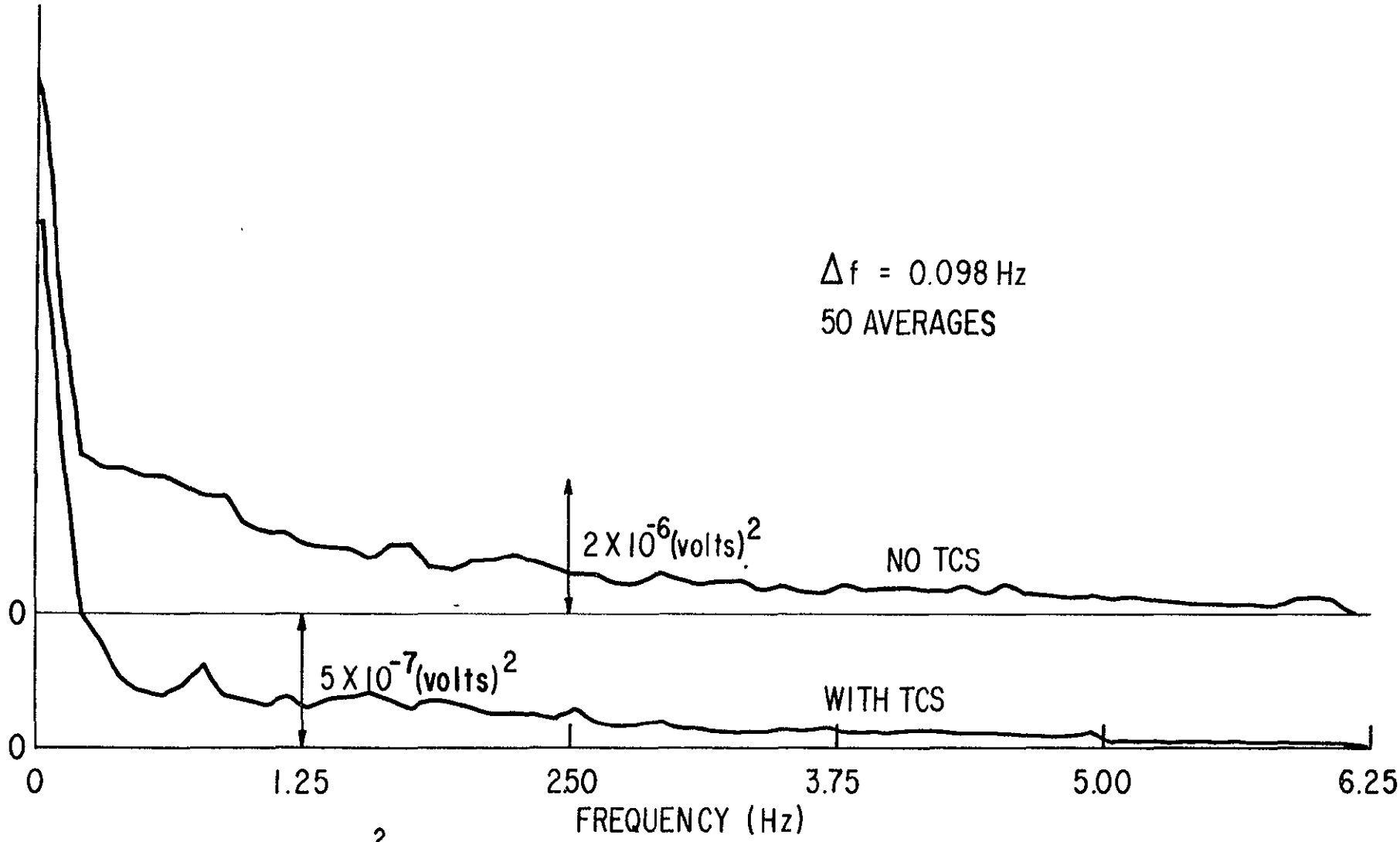

TURBULENT (VELOCITY)^2 SPECTRA, REVERSE CONE INLET, NO SUCTION, EFFECT OF TCS, $\Delta r/R_0 = 0.25$, LOW FREQUENCY, $\theta = 180°$, AXIAL VELOCITY

FIG. 66c

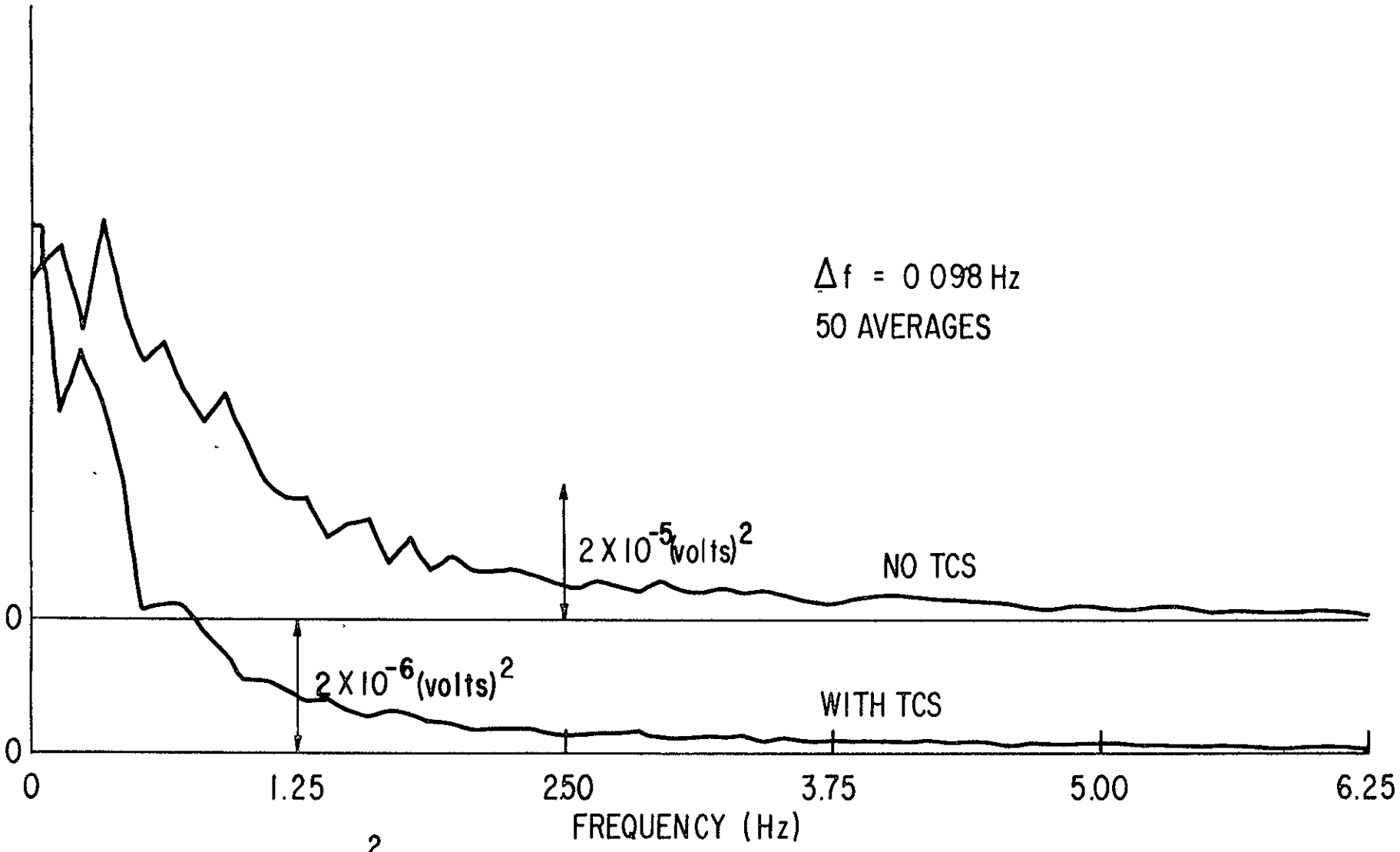

TURBULENT (VELOCITY)^2 SPECTRA, REVERSE CONE INLET, NO SUCTION, EFFECT OF TCS, $\Delta r/R_0 = 0.25$, LOW FREQUENCY, $\theta = 270°$, AXIAL VELOCITY

FIG. 66d

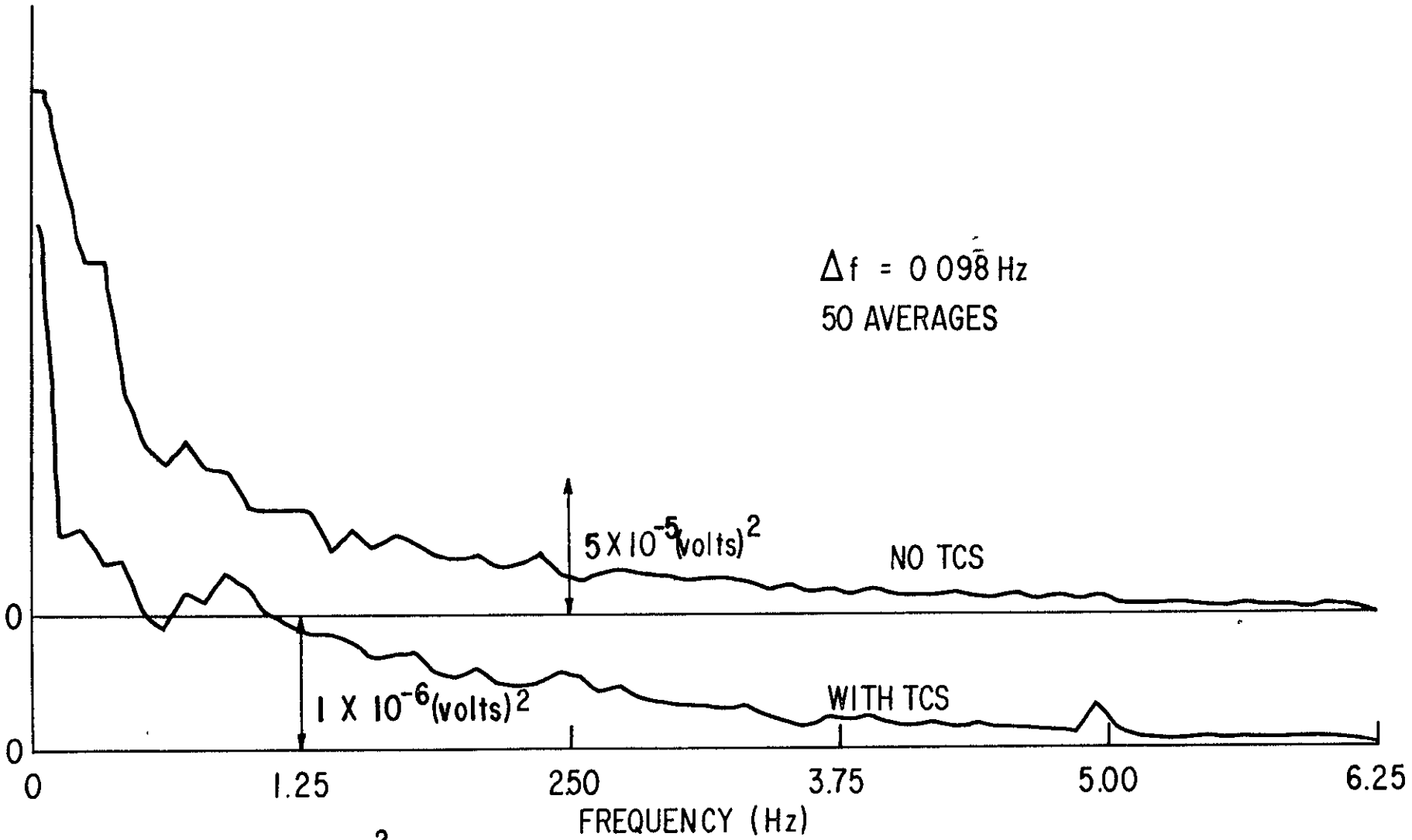

TURBULENT (VELOCITY)^2 SPECTRA, REVERSE CONE INLET, NO SUCTION EFFECT OF TCS,
$\Delta r/R_0 = 0.25$, LOW FREQUENCY, $\theta = 0°$, CIRCUMFERENTIAL VELOCITY

FIG. 67 a

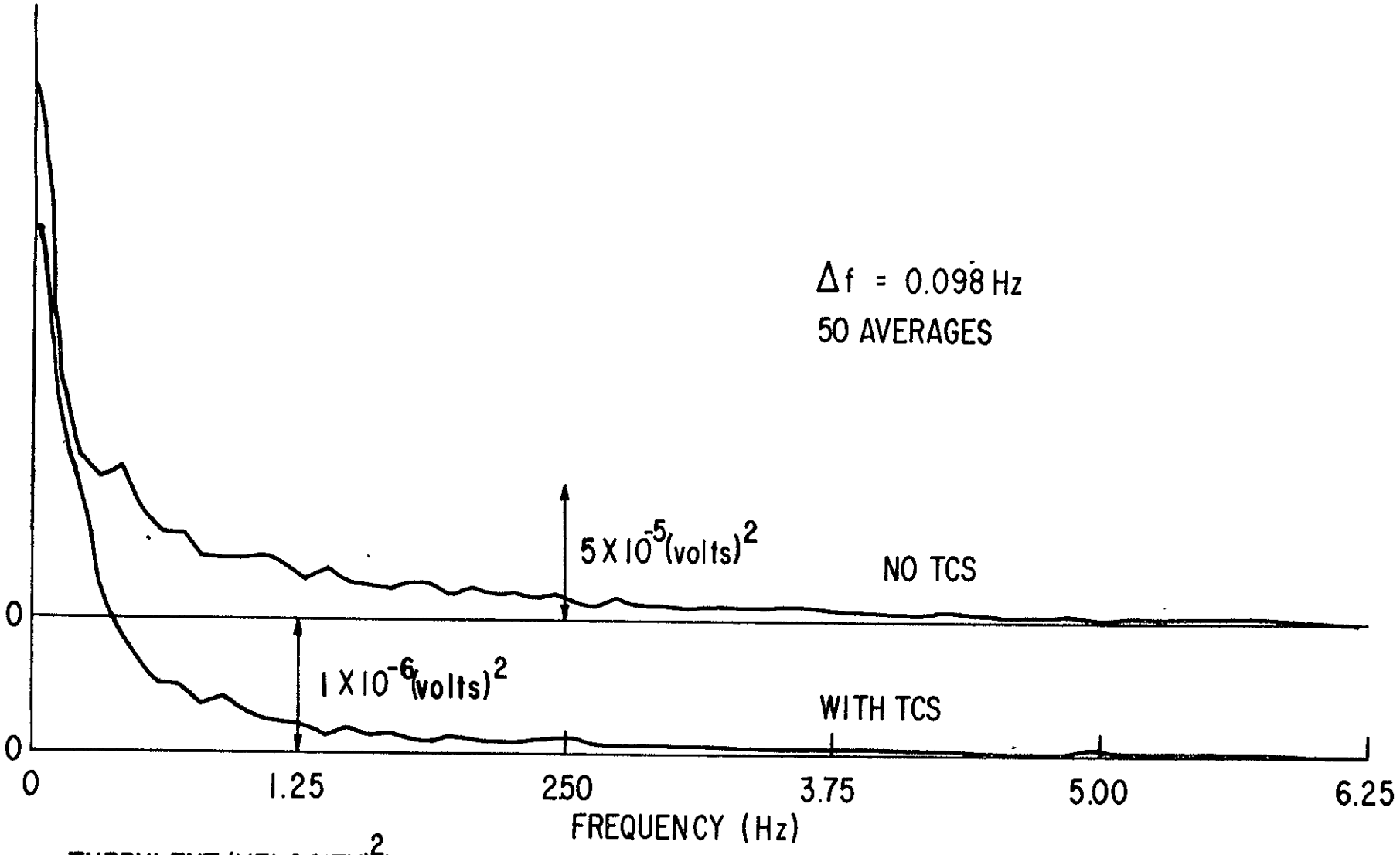

TURBULENT $(\text{VELOCITY})^2$ SPECTRA, REVERSE CONE INLET, NO SUCTION, EFFECT OF TCS, $\Delta r/R_o = 0.25$, LOW FREQUENCY, $\theta = 90°$, CIRCUMFERENTIAL VELOCITY

FIG. 67 b

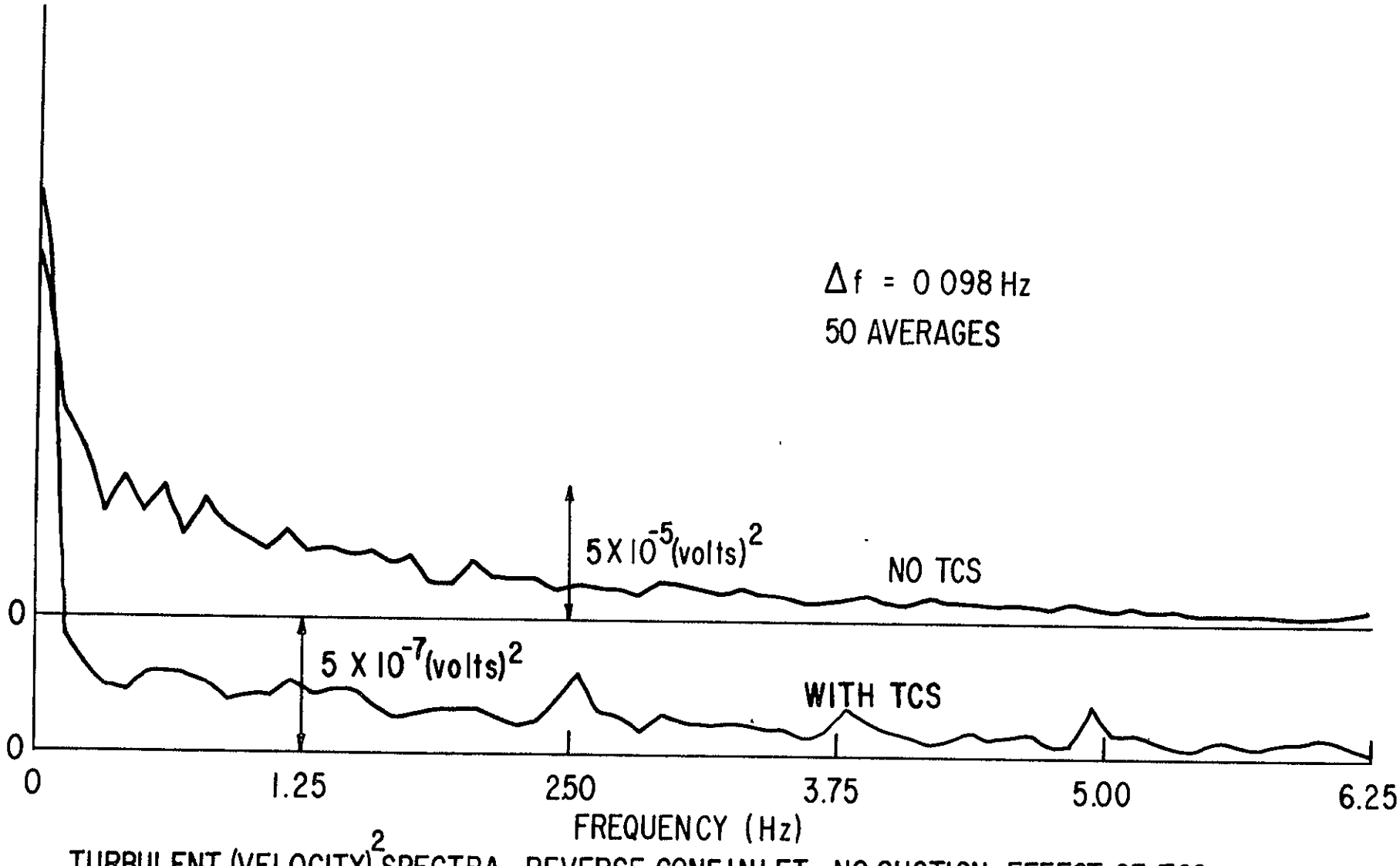

TURBULENT (VELOCITY)^2 SPECTRA, REVERSE CONE INLET, NO SUCTION, EFFECT OF TCS, $\Delta r/R_0 = 0.25$, LOW FREQUENCY, $\theta = 180°$, CIRCUMFERENTIAL VELOCITY

FIG. 67 c

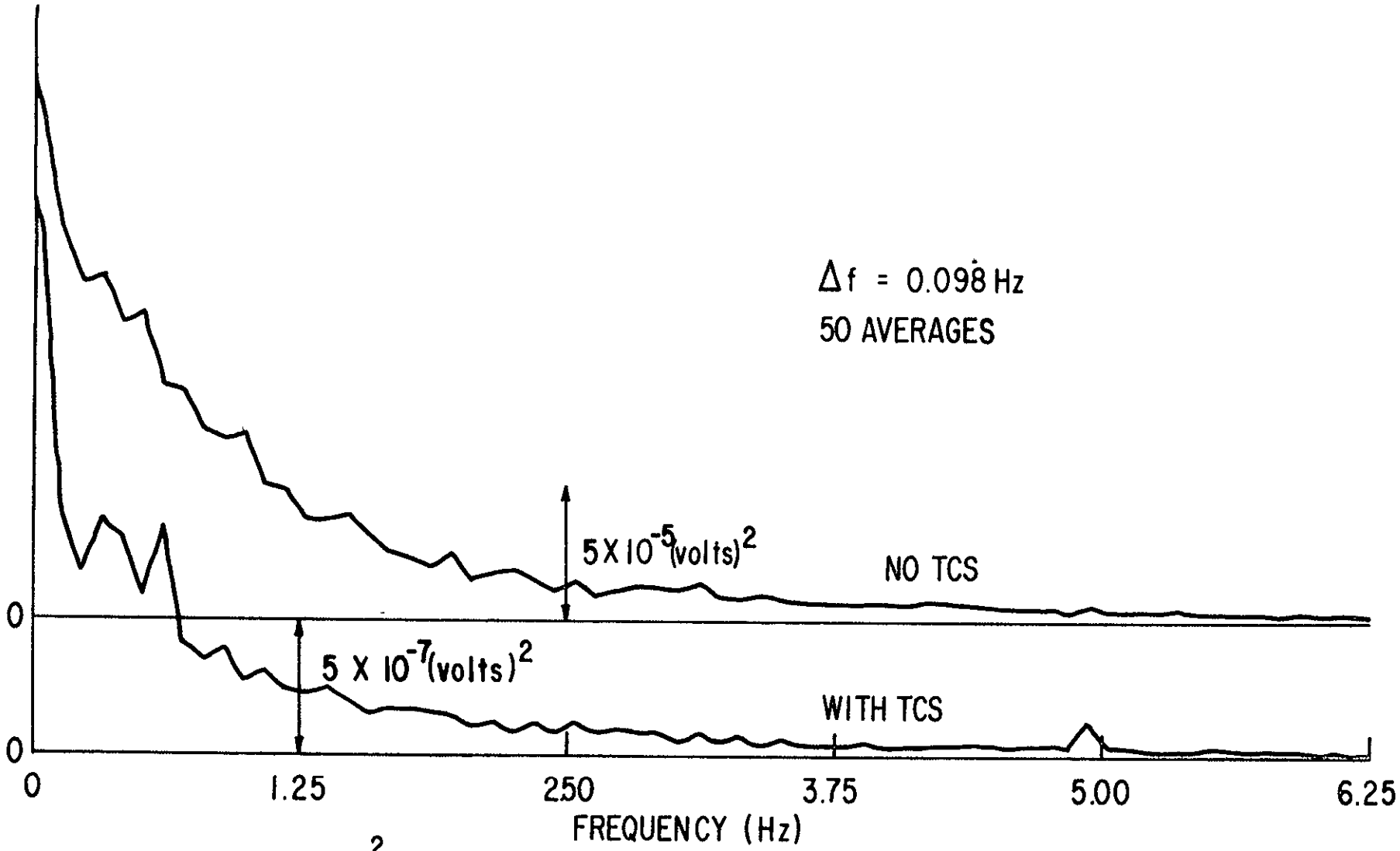

TURBULENT (VELOCITY)^2 SPECTRA, REVERSE CONE INLET, NO SUCTION, EFFECT OF TCS, $\Delta r/R_0 = 0.25$, LOW FREQUENCY, $\theta = 270°$, CIRCUMFERENTIAL VELOCITY

FIG. 67 d

Rotor Inlet Tip Diameter	0.504m (19.84 in)
Pressure Ratio	1.574
Rotor Blade Number	44
Stator Vane Number	86
Vane/Blade Ratio	1.95
Inlet Guide Vanes	None
Rotor Inlet Hub/Tip Radius Ratio	0.50
Rotor-Stator Tip Spacing	1.27 Rotor Chords
Rotor Rotative Speed	16100 RPM
Rotor Tip Speed	424.9m/sec (1394 ft/sec)
Rotor Tip Inlet Relative Mach No.	1.394
Rotor Chord (Midspan)	4.62cm (1.817 in)
Stator Chord (Midspan)	4.06cm (1.597 in)
Rotor Aspect Ratio	2.5
Stator Aspect Ratio	2.3
Rotor Tip Solidity	1.298
Stator Tip Solidity	1.270
Corrected Inlet Weight Flow	29.5Kg/sec(65 lb/sec)
Adiabatic Efficiency	85.5%(80.9% Measured)

Table 1: Test Fan Stage Design Characteristics

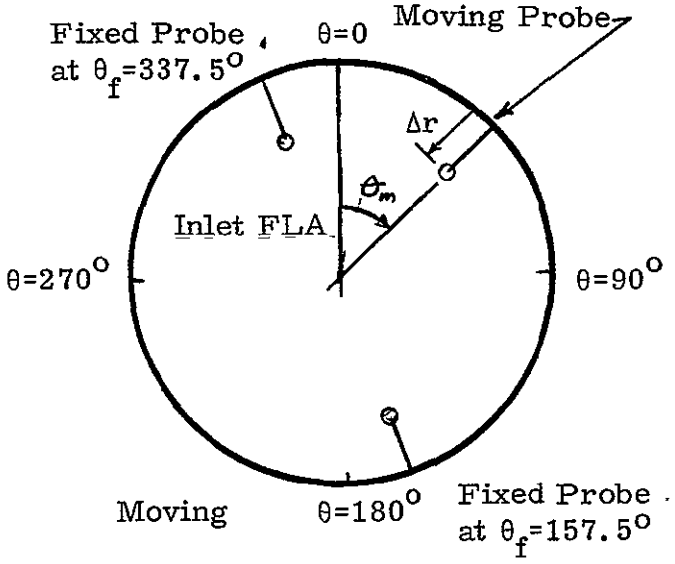

At $\Delta r/R_o$ = 0.05, No fixed probe, θ_m = 0°, 90°, 180°, 270°

At $\Delta r/R_o$ = 0.25, θ_f = 337.5°
θ_m = 342.5°, 347.5°, 352.5°, 0°, 30°, 90°
θ_f = 157.5°
θ_m = 162.5°, 167.5°, 172.5°, 130°, 192.5°*, 270°

With TCS w_s/w_{in} = 0
w_s/w_{in} = 0.08

Without TCS, w_s/w_{in} = 0
w_s/w_{in} = 0.08

Rotor Speed = 54%, Discharge Valve Full Open

*Only when the TCS was not used.

Table 2: Turbulent Spectra and Length Scales, Test Points

APPENDIX A: CALIBRATION OF THE TURBULENCE CONTROL STRUCTURE

To determine the acoustic attenuation of the TCS, a duplex loudspeaker, Altec Model 604-8G, was positioned inside the inlet. The speaker axis was coincident with the rotor axis and the sound measurements were made with the same microphone array as was used for the fan noise tests. A random noise generator, with and without a pink noise filter, was used to excite the loudspeaker. Tests with and without the TCS were conducted to determine the noise insertion loss. All the tests were done at zero fan speed and as such, the refractive effects of the inlet potential sink flow are then missing from this measurement.

Also the effect of the flow through the honeycomb will not be included, as this velocity is very low due to the large surface area of the TCS, about 88.5 ft.^{2}, which provides about a 40 to 1 contraction ratio to the inlet flow area. The attenuation of the acoustic power spectra is shown in Figure A-1, where up to and including 12.5 kHz, the attenuation is less than 1 dB, for both the pink and white noise excitation. Above 12.5 kHz, the attenuation increases to 1 to 1 1/2 dB, and above 25 kHz, the speaker output is too diminished for accurate measurements. Acoustic shadowing occurs in the forward arc between 20° and 50° from the rotor axis. Here the maximum attenuation can reach 3 dB. These peak attenuations occur at the fundamental frequency and the fifth harmonic of the half-wave resonances of the two inch depth of the honeycomb. These effects are seen on Figures A-2 and A-3 at a frequency of 3150 Hz and 16,000 Hz, respectively. These measurements were taken with the same one-third octave band analyzer as used for the fan noise measurements.

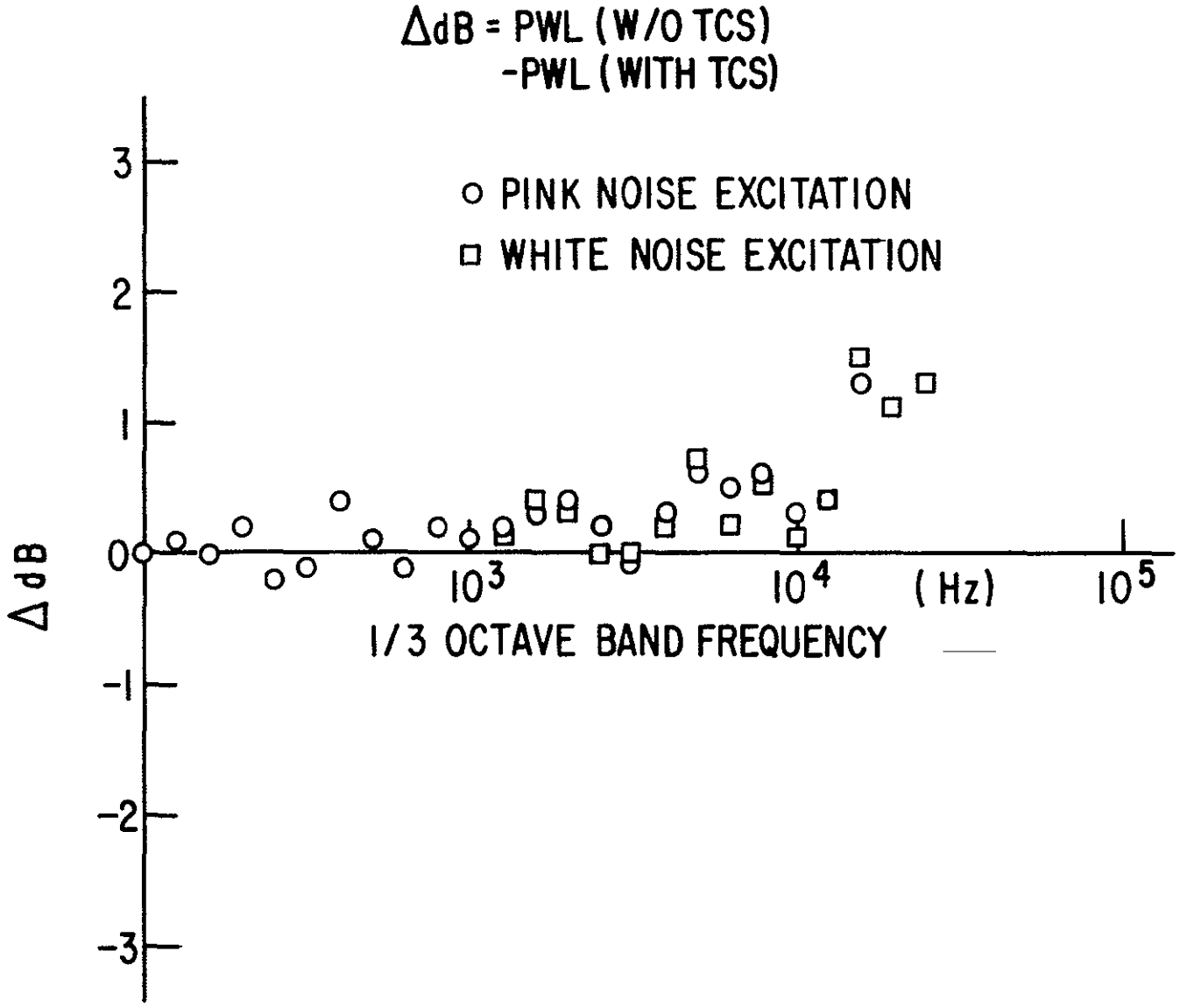

FIGURE A-1 SPEAKER CALIBRATION OF THE TURBULENCE CONTROL STRUCTURE, POWER LEVEL

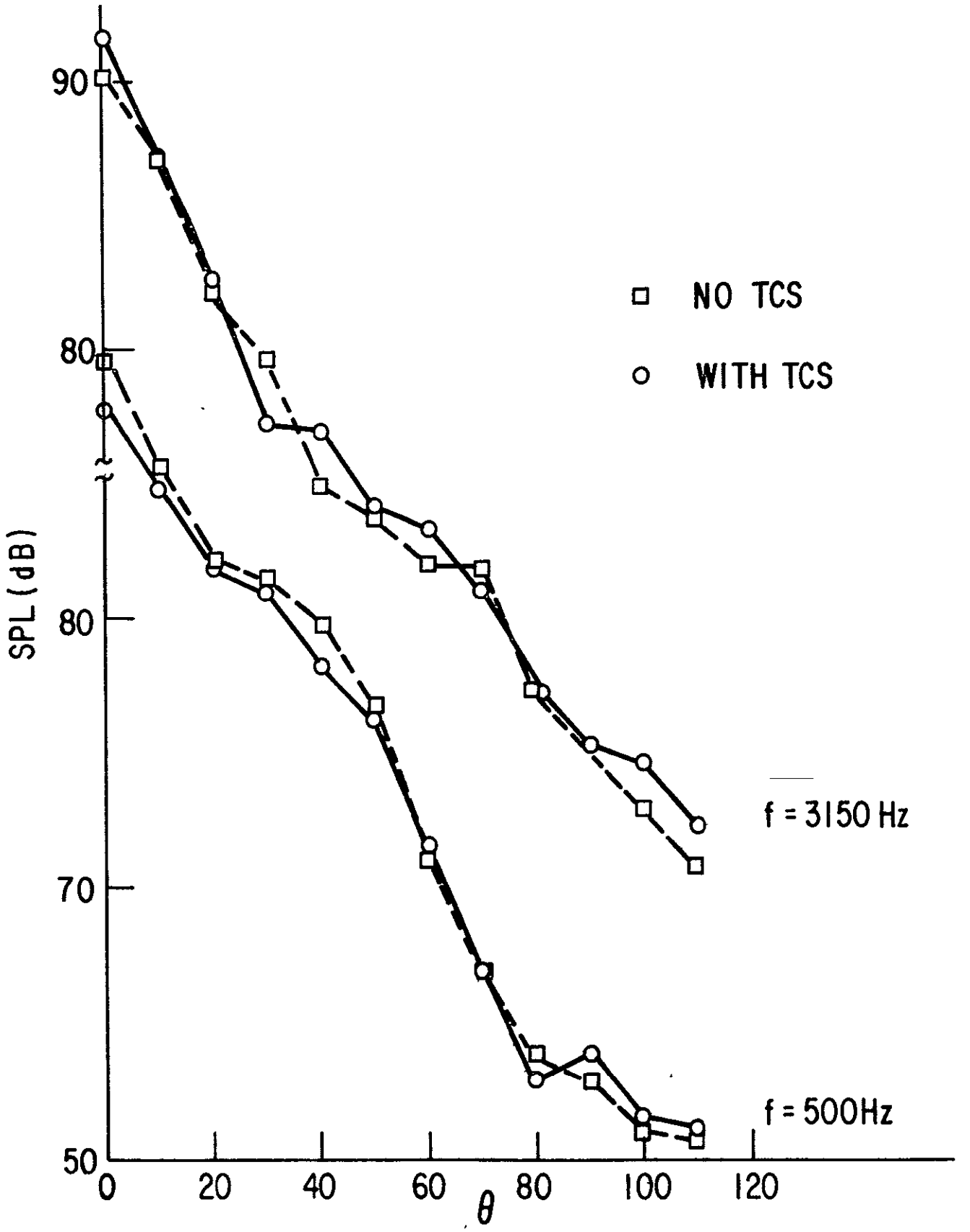

FIGURE A-2 SPEAKER CALIBRATION OF THE TCS DIRECTIVITY EFFECTS, PINK NOISE EXCITATION LOW FREQUENCY

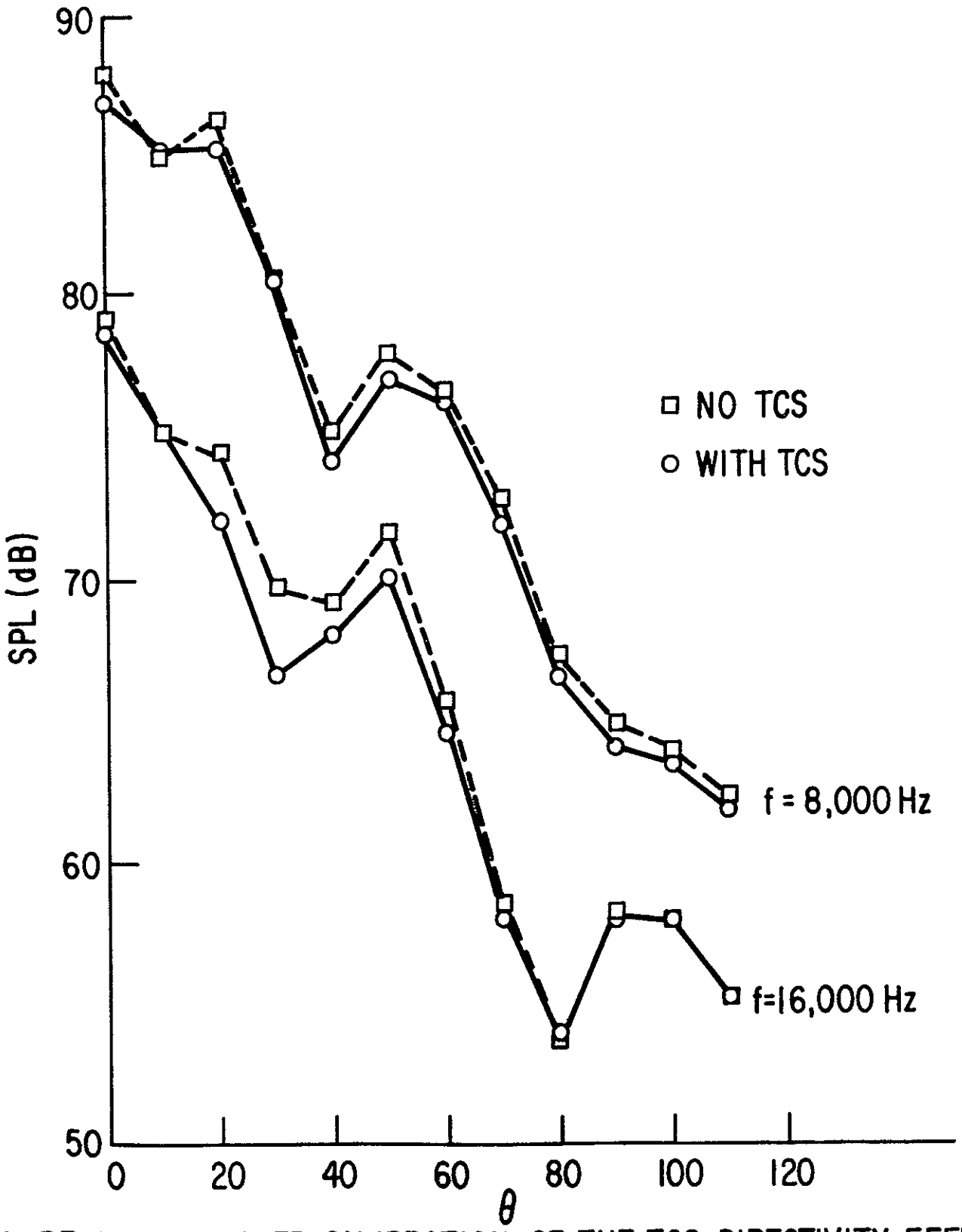

FIGURE A-3 SPEAKER CALIBRATION OF THE TCS DIRECTIVITY EFFECTS, PINK NOISE EXCITATION

DISTRIBUTION LIST

NASA Lewis Research Center
21000 Brookpark Road
Cleveland, OH 44135

Attn:	J.H. Dittmar	MS 500-208	30
	L.W. Schopen	MS 500-305	1
	Dr. B. Lubarsky	MS 3-3	1
	W.L. Stewart	MS 3-5	1
	R.W. Schroeder	MS 500-207	1
	C.E. Feiler	MS 500-208	1
	E.J. Rice	MS 500-208	1
	J.F. Groeneweg	MS 500-208	1
	N.T. Musial	MS 500-311	1
	Library	MS 60-3	2
	Report Control Office	MS 5-5	1
	Dr. J. McCarthy	MS 3-3	1

NASA Scientific and Technical
Information Facility
P.O. Box 33
College Park, MD 20740
Attn: Acquisitions Branch 30

NASA Langley Research Center
Hampton, VA 23665

Attn:	Mr. Homer Morgan	MS 239	1
	Mr. David Chestnutt	MS 239	1
	Mr. Donald L. Lansing	MS 239	1
	Mr. Joseph Posey	MS 239	1

Dr. Sanford Davis
NASA Ames Research Center
Mail Stop 227-9
Moffett Field, CA 94035 1

NASA Headquarters
600 Independence Ave., SW
Washington, DC 20546

Attn:	Harry W. Johnson (Code RL)	1
	Gordon Banerian (Code RLN)	1

Mr. Alan Hersh
Hersh Acoustical Engineering
9545 Cozycroft Avenue
Chatsworth, CA 91311 1

Mr. Richard Hayden
Bolt, Beranek & Newman, Inc.
50 Moulton Street
Cambridge, MA 02138 1

AFAPL, Turbine Engine Division
Attn: Robert McGregor
Wright-Patterson AFB, OH 45433 1

Dr. Ali H. Nayfeh
Virginia Polytechnic Institute
Dept. of Engineering Science & Mechanics
Blacksburg, VA 24061 1

Professor John Cole
Tufts University
Dept. of Mechanical Engineering
Medford, MA 02155 1

General Electric Company
Aircraft Gas Turbine Division
Evendale, OH 45125

Attn:	Mr. R.E. Kraft	1
	Mr. R. Mottsinger	1

Dr. Andrew Bauer
McDonnell-Douglas Aircraft
3855 Lakewood Boulevard
Long Beach, CA 90846 1

Dr. Harry E. Plumbee, Jr.
Lockheed-Georgia Company
Marietta, GA 30061 1

Mr. Abbott A. Putnam
Combustion Systems Section
Battelle Columbus Laboratories
505 King Avenue
Columbus, OH 43201 1

Dr. B. Lakshminarayana
Aerospace Engineering Department
Penn State University
University Park, PA 16802 1

Professor K. Uno Ingard
Massachusetts Institute of Technology
Dept. of Aeronautics & Astronautics
Cambridge, MA 02139 1

Dr. S.H. Ko
Naval Underwater System Center
Code TD-12
New London, CT 06320 1

DISTRIBUTION LIST (Cont'd)

Dr. Ronald L. Panton
University of Texas at Austin
Austin, TX 78712 1

Department of Transportation
Attn: Charles R. Foster
400 7th Street
Washington, DC 20590 1

Mr. Mark Orelup
Detroit Diesel Allison Division
P.O. Box 894
Indianapolis, IN 46206 1

Dr. John J. Schauer
University of Dayton
School of Engineering
Dept. of Mechanical Engineering
Dayton, OH 45469 1

Mr. A. Anderson
The Boeing Company
P.O. Box 3707
Seattle, WA 98124 1

Mr. Les Wirt
Lockheed of California
Burbank, CA 91503 1

Wyle Laboratories
Huntsville, AL 1

Office of Environmental Quality
Attn: John O. Powers
800 Independence Ave., SW
Washington, DC 20591 1

Ms. Sandra Gordon
AVCO-Lycoming Division
550 South Main Street
Stratford, CT 06497 1

Environmental Protection Agency
Crystal Mall, Building 2
1921 Jefferson Davis Highway
Arlington, VA 20460
Attn: John Schettino 1
William Sperry 1

Federal Aviation Administration
800 Independence Ave., SW
Washington, DC 20591
Attn: Robert J. Koenig (Code ARD-551) 1
James F. Woodall (Code ARD-500) 1

Mr. Marvin Schnee
Grumman Aerospace Corporation
Building 35, Dept. 454
Bethpage, NY 11714 1

Mr. M.D. Nelson
The Boeing Company
Nacelle and Noise Abatement Group
Wichita Division
Wichita, KS 67210 1

Mr. R.N. Yurkovich
McDonnell-Douglas Aircraft
St. Louis, MO 63178 1

Dr. L.W. Dean
Pratt & Whitney Aircraft
400 Main Street
East Hartford, CT 06108 1

Dr. D.B. Hanson
Hamilton Standard Division
United Technologies Corporation
Windsor Lakes, CT 06906 1